ILLINOIS CENTER FOR TRANSPORTATION

CIVIL ENGINEERING STUDIES
Illinois Center for Transportation Series No. 21-020
UILU-ENG-2021-2020
ISSN: 0197-9191

Rheology-Chemical Based Procedure to Evaluate Additives/Modifiers Used in Asphalt Binders for Performance Enhancements: Phase 2

Prepared By
Punit Singhvi
Javier J. García Mainieri
Hasan Ozer
Brajendra K. (BK) Sharma
Imad L. Al-Qadi
University of Illinois at Urbana-Champaign

Research Report No. FHWA-ICT-21-015

A report of the findings of

ICT PROJECT R27-196-HS
Rheology-Chemical Based Procedure to Evaluate Additives/Modifiers used in Asphalt Binders for Performance Enhancements

https://doi.org/10.36501/0197-9191/21-020

Illinois Center for Transportation

June 2021

TECHNICAL REPORT DOCUMENTATION PAGE

1. Report No.	2. Government Accession No.	3. Recipient's Catalog No.
FHWA-ICT-21-015	N/A	N/A

4. Title and Subtitle	5. Report Date
Rheology-Chemical Based Procedure to Evaluate Additives/Modifiers Used in Asphalt Binders for Performance Enhancements: Phase 2	June 2021
	6. Performing Organization Code N/A

7. Authors	8. Performing Organization Report No.
Punit Singhvi, https://orcid.org/0000-0002-0468-2702 Javier J. García Mainieri, https://orcid.org/0000-0002-8302-474X Hasan Ozer, https://orcid.org/0000-0003-1526-6840 Brajendra K. (BK) Sharma, https://orcid.org/0000-0002-7035-9380 Imad L. Al-Qadi, https://orcid.org/0000-0002-5824-103X	ICT-21-020 UILU-2021-2020

9. Performing Organization Name and Address	10. Work Unit No.
Illinois Center for Transportation Department of Civil and Environmental Engineering University of Illinois at Urbana-Champaign 205 North Mathews Avenue, MC-250 Urbana, IL 61801	N/A
	11. Contract or Grant No. R27-196-HS

12. Sponsoring Agency Name and Address	13. Type of Report and Period Covered
Illinois Department of Transportation (SPR) Bureau of Research 126 East Ash Street Springfield, IL 62704	Final Report 7/1/18–6/30/21
	14. Sponsoring Agency Code

15. Supplementary Notes
Conducted in cooperation with the U.S. Department of Transportation, Federal Highway Administration.
https://doi.org/10.36501/0197-9191/21-020

16. Abstract
The increased use of softer binders in Illinois over the past decade is primarily attributed to the increased use of recycled materials in asphalt pavement construction. The shift in demand of using PG 58-28 over PG 64-22 has resulted in potential alternative methods to produce softer binders more economically using proprietary products. However, there are challenges in using these proprietary products for asphalt modification because of uncertainty in their long-term performance and significant variability in binder chemistry. The current SuperPave performance grading specification for asphalt binders is insufficient in differentiating binders produced from these modifiers. Therefore, the objective of this study is to evaluate the performance of various softener-type asphalt binder modifiers using a wide array of rheological and chemistry tests for their integration into the Illinois Department of Transportation's material specifications. The small-strain rheological tests and their parameters allowed for consistent grouping of modified binders and can be used as surrogates to identify performing and nonperforming asphalt binders. A new parameter, $\Delta|G^*|_{peak\,\tau}$, was developed from the linear amplitude sweep test and showed potential to discriminate binders based on their large-strain behavior. Chemistry-based parameters were shown to track aging and formulation changes. The modifier sources were identified using fingerprint testing and were manifested in the modified binder chemical and compositional characteristics. The two sources of base binders blended with the modifiers governed the aging rate of the modified binders. Mixture performance testing using the Illinois Flexibility Index Test and the Hamburg Wheel-Track Test were consistent with the rheological and chemical findings, except for the glycol amine-based modified binder, which showed the worst cracking performance with the lowest flexibility index among the studied modifiers. This was contrary to its superior rheological performance, which may be attributed to lower thermal stability, resulting in high mass loss during mixing. According to the characterization of field-aged binders, laboratory aging of two pressurized aging vessel cycles or more may represent realistic field aging of 10 to 15 years at the pavement surface and is able to distinguish modified binders. Therefore, an extended aging method of two pressurized aging vessel cycles was recommended for modified binders. Two different testing suites were recommended for product approval protocol with preliminary thresholds for acceptable performance validated with field-aged data.

17. Key Words	18. Distribution Statement
Softener-type Modifiers, Bio-based Modifiers, Long-term Field Aging, Asphalt Rheology, Asphalt Chemistry, I-FIT, Hamburg Wheel-track Test, Glover-Rowe Parameters, Viscoelastic Transition Temperature, Black Angle, FTIR, GPC	No restrictions. This document is available through the National Technical Information Service, Springfield, VA 22161.

19. Security Classif. (of this report)	20. Security Classif. (of this page)	21. No. of Pages	22. Price
Unclassified	Unclassified	92 + appendices	N/A

ACKNOWLEDGMENT, DISCLAIMER, MANUFACTURERS' NAMES

This publication is based on the results of **ICT-R27-196-HS: Rheology-Chemical Based Procedure to Evaluate Additives/Modifiers Used in Asphalt Binders for Performance Enhancements (Phase 2)**. ICT-R27-196-HS was conducted in cooperation with the Illinois Center for Transportation; the Illinois Department of Transportation; and the U.S. Department of Transportation, Federal Highway Administration.

Members of the Technical Review Panel (TRP) were the following:

- Kelly Morse, TRP Chair, Illinois Department of Transportation
- Dennis Bachman, Federal Highway Administration
- Ross Bentsen, Illinois Tollway
- Kevin Burke, Illinois Asphalt Pavement Association
- Andrew Cascione, Flint Hills Resources
- Justin Grant, Illinois Department of Transportation
- Brian Hill, Illinois Department of Transportation
- Brian Pfeifer, Illinois Department of Transportation
- Ronald Price, Illinois Department of Transportation
- William Snyder, Illinois Department of Transportation
- Megan Swanson, Illinois Department of Transportation
- Jim Trepanier, Illinois Department of Transportation

EXECUTIVE SUMMARY

The increased use of softer binders in Illinois over the past decade is primarily attributed to the increased use of recycled materials in hot-mix asphalt (HMA) pavement construction. The shift in demand of using PG 58-28 over PG 64-22 has resulted in potential alternative methods to produce softer binders more economically. One such approach is to modify a stiffer binder to a softer grade by using proprietary products such as bio-based oils. However, the use of bio-based oils for asphalt modification is not permitted in Illinois because of uncertainty in its long-term impacts on pavement performance. Furthermore, these proprietary bio-based modifiers vary from one source to the other, which may significantly affect binder chemistry and rheology. The current SuperPave performance grading specification for asphalt binders is insufficient in differentiating binders produced from softening-type modifiers. Therefore, the objective of this study was to evaluate the performance of various softener-type asphalt binder modifiers using a wide array of rheological and chemistry tests for their potential integration into the Illinois Department of Transportation's material specifications.

The scope of the study included rheological and chemical characterization of the softening type of proprietary modifiers currently available in the market and proposed for use in Illinois. The outcome of this study was the development of a qualification protocol for screening proprietary modifiers to ensure the long-term performance of asphalt binders. A set of preliminary thresholds for acceptable performance was developed based on the two sources of binder and proprietary modifier combinations evaluated. The thresholds were further validated with field-aged data. The field performance data was established from aged pavement cores collected from Illinois' various regions, representing different climatic conditions.

A range of small- and large-strain binder tests were conducted to evaluate binder behavior over extended laboratory aging conditions: one pressurized aging vessel cycle (PAV), two PAV cycles (2PAV), and three PAV cycles (3PAV). The rheological parameters resulted from small-strain tests conducted at low and intermediate test temperatures and correlated well with each other. They can be used as surrogates to identify performing and nonperforming asphalt binders. The parameters from the small-strain tests included Glover-Rowe parameters, crossover parameters, and black angle for intermediate temperatures. These parameters were obtained using a dynamic shear rheometer. The ΔT_c parameter for low temperatures was determined using a bending beam rheometer. The study showed that laboratory aging of 2PAV cycles or more was able to distinguish binders based on the small-strain tests. All small-strain parameters resulted in similar rankings of modified binders. In contrast, the linear amplitude sweep (LAS) test, a large-strain binder test, was evaluated for determining binder fatigue properties. A new LAS parameter was developed, $\Delta|G^*|peak_{\tau}$, which showed potential to discriminate binders based on their fatigue performance. The performance ranking with respect to the large-strain parameter $\Delta|G^*|peak_{\tau}$ was different than that resulting from small-strain parameters, except for the refined engine oil bottom (ReOB)-based binder. The ReOB-based binder performed the worst among the studied modifiers. Overall, the rheological tests and the test parameters allowed for consistent grouping of modified binders based on the source of modifiers (vegetable oil, bio based, fatty acid derivatives, glycol amines, and petroleum based). The mass loss from rolling thin-film oven (RTFO) testing suggested low thermal stability of the glycol

amine–based modifier, but the rheological findings still suggested this modifier to be the best performing, followed by fatty acid derivatives.

The source material of each modifier provided by the manufacturer was confirmed by performing chemical analyses using Fourier transform infrared (FTIR) spectroscopy. Most modifiers were the vegetable oil type. The fingerprint of the modifier was manifested in distinctive functional groups in the FTIR analysis of modified binders. Molecular weight distribution using gel permeation chromatography (GPC) was further able to differentiate specific modifiers and the impact of aging. Chemical techniques such as FTIR spectroscopy as well as GPC were able to capture the effect of aging on chemical functional groups and molecular size, respectively, in modified binders. FTIR analysis showed that only specific carbonyl functional groups (1,670–1,725 cm^{-1}) captured the effect of aging, unlike what had been reported in the literature (1,600–1,800 cm^{-1}). The molecular weight distribution for asphalt binders was observed to be bimodal and aging the ratio of the peak corresponding to the large to small molecular weight increased with aging. Chemistry-based parameters were effective in distinguishing functional groups or molecular weight distributions of modified binders, except for the ReOB-based modified binder. However, the ReOB-modifier showed the presence of a significantly high content of insolubles (including asphaltenes), which is usually not distinguishable in FTIR and GPC. The glycol amine–based modifier was least susceptible to aging, as observed from FTIR and GPC. Limited thermal analysis of modifiers showed the glycol amine–based modifier to be the least stable (most volatile), which supported the findings from RTFO mass loss. The effect of binder source on modified binder performance was also evaluated. In all the modified binder cases, source binders governed the aging rate, resulting in a similar performance with respect to aging. Therefore, it may not be possible to develop performance-related thresholds based on chemistry parameters. However, chemical characterization was shown to track formulation changes.

Rheological properties of field-aged extracted binders showed a gradient through the pavement depth. The effect of field aging on the surface was more severe than 2PAV for binders aged between 10 to 15 years. It was verified that PAV aging was not sufficient to represent realistic long-term aging for binders. Furthermore, rheological testing of modified binders showed that a 2PAV or more aging protocol better distinguished binders. Therefore, a laboratory aging protocol of 2PAV was recommended to capture the long-term impacts on modified binder properties. Additionally, the chemical characteristics of field-aged binders validated that the carbonyl functional group from 1,670–1,725 cm^{-1} captured the effect of field aging. Based on the rheological results obtained for modified binders from the laboratory aging condition of 2PAV and results from field-aged-extracted binders from surface lifts, initial thresholds were suggested for modified binder acceptance criteria.

Mixture performance testing using the Illinois Flexibility Index Test and Hamburg Wheel-Track Test was conducted to validate the rheological and chemical findings for modified binders. All modified binders showed acceptable cracking and rutting performance as per Illinois standards. The ReOB-based modified binder was among the worst performing, as predicted by rheological findings. The glycol amine–based modified binder showed the worst cracking performance with the lowest flexibility index, contrary to its superior rheological performance. This may be attributed to lower thermal stability/higher volatility, which resulted in high mass loss during mixing. High mass loss in the glycol amine–based modified binder may have reduced the effective binder content, affecting its

cracking performance. Therefore, it was also recommended to consider the thermal stability of modifiers and RTFO mass loss of modified binders to ensure long-term mixture performance.

Both rheological and chemical characterization of softener-type modified binders were able to group binders based on their modifier source. The ReOB-based modified binder was the worst performing while glycol amine was among the best performing except for its low thermal stability. Low thermal stability proved to be a critical property resulting in potentially poor mixture cracking performance.

As a result of the comprehensive rheological and chemistry testing program, two different testing suites were recommended as part of a product approval protocol. An extended aging method of 2PAV was recommended for modified binders. The first testing suite is to support IDOT's existing quality assurance protocols. With a minor addition to the current quality assurance program, the performance of modified binders could be monitored. The second is a new protocol that can be implemented at the product approval stage and repeated yearly or when product formulation changes to incorporate the effect of binder source and modifiers used.

TABLE OF CONTENTS

LIST OF FIGURES

LIST OF TABLES

CHAPTER 1: INTRODUCTION

BACKGROUND

In the United States, roughly 20 million tons of asphalt binder (AB) are used in pavement construction annually (Williams et al., 2018). Asphalt binder is an important component for the construction of hot-mix asphalt (HMA). It is currently produced from the fractional distillation of crude petroleum at refineries. In recent years, the increasing use of harder and aged recycled asphalt materials in HMA applications has significantly increased the need for softer binders (Williams et al., 2018). Logistical limitations and the cost of refineries to produce softer ABs, instead of products of higher value, result in a shortage of straight-run or unmodified AB in the market (Kriz et al., 2019).

To overcome the current demand for softer ABs, traditionally petroleum-based "softeners," like AB flux and aromatic oils, are blended with straight-run AB (Asphalt Institute, 2015). A variety of proprietary products are available to modify AB to achieve softer grades. Blending "softeners," such as recycled oils and bio-based oils, with readily available asphalt binder products is an opportunity to produce the required AB economically and reduce the dependence on petroleum-based products.

A problem arises with the limited information regarding the long-term performance of ABs modified with proprietary modifiers. Poor durability and/or extended cracking issues were identified when re-refined engine oil bottoms (ReOB) and waste engine oils were blended in AB (Ozer et al., 2016; Rose et al., 2016; Jia et al., 2015; Reinke et al., 2016; Golalipour & Bahia, 2016). In addition, the use of certain bio-based oils in ABs increases the oxidation potential, which makes pavements vulnerable to long-term cracking (Fini et al., 2015).

Proprietary products used for AB modification possess unique chemical characteristics and vary significantly from one product to another (Gökalp & Uz, 2019; Haddock, Tao, & Seidel, 2009; Sadek et al., 2020). These modifiers may not only alter the chemical makeup of asphalt binder, but also might affect its rheological performance. Understanding the effects of binder modification on its chemistry, rheology, blend compatibility, and asphalt concrete performance is key to the successful implementation of such modifiers. Previous studies report that some of these modifiers/products show improvements in resisting fatigue and low-temperature cracking of AC, while other studies are inconclusive (Lei, Bahia, & Yi-Qiu, 2015; Paliukaite, Assuras, & Hesp, 2016; Sadek et al., 2020).

Another challenge to the widespread use and implementation of a range of modifiers is the limitations of the standard testing and acceptance protocols. Most agencies in the United States currently use the SuperPave performance grading (PG) system for binder selection and acceptance. The SuperPave grading system was developed in the 1990s and was accepted to be a performance-related material selection system (Anderson & Kennedy, 1993). SuperPave uses rheological properties of AB under various temperature and aging conditions. However, since the inception of PG, technological advancements, along with global economic, political, and environmental considerations, have led to significant changes in AB chemistry and overall quality. Increasing demand for the lighter fractions of crude petroleum has resulted in a much stiffer residue for binder production. The proprietary modifiers may provide some of the desired AB characteristics in the short

term; however, their impact on the rheology and chemistry of asphalt binder is relatively unknown, especially when long-term aging is considered. The testing protocols of the SuperPave PG system do not capture the true performance of those modifiers because of performance parameters and aging conditions' limitations.

The long-term aging of asphalt binder is an ongoing research topic. There is no consensus whether the current binder aging protocol simulates the realistic field aging of asphalt mixtures. This becomes challenging for proprietary modifiers. When modifiers like ReOB or waste engine oils were used as modifiers, deterioration of rheological properties after long-term aging was evident (Paliukaite, Assuras, & Hesp, 2016; Ozer et al., 2016; Rose et al., 2016; Jia et al., 2015; Reinke et al., 2016; Golalipour & Bahia, 2016). Concerns regarding similar deterioration are impeding the use of proprietary modifiers. In Illinois, the use of such proprietary modifiers, except SBS polymer, is restricted because of long-term performance concerns. There is a need for an experimental study to understand the impact of proprietary modifiers on the chemistry and rheological characteristics of asphalt binder beyond what is required with the SuperPave grading system.

RESEARCH OBJECTIVES AND SCOPE

The main goal of this study is to evaluate the performance of various softener-modified asphalt binders for their potential integration into the Illinois Department of Transportation's material specifications.

The scope of the study includes rheological and chemical characterization of the softening type of proprietary modifiers currently available in the market and proposed for use in Illinois. The outcome of this study is the development of a qualification protocol for screening proprietary modifiers to ensure the long-term performance of ABs used in asphalt mixtures. A set of preliminary thresholds for acceptable performance was developed based on the limited binder and proprietary modifier combinations evaluated. The thresholds were further validated with field-aged data. Binder performance was established based on the data collected from aged pavement cores collected from Illinois' various regions, representing different climatic conditions.

CHAPTER 2: MATERIAL INVENTORY AND TEST METHODOLOGY

MATERIAL INVENTORY

Binders and Modifiers

A diverse set of proprietary modifiers that can soften asphalt binder and alter high- and low-temperature performance grading (PG) were used to modify commercially available PG 64-22 base binder, herein referred to as S1. The binder S1 was sampled from an asphalt terminal in Illinois. Table 1 lists the proprietary modifiers with softening properties that were collected for the study. Their identities are kept confidential to avoid any potential conflict of interest. The modifiers are labeled as shown in Table 1. Modifier dosages were chosen to achieve PG 58-28 for the modified binders. All modified binders in this study are labeled with their base binder, followed by the modifier's letter (as presented in Table 1) and the dosage. The modifier's dosage was added as percent (%) by weight of asphalt binder. Table 1 lists the modifier type as identified by the suppliers. A PG 58-28 unmodified binder (S5) was included as a benchmark.

Additionally, S8 and S9-L-NA are unmodified and modified PG 58-28 binders, respectively, sampled from an asphalt terminal and used in the asphalt concrete (AC) of a control section and a test section in Illinois. S9 was verified to be a PG 64-22 base binder. S9-L-NA is the only binder in this study that was not blended in-house. The modifier type and dosage for L were not reported by the supplier. To study the impact of binder source on modified binders, another PG 64-22 binder was procured (S2); it was modified using a selection of the modifiers.

Table 1. Asphalt Binders Tested in This Study

Modifier	Modifier type as indicated by the manufacturer	Binder	Dosage %	Base binder
–	Original binder (PG 58-28) from source 1	S5	–	–
–	Original binder (PG 58-28) from source 2	S8	–	–
–	Original binder (PG 64-22) from source 1	S1	–	–
–	Original binder (PG 64-22) from source 2	S2	–	–
A	Bio-oil	S1-A-3.5	3.5	S1
B	Fatty acid derivative	S1-B-5.0 / S2-B-5.0	5.0	S1 / S2
C	Fatty acid derivative	S1-C-3.1	3.1	S1
D	Bio-oil blend	S1-D-3.1	3.1	S1
E	Modified vegetable oil	S1-E-3.1	3.1	S1
F	Modified vegetable oil	S1-F-3.1 / S2-F-3.1	3.1	S1 / S2
G	Glycol amine	S1-G-6.5 / S2-G-6.5	6.5	S1 / S2
H	Asphalt	S1-H-10 / S2-H-10	10	S1 / S2
I	Vegetable oil	S1-I-3.5	3.5	S1
J	Vegetable oil	S1-J-3.0	3.0	S1
K	ReOB	S1-K-10 / S2-K-10	10	S1 / S2
L	N/A	S9-L-NA	N/A	S9

Blending Methodology

A blending procedure was developed to produce modified binders in-house (Singhvi et al., 2020). The procedure was developed in consultation with the suppliers. The procedure was developed to collect statistically representative samples from the gallon cans of the base binders collected for this study. A shear mixer (Cafarmo BDC1850) with a ringed propeller (Heidolph PR31) (33 mm diameter fan) was used for blending. The blending was performed at 130 ± 10°C. The blending temperature was maintained using a heating mantle (Glas-Col LLC) capable of handling a 1 L aluminum can. The method for producing representative modified samples is summarized below and found in Figure 1:

1. Asphalt binder from each set (1 gal) was heated to 135°C for 2 hr. in a conventional forced draft oven to reach a flowing state. The asphalt binder was split into 6 qt cans at approximately 500 g each and was stirred before pouring. The samples in the cans were then stored for modification. The weight (measured to a 0.01 g accuracy) of the binder was recorded.

2. Before modification, the split base binder (S1) was heated for 30 min in a heating mantle to reach 130 ± 10°C to ensure that the material was steadily flowing prior to blending.

3. The modifier was added (weight measured to a 0.01 g accuracy), and the propeller was inserted halfway into the depth of the material and was set to 1000 rpm for 20 min. During blending, the temperature was maintained at 130 ± 10°C and the formation of vortexes was prevented to avoid air bubble formation in the blend.

4. After blending, the modified binder was transferred equally to four 240 ml (8 oz) cans.

5. Steps 2 to 4 were repeated for the asphalt binders from the sets mentioned in Step 1 to obtain representative samples.

6. Later, three 240 mL (8 oz) cans from different batches of each modified binder were combined to proceed with aging.

Aging conditions used in the study are unaged (UA), rolling thin-film oven (RTFO), per AASHTO T240-13, and a pressurized aging vessel (PAV), including vacuum degassing following AASHTO T28-12 for 20 hr. (PAV), 40 hr. (2PAV), and 60 hr. (3PAV) conditioning. Conditions with 2PAV and 3PAV were obtained by running continuous 40 hr. and 60 hr. PAV cycles, respectively. Once the samples reached their required aging condition, they were stored in small 30 ml (1 oz) cans until testing, to avoid multiple heating cycles. To control any changes in chemical and rheological properties, cans were not re-used once heated for testing. A similar treatment was applied to all binders used in the study.

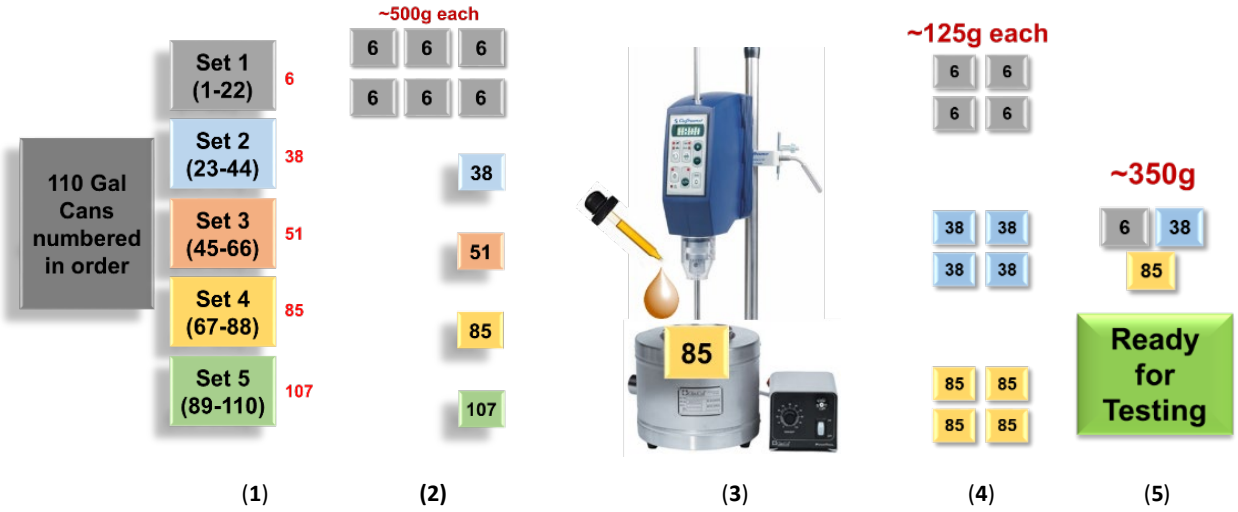

Figure 1. Diagram. Blending and production of representative asphalt binder samples.

Field Core Inventory

Field cores aged more than 10 years were collected from different districts across Illinois, preferably with thicknesses 8 in. or more to characterize aging through the pavement depth. Eight cores per section were collected. Table 2 summarizes the field cores used in the study. Additional details for the cores are provided in Appendix E.

Table 2. Field Core Information

Field Core ID	District	Binder PG	Year of Construction	Year of Coring	Age
I-355	D2	64-22	2007	2018	11 yrs.
I-90	D1	64-22	2006	2018	12 yrs.
22STR2	D2	58-22	2004	2014	10 yrs.
2RT26	D2	76-28	2004	2014	10 yrs.
SMA20	–	NA	1998	2018	20 yrs.
L1-1019	D5	64-22	2008	2019	11 yrs.
L2-1019	D5	64-22	2009	2019	10 yrs.
L3-1019	D5	64-22	2011	2019	8 yrs.
ICT Parking Lot	D5	NA	1989	2020	31 yrs.
IL-125	D6	64-22	2009	2018	9 yrs.
I-72 1E	D6	64-22	2003	2013	10 yrs.
US-51	D8	64-22	2001	2018	17 yrs.

TESTS AND PARAMETERS

Table 3 presents a summary of the experimental program and specifications followed for this study.

Table 3. Summary of Experimental Program

Conditioning		Rheology		Chemistry		Field core binder extraction		Mixture level testing	
Procedure	Specification	Test	Specification	Test	Specification	Extraction	Specification	Test	Specification
Rolling thin-film oven (RTFO) aging	AASHTO T240-13	SuperPave G* measurements	AASHTO T315 and M320	GPC	In-house protocol as described in a later section	Solvent distillation	Binder extraction- Auto extractor from PAVELAB Binder Recovery- AASHTO T319	IFIT	AASHTO TP124
Pressure aging vessel (PAV) aging	AASHTO T28-12	Frequency sweep	An in-house protocol was developed for obtaining the measurements and manual shifting to obtain master curves	FTIR	In-house protocol as described in later sections			HWTT	AASHTO T324
Extended PAV aging	AASHTO T28-12 modified for 40 or 60 hr. of continuous conditioning time and degassing	Linear amplitude sweep	AASHTO TP101 and T391-20, an in-house interpretation method and parameter were developed to analyze the measurements.	Elemental analysis	Conducted at UIUC's Microanalysis Laboratory as per their standard procedure				
		Bending Beam Rheometer	AASHTO T313	TGA	Ramp rate = 20°C/min up to 700°C				
				SARA	In-house protocol as described in a later section				

Rheology

For rheological characterization of binders, tests were performed within and beyond the linear viscoelastic region (LVER). Results are referred to as small- and large-strain testing results, respectively. More information about the importance of small- and large-strain testing can be found in Appendix A, where more information about the parameters discussed in this chapter is also provided. In this chapter, only the methods used to obtain the parameters are explained.

Tests were performed utilizing a bending beam rheometer (BBR) (Cannon TE) and a dynamic shear rheometer (DSR) (Kinexus KNX2712). The rheometers were operated in an active hood for temperature control. Two replicates were tested in each trial, with averages being reported. The coefficient of variation was limited to 7% on any complex modulus measurement on frequency sweeps. Repeatability criteria were followed as reported by Singhvi et al. (2020).

All binders used in this study were initially tested to determine SuperPave PG. The tests were performed per AASHTO T315-19 (DSR) and T313-19 (BBR). Continuous PGs (true grades) were also determined. The BBR measurements for PAV-aged (PAV), double PAV-aged (2PAV), and triple PAV-aged (3PAV) samples were obtained following AASHTO T313-19 specifications.

ΔT_c was computed using the equation shown in Figure 2:

$$\Delta T_c = T^{cr}{}_S - T^{cr}{}_{m-value}$$

Figure 2. Equation. Delta T_c calculation.

where $T^{cr}{}_S$ and $T^{cr}{}_{m\text{-}value}$ are the critical temperatures for stiffness and m-value, respectively. The m-value, which is the slope of the time-stiffness curve, represents the binder's ability to relax under stress. These values were found using the interpolation method recommended by the Asphalt Institute (2019). Some temperatures (S1-K-10 and all 2PAV- and 3PAV-aged samples) were extrapolated to obtain values at critical stiffness (300 MPa) without testing at extra temperatures. Two beams were tested per sample per temperature; the averages were reported. The coefficient of variance (CoV) for the m-value and stiffness was kept below 1.5% and 8%, respectively. If the criteria were not met, extra beams were tested to have confidence in the reported results.

Frequency sweep tests were conducted using DSR equipment and the following protocol:

- Conditioning of samples was applied before testing (10 cycles of 0.1% strain at 15°C and a frequency of 0.5–0.61 rad/s).
- Shear modulus (G*) and phase angle (δ) was obtained for all samples at unaged (UA), RTFO, PAV, 2PAV, and 3PAV conditions.
- Data were measured in isotherms of 15°C, 25°C, and 35°C. Additional frequency sweeps at 45°C isotherms or extended frequencies at 5°C were performed for selected binders to substitute or verify extrapolated results.

- Nineteen data points were collected per isotherm in the frequency range from 1.00 rad/s to 62.83 rad/s at a constant shear strain of 1.6% for OB, 1.2% for RTFO and PAV-aged samples, and 1.0% for 2PAV and 3PAV samples. These strains were selected to ensure measurements within the linear viscoelastic range of the samples.

- Harmonic distortion between strain excitations and stress responses was less than 1% after the first measurement, and measured torque was in the operational range of the equipment for all sweeps performed.

- Additionally, a preconditioning sequence was incorporated before the isotherms to verify that the measurements were recorded within the linear viscoelastic range.

The data were shifted to a 15°C reference temperature to develop master curves. This procedure is reported by Singhvi et al. (2020).

The Glover-Rowe parameter (GRP) was computed using the equation shown in Figure 3:

$$GRP = \frac{|G^*| \times (\cos\delta)^2}{\sin\delta}$$

Figure 3. Equation. Glover-Rowe parameter.

where |G*| and δ are the complex shear modulus and phase angle at 15°C and 0.005 rad/s. G* and δ at 15°C and 0.005 rad/s were obtained from measured data. In some cases, the data was extrapolated using polynomial-fits from master curves and black space diagrams.

Unlike GRP, GRP_f was obtained at a temperature that changes for different binder low-temperature PGs; therefore, it is less dependent on the complex modulus of the binder. The GRP_f was obtained using the same formula (Figure 3) for frequency sweep data at 10 rad/s shifted to the respective temperatures: 22°C for binders with a low PG of −28 and 25°C for binders with a low PG of −22 (Christensen & Tran, 2019). Black angles were interpolated from measured phase angle (δ) data for a |G*| of 8967 kPa using fourth-order polynomial fits.

The crossover complex shear modulus ($|G^*|_c$) is reported as the complex shear moduli |G*| at a 45° phase angle from the respective black-space diagrams at a 15°C reference temperature and a frequency of 10 rad/s. In contrast, the reported crossover reduced frequency (w_c) is the reduced frequency (w_r) at a 45° phase angle interpolated using the shifted measured data for a 15°C reference temperature at a frequency of 10 rad/s. The reported viscous to elastic transition temperature (VETT) was computed using the equation presented in Figure 4:

$$\mathrm{VETT} = \frac{15 \times C_1 - (C_2 - 15) \times (log_{10}(w_c) - 1)}{C_1 + log_{10}(w_c) - 1}$$

Figure 4. Equation. Viscous to elastic transition temperature.

where C_1 and C_2 are the Williams-Landel-Ferry constants determined to develop master curves (Williams, Landel, & Ferry, 1955). The equation in Figure 4 is derived from algebraic manipulation of the Williams-Landel-Ferry equation for a reference temperature of 15°C at a frequency of 10 rad/s.

The R-value was obtained by assuming the glassy complex shear modulus $|G^*|_g$ of all binders is 1 GPa. This assumption is debatable, as $|G^*|_g$ has been portrayed as being significantly different for different binders (Rowe, 2019). However, because of the difficulty measuring G^*_g, limited efforts have been made to determine its value. The assumption made here is that the variability in the crossover modulus is much higher than the variability in the glassy complex modulus. Therefore, the R-value may correlate to the binder properties changing with different modifiers. The R-value was computed using the equation presented in Figure 5:

$$R - value = \log_{10}(1000) - \log_{10}(|G^*|_c)$$

Figure 5. Equation. R-Value.

where $|G^*|_c$ is in MPa.

The standard linear amplitude sweep (LAS) test was performed using DSR equipment (Kinexus KNX2712) with an active hood for temperature control. All samples were tested at 19°C, except the S1 samples, which were tested at 25°C. Tests were performed in isothermal conditions at SuperPave intermediate temperatures to represent field climatic conditions under which those binders are intended to be used. An isostiffness approach could have been pursued; however, an approach that provides isothermal and climate-representative conditions was preferred. S1 is the base binder (PG 64-22) for most of the modified binders in this study. The results for S1 are presented to validate the quality of the base material but are not meant for direct comparison.

Chemistry

Modifiers and asphalt binders were chemically characterized to determine the elemental composition, functional groups, molecular weight distribution, SARA composition, and thermal properties using elemental analysis, Fourier transform infrared (FTIR) spectroscopy, gel permeation chromatography (GPC), thin layer chromatography flame ionization detection (TLC-FID), and thermogravimetric analysis (TGA), respectively. Laboratory- and field-aged binders were also chemically characterized. The test procedures and parameters evaluated in the study are summarized as follows.

Elemental Composition

Elemental analyses of modifiers were conducted in an Exeter Analytical (Chelmsford, MA) CE-440 elemental analyzer at the University of Illinois at Urbana-Champaign's Microanalysis Laboratory. The proportions of carbon, hydrogen, nitrogen, and sulfur elements in the material's composition were expressed in percent. The proportion of oxygen (O) was obtained by subtracting the percentages of carbon, hydrogen, nitrogen, and sulfur from 100.

Chemical Functional Groups

A FTIR spectrometer (Thermo Nicolet Nexus 670) was used to detect the chemical functional groups present in modifiers in the 600–4,000 cm^{-1} wavenumber range. Data was collected at a resolution of 4 cm^{-1} with the number of scans set to 64. Two replicates were tested for each sample. The method was based on attenuated total reflection. Functional groups corresponding to carbonyls and sulfoxides were evaluated for quantifying oxidation in asphalt binders. Several indices based on carbonyl and sulfoxides were proposed; they are presented in Chapter 4. The spectrometer results were also used in fingerprinting modifiers.

Molecular Weight Distribution

The molecular weight analysis was conducted using gel permeation chromatography (GPC). The system consists of a Waters 2695 separation module connected to two Styragel HR1 Size Exclusion Chromatography (SEC) columns (7.8 mm × 300 mm) in series followed by a Waters 2414 Refractive Index (RI) detector and a computer with Empower Pro and data acquisition software. Samples of 3% by weight were prepared in tetrahydrofuran, a carrier solvent with a flow rate of 1.0 mL/min and an injection volume of 20 µL. They were filtered using a 0.45 µm Millipore polytetrafluoroethylene syringe filter to remove suspended particulates. To detect analytes, a constant flow of fresh eluent was supplied to the column via a pump.

The resulting chromatographic data was processed for number-average molecular weight (Mn), weight-average molecular weight (M_w), and polydispersity index (PDI) using the equations presented in Figure 6, Figure 7, and Figure 8, respectively. The molecular weights were calculated based on the component molecular weights (M_i) determined from the retention time calibration curve and signal intensities (N_i). Furthermore, other molecular weight parameters based on small, medium, and large molecular sizes were evaluated. Additional parameters were proposed in Chapter 4.

$$M_n = \frac{\sum M_i N_i}{\sum N_i}$$

Figure 6. Equation. Number-average molecular weight.

$$M_w = \frac{\sum M_i^2 N_i}{\sum M_i N_i}$$

Figure 7. Equation. Weight-average molecular weight.

$$PDI = \frac{M_w}{M_n}$$

Figure 8. Equation. Polydispersity index.

The retention time calibration curve was developed by fitting log-scale molecular weights to their retention time for standard material with known molecular weights (polystyrene standards consisting of peak maxima molecular weights) using a 3° polynomial. The fitted curve was then used to measure the molecular weights of unknown modifiers using chromatographic data. The distributions with shorter retention times correspond to larger molecular sizes, whereas longer retention times represent smaller sizes. The molecular weights are reported in Daltons.

Compositional Characteristics

The thin layer chromatography—flame ionization detection (TLC-FID) technique was used to separate modifiers and asphalt binders into four generic fractions—saturates, aromatics, resins, and asphaltenes (SARA). TLC-FID was performed in a three-stage development process using n-heptane, toluene, and tetrahydrofuran, respectively, as solvents. Two percent (weight by volume) solution of samples were prepared in dichloromethane (for modifiers) or chloroform (for asphalt binders), which dissolves all four SARA fractions. The solution is filtered through a 0.45 µm Millipore polytetrafluoroethylene syringe filter to remove insoluble suspended particles from the solution. The suspended particles are referred to herein as insoluble residue. The sample solution (1 µL) was spotted on chromrods coated with a thin film of silica gel using a microsyringe. The chromrods were dried for 10 min and humidified in $NaNO_2$ for 10 min between each development. The chromrods were scanned with an Iatroscan MK-5 analyzer (Iatron Laboratories Inc., Tokyo) with a flame ionization detection (FID) method, which provided chromatograms with peaks for SARA composition.

Thermal Analysis

Thermogravimetric analysis (TGA) was performed on selected modifiers and binders in the University of Illinois at Urbana-Champaign's Materials Research Laboratory. Q50 TGA equipment was used to conduct thermal degradation of modifiers and asphalt binders. The test used a constant heating rate of 20°C/min (ramp type), heated to 700°C under a nitrogen and oxygen environment. A sample weight of 10–20 mg was used with two replicates tested for each sample.

Field Core Extraction, Distillation, and Recovered Binder Testing

Field cores were cut in 0.5 in. slices through the depth of the core. Four slices from the same depth representing the same section were heated at 140°C in a forced draft oven for 30 min. The heated sample was then used for extraction using a PAVELAB auto extractor. PAVELAB's fast extraction feature was used to extract the binder with trichloroethylene as an extracting solvent. The extracted binder was later recovered using a ROTOVAP extractor based on the solvent distillation method, as per AASHTO T319. The recovered binder was then subjected to chemical and rheological testing, as presented in the above sections.

Mixture Level Testing

Mixture performance tests were used to evaluate the cracking and rutting performance of AC mixtures made from modified binders. A series of laboratory AC mixtures were designed, and certain plant-produced mixtures were procured for the study. The Illinois Flexibility Index Test (I-FIT) was used to evaluate cracking, and the Hamburg Wheel-Track Test (HWTT) was used for determining

rutting resistance of mixes. I-FIT specimens aged for 3 days at 95°C in a forced draft oven were also tested to evaluate the long-term performance of AC mixtures (Al-Qadi et al., 2019).

Illinois Flexibility Index Test

I-FIT was conducted as per AASHTO TP-124. SuperPave gyratory pills of 160 mm height were compacted to obtain resulting I-FIT specimens with 7± 0.5% air voids. The test was conducted at 25°C. I-FIT parameters such as flexibility index (FI), fracture energy (FE), post-peak slope (m), and strength (in psi) were reported for each specimen. Compacted I-FIT specimens were also tested for long-term aging properties as per Al-Qadi et al. (2019). Six to eight replicates were tested for each condition per mix.

Hamburg Wheel-track Test

HWTT was conducted in accordance with AASHTO T324. The samples were compacted to 130 mm height and were cut in half to obtain the Hamburg specimens with target air voids of 7± 0.5%. The test was conducted on specimens submerged in water at 50°C. Variation of rut depth with number of passes was reported.

CHAPTER 3: RHEOLOGICAL CHARACTERIZATION FOR SOFTENER-MODIFIED BINDERS

This chapter presents and discusses the rheological testing results for a subset of binders. Performance grading (PG) is provided for context. Then, small-strain testing results are presented and interpreted, and modified binders are grouped based on performance. Additionally, the relationship between small-strain parameters is evaluated. Then, large-strain testing results are presented using the standard interpretation procedure, limitations are presented for that procedure, and an improved and more practical method is proposed. Finally, a comparison between small- and large-strain behavior is provided in terms of how they rank binders.

SUPERPAVE PERFORMANCE GRADE

True PG grades (continuous) of the source and modified binder are reported in Figure 9. These were obtained per the current SuperPave specification, AASHTO M320. All binders tested in this project have similar stiffnesses and phase angles at intermediate temperatures at the PAV aging condition.

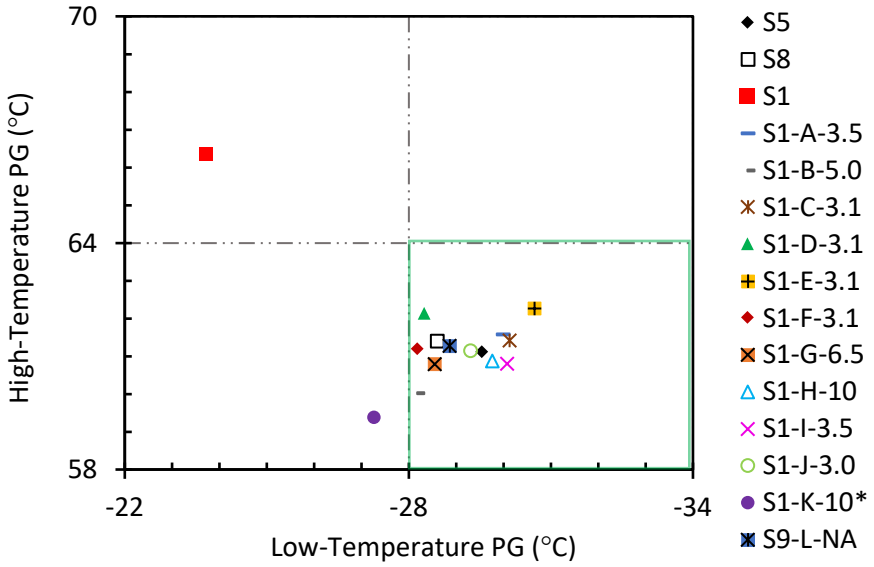

*As detailed by Singhvi et al. (2020), modification to PG 58-28 was attempted and was not possible.

Figure 9. Graph. Continuous PG grade for source and modified binders considered in this study.

However, although modification produced the target PG, the long-term performance of modified binders may be different than unmodified binders (Zhang et al., 2017; Ozer et al., 2016; Reinke et al., 2016). Therefore, the experimental program included various test procedures to obtain a better performance assessment of modified binders at small and large strains.

SMALL-STRAIN TEST RESULTS

Low-temperature Tests and Parameters

ΔT_c results are presented in Figure 10. Modified binders have been identified by the modifier type: vegetable oil (veg. oil), petroleum based, re-refined engine oil bottoms (ReOB), fatty-acid derivative (FA), or glycol amine (GA). Distinct groups of modifiers can be observed based on their binder's ΔT_c results at the 2PAV aging condition:

- Fatty acid and glycol amine (−1.8 to −3.6).
- Vegetable oil and petroleum-based modifiers (−4.2 to −8.1) perform similarly to the S5 unmodified benchmark.
- ReOB (−13.0).

S8 appears to have more desirable ΔT_c than its modified counterpart S9-L-NA. Note that all binders presented in Figure 10 were m-controlled at low temperatures at all aging conditions, i.e., their m-value (relaxation parameter obtained from BBR testing) was more critical than their stiffness.

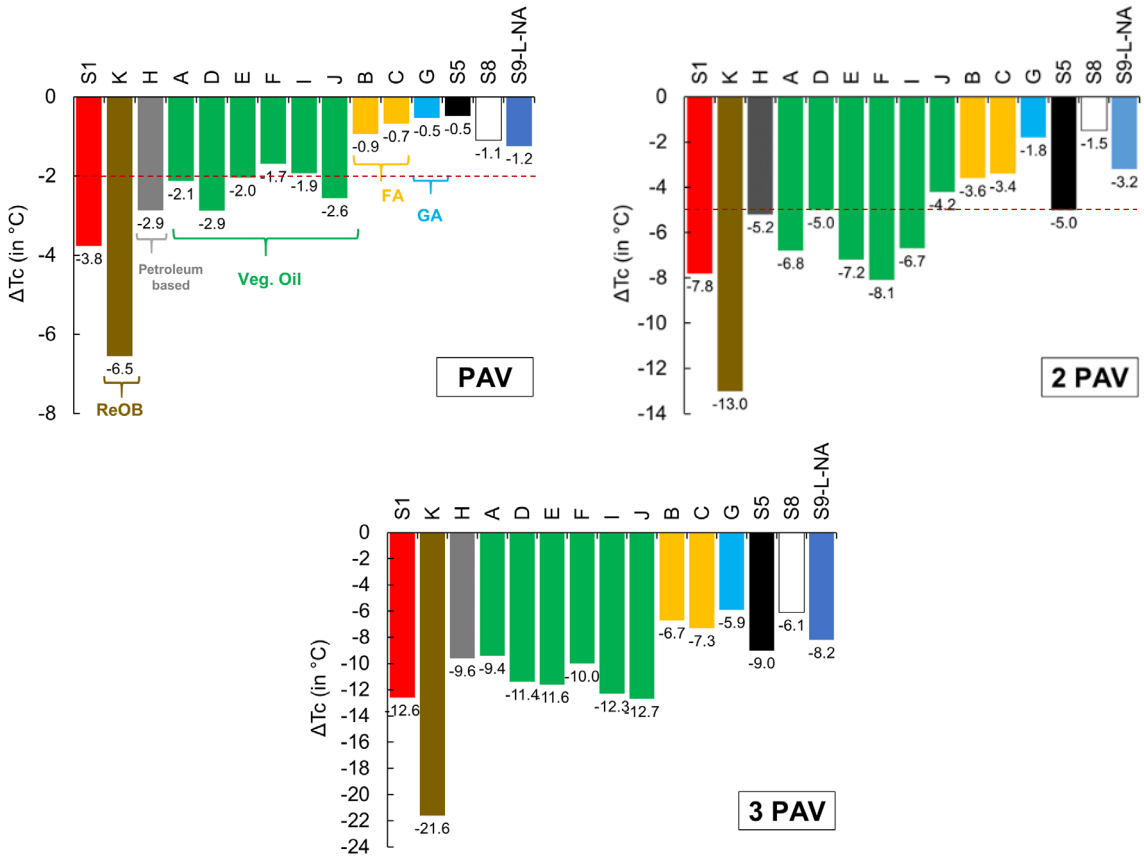

Figure 10. Bar plots. ΔT_c parameter obtained at three aging conditions.

Minimum values of ΔT_c of −2°C and −5°C are used in several states as thresholds for PAV- and 2PAV-aged binders, respectively (Asphalt Institute, 2019). Except for modifier J, all binders that failed the PAV criterion also failed the 2PAV criterion. The unmodified PG 58-28 (S5) was used as a benchmark to evaluate the effect of aging. The ranking of all binders at 2PAV and 3PAV aging conditions are consistent. For example, the binders that had a lower ΔT_c than that of S5 at 2PAV also had a lower ΔT_c than that of S5 at 3PAV. The ranking of binders did not change after 3PAV. Therefore, 2PAV aging is necessary and sufficient to discriminate binders based on ΔT_c.

S1 is a commercially available PG 64-22 binder and is commonly used in Illinois. Its ΔT_c can be compared to the rest of the binders (PG 58-28) because ΔT_c at all aging conditions was determined at the same stiffness level (around 300 MPa). A ReOB-modified binder at 2PAV and 3PAV aging conditions was also tested at different temperatures. In general, a binder that passes the BBR test at −18°C would skip a grade (6°) and pass the test criterion at −12°C and −6°C at the 2PAV and 3PAV aging conditions, respectively. This was not the case for the ReOB-modified binder, which did not pass at −12°C when changing from PAV to 2PAV. Because of this, ΔT_c values for ReOB are at a different magnitude compared to the other modified binders.

The repeatability of ΔT_c presents a concern. The precision of ΔT_c is 0.8°C for a single technician and 1.8°C for multiple laboratories (Asphalt Institute, 2019). A difference of 1.8°C in ΔT_c is within the test's precision range but could represent a significant difference in pavement performance. ΔT_c repeatability was observed to be less achievable at higher than the PAV aging condition. The coefficient of variation (CoV) for two beams tested with the same equipment was observed to be over the AASHTO interlaboratory values. The CoV for the m-value was over the recommended 1% for approximately one-quarter of the tests but rarely over 1.5%. (The CoV was over 1.5% for less than one-sixth of the tests.) The CoV for the stiffness was over the recommended 2% for approximately one-third of the tests, but rarely over 6% (See Appendix B for the data).

Intermediate Temperature Tests and Parameters

Glover-Rowe Parameters

A warning threshold maximum of 180 kPa (damage onset) and a limit maximum of 600 kPa (significant cracking) are recommended for the GRP (Rowe, 2016; Rowe & Sharrock, 2016). The results are reported with S1 (base binder) in Figure 11. However, because GRP is a stiffness-dependent parameter and parameters were obtained from tests at the same temperature, the S1 binder is not comparable to modified binders with a softer grade. The thresholds should be different for binders with different stiffness and PG.

The damage onset threshold for PG 58-28 was reached by most modified binders at the 2PAV aging condition except the C- and G-modified binders as well as the S8 unmodified binder. C- and G-modified binders as well as S5 did not reach the significant cracking threshold at the most intense aging condition (3PAV).

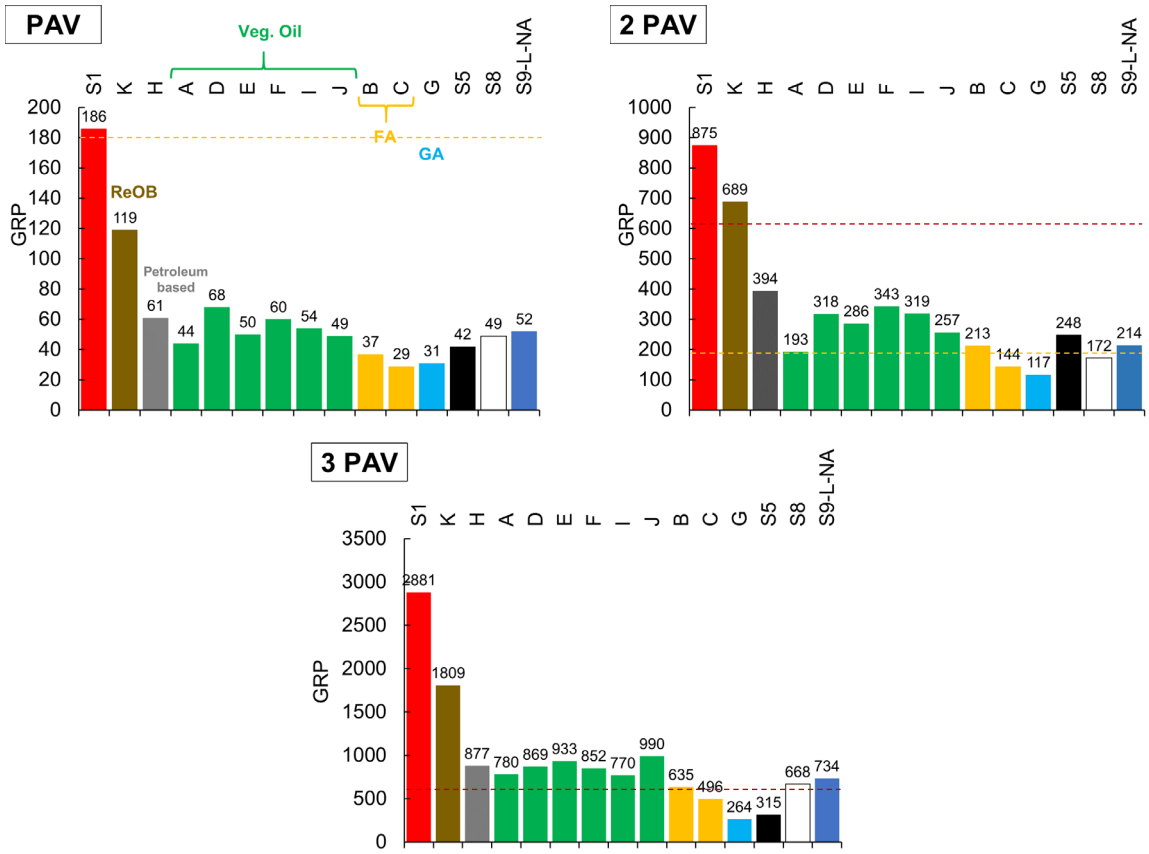

Figure 11. Bar plots. GRP tested binders at various aging conditions.

GRP_f results are presented in Figure 12. Christensen & Soliman (2020) indicate that a limit of 5,000 kPa at the PAV aging condition and an 8,000 kPa limit for the 2PAV aging condition are proposed in the final report for NCHRP Project 9-59. All tested binders are under the threshold limit at the PAV aging condition. At the 2PAV aging condition, the base binder and the binders modified with K, H, D, F, and I exceeded the threshold limit (Figure 12). Binders modified with J and L are borderline cases.

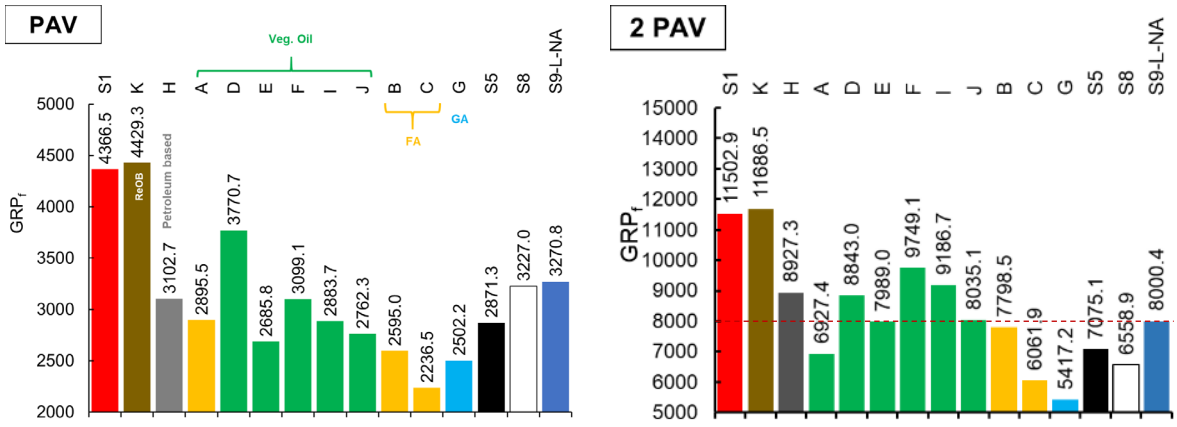

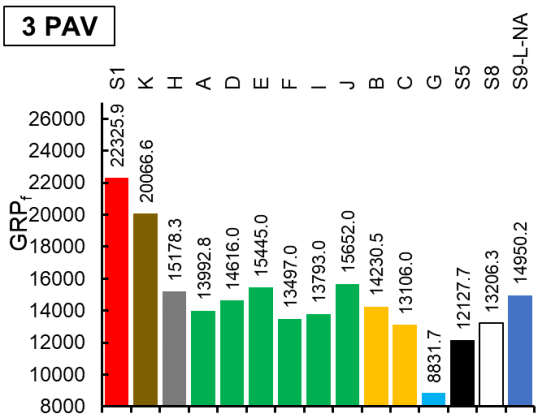

Figure 12. Bar plots. GRP_f for all binders at all tested aging conditions.

Crossover Parameters

The crossover parameters presented include the crossover modulus ($|G^*|_c$ in Figure 13), the crossover frequency (w_c in Figure 14), the VETT (in Figure 15), and the R-value (Figure 16). A first group of modified binders were tested at the RTFO aging condition. Testing at this condition was not continued because it was unnecessary. Clearer trends appeared beyond the PAV aging condition. Crossover parameters are indicative of the predominant viscoelastic behavior by identifying the transition from viscous to more elastic response. For example, when a recently placed HMA pavement layer with a binder like S1-E-3.1 (RTFO aging condition) is subjected to a load at a frequency greater than 16 Hz (at 15°C), the binder is expected to have a predominantly elastic response.

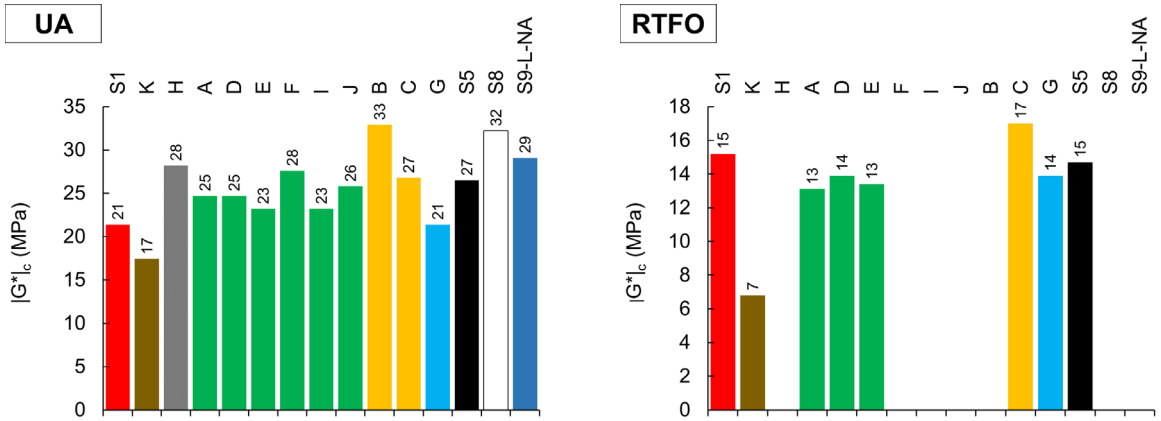

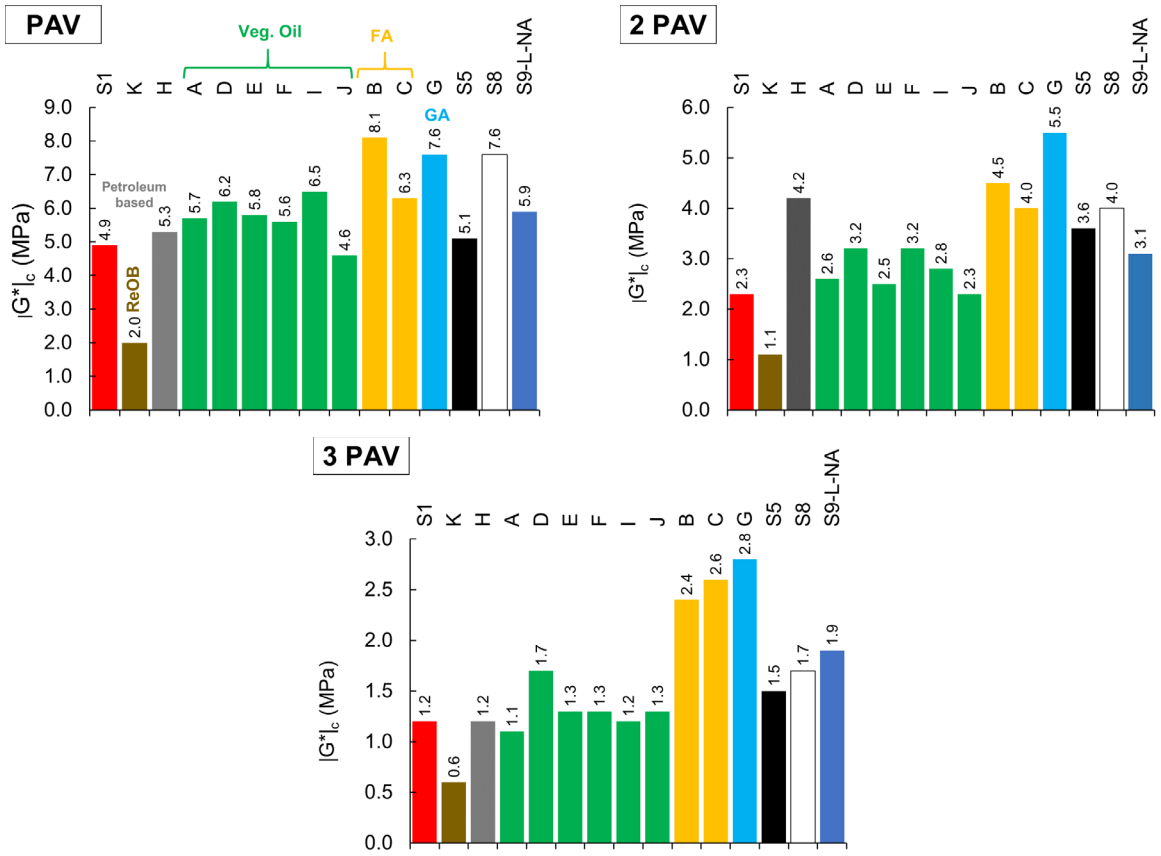

Figure 13. Bar plots. $|G^*|_c$ for all binders at all tested aging conditions.

A distinct grouping of modifiers can be observed based on their binder's crossover modulus results at any aging condition:

- Unmodified benchmark S5 and control S1, the vegetable oil modifiers, and the petroleum-based modifiers (2.3 to 4.2 MPa at 2PAV). The petroleum-based modifier appears to break the trend at the 2PAV aging condition.
- Fatty acids and glycol amine (4.0–5.5 MPa at 2PAV).
- ReOB (1.1 MPa at 2PAV).
- S8 and S9-L-NA appear to have a similar $|G^*_c|$.

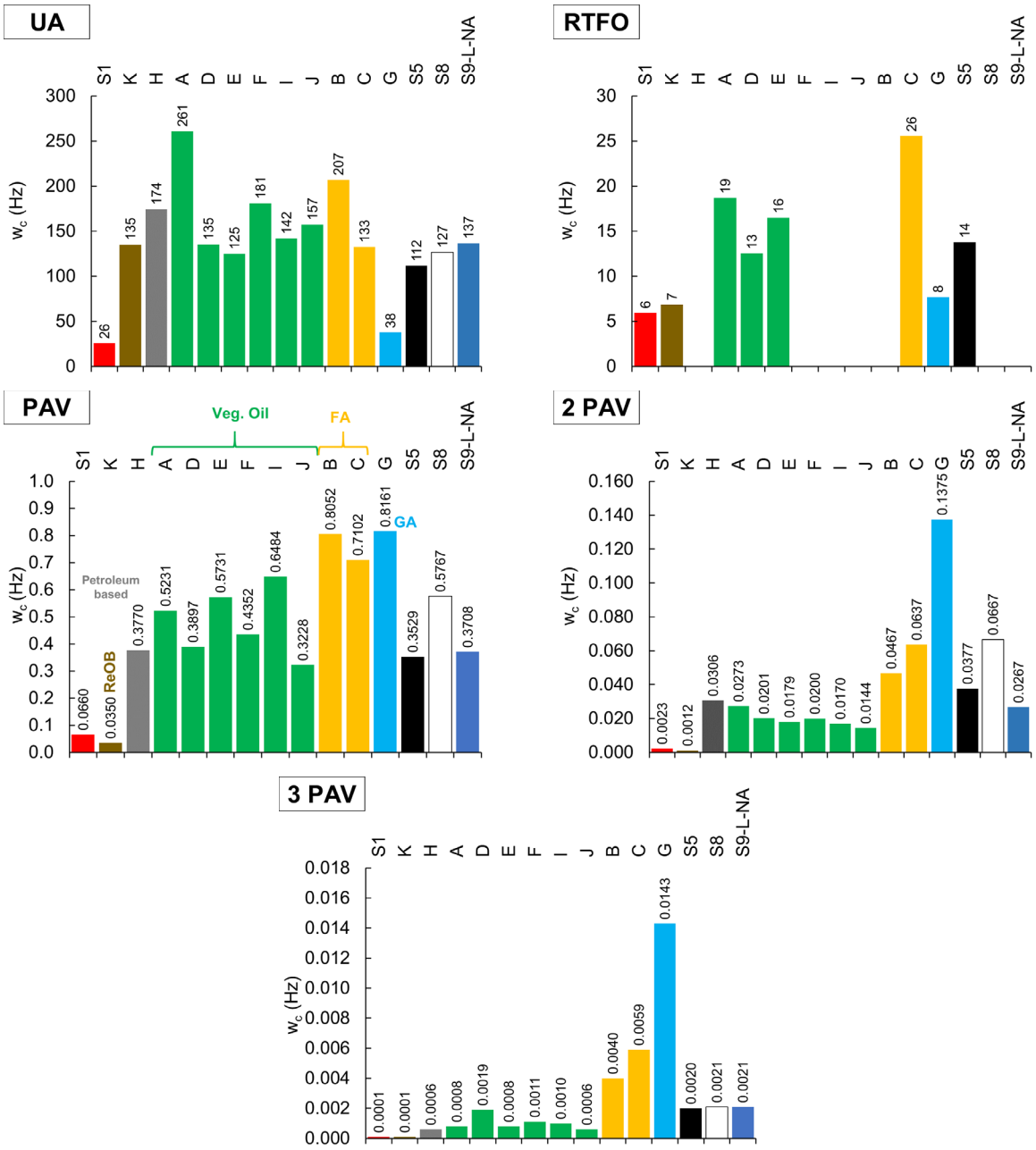

Figure 14. Bar plots. w_c for tested binders at various aging conditions.

VETT varied between 18.4°C and 21.1°C for vegetable oil modifiers after PAV while fatty acid– and glycol amine–based modifiers exhibited smaller VETT (17.5°C to 18.0°C). In contrast, VETT for the modifier K is consistently and significantly higher at all PAV conditions. Despite the increase in VETT values with additional PAVs, the trend is preserved. As the binder ages, it loses viscous characteristics and becomes more brittle (as shown with a predominant elastic behavior). If the pavement is in a climatic region where the average temperature is greater than the respective VETT, then the mechanical response of the asphalt binder would be predominantly viscous. For example, the modifier E has a VETT of 6.4°C, 18.9°C, 31.6°C, and 42.0°C after RTFO, PAV, 2PAV, and 3PAV,

respectively. Because the intermediate temperature in Illinois is around 19°C, modifier E will have a predominantly elastic response after it surpasses the PAV aging condition.

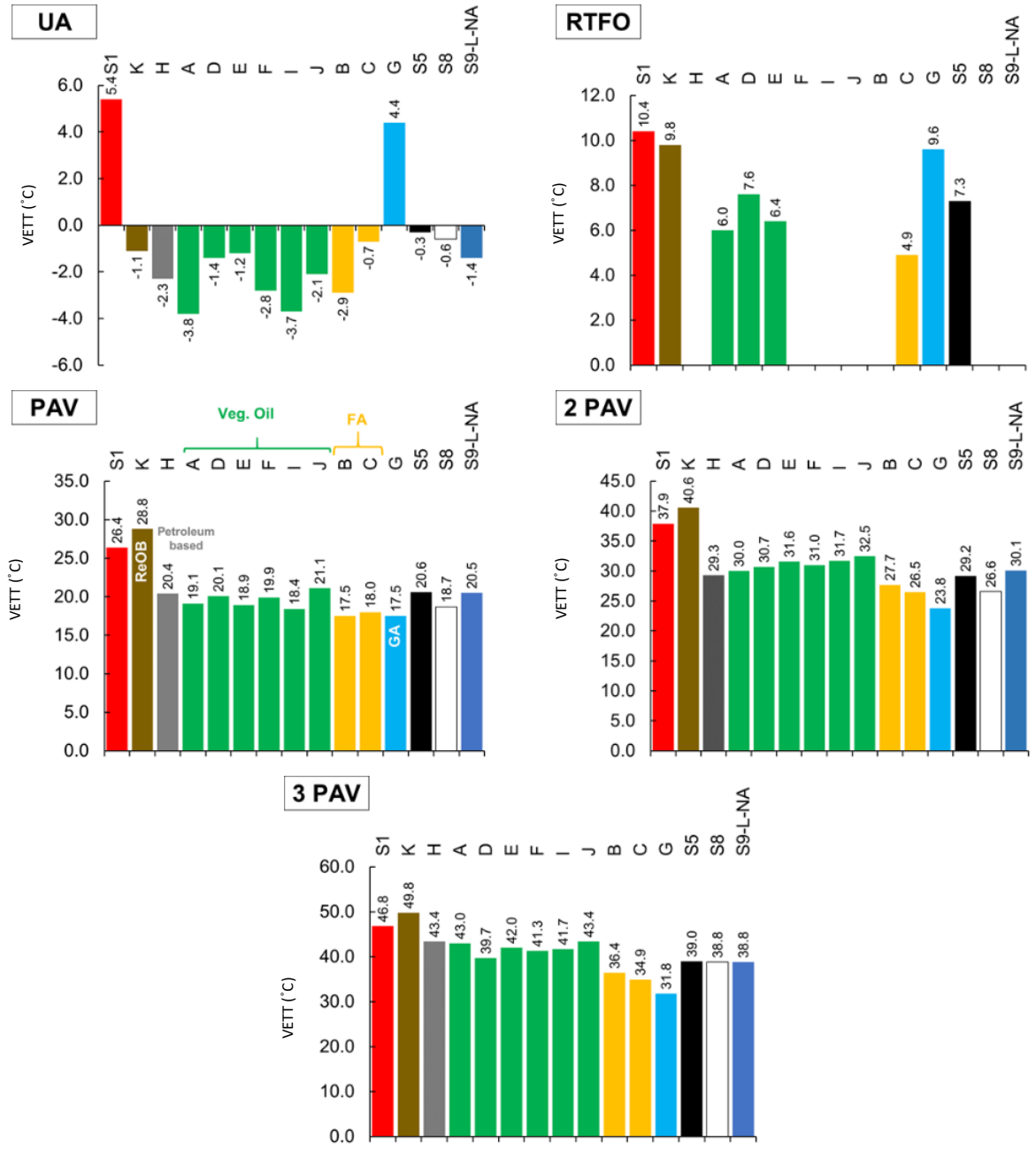

Figure 15. Bar plots. VETT for tested binders at various aging conditions.

NCHRP 9-59 recommends an acceptable fatigue performance if the R-value ranges from 1.5–2.5 for the PAV-aged condition and 2.5–3.2 for the 2PAV-aged condition (Christensen & Tran, 2019). S1-K-10 under the PAV-aged condition is the only binder that is out of range, while in the 2PAV-aged condition, all binders in this study are within the suggested NCHRP recommendations for R-value.

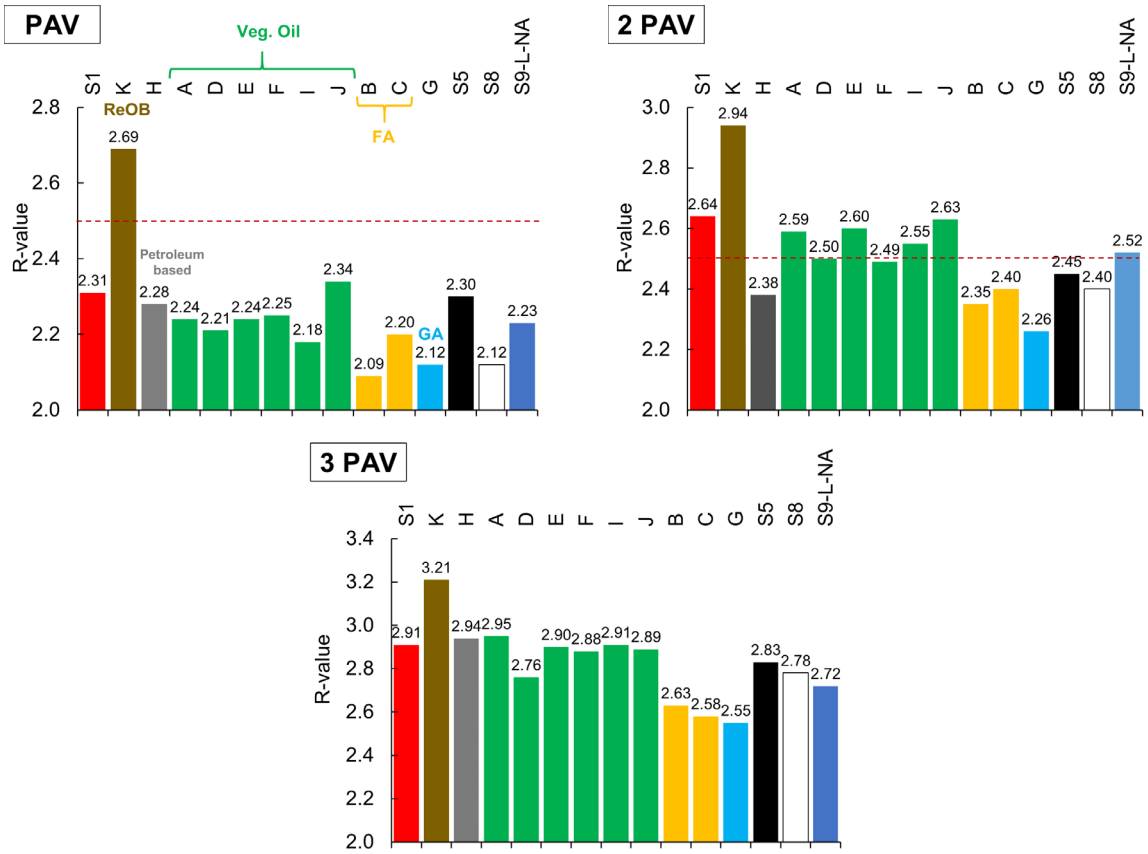

Figure 16. Bar plots. R-value for all binders at all tested aging conditions.

Black Angle: Phase Angle at G of 8,967 MPa*

Black angle results are presented in Figure 17. A distinct group of modifiers can also be observed based on their binder's phase angle results. Vegetable oil and petroleum-based modifiers (41.0° to 41.9°) are distinguished from fatty acid (43.2° to 44.8°), glycol amine (44.5°), and ReOB (36.8°) after PAV aging. The trends are preserved after extended PAV aging, and phase angles decreased with aging. If a minimum threshold of 40° was chosen for the PAV condition, only the S1-K-10 binder would be expected to have a more elastic than typical behavior at in-service conditions.

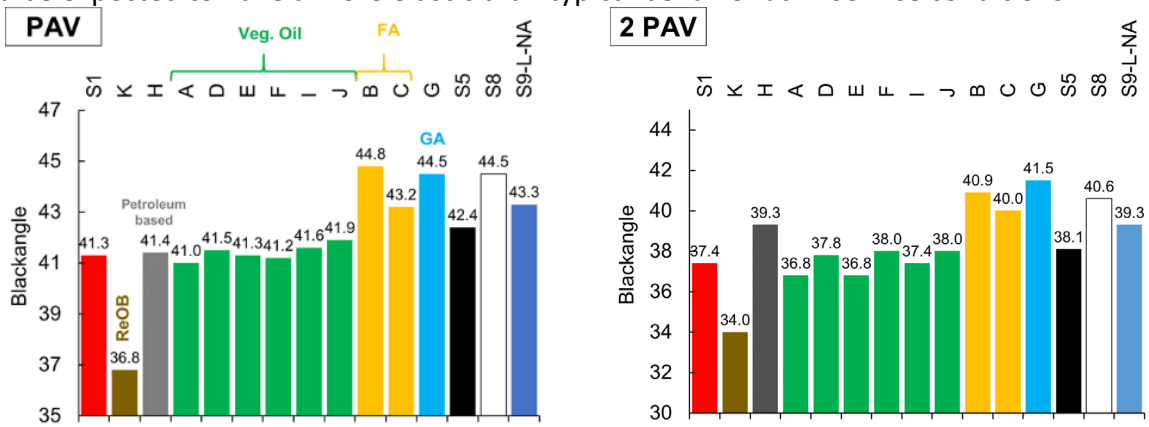

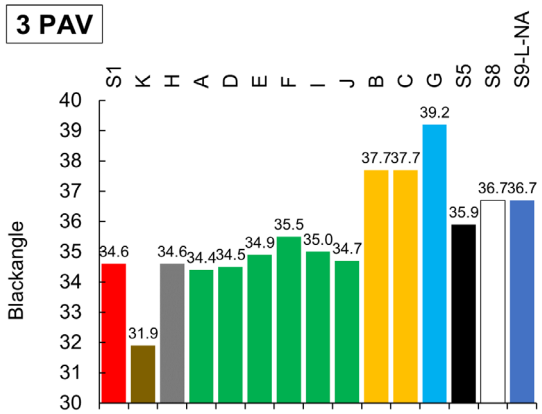

Figure 17. Bar plots. Black angle for all binders at all tested aging conditions.

Relationships between Small-strain Testing Parameters

The correlation between different small-strain parameters is sought. Table 4 presents the covariance between the binders' parameters at PAV, 2PAV, and 3PAV aging conditions. Some are correlated, and there are aging trends evident in (a) that disappear when only one aging condition is considered, such as in (b). The key takeaways of this section can be identified in these correlation matrices; any correlation under 0.85 was considered inconclusive, and the rest are described ahead. Correlation does not imply causation, but in some cases elaborated below, these correlations rise from conceptual relationships.

Table 4. Correlation Matrix for Small-Strain Parameters at (a) PAV, 2PAV, and 3PAV Aging Conditions and (b) at 2PAV Aging Condition Only

(a)	w_c	$\|G^*_c\|$	VETT	R-value	Black angle	GRP_f	GRP	ΔT_c
w_c	**1**	**0.88**	*−0.80*	*−0.76*	*0.80*	*−0.72*	*−0.49*	*0.65*
$\|G^*_c\|$	**0.88**	**1**	**−0.94**	**−0.96**	**0.96**	*−0.86*	*−0.68*	*0.84*
VETT	*−0.80*	**−0.94**	**1**	**0.97**	**−0.95**	**0.97**	*0.82*	**−0.91**
R-value	*−0.76*	**−0.96**	**0.97**	**1**	**−0.97**	**0.9**	*0.77*	**−0.92**
Black angle	*0.80*	**0.96**	**−0.95**	**−0.97**	**1**	**−0.88**	*−0.73*	**0.92**
GRP_f	*−0.72*	**−0.86**	**0.97**	**0.9**	**−0.88**	**1**	**0.89**	**−0.88**
GRP	*−0.49*	−0.68	**0.82**	0.77	−0.73	**0.89**	**1**	*−0.80*
ΔT_c	*0.65*	**0.84**	**−0.91**	**−0.92**	**0.92**	**−0.88**	*−0.80*	**1**
(b)	**w_c**	**$\|G^*_c\|$**	**VETT**	**R-value**	**Black angle**	**GRP_f**	**GRP**	**ΔT_c**
w_c	**1**	**0.85**	*−0.80*	*−0.74*	*0.77*	*−0.77*	*−0.6*	*0.69*
$\|G^*_c\|$	*0.85*	**1**	**−0.90**	**−0.97**	**0.93**	*−0.71*	*−0.62*	*0.80*
VETT	*−0.80*	**−0.9**	**1**	**0.92**	**−0.86**	**0.91**	**0.88**	**−0.87**
R-value	*−0.74*	**−0.97**	**0.92**	**1**	**−0.93**	*0.72*	*0.66*	*−0.84*
Black angle	*0.77*	**0.93**	**−0.86**	**−0.93**	**1**	*−0.70*	*−0.61*	0.91
GRP_f	*−0.77*	*−0.71*	**0.91**	*0.72*	*−0.70*	**1**	**0.91**	−0.81
GRP	*−0.60*	*−0.62*	**0.88**	*0.66*	*−0.61*	**0.91**	**1**	−0.73
ΔT_c	*0.69*	*0.80*	**−0.87**	*−0.84*	**0.91**	*−0.81*	*−0.73*	**1**

The GRP and ΔT_c parameters have been associated with non-vehicular load low-temperature cracking in literature. Figure 18 presents the relationships for the tested binders. As GRP increases and ΔT_c decreases, cracking susceptibility increases. Low-temperature cracking susceptibility is expected to increase with aging. Nevertheless, the presented threshold criteria would classify binders differently: some binders would fail the 180 kPa GRP criterion but pass the −5°C ΔT_c criterion (yellow dotted oval) and some binders would pass the 600 kPa GRP criterion but not the −5°C ΔT_c criterion (red oval).

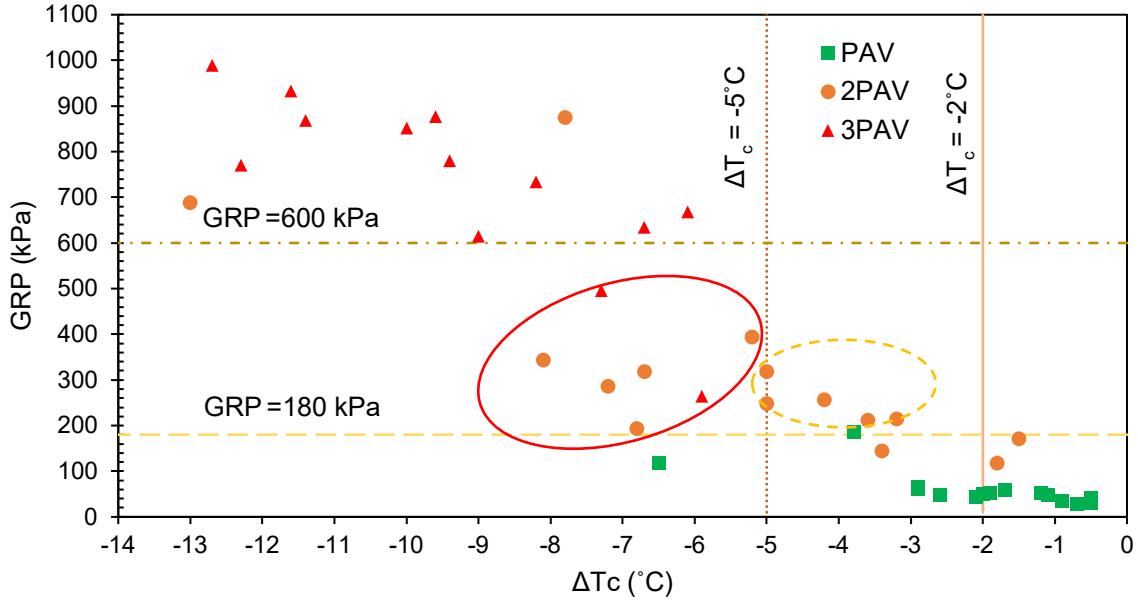

Figure 18. Graph. GRP—ΔT_c relationship.

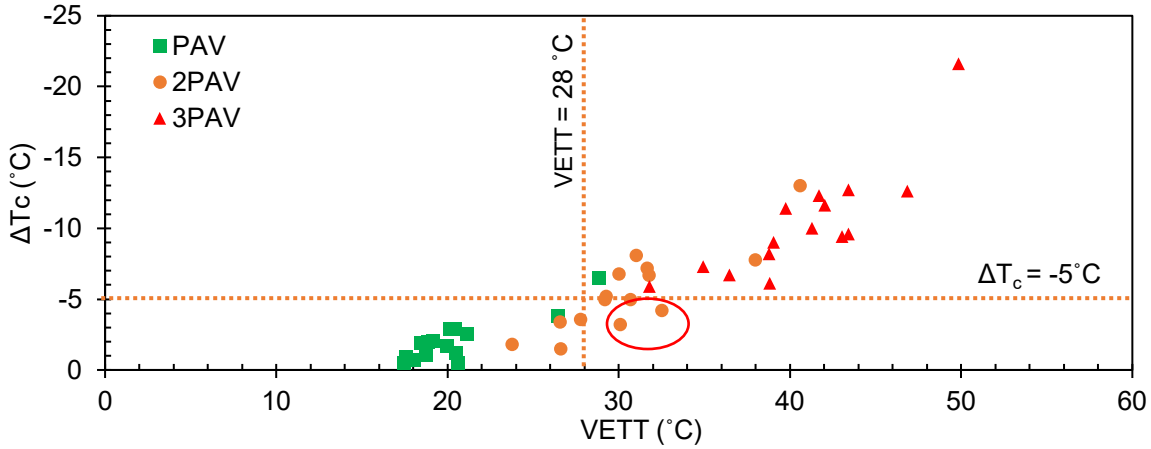

Figure 19. Graph. ΔT_c—VETT relationship.

Figure 19 presents the relationship between ΔT_c and VETT. At 28°C, the maximum threshold for VETT would be a consistent threshold for a −5°C minimum ΔT_c for all but two cases in the oval: S9-L-NA and S1-J-3.0. Hence, VETT or the black angle (see Figure 19) could be potential surrogates for ΔT_c that can

be obtained from selected sweep measurements with the DSR. A threshold value for VETT of 32°C was used to assess adequate rejuvenation on recycled binders by García Cucalón et al. (2018). S9-L-NA, S1, and S1-K-10 would not pass this criterion. The threshold was selected based on its ability to discriminate between binders near the GRP threshold limit of 180 kPa. This is better illustrated by the relationship between low- and intermediate-temperature small-strain parameters, presented in Figure 20.

GRP and GRP_f are closely related under 10 MPa GRP_f, and thus would provide a similar ranking of binders as well as the ability to distinguish between them. Ten MPa GRP_f would separate 2PAV- and 3PAV-aged binders, with the exceptions of S1-K-10 and S1.

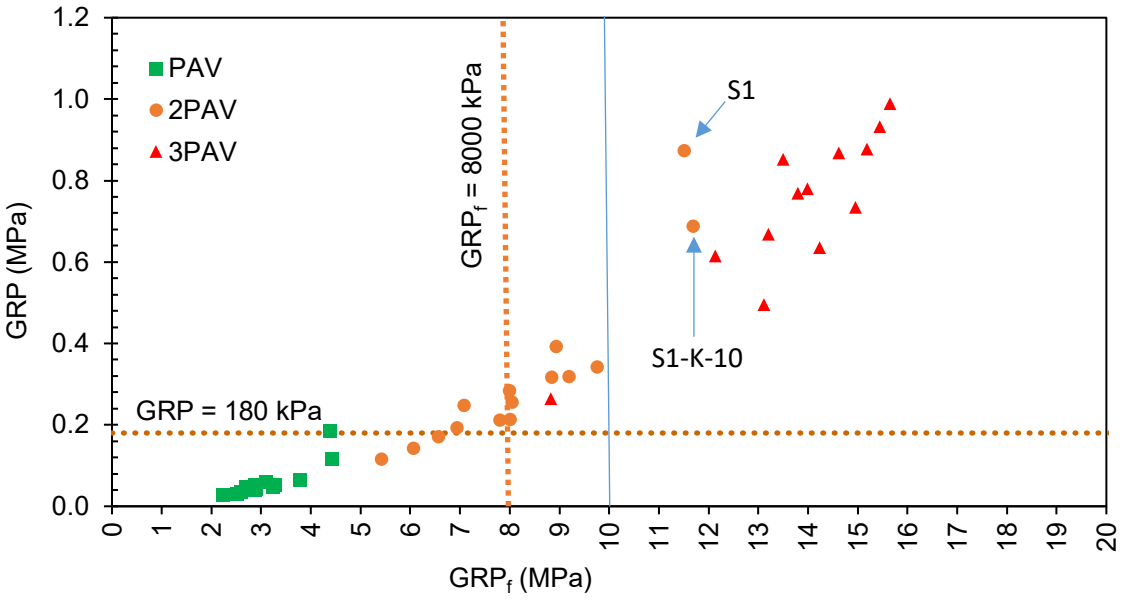

Figure 20. Graph. GRP—GRP_f relationship.

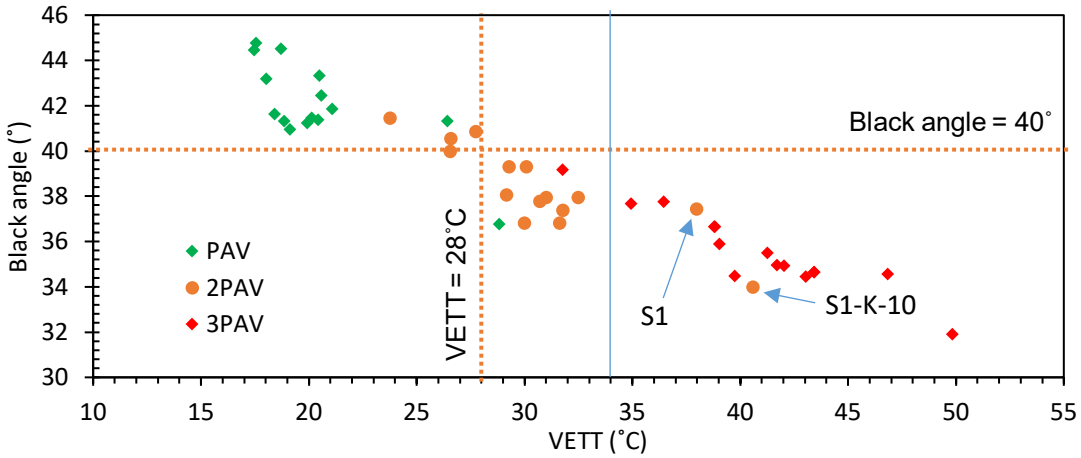

Figure 21. Graph. Black angle—VETT relationship.

The black angle is an indicator of the predominant behavior of a binder's mechanical response at intermediate-temperature loading conditions. VETT and black angle are conceptually and empirically related (Figure 21). A linear regression of the data yields the equation presented in Figure 22:

$$Black\ angle = -0.4233 \times VETT + 51.863;\ R^2 = 0.9522$$

Figure 22. Equation. Equation. Black angle correlation to VETT.

A minimum black angle threshold of 40° would correspond to a VETT of 28°C for all cases. Thresholds should be developed for the VETT based on a statistical analysis of temperature measurements at the location where the binder would be used. A VETT of 34°C separates 2PAV- and 3PAV-aged binders, with the exceptions of S1-K-10 and S1.

In general, there is a good correlation between all small-strain parameters considered. However, there are some inconsistencies in determining passing and failing binders when the threshold values from the literature are used. For example, some binders would fail the GRP criterion but not the ΔT_c criterion, and vice versa. Inconsistencies can be due to the stiffness dependence of each parameter. In contrast, there was a clear trend in all those parameters with increasing aging. Most of the modifiers followed a similar trend, and their behavior can be grouped in three categories, as follows:

- Stiffening at a critical rate: S1-K-10 (ReOB-modified binder).
- Stiffening at a normal rate: S1, S5, S8, S9-L-NA, S1-A-3.5, S1-B-5.0, S1-C-3.1, S1-D-3.1, S1-E-3.1, S1-F-3.1, S1-H-10, S1-I-3.5 and S1-J-3.0 (vegetable oil, fatty acid derivatives, and petroleum-based modified and unmodified binders).
- Stiffening at a lower than normal rate: S1-G-6.5 (glycol amine–modified binder).

LARGE-STRAIN TESTING

During the pavement's service life, this thin asphalt binder layer is subjected to significant stress concentration and strain, ranging, on average, between 7.8 and 510 times the bulk strain of the AC mixture (Kose et al., 2000). It is critical to characterize the binders at large strains to represent loading conditions in the field (Bahia et al., 1999). The linear amplitude sweep (LAS) test characterizes asphalt binders' damage tolerance to fatigue loading (Hintz et al., 2011a). The LAS test was performed in accordance with AASHTO TP101. Table 5 presents a summary of the results. Figure 23 presents the obtained model for the binders studied in this chapter.

Table 5. Summary of LAS Parameters Required on AASHTO TP-101

Sample	Aging condition	C_0	C_1	C_2	Fitting summed error	α	$\|G^*\|\sin(\delta)_{initial}$	D_f	k	A	B
S1	3PAV	1	0.086	0.409	0.374	2.949	13.13	31	2.743	2.84E+07	-5.898
S1	2PAV	1	0.097	0.39	0.298	2.504	12.079	27	2.527	3.26E+06	-5.008
S1	PAV	1	0.09	0.399	0.147	1.978	9.326	30	2.189	5.87E+05	-3.956
S1-A-3.5	3PAV	1	0.089	0.411	0.358	2.949	13.154	28	2.737	2.07E+07	-5.899
S1-A-3.5	2PAV	1	0.092	0.399	0.255	2.525	12.448	28	2.516	4.12E+06	-5.049
S1-A-3.5	PAV	1	0.19	0.286	0.138	2.06	12.83	8	2.472	6.13E+05	-4.056
S1-B-5.0	3PAV	1	0.092	0.401	0.364	2.686	16.635	28	2.608	7.06E+06	-5.372
S1-B-5.0	2PAV	1	0.091	0.407	0.276	2.29	15.168	27	2.358	1.40E+06	-4.58
S1-B-5.0	PAV	1	0.111	0.378	0.34	1.841	15.373	21	2.154	3.12E+05	-3.674
S1-C-3.1	3PAV	1	0.093	0.399	0.328	2.862	15.031	28	2.721	1.43E+07	-5.725
S1-C-3.1	2PAV	1	0.091	0.406	0.207	2.277	12.395	28	2.353	1.41E+06	-4.554
S1-C-3.1	PAV	1	0.08	0.429	0.117	1.854	10.012	31	2.059	3.50E+05	-3.708
S1-D-3.1	3PAV	1	0.084	0.42	0.283	2.928	13.609	30	2.698	2.27E+07	-5.856
S1-D-3.1	2PAV	1	0.092	0.399	0.255	2.525	12.448	28	2.516	4.12E+06	-5.049
S1-D-3.1	PAV	1	0.087	0.414	0.148	2.028	10.169	29	2.188	6.13E+05	-4.056
S1-E-3.1	3PAV	1	0.091	0.401	0.351	2.95	14.814	29	2.769	2.37E+07	-5.901
S1-E-3.1	2PAV	1	0.094	0.395	0.239	2.474	11.955	28	2.497	3.34E+06	-4.949
S1-E-3.1	PAV	1	0.081	0.423	0.131	1.989	9.02	32	2.148	6.65E+05	-3.978
S1-F-3.1	3PAV	1	0.091	0.401	0.284	2.812	13.511	29	2.685	1.39E+07	-5.624
S1-F-3.1	2PAV	1	0.094	0.396	0.269	2.469	13.469	28	2.492	3.15E+06	-4.938
S1-F-3.1	PAV	1	0.084	0.415	0.141	2.022	9.22	31	2.183	7.36E+05	-4.044
S1-G-6.5	3PAV	1	0.095	0.4	0.242	2.457	15.506	26	2.474	2.32E+06	-4.915
S1-G-6.5	2PAV	1	0.095	0.4	0.179	2.145	12.503	26	2.288	7.40E+05	-4.29
S1-G-6.5	PAV	1	0.082	0.427	0.134	1.846	11.048	30	2.058	3.11E+05	-3.693
S1-H-10	3PAV	1	0.087	0.416	0.453	2.884	13.445	29	2.684	1.59E+07	-5.769
S1-H-10	2PAV	1	0.102	0.379	0.285	2.493	11.879	26	2.547	2.89E+06	-4.985
S1-H-10	PAV	1	0.088	0.406	0.132	2.01	9.915	30	2.194	6.68E+05	-4.02

Sample	Aging condition	C_0	C_1	C_2	Fitting summed error	α	$\|G^*\|\sin(\delta)_{initial}$	D_f	k	A	B
S1-I-3.5	3PAV	1	0.095	0.398	0.228	2.88	14.873	26	2.733	1.26E+07	-5.76
S1-I-3.5	2PAV	1	0.1	0.383	0.281	2.485	12.759	26	2.534	3.06E+06	-4.969
S1-I-3.5	PAV	1	0.084	0.414	0.134	1.978	9.44	31	2.159	6.35E+05	-3.955
S1-J-3.0	3PAV	1	0.093	0.395	0.334	2.908	14.958	28	2.759	1.98E+07	-5.816
S1-J-3.0	2PAV	1	0.097	0.391	0.218	2.411	12.476	27	2.467	2.25E+06	-4.821
S1-J-3.0	PAV	1	0.085	0.412	0.11	1.964	9.128	31	2.155	5.92E+05	-3.929
S1-K-10	3PAV	1	0.088	0.415	0.454	3.371	10.385	28	2.974	1.04E+08	-6.743
S1-K-10	2PAV	1	0.099	0.395	0.395	2.871	9.764	24	2.737	9.10E+06	-5.743
S1-K-10	PAV	1	0.105	0.38	0.356	2.346	8.228	23	2.454	1.21E+06	-4.693
S5	3PAV	1	0.092	0.402	0.313	2.752	14.217	28	2.646	9.62E+06	-5.504
S5	2PAV	1	0.101	0.386	0.245	2.453	13520	25	2.506	2.28E+06	-4.907
S5	PAV	1	0.089	0.411	0.179	1.965	11.321	28	2.157	4.29E+05	-3.93
S8	3PAV	1	0.1	0.386	0.324	2.693	15.175	25	2.654	5.89E+06	-5.386
S8	2PAV	1	0.1	0.387	0.251	2.248	14.227	25	2.377	1.04E+06	-4.495
S8	PAV	1	0.087	0.415	0.146	1.902	10.549	28	2.113	3.51E+05	-3.805
S9-L-NA	3PAV	1	0.091	0.405	0.325	2.819	16.33	27	2.676	1.13E+07	-5.637
S9-L-NA	2PAV	1	0.098	0.397	0.368	2.311	12.046	24	2.393	1.11E+06	-4.622
S9-L-NA	PAV	1	0.081	0.429	0.145	1.936	10.759	31	2.106	4.72E+05	-3.873

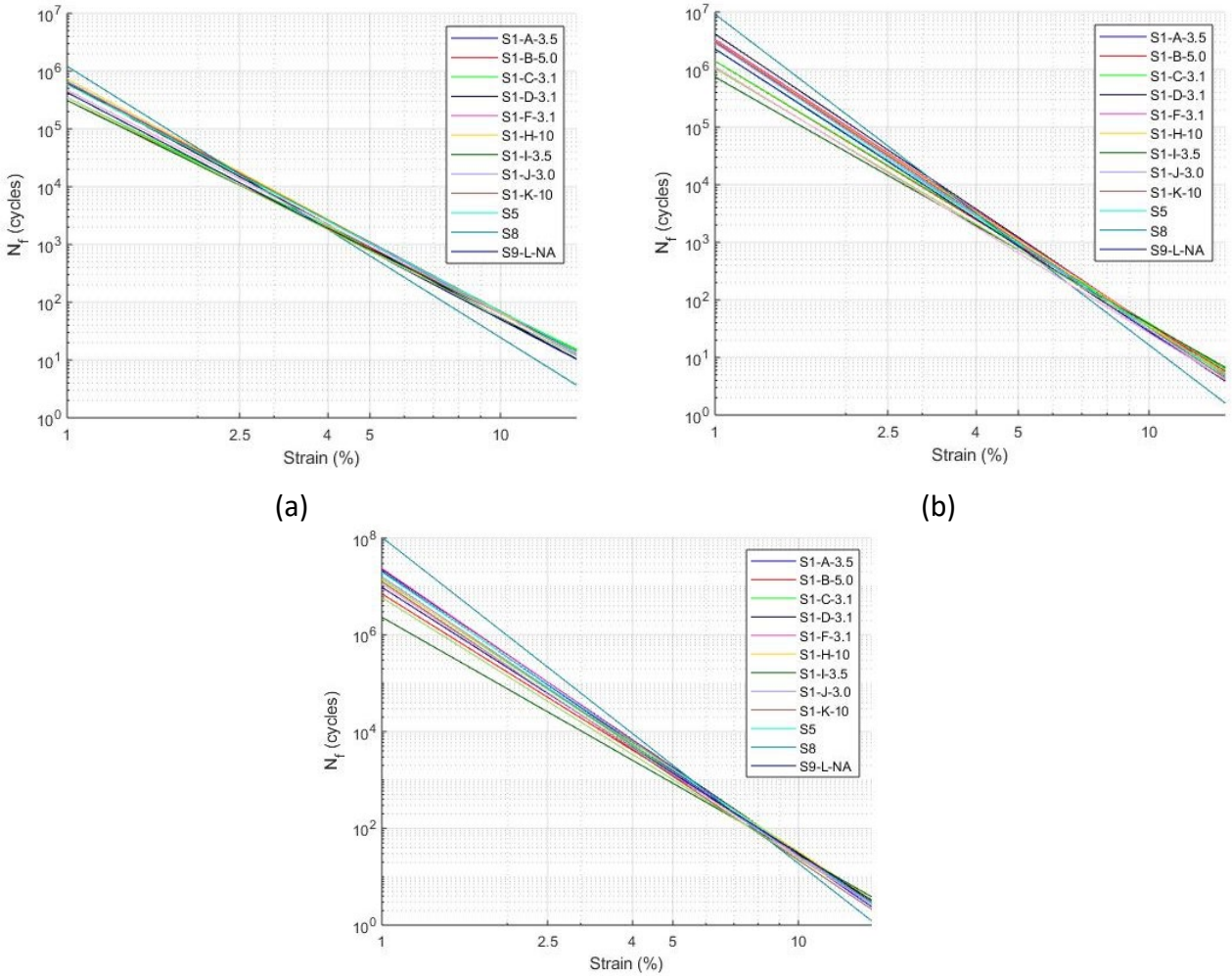

Figure 23. Graphs. LAS results in accordance with AASHTO TP-101 at (a) PAV, (b) 2PAV, and (c) 3PAV aging conditions.

To evaluate the binders, a strain level such as 2.5%, 4%, or 5% should be selected. Figure 23 shows how such an evaluation would be dependent on the strain selected and therefore inconclusive for asphalt-binder ranking purposes. Binder comparison would depend on an arbitrarily selected strain. Furthermore, the analysis chooses 35% reduction in stiffness as a failure definition to define parameters required for the model's predictions. This is also debatable because it does not correspond to any marked change in the sample's mechanical response.

LARGE-STRAIN TESTING PARAMETER: $\Delta|G^*|_{PEAK\ T}$

In addition to the limitations mentioned above, García Mainieri et al. (2021) identified that there is a material ejection problem during the LAS test when the binder's phase angles are low enough or the material is stiff enough (Figure 24-A and Figure 24-B). When this happens, normal stresses are sustained or increase after dilation (Figure 24-C) and the linear viscoelastic constitutive relationship

used to calculate modulus is no longer valid. Additionally, binders at the LAS testing range could develop significant amounts of viscous dissipated energy prior to any indication of cracking or failure. Therefore, any approach based on dissipated energy or pseudo-strain energy may not directly describe fatigue resistance.

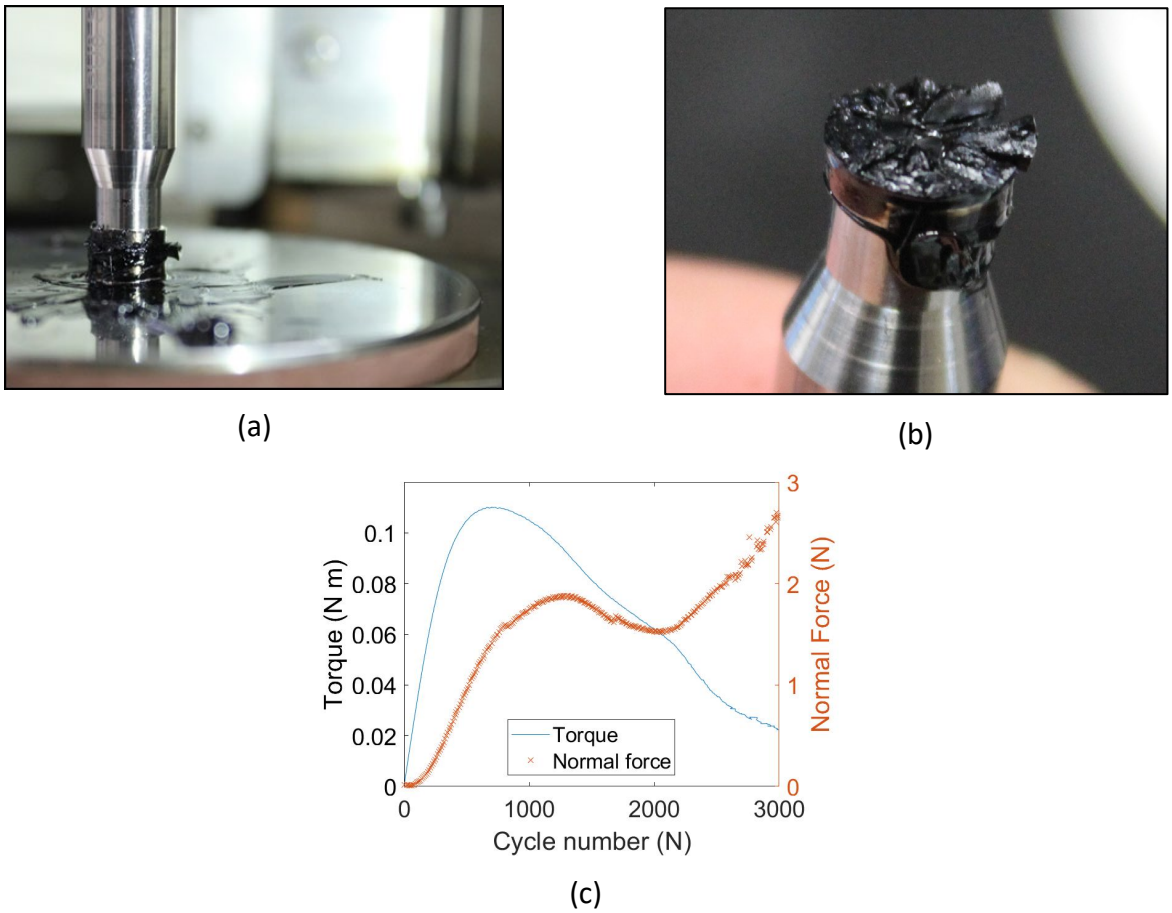

(c)

Figure 24. Photos and Graph. (a) Material ejected during LAS, (b) wedges on asphalt binder attached to top spindle after the LAS test, and (c) normal stresses increasing after dilation during the LAS test.

For the data presented in Figure 24, material ejection happened for the S1-K-10 sample at the PAV aging condition and all samples at the 2PAV and 3PAV aging conditions. Consequently, an alternative method was developed in this study to provide a more practical and reliable parameter while recognizing the inherent assumptions and drawbacks of the LAS test: the reduction in $|G^*|$ measured from the start of the test until the peak shear-stress condition ($\Delta|G^*|_{peak\,\tau}$). The method's development was discussed in detail by García Mainieri et al. (2021). Details of the procedure to obtain $\Delta|G^*|_{peak\,\tau}$ are presented in Appendix C.

The $\Delta|G^*|_{peak\,\tau}$ values obtained for each binder from LAS test measurements are presented in Table 6. Applying a minimum $\Delta|G^*|_{peak\,\tau}$ requirement of 56% at the 2PAV aging condition would differentiate S1-K-10, S1-B-5.0, S9-L-NA, and S1 from the rest of the binders.

Table 6. $\Delta|G^*|_{peak\,\tau}$ (%) for Tested Binders at Various Aging Conditions (García Mainieri et al., 2021)

Binder	Aging condition				
	UA	RTFO	PAV	2PAV	3PAV
S1-K-10			56.7	53.1	50.7
S1-B-5.0			60.1	53.6	50.9
S9-L-NA			60.4	54.8	52.2
S1			62.0	55.6	54.8
S1-C-3.1	40.1	49.8	61.8	56.5	54.2
S1-F-3.1			61.6	56.5	54.0
S1-H-10			61.5	56.6	53.2
S1-J-3.0			61.4	56.6	54.3
S1-D-3.1	40.3	51.5	59.0	57.2	52.6
S5			60.4	57.3	53.3
S1-E-3.1			61.0	57.6	52.4
S1-G-6.5			60.6	58.0	53.6
S1-I-3.5			61.5	58.0	53.4
S1-A-3.5	31.3	52.3	61.6	58.4	53.5
S8			61.5	59.0	54.0

Figure 25 presents $\Delta|G^*|_{peak\,\tau}$ for the tested binders at various aging conditions. The coefficient of variation for this parameter was generally under 3%. At the PAV aging condition, S1-D-3.1, S1-B-5.0, and especially S1-K-10 underperformed, while the rest of the modified asphalt binders performed similarly to the unmodified asphalt binders (S5 and S8). As expected, damage tolerance decreased with extended aging.

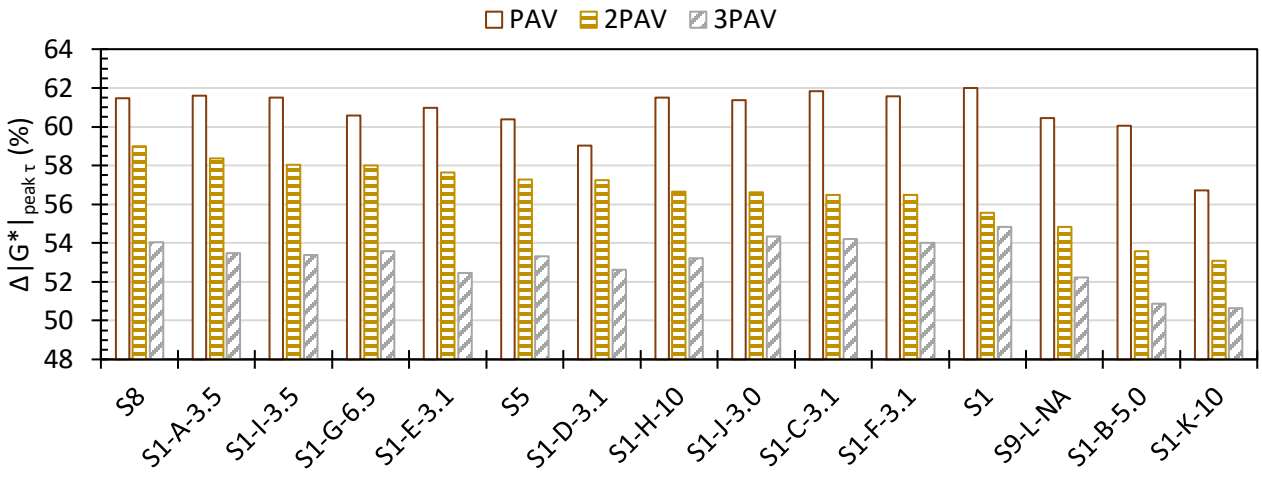

Figure 25. Bar plot. $\Delta|G^*|_{peak\,\tau}$ for all tested binders at PAV, 2PAV, and 3PAV aging conditions.

García Mainieri et al. (2021)

Figure 26 presents a curve in the ($\Delta|G^*|_{peak\,\tau}$, $N_{f,\,peak\,\tau}$) space, connecting all aged binders tested. The figure presents binders tested at the five aging conditions to monitor aging progression. A softer binder (such as an unaged binder) would have a lower tolerance to integrity loss under LAS fatigue loading than a stiffer binder (such as an RTFO-aged binder) (García Mainieri et al., 2021). The test was conducted using strain control, and observations are consistent with typical strain control cyclic experiments. Asphalt binder forms a more connected microstructure and gains stiffness and strength during initial aging. As illustrated in the first part of the curve, $N_{f,\,peak\,\tau}$ and damage tolerance increase. Once an optimum structure is reached, binders become brittle, which results in a decrease in damage tolerance and $N_{f,\,peak\,\tau}$. In other words, damage initiates and propagates faster, as shown in the second distinctive part of the curve. The distinction between the two phases, illustrating an optimal blend of stiffness and damage tolerance, is closely preceding PAV aging condition.

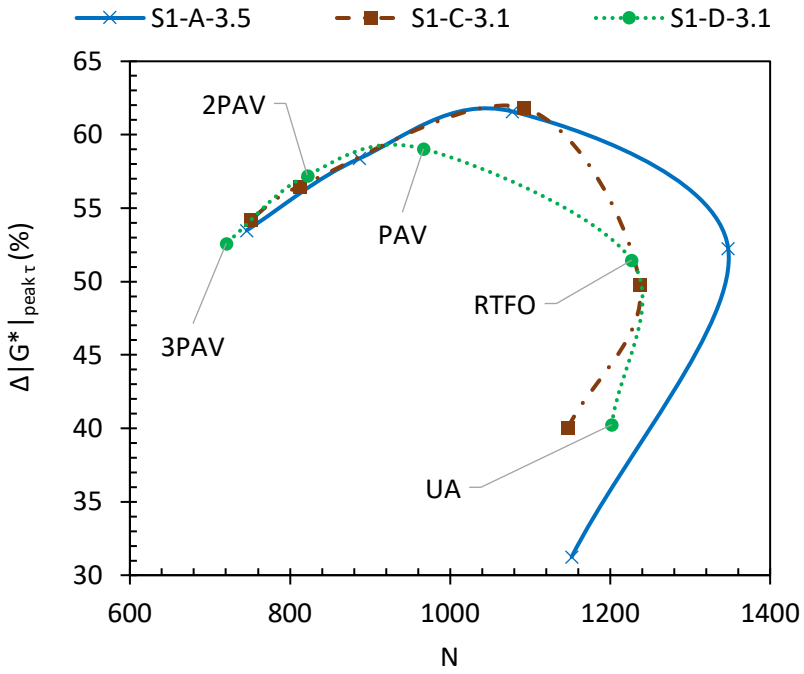

Figure 26. Graph. Curves connecting results at all aging conditions for selected binders.

García Mainieri et al. (2021)

RELATIONSHIP BETWEEN SMALL- AND LARGE-STRAIN TESTING PARAMETERS

The correlation between different small-strain parameters and the large-strain parameter $\Delta|G^*|_{peak\,\tau}$ is presented in Table 7. The covariance between the binders' parameters at PAV, 2PAV, and 3PAV aging conditions is reported. There are aging trends evident in (a) that disappear when only one aging condition is considered, such as in (b). The binders' large-strain behavior is shown to be different than their small-strain behavior. A comparison of ranking based on large- and small strain behavior will be discussed next.

Table 7. Correlation between Large-Strain and Small-Strain Parameters at (a) PAV, 2PAV, and 3PAV Aging Conditions and (b) at 2PAV Aging Condition Only

(a)	w_c	$\lvert G^*_c \rvert$	VETT	R-value	Black angle	GRP_f	GRP	ΔT_c	$\Delta\lvert G^* \rvert_{peak\,\tau}$
$\Delta\lvert G^* \rvert_{peak\,\tau}$	0.76	0.84	−0.89	−0.85	0.82	−0.88	−0.64	0.78	1
(b)	w_c	$\lvert G^*_c \rvert$	VETT	R-value	Black angle	GRP_f	GRP	ΔT_c	$\Delta\lvert G^* \rvert_{peak\,\tau}$
$\Delta\lvert G^* \rvert_{peak\,\tau}$	0.35	0.29	−0.51	−0.4	0.22	−0.54	−0.47	0.41	1

Aging trends can relate small-strain testing parameters and the large-strain parameter, $\Delta\lvert G^* \rvert_{peak\,\tau}$. As shown in Figure 27, ΔT_c becomes more negative as binders lose their relaxation properties with aging. Furthermore, $\Delta\lvert G^* \rvert_{peak\,\tau}$ increases as binders stiffen with aging and then, after PAV aging condition, decreases with extended aging. Also, VETT increases with aging along with the elastic and brittle behavior of the binders. However, a higher-resolution analysis is needed to discern between a behavioral relationship and a correlation. At each aging condition, there is no apparent trend between ΔT_c and $\Delta\lvert G^* \rvert_{peak\,\tau}$ or VETT and $\Delta\lvert G^* \rvert_{peak\,\tau}$.

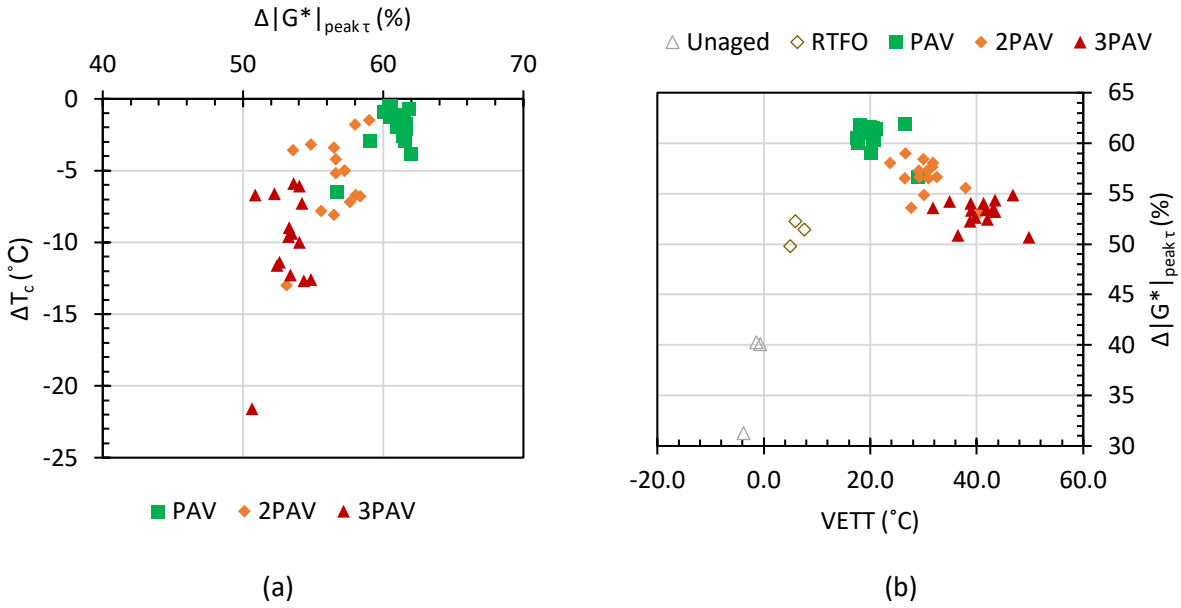

Figure 27. Graph. (a) ΔT_c vs. $\Delta\lvert G^* \rvert_{peak\,\tau}$ and (b) $\Delta\lvert G^* \rvert_{peak\,\tau}$—VETT relationship.

Christensen and Tran (2019) proposed that when the m-value was critical (m = 0.300), the stiffness, S@(m = 0.300), should be examined as an indicator of fatigue tolerance in asphalt concrete (AC) mixes. This is compared to $\Delta\lvert G^* \rvert_{peak\,\tau}$ in Figure 28. Although trends may be observed between S and $\Delta\lvert G^* \rvert_{peak\,\tau}$, no relation is apparent between the parameters for each aging condition.

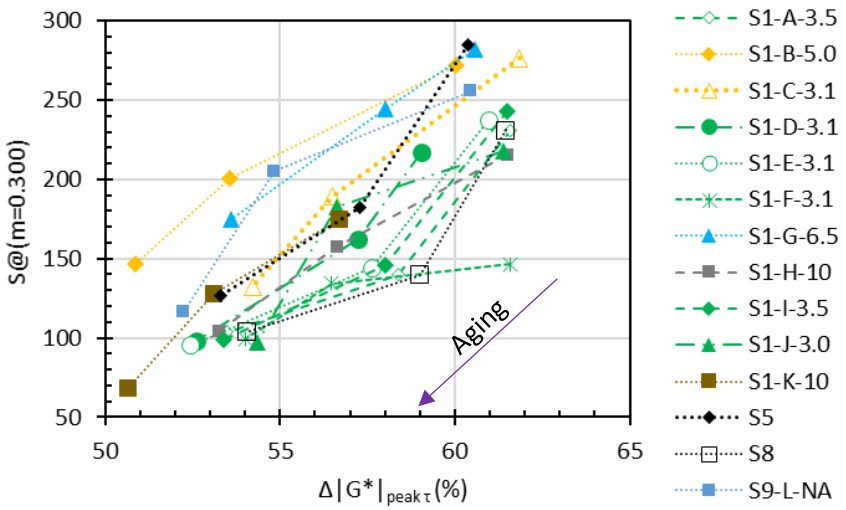

Figure 28. Graph. S@(m = 0.300) - Δ|G*|$_{peak\ \tau}$ relationship.

Binder Ranking

Figure 29-A to Figure 29-C show a comparison of all small-strain parameters and the large-strain parameter for PAV, 2PAV, and 3PAV aging conditions. Binders were ranked from 1 to 14 based on the different small-strain parameters derived from the mean value of each parameter. This ranking is presented on the y-axis. The binders were also ranked based on Δ|G*|$_{peak\ \tau}$ on the x-axis, from left (best) to right. The rankings based on small-strain testing parameters tend to be similar, except for |G*|sin(δ). In general, binders may not be ranked consistently considering both small-strain parameters and Δ|G*|$_{peak\ \tau}$.

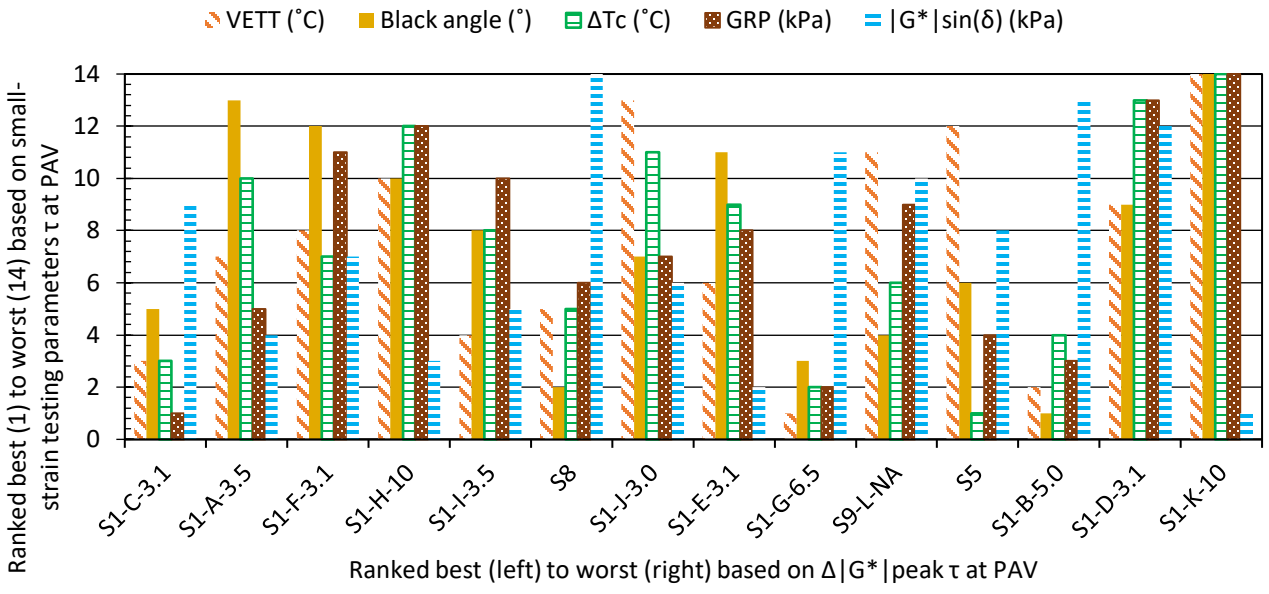

(a)

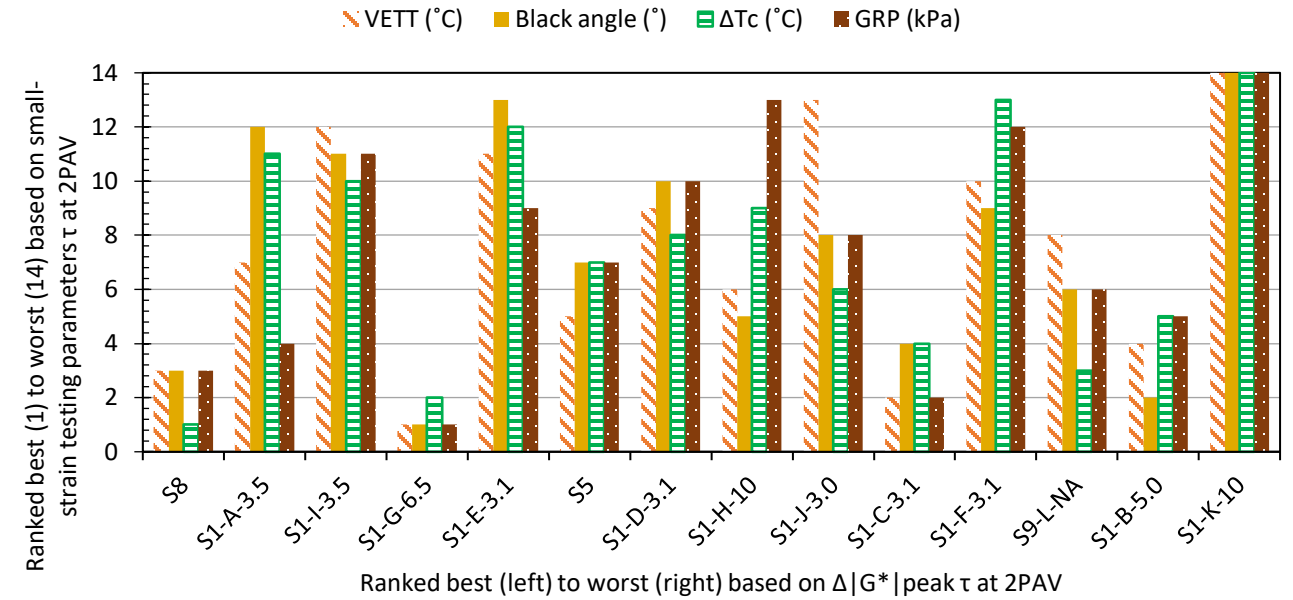

(b)

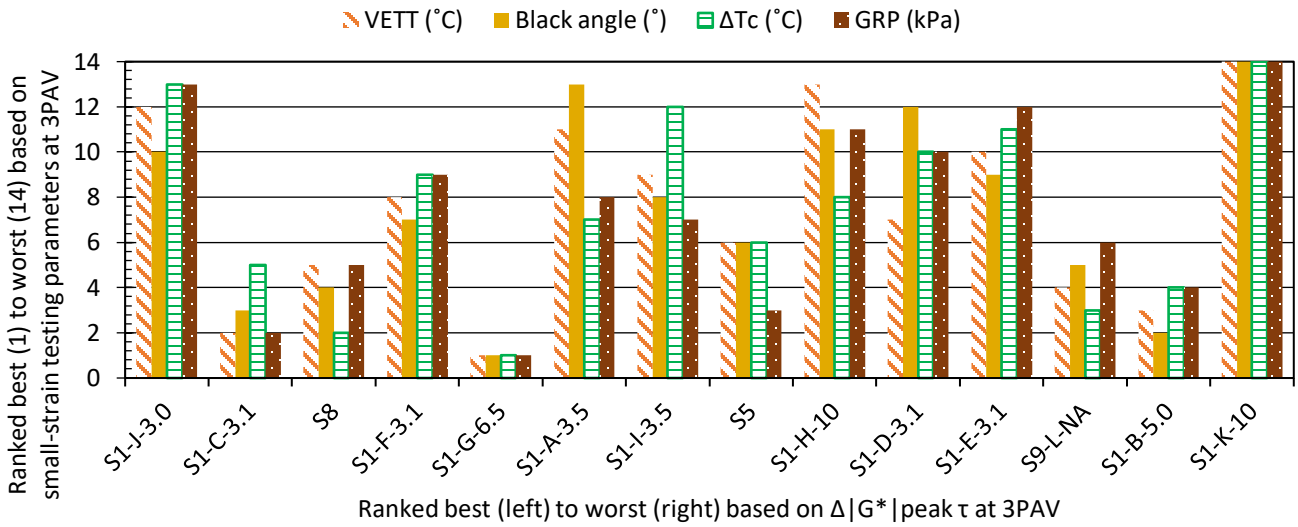

(c)

Figure 29. Bar plots. Ranking comparison between small- and large-strain testing parameters at (a) PAV, (b) 2PAV, and (c) 3PAV aging conditions.

Binder ranking at the PAV aging condition is not consistent among the small-strain parameters. Ranking varied significantly between the parameters. However, there is more uniformity observed after 2PAV and 3PAV between small-strain parameters. The binders ranking among the best four performers based on small-strain testing parameters (S1-G-6.5, S8, S1-C-3.1, and S1-B-5.0) are the same for parameters obtained at the 2PAV aging condition and parameters obtained at the 3PAV

aging condition. However, rankings are not consistent between small- and large-strain parameters at any aging level except for S1-K-10, which is the only binder ranked the worst under all three PAV aging conditions.

Summary

A range of small- and large-strain asphalt binder tests were conducted on the modified and original binders. The relationships, discrimination, and ranking based on small- and large-strain testing parameters for unmodified and modified asphalt binders at long-term aged and extendedly aged conditions were analyzed and compared. Except for two binders (S1-K-10 and S1), it is possible that all binders in this study performed similarly, which led to slight differences in $\Delta|G^*|_{peak\,\tau}$. Greater differences in $\Delta|G^*|_{peak\,\tau}$ might be detected by small-strain testing parameters. This limitation as well as the effect of chemical composition on cracking parameters should be investigated in the future. Below are the findings and conclusions of this chapter.

- Small-strain testing parameters and the large-strain parameter $\Delta|G^*|_{peak\,\tau}$ show different engineering properties of asphalt binders. They do not necessarily correlate well with each other.

- The intermediate-temperature small-strain behavior of binders can be predicted using low-temperature small-strain parameters, and vice versa. Repeatability, adequate stiffness (or modulus), and phase angle limits should be considered if an intermediate-temperature small-strain parameter is selected to identify thresholds for both low- and intermediate-temperature asphalt binder behavior.

- There is a trend of enforcing unique thresholds to parameters used for binder discrimination. This may not be valid for stiffness-dependent parameters, like GRP, $\Delta T_{c,}$ and GRP_f. Unique thresholds may be selected for stiffness-independent parameters, like VETT and black angle. This may be applied to various aging conditions.

- Performance prediction of modified asphalt binder using PAV-, 2PAV-, and 3PAV-aged samples' parameters is different. There is more uniformity in the rankings after a single PAV. To select an optimal aging condition between 2PAV and 3PAV, data from the field cores is needed. The 3PAV aging of binders may reflect aging beyond that experienced during the life expectancy of a pavement. Chapter 5 presents the data from the field cores and corresponding analysis and discussions.

CHAPTER 4: CHEMICAL CHARACTERIZATION OF MODIFIERS AND SOFTENER-MODIFIED BINDERS

MODIFIER CHEMISTRY

The modifiers used in the project are shown in Table 1. Most of these modifiers are bio-based proprietary products like modified vegetable oil, fatty acid derivatives, and glycol amines. A ReOB-based modifier, known to have poor cracking performance, was included as a benchmark to evaluate the relative performance of different modifiers. An asphalt-based modifier was also included in the study. The experimental plan introduced in Chapter 2 was followed. Chemical characterization for modifier fingerprinting was conducted; the results are presented in this chapter.

Elemental and Compositional Analysis

Table 8 summarizes the elemental analysis results for the modifiers used in the study. Typical composition of modifiers identified as vegetable oils, modified vegetable oils, or bio-oils were high in carbon, ranging from a low of 76.4% for modifier D to a high of 78.8% for modifier I; elemental hydrogen ranged from 11.3% to 11.7% for F and I, respectively. The elemental nitrogen in vegetable oil-based modifiers was less than 1.4% (for modifier D), while the sulfur content was usually absent in these type of modifiers except for modifiers F (1%), L (0.25%), E (0.19%), and D (0.04%). Modifier G had a significantly different elemental composition compared to the rest of the modifiers, with exceptionally lower carbon content (49.4%), slightly lower hydrogen (9.9%), and significantly higher nitrogen (10.1%) and oxygen (30.6%). Exceptionally high nitrogen and oxygen in modifier G may be attributed to its chemical make-up, which is primarily a glycol amine–based modifier (Table 1). The ReOB-based modifier K and the asphalt-based modifier H had carbon, hydrogen, and nitrogen in a similar range to that of vegetable oils. However, they were relatively high in sulfur—2.5% and 0.7% for H and K, respectively.

Table 8. Elemental Carbon, Nitrogen, Hydrogen, Sulfur, and Oxygen Composition for Modifiers

Modifier ID	Carbon (%)	Hydrogen (%)	Nitrogen (%)	Sulfur (%)	Oxygen (%)
A	77.3	11.7	1.0	0.0	10.0
B	77.7	11.0	0.9	0.0	10.5
C	70.0	11.2	4.0	0.0	14.8
D	76.4	11.6	1.4	0.0	10.6
E	77.4	11.5	0.9	0.2	10.0
F	76.3	11.3	1.0	1.0	10.3
G	49.4	9.9	10.0	0.0	30.6
H	81.7	10.5	1.5	2.5	3.9
I	78.8	11.7	1.0	0.0	8.4
J	77.3	11.6	1.0	0.0	10.1
K	79.9	12.4	1.5	0.7	5.4
L	78.0	11.5	0.9	0.3	9.3

Each modifiers' composition was characterized based on the relative proportions of saturates, aromatics, resins, and asphaltenes (SARA). Table 9 summarizes the SARA composition for each modifier. All modifiers, except K (ReOB), were primarily comprised of resins as their major fraction, ranging from 62.4% (for A and H) to 87.8% (for B). Modifier K had high saturates and significantly high insoluble residue. Contrastingly, the bio-based oil modifiers' (A, B, C, D, E, F, I, and J) indicates the presence of asphaltenes. This may be an artifact of the TLC-FID testing technique; asphaltenes were not expected in any of the modifiers except H and K. The TLC-FID used in the present study separates the SARA fractions in three stages based on polarity. The modifier solution is prepared in dichloromethane, which is capable of dissolving highly polar compounds. In the first stage, n-heptane separates non-polar saturates. The second and third stages separate aromatics, resins, and asphaltenes, respectively, as per their increasing polarity. The proportion classified as asphaltenes in modifiers may represent high polarity resins instead. Modifier G was insoluble in the solvent used for conducting SARA; hence, the test could not be completed. Interestingly, modifier G was also soluble in water.

Furthermore, modifier K may result in a gel-type structure with a high amount of saturates (paraffins) and insoluble residue. Excess of saturates and insoluble residue may lead to gelation in the asphalt binder structure, causing compatibility issues. The gel-type structure retains residual thermal stresses, leading to cracking in the asphalt (Asphalt Institute, 2016).

Table 9. SARA Composition for Modifiers

Modifier ID	Saturates (%)	Aromatics (%)	Resins (%)	Asphaltenes (%)	Insoluble Residue (%)
A	8.3	19.7	62.5	4.6	4.9
B	0.0	0.2	87.8	7.2	4.8
C	0.0	0.0	70.1	23.2	6.6
D	1.1	10.5	78.5	7.5	2.3
E	0.0	0.1	83.4	13.0	3.5
F	0.0	0.0	87.4	8.4	4.2
H	5.0	18.0	62.4	10.5	4.1
I	0.0	14.8	77.9	4.1	3.2
J	0.0	0.3	85.5	10.3	3.9
K	59.3	0.5	10.3	4.0	26.0

Chemical Functional Groups

Fourier transform infrared (FTIR) spectroscopy was used to fingerprint the chemical functional groups present in each modifier. The region between 1,000–1,500 cm^{-1} wavenumbers is a characteristic of vegetable oil (Rabelo et al., 2015). Figure 30-A demonstrates a characteristic peak at 1,743 cm^{-1}, representing carbonyl stretching (C=O) in the vegetable oils. The peaks at 1,465 cm^{-1} and 1,377 cm^{-1} correspond to the bending vibration peak of methylene, while the peak at 1,099 cm^{-1} represents the vibration from C-O ester linkage and 1,160 cm^{-1} indicated the presence of C-O from triglycerides (Shi et al., 2017; Rabelo et al., 2015; Rohman & Man, 2013). As shown in Table 1 and Figure 30-A, modifiers A, D, E, F, I, and J indicate the presence of some type of vegetable oil.

In Figure 30-B, the wavenumbers 3,009, 3,955, 2,933, and 2,852 cm^{-1} represent the C-H stretching vibrations typical of hydrocarbons. Modifier H, which was disclosed by the supplier to be an asphalt-based modifier, also has the presence of some vegetable oil-based peaks as found in the spectra presented in Figure 30-A. In Figure 30-C, the spectral response of fatty acid–based modifiers B and C have peaks at 1,702 and 1,735 cm^{-1}, representing carbonyl from the acid or ketone group. The peak at 1,270 cm^{-1} for modifier B corresponds to the -C-O- (alkoxy) functional group, while for modifier C, the peaks at 1,073 and 1,037 cm^{-1} also represents the presence of alkoxy functional groups (Shi et al., 2017; Tarhan et al., 2017; Sinclair et al., 1952). This suggests that the carbonyl peak belongs to acid derivative (-COO-) in modifiers B and C. In Figure 30-E, a wide peak at 1,120 cm^{-1} for modifier G shows the aliphatic alkoxy functionality. Furthermore, a peak at 1,665 cm^{-1} is characteristic of either an amide or an aldehyde group. However, the broad peak at 2,852 cm^{-1} (Figure 30-F) is a characteristic of an amine salt, which emphasizes that the peak at 1,665 cm^{-1} belongs to the amide group (Sigmaaldrich, n.a.).

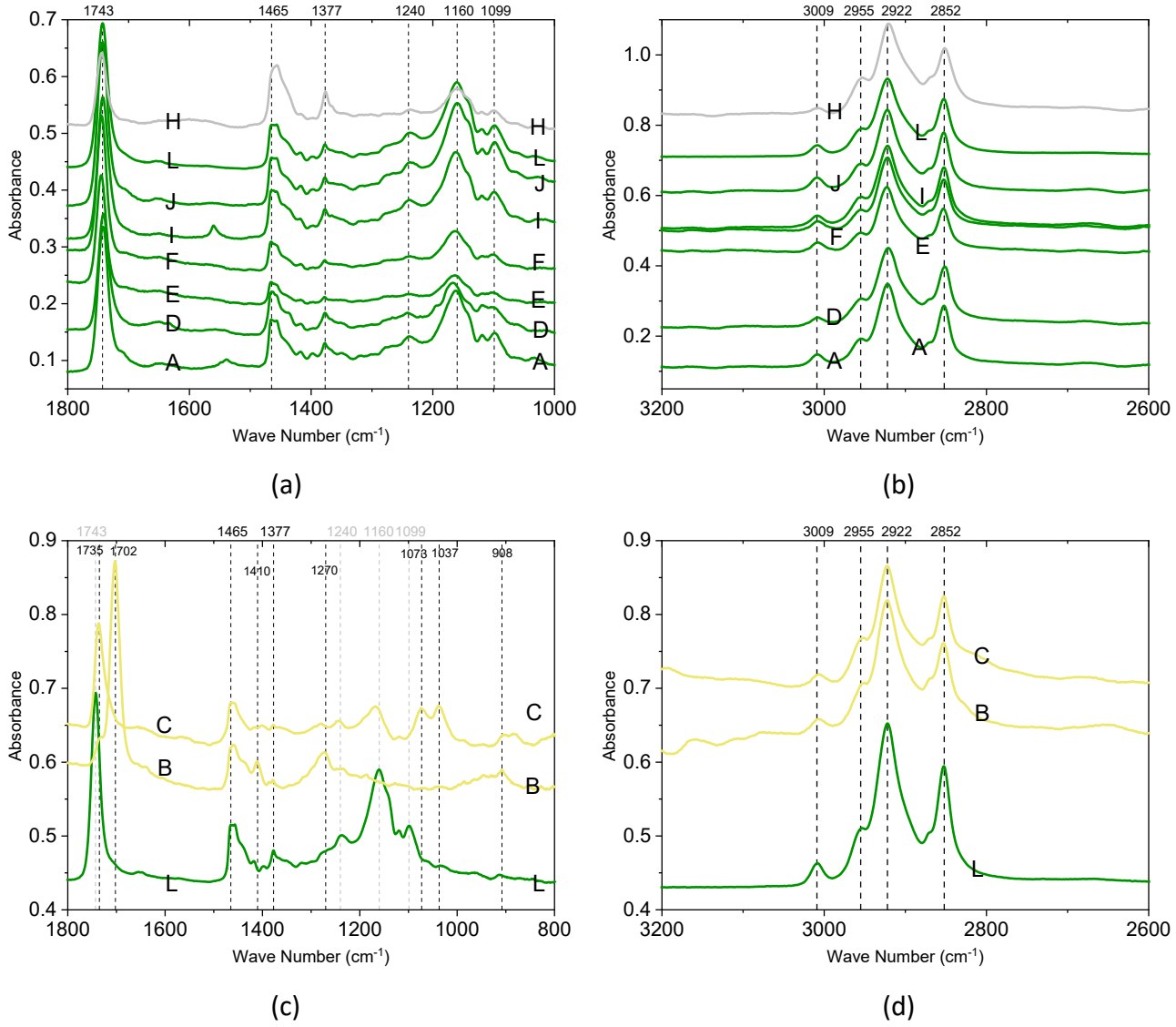

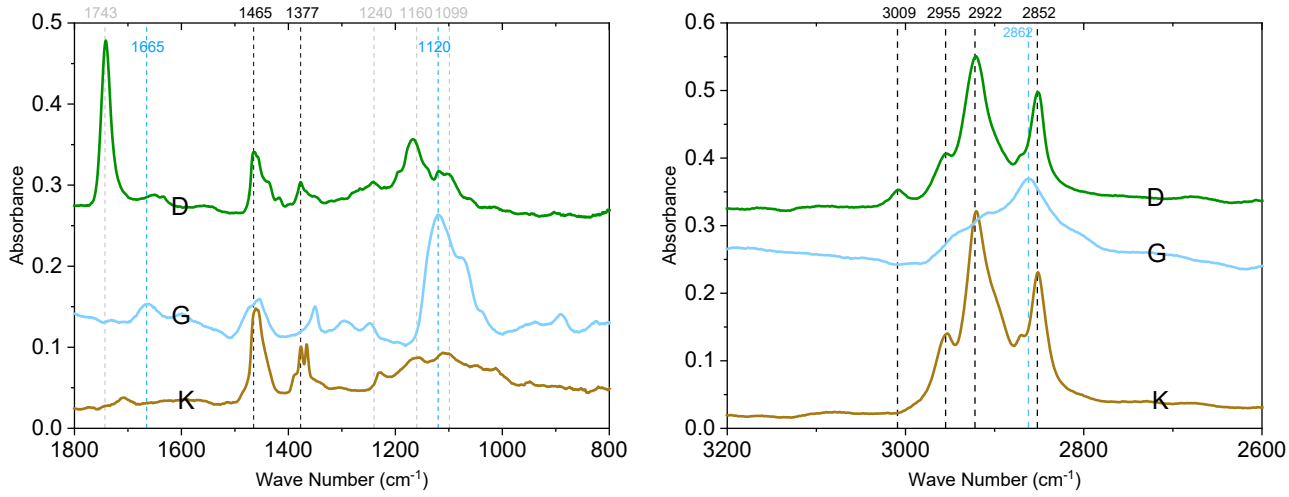

(e) (f)

Figure 30. Graph. FTIR results of modifiers.

Molecular Size Distribution

The molecular weight distribution results from the gel permeation chromatography technique further differentiate the modifiers. Figure 31-A shows the presence of bimodal distribution for modifiers A and D, which identifies the presence of two types of molecular species, while Figure 31-B shows modifiers E, I, J, and L with a single peak; these modifiers consist of one molecular species. Modifier F (Figure 31-C) has a broad distribution at a lower retention time (high molecular weight) and a predominant single peak at a higher retention time (low molecular weight). In Figure 31-D, modifier K shows a wider distribution in molecular weights compared to other modifiers. Modifier H showed a distribution with characteristics found in asphalt binder (Figure 39), as expected. The molecular weight distribution result in Figure 31-D reinforce the FTIR results presented in Figure 30-A, indicating modifier H may have both vegetable oil and asphalt-like properties. The fatty acid derivatives B and C differ in their molecular weight distribution (Figure 31-E). Their distribution shows three peaks, which suggests they have three types of distinct molecular species. Modifier G is a single peak distribution and has the lowest molecular weight among all modifiers (Figure 31-F). The number average (M_n), weight-average molecular weights (M_w), and polydispersity index (PDI) for modifiers is presented in Table 10. All modified vegetable oils show similar range of Mn and Mw with PDI close to one, except modifier F. The molecular weights for glycol amine and fatty acid derivatives are significantly lower than all modifiers tested. The value of molecular weights and PDI for modifier H and K is similar to asphalt binders.

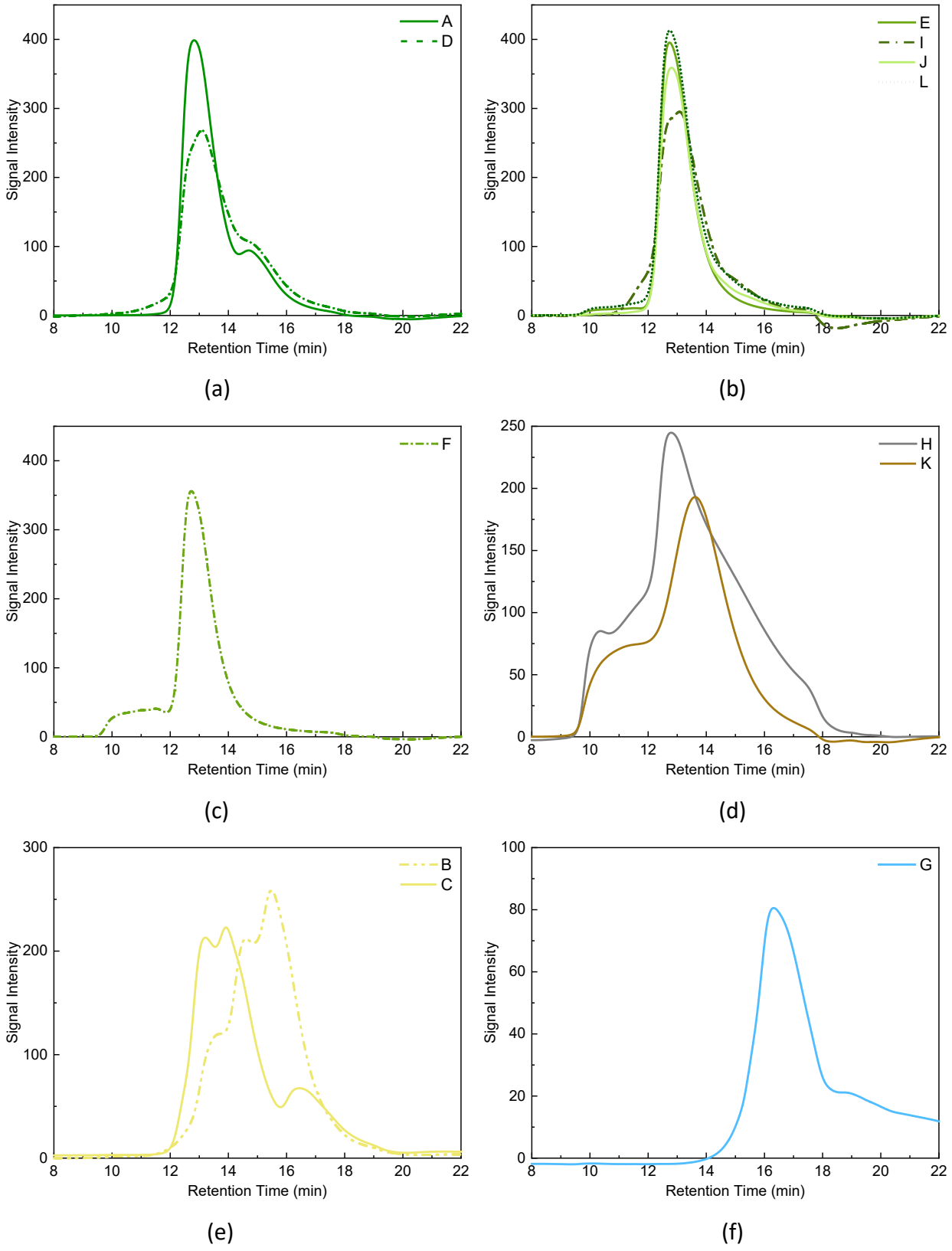

Figure 31. Graph. Molecular weight distribution of modifiers.

Table 10. Molecular Weights (M_n and M_w) and Polydispersity Index for Modifiers

Modifier ID	M_n (Daltons)	M_w (Daltons)	PDI
A	1097	1272	1.16
B	514	828	1.61
C	736	1030	1.40
D	1033	1480	1.43
E	1435	3413	2.38
F	2096	7269	3.47
G	102	272	2.65
H	2255	9676	4.29
I	1232	1573	1.28
J	1175	1323	1.13
K	2414	9631	3.99
L	1413	3702	2.62

Thermal Analysis

Thermogravimetric analysis (TGA) was performed to determine the decomposition temperature of selected modifiers. The TGA of the modifiers was performed by heating the sample in the presence of air at a constant heating rate of 20°C/min to 700°C. The modifiers were decomposed at temperatures higher than 600°C. The rate of weight change with increasing temperature was fastest for modifier G, indicating a lower thermal stability (Figure 32). This is an undesirable trait considering that the mixing and compaction temperature for asphalt mixtures is around 150°C. In contrast, modifier E was the most stable out of the tested modifiers. The changes in weight in the mixing temperature range is greater than 2% for modifier G and is less than 1% for modifiers A, C, D, and E (Figure 32). Further evaluation of modifiers using TGA can help understand thermal properties of these modifiers, which was beyond the scope of this study.

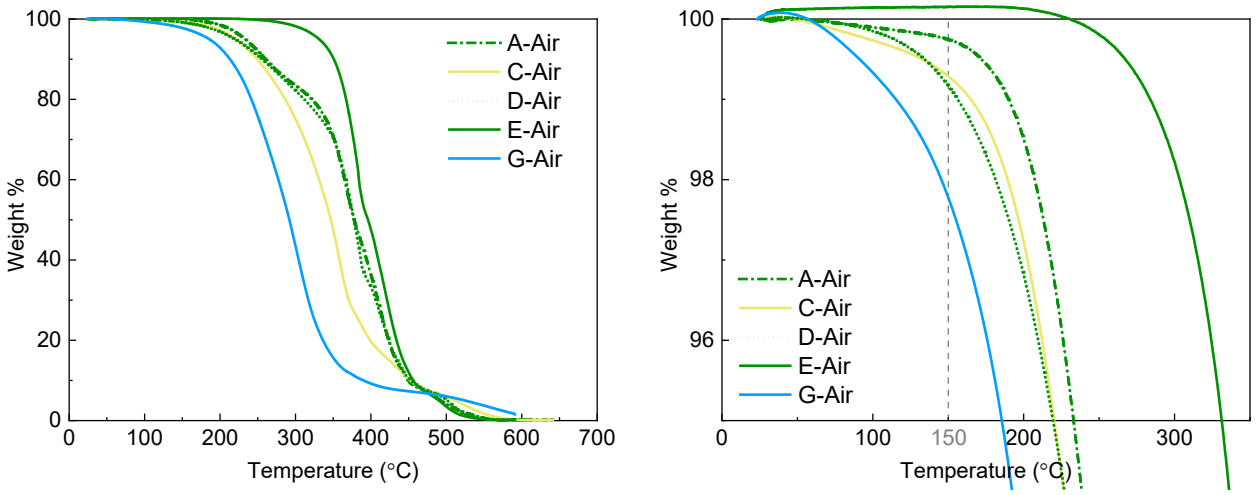

Figure 32. Graph. Thermogravimetric analysis of modifiers.

SOFTENER-MODIFIED BINDER CHEMISTRY

The results from the chemical characteristics of modified binders produced from the base binder S1 and unmodified binders S1, S5, and S8 are presented in the section below. In addition, modified binder S9-L-NA was included for comparison with S8, as these binders were used in a test section constructed in Illinois. Laboratory-aged binders including unaged, RTFO-, PAV-, 2PAV-, and 3PAV-aged conditions were considered to investigate the impact of the modifiers on asphalt binder chemistry.

Chemical Functional Groups

Figure 33-A presents a typical FTIR spectrum for asphalt binders. The spectral window from 800 to 1,800 cm^{-1} is a region that provides a fingerprint for the asphalt binder tested. The changes in binder chemistry because of laboratory aging, field aging, or chemical modifications can also be identified in this region. The fingerprint region is sub-divided into 10 regions as shown in Figure 33-B; each region corresponds to specific chemical functional groups described in Table 11.

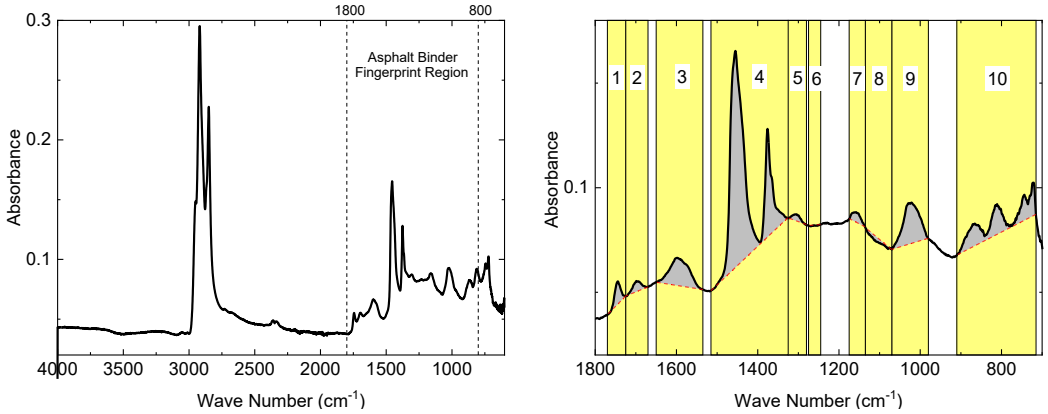

(a) (b)

Figure 33. Graph. (a) Typical FTIR spectra for asphalt binders, (b) fingerprint regions for binders.

Table 11. Highlighted Regions Representing Possible Functional Group and Their Range of Wavenumbers in the Fingerprint Region

Highlighted Region	Wavenumber Range (cm^{-1})	Possible Functional group
1	1,725–1,770	Esters (C=O stretching)
2	1,670–1,725	Aldehydes, Ketones, Acids (C=O stretching) Amides (C=N)
3	1,535–1,650	C=C aromatic stretching
4	1,325–1,515	sp^3 C-H bending
5	1,280–1,325	C-O (acyl, phenol), nitro
6	1,245–1,275	C-O (acyl, phenol), C-N
7	1,135–1,175	Alkoxy
8	1,070–1,135	Alkoxy
9	980–1,070	Sulfoxide
10	715–910	Alkene sp^2 C-H bending Aromatic sp^2 C-H bending

Effect of Aging in FTIR Spectra for Modified Binders

The binders' spectral response changes with laboratory aging because of the exposure to high temperature and pressure conditions. Figure 34 presents a typical spectral response. With aging, certain chemical functionalities change because of laboratory aging (e.g., region 9). Some do not have any significant change (e.g., regions 3, 4, and 10).

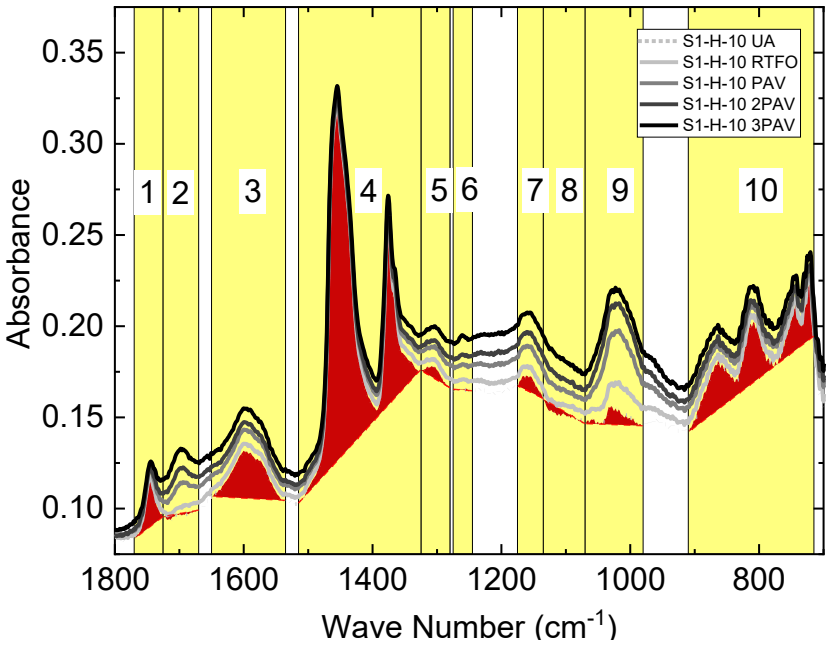

Figure 34. Graph. Typical FTIR spectra for asphalt binders with different aging conditions from wavenumbers 800 to 1,800 cm^{-1}.

The spectral response for selected modified and base binders from wavenumbers 800–1,800 cm^{-1} are presented in Figure 35. With aging, the area under the sulfoxide group (980–1,070cm^{-1}) and areas for some specific carbonyl groups (around the peak of 1,700 cm^{-1}) increases. However, in the case of modified binders obtained from E, C, and H (Figure 35), the carbonyl area centered around the peak of 1,750 cm^{-1} decreases with aging. The spectral areas corresponding to aromatic (region 3), aliphatic (region 4), and methylene peaks (region 10) do not change significantly with aging relative to sulfoxide and carbonyl areas, as these functional groups are less prone to change with aging.

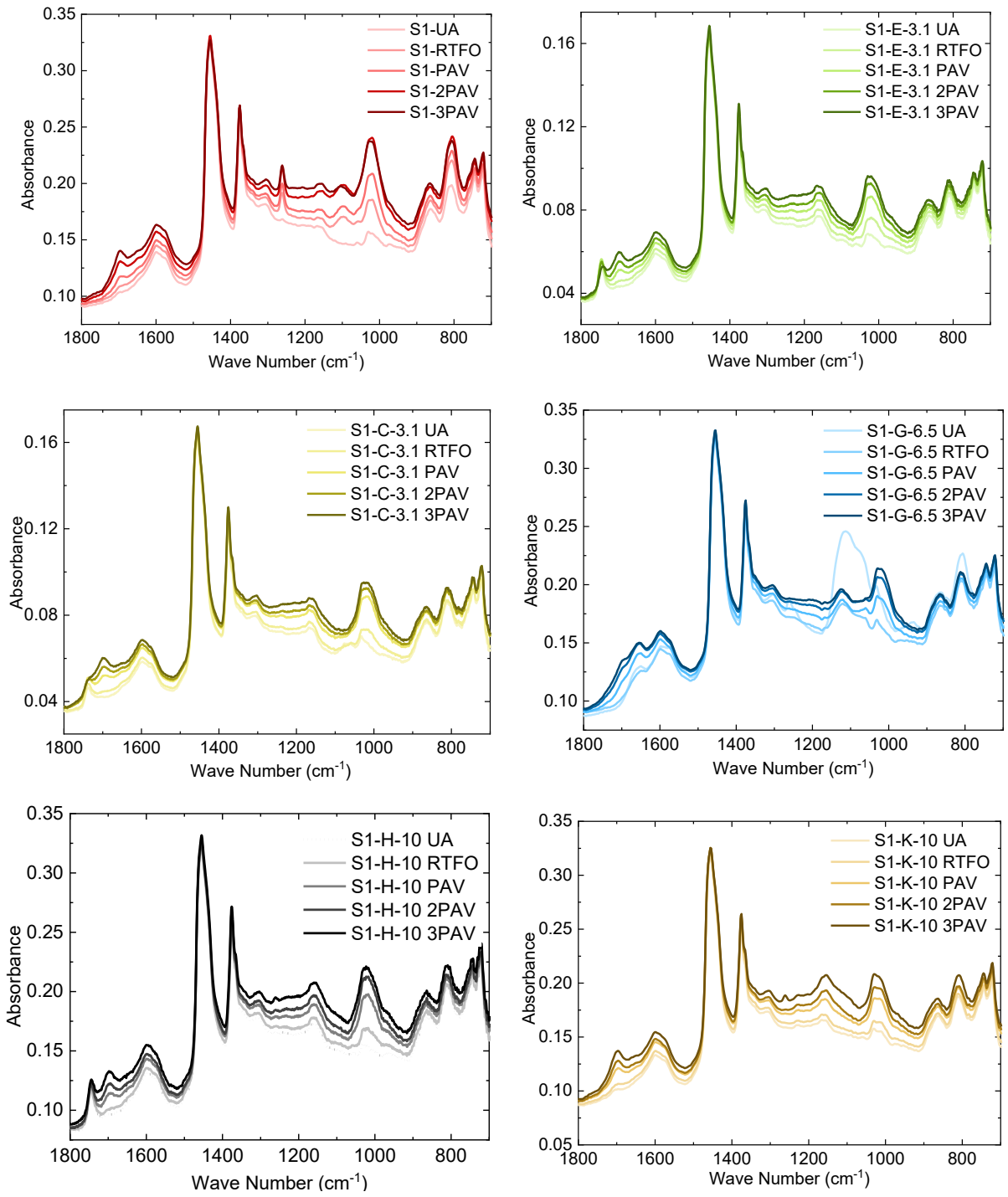

Figure 35. Graph. FTIR spectra for modified and modified binders for different aging conditions.

Oxidation Indices

To quantify the effect of laboratory aging, several indices were calculated using the area under the highlighted regions presented in Figure 34 (see Appendix D). The two most suitable indices for capturing the effect of aging are calculated using the equations in Figure 36 and Figure 37. The indices

were selected based on the findings from chemical characterization of extracted binders from field-aged cores presented in Chapter 5.

$$FTIR_{C=O} = \frac{A_2}{(A_3 + A_4)}$$

Figure 36. Equation. Carbonyl-based FTIR oxidation index.

$$FTIR_{C=O+S=O} = \frac{(A_2 + A_9)}{(A_3 + A_4)}$$

Figure 37. Equation. Carbonyl- and sulfoxide-based FTIR oxidation index.

where A_2 is the area under FTIR spectra between 1,670–1,725 cm^{-1}; A_3 is the area under FTIR spectra between 1,535–1,650 cm^{-1}; A_4 is the area under FTIR spectra between 1,325–1,515 cm^{-1}; and A_9 is the area under FTIR spectra between 980–1,070 cm^{-1}. The indexes presented are normalized with aromatic and aliphatic peaks to eliminate the differences caused by the change in the order of magnitude in absorbance peaks. Appendix D summarizes the areas highlighted in Figure 34 for modified and unmodified binders at different aging conditions.

Figure 38 presents the aging evolution of the modified binders. The data presented is shown for RTFO, PAV, 2PAV, and 3PAV conditions because the extent of aging is similar for each step from RTFO to PAV, PAV to 2PAV, and 2PAV to 3PAV. The unaged condition was excluded because the aging extent from the unaged to RTFO-aged condition is different from the latter scenarios. The rate of change in two oxidation indices was determined by the equation shown in Figure 37 and is presented in Figure 38. In addition to the absolute value of the oxidation index, the rate of change in the oxidation index also plays an important role in determining the oxidation potential of a modified binder. The findings based on the evaluation of oxidation indices are as follows:

- $FTIR_{C=O+S=O}$ and $FTIR_{C=O}$ show similar impacts on binder modified with vegetable oils and can be useful in quantifying the oxidation potential. However, the $FTIR_{C=O+S=O}$ index shows a reduction in the rate of oxidation after the 2PAV condition (40 hr. in PAV from Figure 38) in all the binders except modifiers G and S5.

- Modifier G has a lower rate of change for the $FTIR_{C=O}$ index compared to other modifiers. In addition, it has lower values for oxidation indexes at different aging conditions.

- The $FTIR_{C=O}$ index shows a consistent change in the aging rate (Figure 38) except B-modified binder. Like the $FTIR_{C=O+S=O}$ index, the $FTIR_{C=O}$ index also shows a lower rate and lower oxidation index for G-modified binder.

In general, the modifiers used in the study show a similar range of oxidation indexes as well as the rate of aging except modifier G, which shows the lower index (intercept) and aging rate (slope).

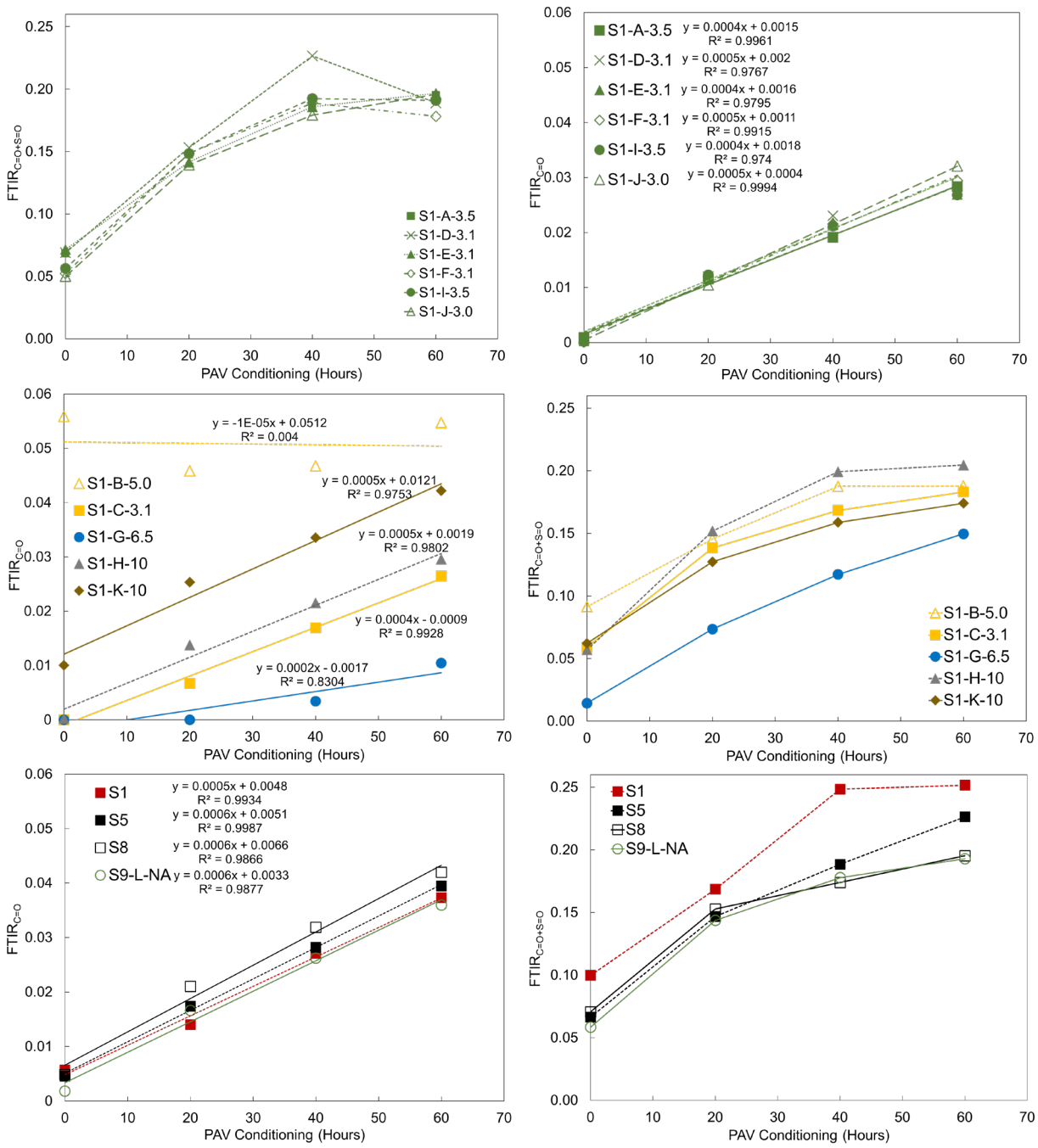

Figure 38. Graphs. Aging evolution for different binders expressed using FTIR oxidation indices.

Molecular Size Distribution

Figure 39 presents the molecular size distribution for base binder S1 at different aging conditions. The molecular distribution for the modified and unmodified binders had a bimodal distribution, suggesting the presence of two types of dominating molecular species. The retention time in Figure 39 is used to determine the average molecular weights for binders. A lower retention time corresponds to a higher molecular weight, and vice versa. The number-average molecular weight

(M_n), weight-average molecular weight (M_w), and polydispersity index (PDI) for modified binders are included in Appendix D.

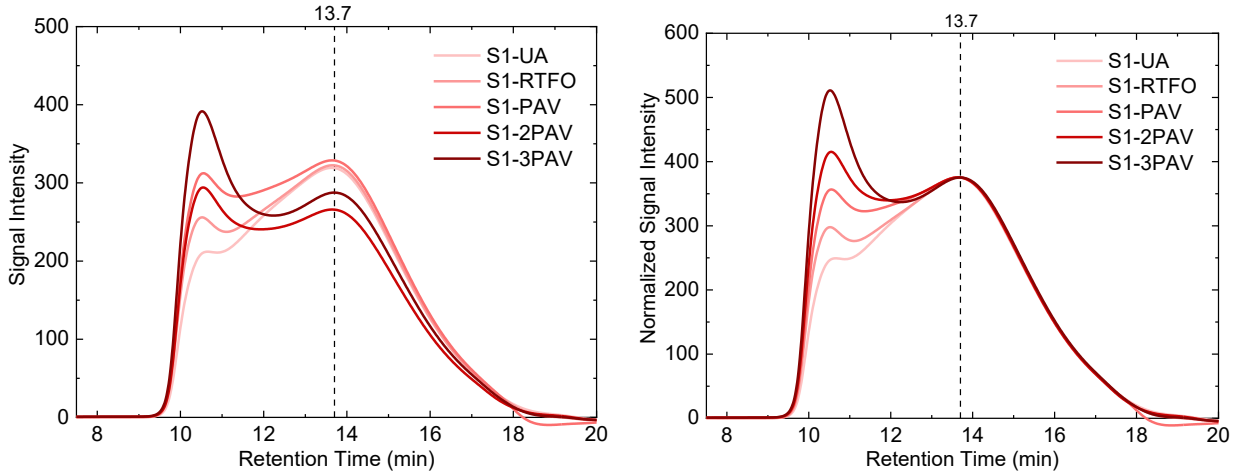

Figure 39. Graphs. (a) Typical molecular weight distribution for asphalt binders with aging; (b) normalized molecular weight distribution at retention time 13.7 min.

Effect of Aging on Molecular Weight of Modified Binders

In Figure 42, the peak on the left has a higher molecular weight than the peak on the right. Therefore, the areas near the left and right peaks are referred to as large and small molecular size, respectively, as shown in Figure 42. The peak corresponding to the large molecular size increases relative to the small molecular size for all binders with aging. To better visualize the effect of aging, the molecular distribution plots were normalized with respect to the peak at a retention time of 13.7 min, as shown in Figure 42. Figure 42 presents the relative change in peak heights and corresponding areas between the large and small molecular sizes. To capture the change in molecular weight distribution, two parameters are calculated as per the equations shown in Figure 40 and Figure 41.

$$MWD_{N,Peak} = \frac{P_{LM1}}{P_{SM1}}$$

Figure 40. Equation. Index based on peak intensity representing large and small molecular weights.

$$MWD_{N,Area} = \frac{A_{LM1}}{A_{SM1}}$$

Figure 41. Equation. Index based on area representing large and small molecular weights.

where P_{LM1} is the signal intensity at a 10.5 min retention time; P_{SM1} is the signal intensity at a 13.7 min retention time; A_{LM1} is the area under the molecular weight distribution from a 9 to 12.5 min retention time; and A_{SM1} is the area under the molecular weight distribution from a 12.5 to 19 min

retention time. The retention times were chosen based on the binder data set tested for this study, which showed bimodal peak distribution with a peak centered at 10.5 min and 13.7 min for large and small molecular weights, respectively. The selected times may vary with from one GPC technique to another.

Figure 40 quantifies the change in molecular size using the ratio of peak heights corresponding to the peak representing the large molecular size (P_{LM1}) to the small molecular size (P_{SM1}). Peak P_{LM1} was measured at a 10.5 min retention time, and peak P_{SM1} was measured at a 13.7 min retention time. The retention times considered were based on the entire data set of modified binders considered in the study and are shown in Appendix D.

In contrast, the parameter from Figure 41 quantifies the molecular weight change in the large and small molecular sizes using areas corresponding to each region shown in Figure 42. For consistency in determining the areas, retention time representing the bell-shaped curve was 9 to 12.5 min and 12.5 to 19 min for large and small molecular weights, respectively.

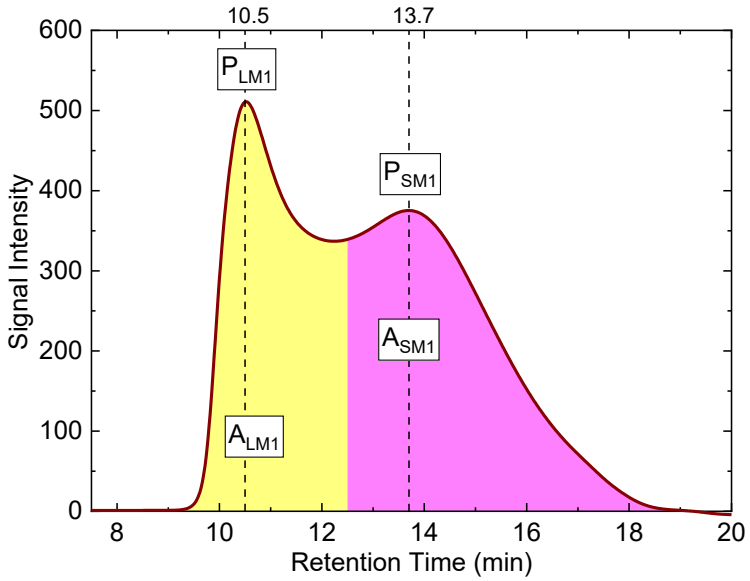

Figure 42. Graph. Peaks and areas for regions representing large and small molecular weights.

Figure 43 presents the molecular weight distribution for selected modified binders after aging. The modifiers have a significant effect on molecular weights and their rate of change with aging. Modifier G shows the least potential to change compared to the rest of the modifiers. However, differences are not distinguishable for the remaining modifiers.

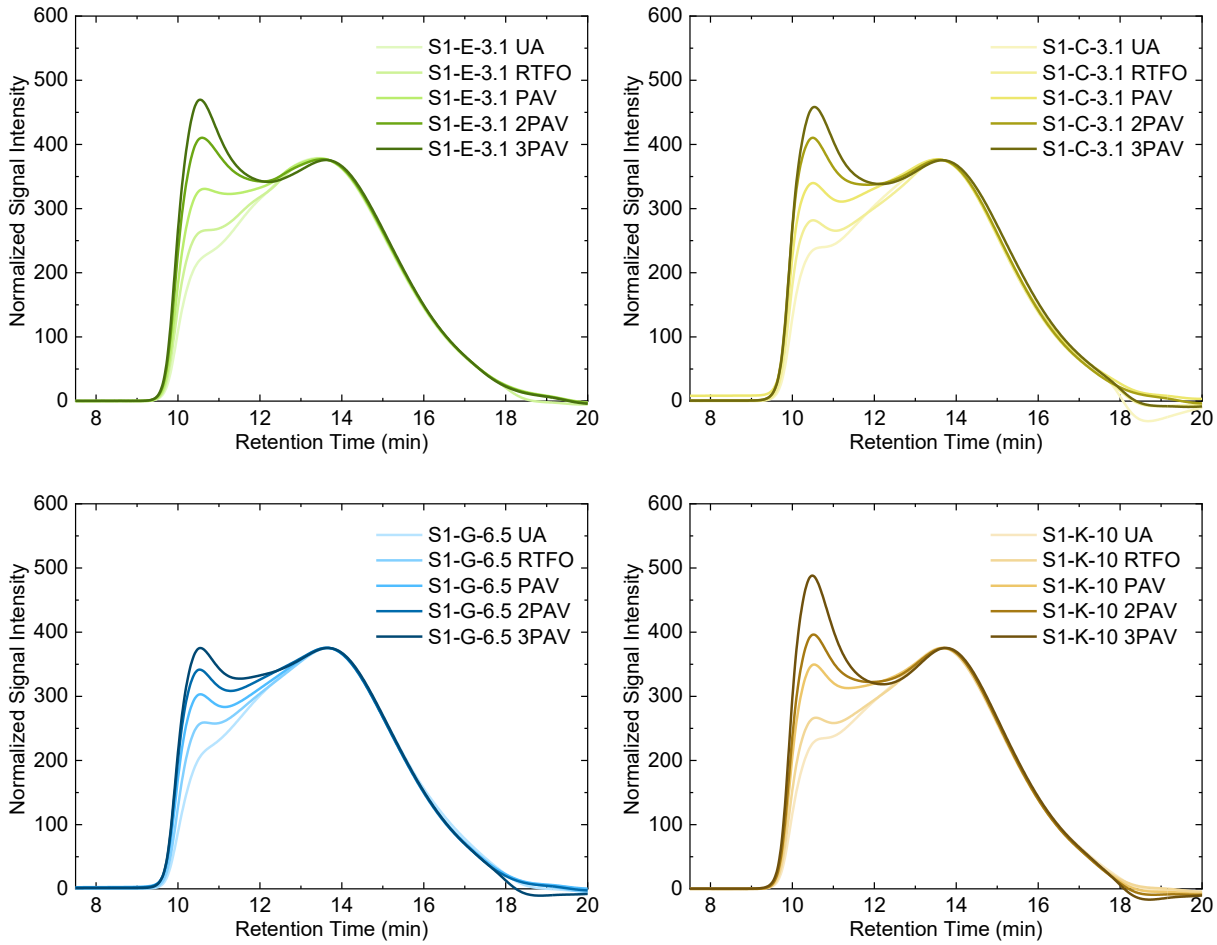

Figure 43. Graphs. Molecular weight distribution for modified binders with aging.

Figure 44 presents the aging evolution based on the change in molecular size from small to large for different modified binders. Both parameters presented show consistent trends with aging and either parameter can be used for developing kinetic parameters.

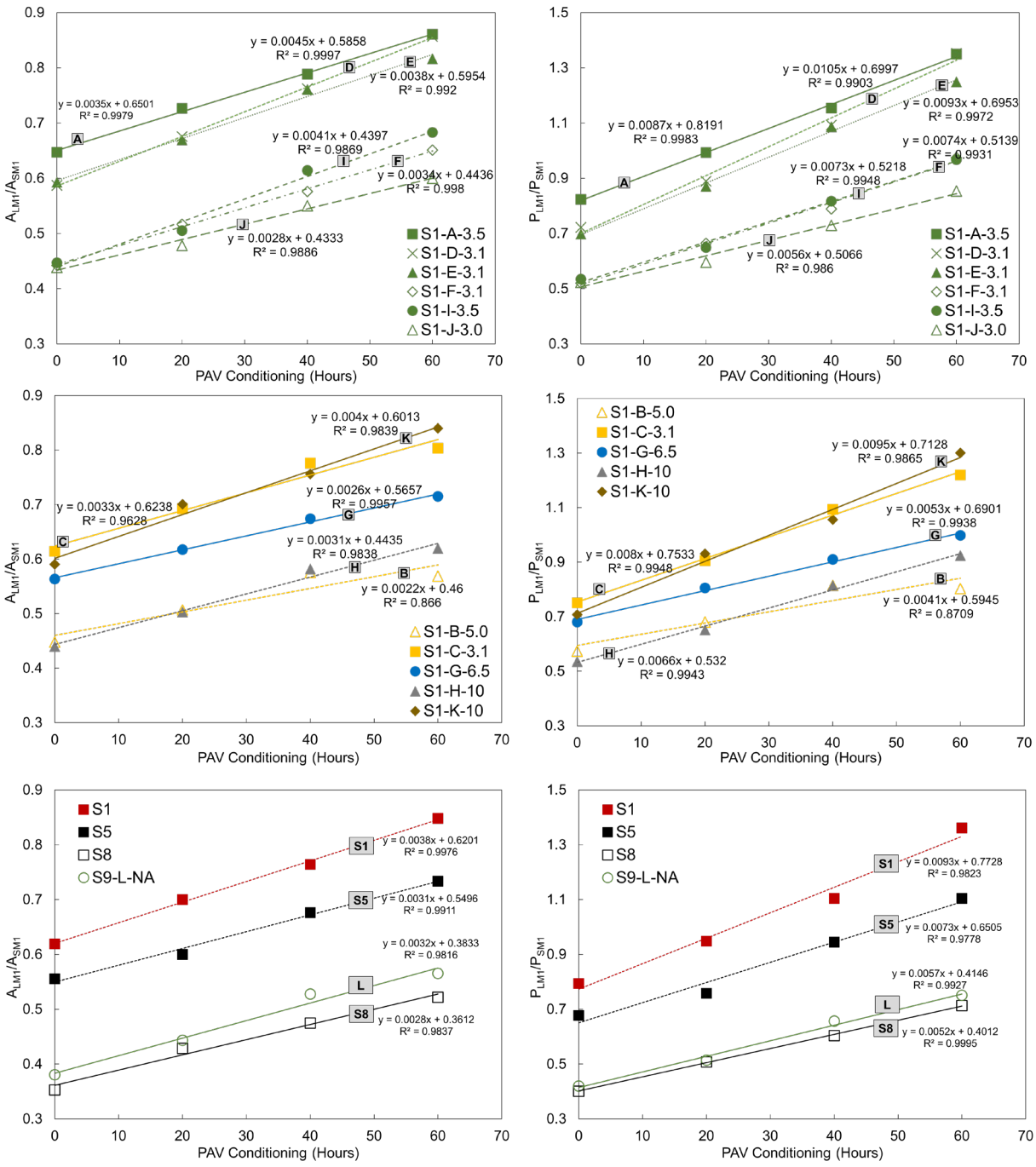

Figure 44. Graphs. Aging evolution for different binders expressed using molecular weight indices.

The molecular size increased with aging for all modified and unmodified binders (Figure 44). All modified binders showed a similar rate of aging except modifier G, which showed the lowest rate of change. Furthermore, the molecular weight for modifier G was the lowest compared to other modifiers at various aging levels (see Appendix D).

SUMMARY

The main findings of the chemical characterization of modifiers and the modified binders are as follows:

- The chemical characterization of the modifiers confirmed the modifier types provided by the manufacturers.
- The chemical analysis suggests that all vegetable oil–based modifiers have similar compositions, while modifier G (glycol amine) varies significantly from other modifiers.
- SARA analysis suggests that modifier K (ReOB) has a significantly high content of insoluble residue and its composition is significantly different from others. The rest of the modifiers are mainly composed of resins.
- A limited examination of thermal analysis suggests modifier G has low thermal stability, which supports the high mass loss percentage after RTFO reported in Chapter 8.
- Aging trends of modified binders were examined using GPC and FTIR data. The sensitivity of modified binders to aging was consistent among different modifiers, except modifier G. Furthermore, FTIR analysis showed that only specific carbonyl (1,670–1,725 cm^{-1}) captures the effect of aging, unlike what has been variably used in literature (1,600–1,800 cm^{-1}) (Prapaitrakul, 2009; Yut & Zofka, 2011; Zhu, 2015.
- Although modifier K showed poor rheological performance, the same was not evident from the chemical testing of modified binders. However, the compositional analysis of modifier K does indicate the presence of high insoluble residue, which is filtered out for the chemical tests and is not evident in chemical testing of the modified binder. In addition, modifier K also has high saturates; combined with the insoluble residue, this may lead to a gel-type structure, which may explain the poor rheological performance. Meanwhile, modifier G shows exceptional rheological performance, which is evident from its lower aging susceptibility.

CHAPTER 5: LONG-TERM FIELD AGING OF BINDERS IN ILLINOIS

The effect of field aging on asphalt binders exposed to Illinois' climate was studied. Field cores were selected from full-depth and conventional asphalt pavements. Twelve field cores aged from 8 to 31 years were collected across Illinois. Table 2 summarizes the field cores used in the study. Extracted binders from the field cores were tested for the frequency sweep and LAS tests for rheology. The binders were also tested for FTIR and GPC to determine chemical characteristics. The same binder grade (PG 64-22) was used through the depth of cores selected to obtain aging gradients. Data from the rest of the field cores are presented to compare field aging trends with that of binders aged in the laboratory.

AGING GRADIENT ANALYSIS OF FIELD-AGED BINDERS

Aging in asphalt concrete varies through the depth of the pavement structure. The surface of the pavement is directly exposed to climatic changes, traffic, and atmosphere, which makes it more susceptible to aging. Aging intensity can be expected to decrease with depth.

Field cores from three locations—US-51, IL-125, and L2-1019—with varying depths were used to evaluate the impact of aging through the pavement depth. Slices of 0.5 in. thickness were obtained from the US-51 and IL-125 field cores at various depths: surface, 4 in., 9 in., and 12 in. Because the only information known for the binders used in the field cores is their SuperPave performance grade, it is not possible to make a one-to-one comparison with the binders used in this study. However, the aging trends in the field cores were evaluated by comparing to the extracted binder from the bottom of the core. For L2-1019, slices were obtained from other depths: 1 in., 1.5 in., and 4 in.

Rheological Characterization of Field-aged Binders along Pavement Depth

Frequency sweep tests (1-62.83 rad/s) were conducted at isotherms of 15°C, 25°C, 35°C, and 45°C, and 1% strain. Figure 45 presents complex modulus master curves and phase angles at a reference temperature of 15°C. Because most of the binders in the field cores were PG 64-22, the complex modulus master curves for different aging conditions from the base binder S1 were also plotted for comparison.

There is a significant change in asphalt binder rheology through the pavement depth with aging (Figure 45). The shape of the complex modulus master curves from the extracted binder (US-51 and IL-125) at depths below 8 in. are similar to that of the base binder S1. The values for complex modulus are close to the RTFO-aged S1. For US-51, the modulus for a binder at a 12.5 in. depth is close to the unaged S1. However, as the binder is extracted from shallower slices, the shape of the master curves significantly deviates from the aged S1 binders (Figure 45).

In Figure 45, the binders extracted from the surface show stiffnesses between 2PAV and 3PAV aging for S1 master curves at lower reduced frequencies, while at higher reduced frequencies, the binder at the surface behaves much stiffer than S1 at 3PAV. At a 4 in. depth, binder stiffness is closer to PAV-aged S1 at lower frequencies, while it ranges from 2PAV to 3PAV at a higher reduced frequency. The binder phase angles at the surface were between 2PAV to 3PAV for low frequencies and PAV to 2PAV

for higher frequencies. At depths below 8 in., phase angle distribution of the extracted binders is similar to unaged and RTFO-aged master curves for S1 in shape as well as in values. Based on a preliminary investigation, the phase angles tend to increase after extraction using TCE solvent. This needs to be further investigated and a suitable correction factor should be incorporated, if required.

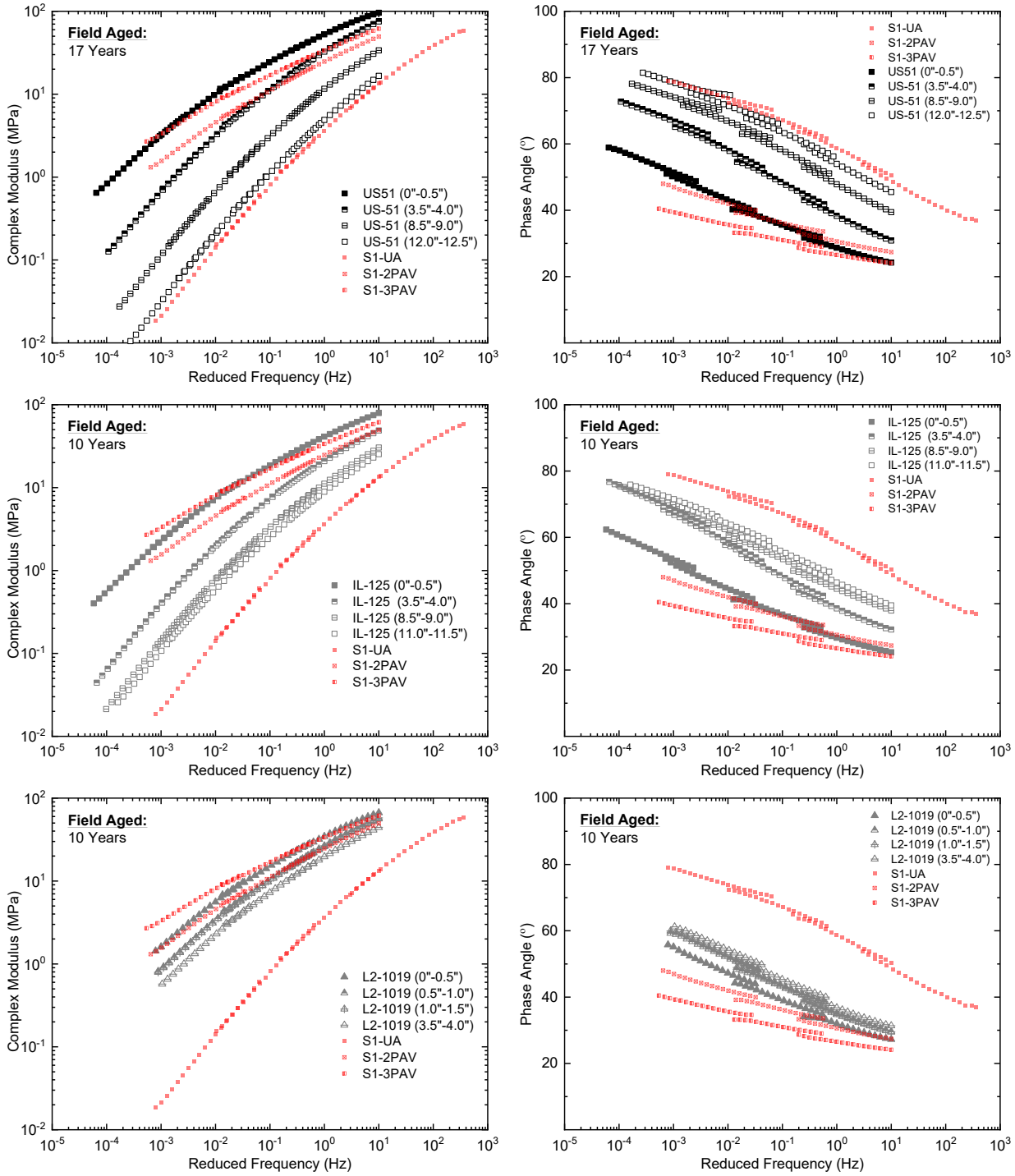

Figure 45. Graphs. Complex modulus and phase angle master curves at various depths for field core sections: US-51, IL-125, and L2-1019.

The binder from US-51 shows typically stiffer behavior, which is expected for a 17-year-old specimen. The binder from IL-125 is stiffer than L2-1019 (Figure 45). One of the possible reasons may be attributed to higher binder content in L2-1019, which is around 7%, while the binder content is around 5% for IL-125. The higher asphalt binder content in L2-1019 likely has higher asphalt film thickness, which may have limited the aging extent within the film. The binder properties at a 4 in. depth for IL-125 and L2-1019 show similar behavior, which may be attributed to limited influence from the surface aging. This also suggests that these binders may have started with a similar stiffness range. In general, the findings suggest that PAV aging may not represent the severity of binder aging at the surface. PAV is more closely associated with aging at 4 in. below the surface for long-term aging (>10 years) in two of the sites analyzed. Aging at the surface (up to 0.5 in.) is much more severe than the aging intensity for S1 at the 2PAV condition in those and in the cores. However, the severity of aging may also depend on the mix design or other factors not evaluated in this study such as in-place density.

Aging Effects on Rheological Parameters

Figure 46 presents the variation of various rheological parameters through the depth of the pavement as well as a comparison of GRPs between field- and lab-aged binders. GRPs are significantly higher on the surface than at the bottom layers. GRP for the surface is in the range of 2PAV-aged S1; in contrast, GRP_f is in between 2PAV to 3PAV. This deviation is because the GRP_f was calculated at a higher frequency and GRP at 15°C was measured at a lower frequency (Figure 46-A and Figure 46-B). Both GRPs at a 4 in. depth are similar to that of PAV-aged S1, while at depths lower than 8 in., the values are closer to lower aging intensity (RTFO or unaged) values for S1.

Figure 46-C to Figure 46-F present other rheological parameters. Parameters such as VETT and black angle do not correspond to a similar level of aging effect compared to Glover-Rowe parameters at the surface. R-values correspond to an aging extent less than that of a typical PAV-aged binder, with higher values at the surface but similar values for the underlying layers. Similar observations for black angle were observed as well. However, VETT shows a more visible decreasing trend in its values through the depth of the cores. Furthermore, aging levels at the surface correspond to PAV to 2PAV aging levels. Meanwhile, the observed trends were still consistent for some parameters evaluated at the small strain; not all parameters capture the aging gradient across the pavement depth. GRPs and VETT are good indicators of the aging gradient. Still, further investigation is required to explain the observations for phase angle, black angle, and R-value.

From the LAS test on extracted binders, the large-strain parameter, $\Delta G^*_{peak\ T}$, shows a trend similar to the one discussed in Chapter 3. The parameter shows a lower value for unaged binders and increases upon aging to a maximum around PAV aging and decreases further with extended aging. In Figure 46, at a 12 in. depth, $\Delta G^*_{peak\ T}$ is low, the parameter increases at an 8 in. depth, and then decreases towards the surface (at 4 in.). However, the absolute values for $\Delta G^*_{peak\ T}$ show much lower values (stiffer than 3PAV aged) compared to S1 aged binders; the trends are consistent through the depth.

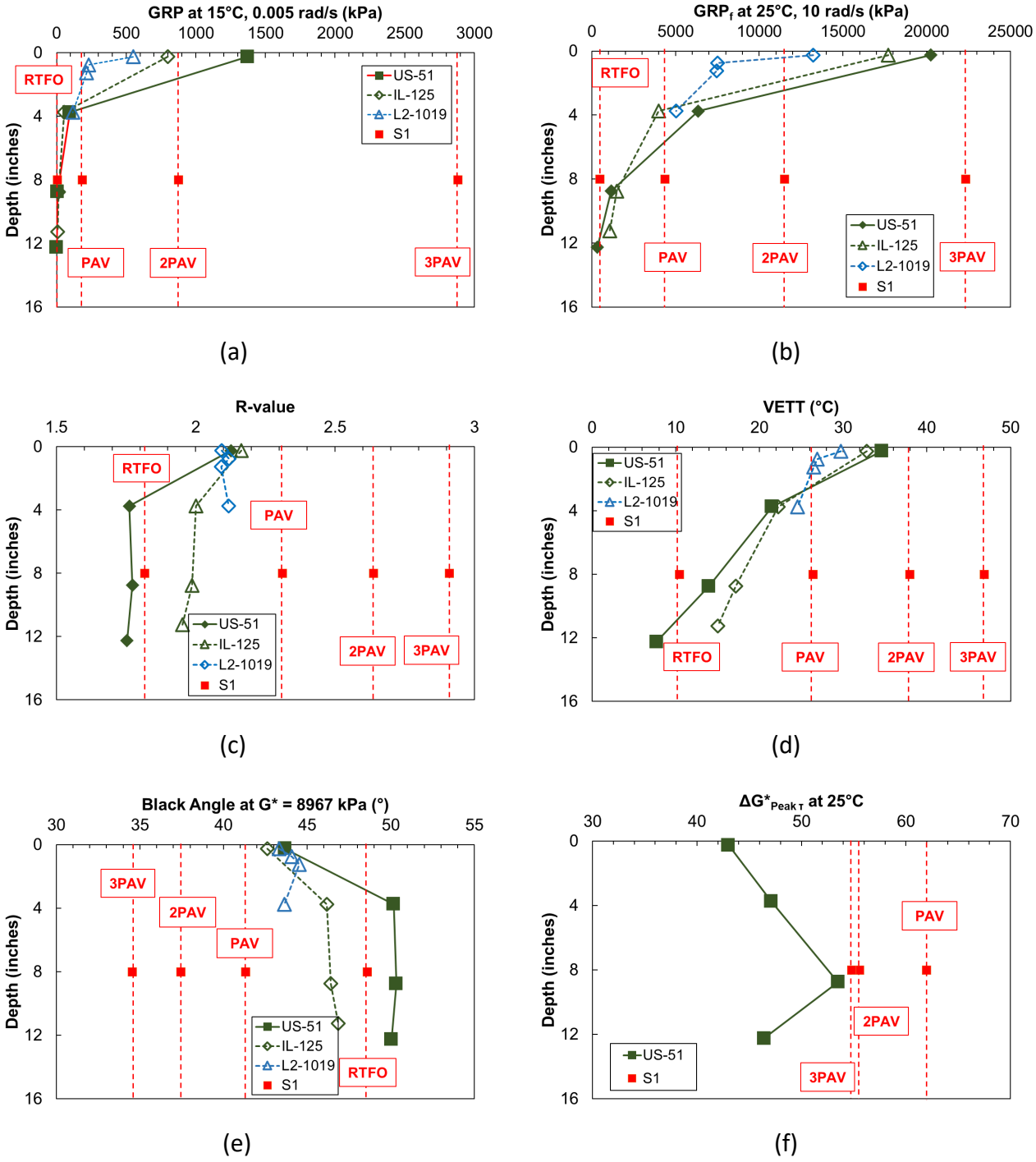

Figure 46. Graphs. Rheological parameters—(a) GRP; (b) GRP_f; (c) R-value; (d) VETT; (e) black angle; and (f) $\Delta G^*_{peak\ \tau}$ for binders extracted from field cores US-51, IL-125, and L2-1019 plotted with reference binder S1.

Chemical Characterization of Field-aged Binders through Pavement Depth

The rheological changes across the pavement depth may be attributed to changes in chemistry. The following section presents the effect on chemical parameters for extracted binders through the depth of the pavement.

Aging Effects on Chemical Parameters

Oxidation Indices from FTIR

Carbonyl and sulfoxide functional groups tend to increase with binder oxidation. However, there is a wide wavenumber range that corresponds to the carbonyl functional groups. Figure 47 indicates that only the intensity of the carbonyl peak centered around 1,696 cm^{-1} increases moving toward the surface. In contrast, the carbonyl centered around 1,727 cm^{-1} decreases with depth. This suggests that only specific carbonyl groups should be considered to quantify the effect of aging in asphalt binders. Furthermore, the sulfoxide functional group is consistently high at the surface and decreases with depth. Apart from carbonyls and sulfoxides, other -C-O- functional groups did not show any effect with varying aging extents through pavement depth. The carbonyl-based and combination of sulfoxide- and carbonyl-based oxidation indices decrease with the aging extent moving through the depth of the pavement.

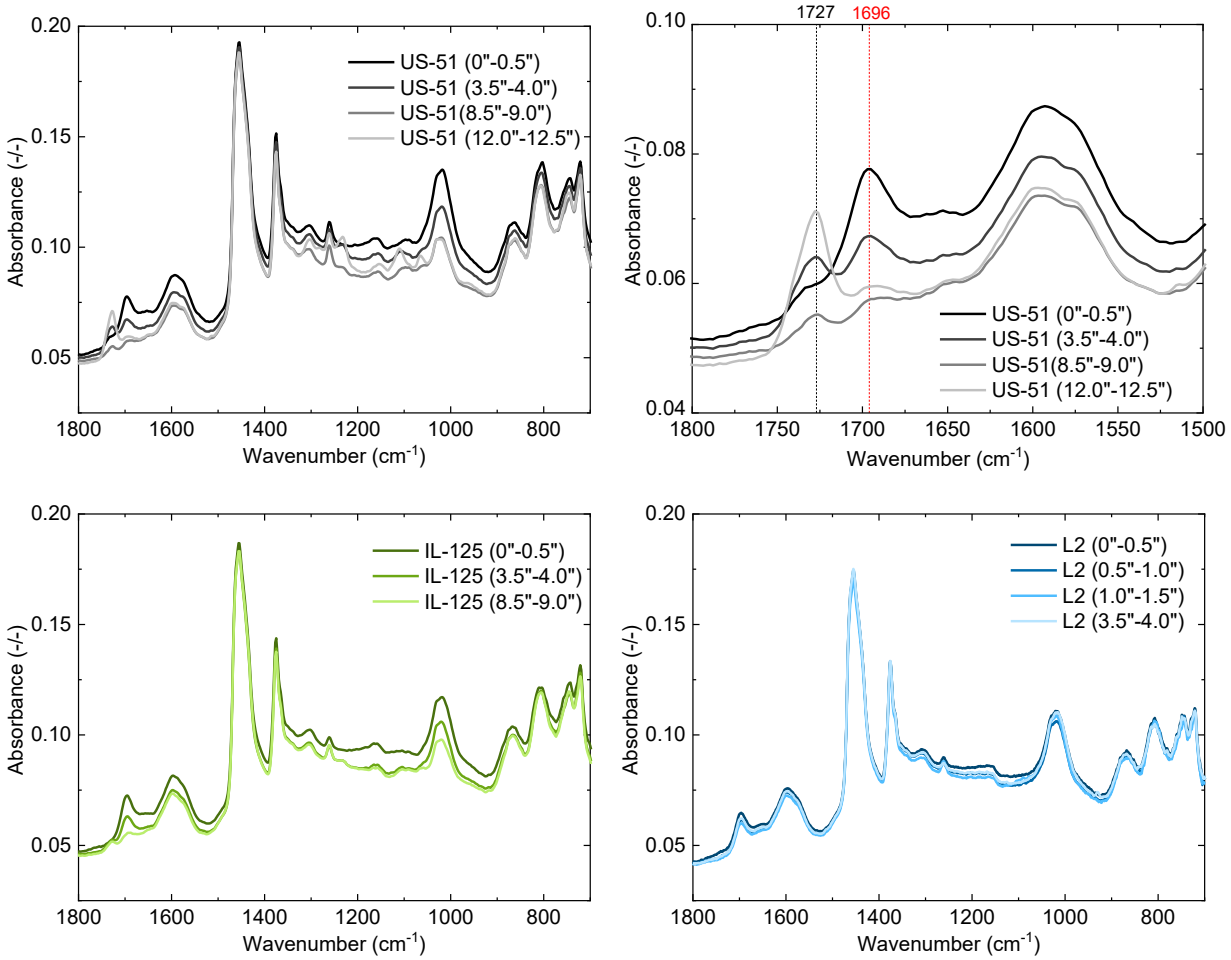

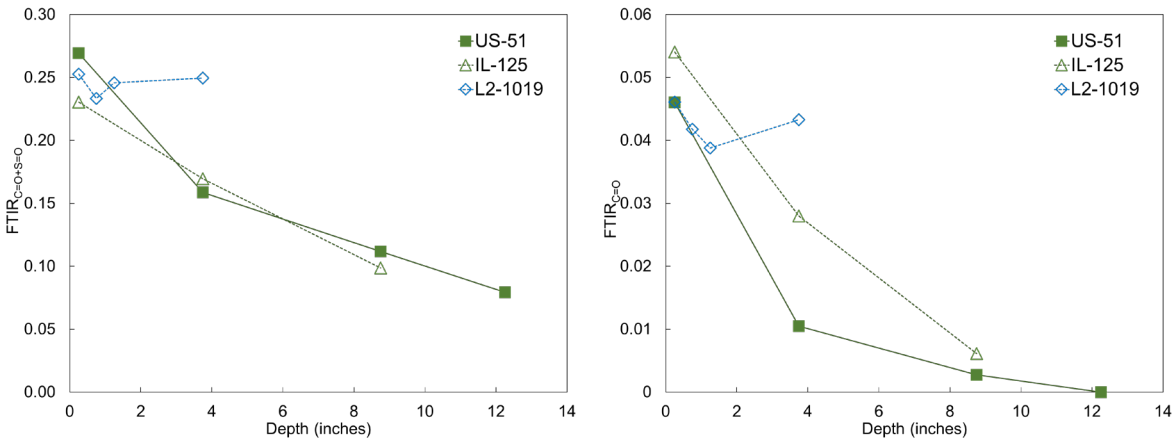

Figure 47. Graphs. FTIR spectra and oxidation indices at various depths for field core sections: US-51, IL-125, and L2-1019.

Molecular Weight Indices from GPC

Oxidation is also associated with the change in molecular weights. The extracted binders at the surface showed an increase in average molecular weights compared to the binders in the lower layers. In Figure 48, the normalized molecular weight parameter defined based on the area of large to small molecular weight decreases with depth, suggesting higher molecular weight for binders exposed to the surface compared to lower layers.

EFFECT OF LONG-TERM AGING ON BINDERS AT PAVEMENT SURFACE

This section determines a more realistic binder-aging protocol. The findings were further utilized to establish preliminary thresholds for rheological and chemical parameters.

Rheological Characterization of Field-aged Binders at Pavement Surface

Figure 49 presents the complex modulus and phase angle master curves for field-aged binders collected from 0.5 in. surface lifts of the field cores. The cores presented below are aged from 8 to 31 years (Table 2). When compared to S1, the stiffness of the extracted binders ranges from 2PAV to 3PAV at lower reduced frequencies and greater than 3PAV for high reduced frequencies. While for phase angles, the distribution was from PAV to 2PAV and 2PAV to 3PAV for low and high reduced frequencies, respectively.

The rheological parameters from small- and large-strain binder tests of aged binder extracted from field core surfaces were evaluated. Figure 50-A and Figure 50-B show the range of GRPs for 12 field cores aged 8 to 31 years. For cores aged less than 15 years in the field, the GRP ranged from 300 kPa to 1,200 kPa, while cores aged more than 15 years ranged from 1,400 kPa to 2,100 kPa. Most of these GRPs were more than the suggested threshold of 180 kPa for the onset of cracking and 600 kPa for severe cracking. The GRP at 15°C for extracted binders at the surface for cores aged less than 15 years were close to 2PAV-aged S1 binders.

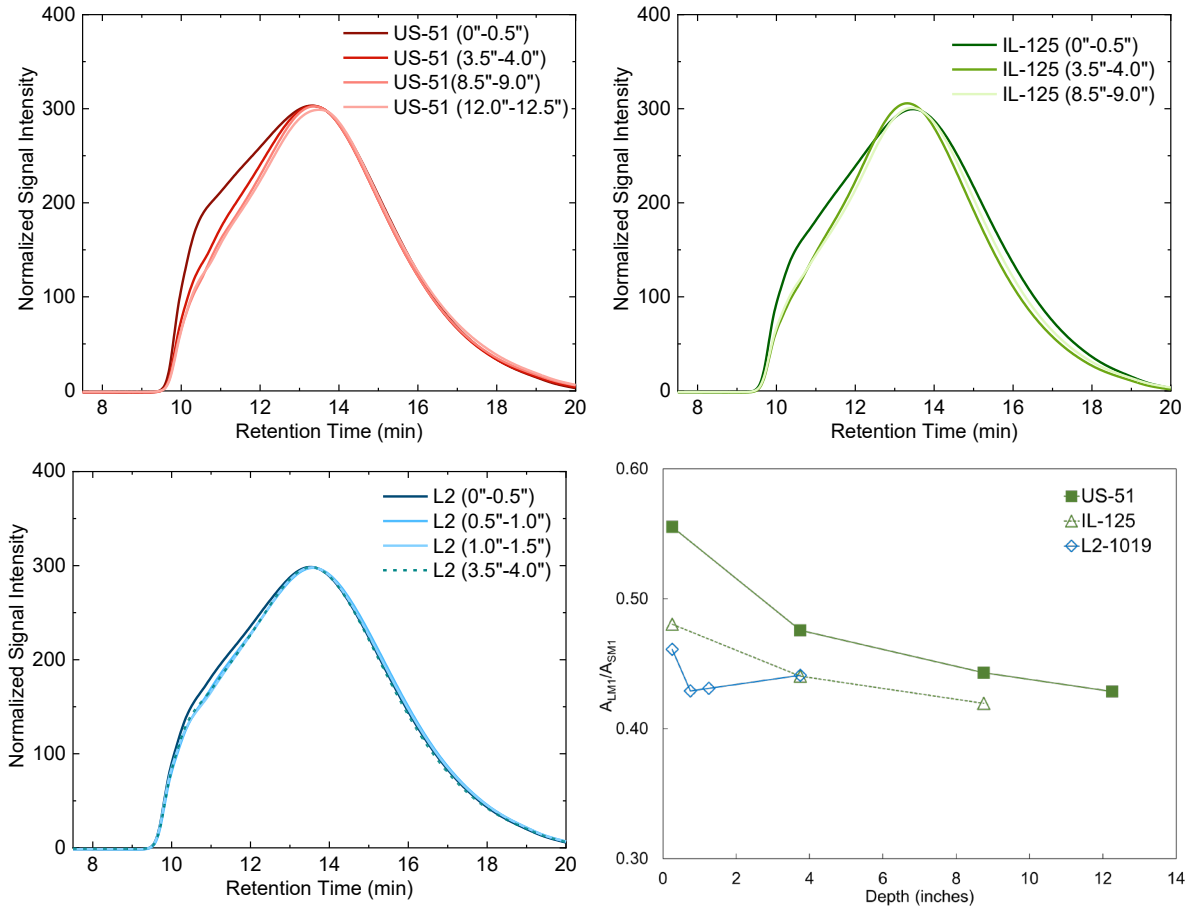

Figure 48. Graphs. Molecular weight distribution and area-based index at various depths for field core sections: US-51, IL-125, and L2-1019.

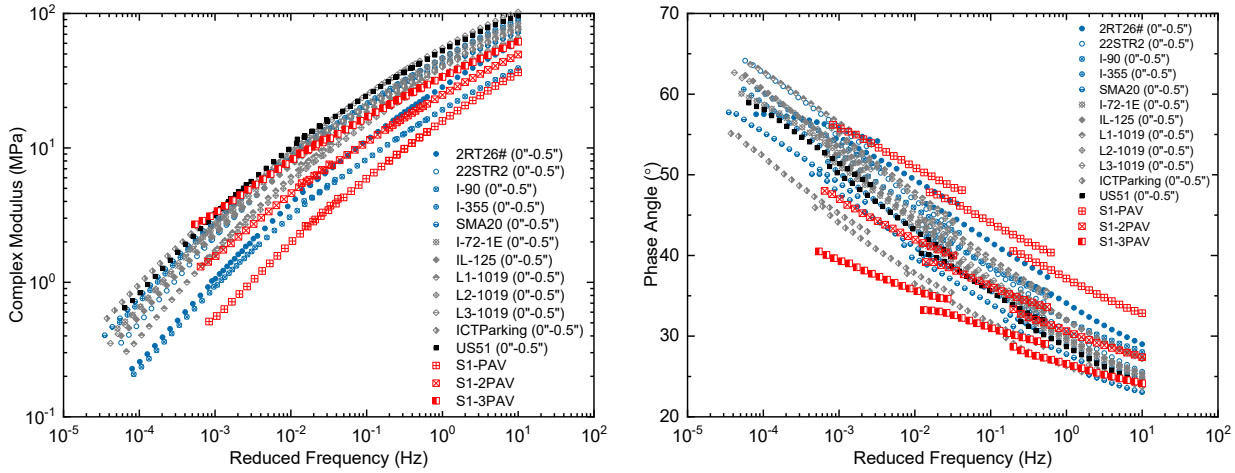

(a) (b)

Figure 49. Graphs. (a) Complex modulus and (b) phase angle master curves for binders extracted from the surface of the field cores.

Figure 50-B shows the GRP_f for extracted surface binders ranged from 8,000 kPa to 22,000 kPa for cores aged less than 15 years and from 20,000 kPa to 25,000 kPa for more than 15 years. The values for GRP_f for surface binders from field cores aged less than 15 years were between GRP_f of 2PAV- to 3PAV-aged S1 binder. Christensen and Tran (2019) recommend an upper limit for GRP_f of 5,000 kPa and 8,000 kPa for PAV- and 2PAV-aged binders, respectively. However, the presented findings suggest that binders aged more than 10 years (long term) have significantly higher GRP_f (8,000 kPa), as suggested by Christensen & Tran (2019).

Similarly, Figure 50 presents the range of crossover parameters, black angle, and $\Delta G^*_{peak\,\tau}$ for long-term-aged cores. The parameters dependent on phase angles suggest a lower aging extent when compared to parameters from S1 aged binders. As stated previously, the effect of solvent extraction on phase angles needs further investigation, which will affect the values of phase-angle dependent parameters. The $\Delta G^*_{peak\,\tau}$ parameter consistently showed a much more severe effect of field aging. This observation may indicate that some changes in binders' microstructure captured by the large-strain test were not captured by other small-strain tests.

Chemical Characterization of Field-aged Binders at Pavement Surface

Oxidation and molecular weight indices for surface-extracted binders are presented in Table 12. In general, the indices for field cores aged more than 15 years were higher than field cores aged less than 15 years except for the carbonyl-based index. Hence, a sulfoxide- and carbonyl-based index is more suitable to quantify aging effects in binders. The area-based molecular weight index was also able to discriminate the extensively aged binder. Even though the chemical parameters complement findings from rheology, further investigation is required to quantify thresholds for chemical parameters.

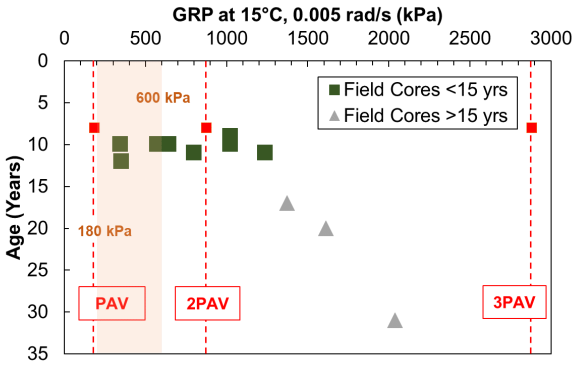

(a)

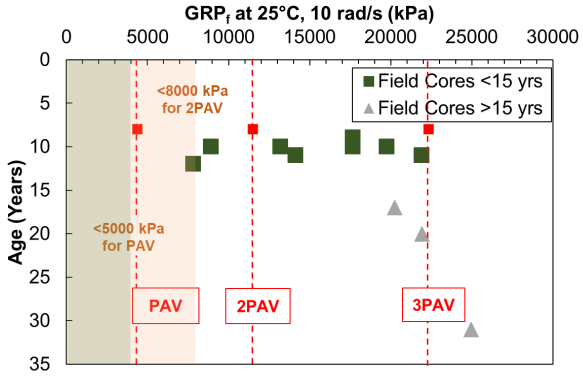

(b)

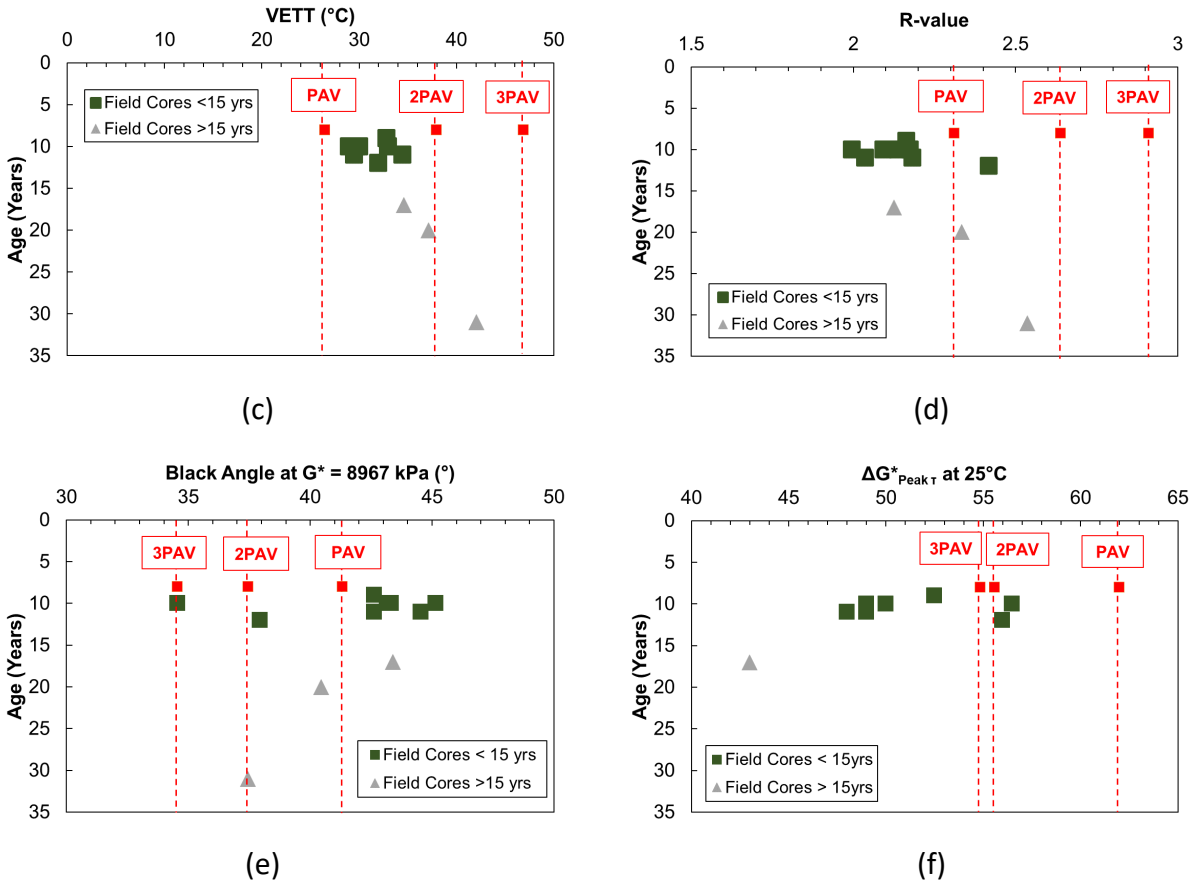

Figure 50. Graphs. Rheological parameters—(a) GRP, (b) GRP_f, (c) R-value, (d) VETT, (e) black angle, and (f) $\Delta G^*_{peak\ \tau}$ for binders extracted from the surface of the field cores plotted with reference binder S1.

Table 12. FTIR and GPC Parameters for Binders Extracted from the Surface (0–0.5 in.) of the Field Cores

Field Core ID	$FTIR_{C=O}$	$FTIR_{C=O+S=O}$	MWD_{Area}
US-51	0.046	0.269	0.555
L2-1019	0.046	0.253	0.461
L1-1019	0.038	0.224	0.490
IL-125	0.054	0.230	0.480
I-90	0.043	0.228	0.492
I-72 1E	0.045	0.262	0.554
I-355	0.049	0.250	0.493
2RT26	0.037	0.209	0.417
22SRT2	0.043	0.245	0.528
S1-UA	0.003	0.042	0.558
S1-RTFO	0.006	0.100	0.619
S1-PAV	0.014	0.169	0.700
S1-2PAV	0.027	0.248	0.764
S1-3PAV	0.037	0.252	0.848

LONG-TERM AGING PROTOCOL FOR MODIFIED BINDERS AND THRESHOLDS

The field aging analysis of a standard binder grade used in Illinois showed the severity of field aging. Most of the rheological and chemistry parameters used in the experimental program demonstrated the impact of aging after 10 years. The effect of aging severity converges from approximately unaged conditions to approximately 3PAV equivalent conditions closer to the surface. While some parameters showed that aging can be as severe as 2PAV or 3PAV equivalent in the field, others showed less severe aging than 2PAV.

The results from rheological characterization of field cores can be used to establish a realistic long-term aging protocol for modified binders. The chemical parameters complement the findings from rheological-derived parameters. Field aging of 10–15 years is assumed to represent long-term aging for this study. Anything beyond 15 years is considered extra long-term aging and may not need to be used as a performance target. Most of the field-aged binders from Illinois suggested aging levels of more than 2PAV as per stiffness-based rheological parameters. Furthermore, findings from Chapter 3 suggest that modified binders are better distinguished at aging conditions of 2PAV and higher. The PAV aging condition was shown to be insufficient to distinguish modified binders. The field cores' data showed the PAV aging condition does not represent realistic aging at the pavement surface for Illinois' climate. Therefore, binder aging of 2PAV or higher appears to be more suitable for any parameter corresponding to the long-term behavior of binders and modified binders.

Based on the presented data, thresholds reported in the literature for rheological parameters like GRP and GRP_f may not represent Illinois' conditions. These thresholds may need to be adjusted for Illinois' binders and require further investigation. For example, a GRP of 180 to 600 kPa, representing cracking onset and severe cracking, respectively, is significantly lower than the GRP of binders aged less than 15 years in Illinois. Similarly, Christensen and Tran (2019) suggest a maximum GRP_f of 8,000 kPa for 2PAV-aged binders at 25°C for PG 64-22. This recommendation may not comply with binders aged in Illinois for 10–15 years, which is considered the long-term aging target.

Preliminary Threshold Selection

Because aging in Illinois is more severe than 2PAV and modified binders are better distinguished at 2PAV, the 2PAV aging condition was used as a reference to establish thresholds for modified binder selection. The following section presents threshold selection for the different rheological parameters. All thresholds are based on the limited data set tested and require further validation. Note that most binders from the field cores were PG 64-22. However, the modified binders evaluated in other chapters focus on PG 58-28 as the target binder grade.

Glover-Rowe Parameters

GRP is a stiffness-dependent parameter and is calculated at 15°C and a frequency of 0.005 rad/s. For example, PG 58-28 will have a lower GRP than PG 64-22 at 15°C. However, the current threshold for GRP is 180 kPa (cracking onset) and 600 kPa (severe cracking) irrespective of the binder grade, which may not be applicable for all binder grades. Therefore, a unique threshold for binders should be established based on their PG if GRP at 15°C, 0.005 rad/s is used to compare binder performance. Figure 50 presents GRP for field-aged binders representing long-term-aged PG 64-22. The GRP

thresholds of 180 kPa and 600 kPa do not seem to be applicable for Illinois binders, as they fail most of the binders. These thresholds seem to represent the PAV aging condition, while the field evaluation suggests aging of 2PAV or higher, which is a more representative state of aging in Illinois for surface binders. Therefore, based on 2PAV aging as the long-term aging duration, the maximum allowable GRP of 1,000 kPa is more realistic based on the limited field data evaluated. In Figure 51, for modified binders with PG 58-28, the maximum allowable GRP of 500 kPa at 2PAV is the suggested threshold as it differentiates the worst-performing binder. Given the variability, the threshold was chosen to account for the range of test output of lowest ranked modified binder except ReOB.

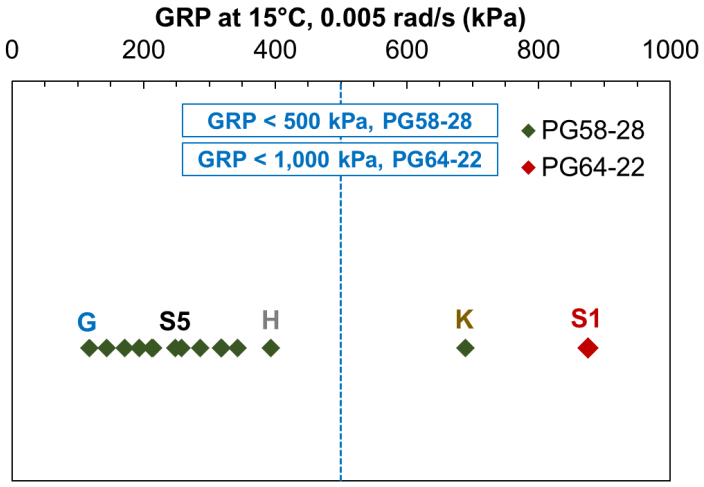

Figure 51. Graph. Suggested thresholds for GRP at 15°C, 0.005 rad/s for different PG grades.

The GRP_f presented by Christensen & Tran (2019) also defines a unique allowable threshold of 5,000 kPa for PAV and 8,000 kPa for 2PAV-aged binders, irrespective of their grade. The thresholds are determined at fatigue test temperatures proposed in Christensen and Tran (2019) (e.g., 25°C for PG 64-22 and 22°C for PG 58-28). However, these binders may still be at different stiffness levels as a 3°C shift in temperature does not correspond to a 6° grade change (see Figure 52). A fixed maximum threshold may be unnecessarily stricter for the binder with higher stiffness. An alternative is to obtain the GRP_f at the SuperPave intermediate temperature (25˚C for PG 64-22 and 19°C for PG 58-28), as presented in Figure 52, which is at a 6°C difference. The GRP_f at the SuperPave intermediate temperature is referred to as $GRP_{f,\ adjusted}$ herein. A maximum $GRP_{f,\ adjusted}$ of 14,000 kPa at the 2PAV aging condition is recommended for Illinois binders to ensure long-term performance as per Figure 50. The selected $GRP_{f,\ adjusted}$ also distinguishes modified binders (Figure 53).

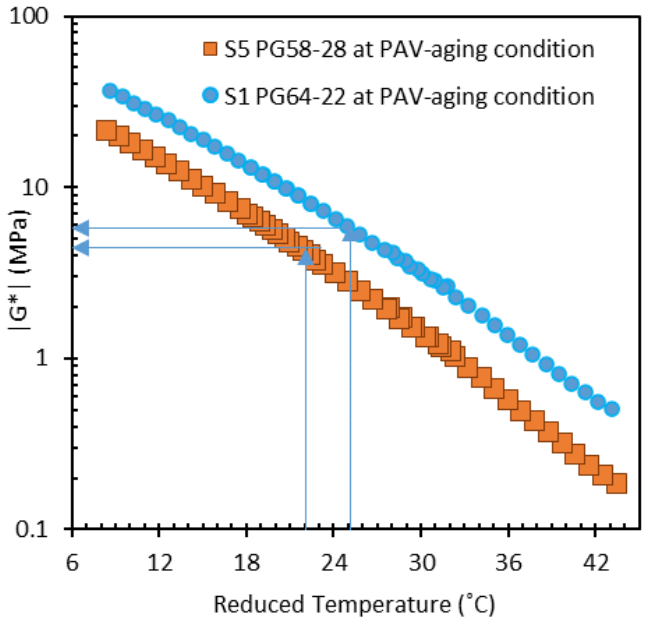

Figure 52. Graph. Temperature dependence of two binders: PG 64-22 and PG 58-28.

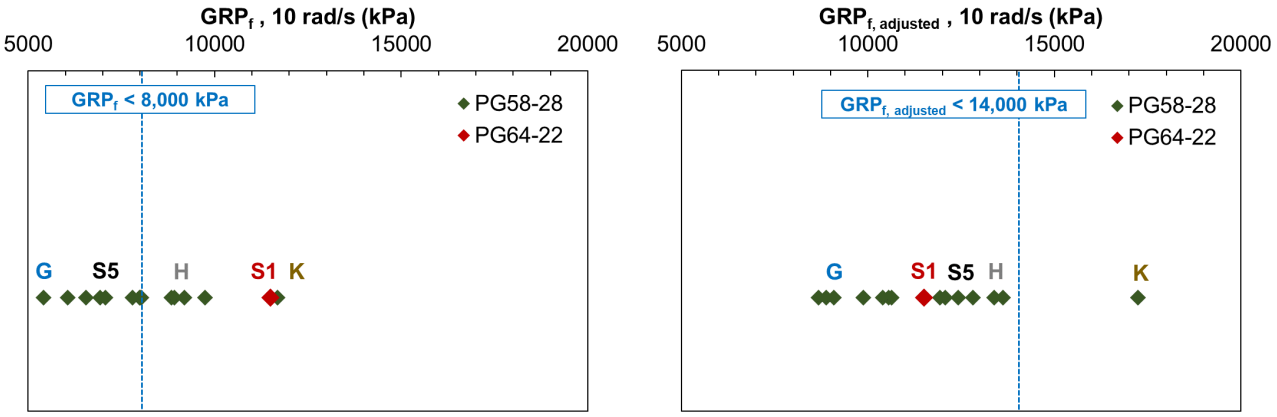

Figure 53. Graphs. Thresholds for GRP_f and $GRP_{f,\ adjusted}$ for modified binders.

Other Rheological Parameters

Similarly, thresholds for crossover parameters, the black angle, and the LAS parameter $\Delta G^*_{peak\ \tau}$ to ensure the long-term performance of modified binders are presented in Figure 54. The thresholds are chosen to distinguish worst-performing binders (modifier K in this study) based on the limited data set tested and require further validation.

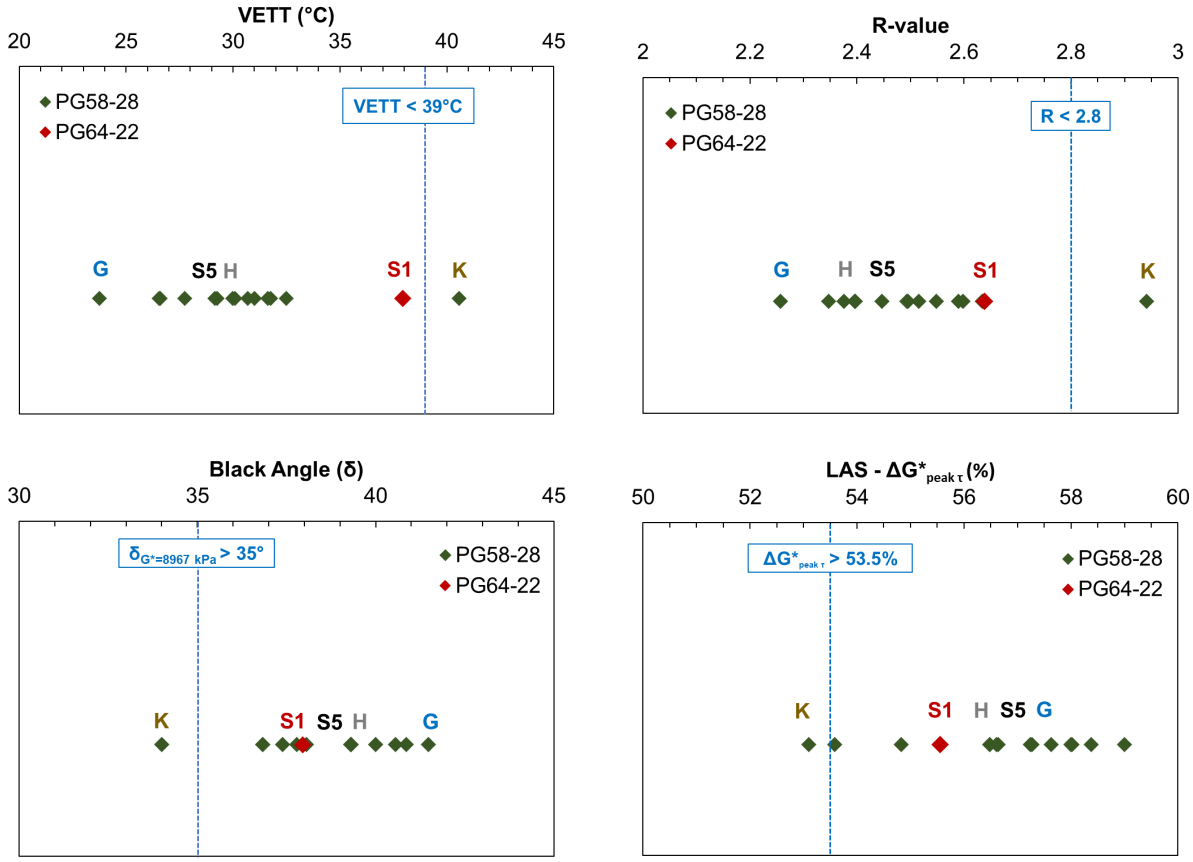

Figure 54. Graphs. Thresholds for VETT, R-value, black angle, and $\Delta G^*_{peak\ \tau}$ for modified binders.

CHAPTER 6: MIXTURE PERFORMANCE

This chapter discusses the effects of the modified binders on mixture cracking and rutting performance characteristics. The Illinois Flexibility Index Test (I-FIT) and the Hamburg Wheel-Track Test (HWTT) were conducted. A selected set of modified binders representing different types of modifiers (vegetable oil, fatty acid derivative, glycol amine, ReOB, and petroleum based) along with an unmodified counterpart (S5) were used to develop a laboratory design asphalt concrete (AC) mixture. In addition, a set of plant mixtures with and without modifiers from two field study sections were also investigated. Table 13 provides a summary of laboratory and plant mixtures with their respective modified binders used in this study. (Refer to Appendix F for mix design details.) The mixtures were also evaluated for long-term cracking performance by aging compacted I-FIT specimens for 3 days at 95°C in a conventional forced draft oven as per Al-Qadi et al. (2019).

Table 13. Asphalt Concrete Mix Design Information for Laboratory and Plant Mixtures

Mix ID	Mixture Type	Binder ID	Binder PG	Modifier Used	N Design	NMAS[3] (mm)	AC	Design VMA[4]	AV[5]
S5	Lab Mix; CDG[1]	S5	58-28	–	N70	9.5	6.3%	15.4%	4.5%
C	Lab Mix; CDG	S1-C-3.1	58-28	C	N70	9.5	6.3%	15.4%	4.5%
F	Lab Mix; CDG	S1-F-3.1	58-28	F	N70	9.5	6.3%	15.4%	4.5%
G	Lab Mix; CDG	S1-G-6.5	58-28	F	N70	9.5	6.3%	15.4%	4.5%
H	Lab Mix; CDG	S1-H-10	58-28	G	N70	9.5	6.3%	15.4%	4.5%
K	Lab Mix; CDG	S1-K-10	58-28	H	N70	9.5	6.3%	15.4%	4.5%
PM1	Plant Mix; CDG	S8	58-28	NA[6]	N70	9.5	6.0%	15.5%	4.0%
PM2	Plant Mix; CDG	S9-L-NA	58-28	L	N70	9.5	6.0%	15.5%	4.0%
PM3	Plant Mix; FDG[2]	NA	NA	NA	N100	12.5	5.1%	15.1%	4.1%
PM4	Plant Mix; FDG	NA	NA	F	N100	12.5	5.1%	15.1%	4.1%

CDG[1]—coarse dense graded; FDG[2]—fine dense graded; NMAS[3]—nominal maximum aggregate size; VMA[4]—voids in mineral aggregates; AV[5]—air voids; NA[6]—not available.

ILLINOIS FLEXIBILITY INDEX TEST

I-FIT was conducted on laboratory and plant mixtures for both unaged and long-term-aged conditions as per Illinois Modified AASHTO TP 124-18. Figure 55 presents the I-FIT parameters for unaged and aged laboratory mixtures. The flexibility index (FI) indicates the cracking resistance of an AC mixture. A higher value represents better cracking resistance. The highest average unaged FI of 17.3 occurred in the C-modified mixture, while it was the lowest (11.1) for the G-modified mixture followed by the K-modified mixture.

With long-term laboratory aging (LTA) of 3 days at 95°C, the C-modified mixture still outperformed the rest of the modifiers, while K- and G-modified mixtures showed lower cracking performance than the rest of the mixtures. The superior performance of the C-modified mixtures and poor performance of the K-modified mixtures complement the findings from binder rheology. Modifier G showed the best performance in binder rheology testing but performed the worst in I-FIT mixture testing. This may be attributed to modifier G's high volatility and consequent material loss during mixing (lower binder content or loss of softening components) or its susceptibility to dissolve in water and

consequent moisture susceptibility in mixture level. As a future work, we recommend testing of recovered binder to check for the loss of volatiles and exploring other potential reasons that may include loss of adhesion.

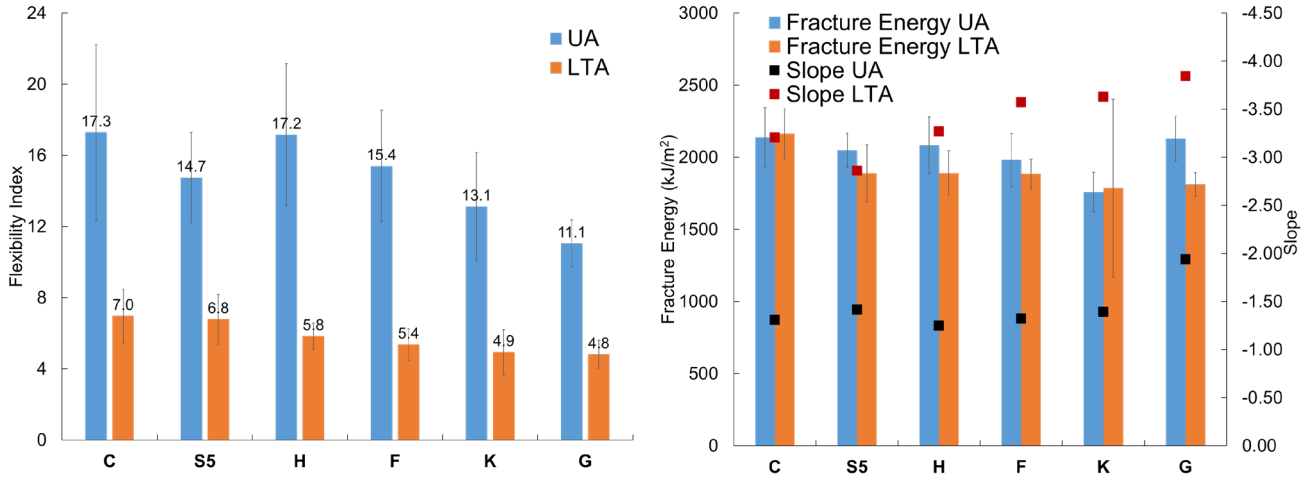

Figure 55. Graphs. I-FIT parameters for laboratory asphalt concrete mixtures.

Figure 56 presents the I-FIT parameters for mixtures collected from two field sections. Plant mixes (PM) 1 and 2 were collected from a field section paved near Chicago, Illinois, in August 2019. An unmodified binder S8 was used in PM1, while PM2 was designed with a modified binder S9-L-NA. The average FI for unaged PM1 was 11.3 and that of PM2 was 9.3. The FI for the LTA condition was 4.6 for the PM1 mixture and 4.3 for the PM2 mixture. As a result, the I-FIT results for those two mixtures were comparable to each other.

PM3 and PM4 were sampled from a pilot study conducted by the Minnesota Department of Transportation on modifiers. PM3 is a control fine, dense-graded mix with 25% reclaimed asphalt pavement (RAP), while PM4 is a high recycled fine, dense-graded mix with 45% RAP and modifier F. The mixes were placed in 2018 with the objective to evaluate the effectiveness of modifiers for improving mixture cracking performance for high recycled mixes. These mixtures were stored in a temperature-controlled environment (at 4°C) until tested in 2021. The average FIs for PM3 and PM4 were close to each other and were equal to 7.9 and 7.7, respectively, for unaged conditions. However, the long-term aging performance of a high recycled mix with modifier F showed a slightly higher FI of 4.1 compared to the control mix with FI of 3.3, indicating better cracking performance. The post-peak slope before and after aging was higher for PM2 than PM1, while it was lower for PM3 in the unaged condition but increased compared to PM4 after long-term aging. The fracture energies for PM1 and PM2 were higher than PM3 and PM4 at both unaged and LTA conditions.

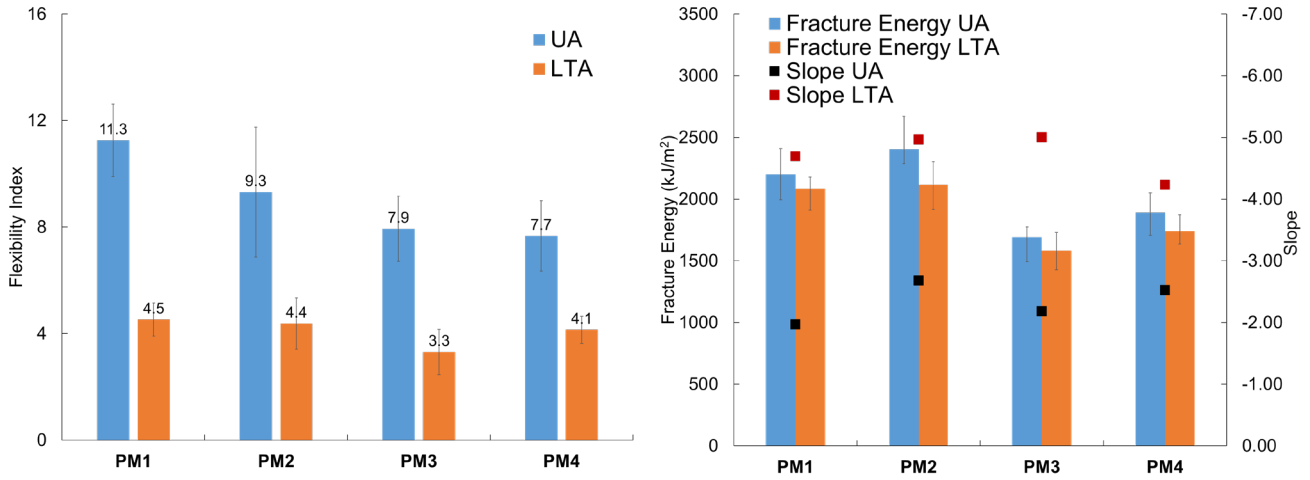

Figure 56. Graphs. I-FIT parameters for plant asphalt concrete mixtures.

HAMBURG WHEEL-TRACK TEST

Rutting potential for the mixes was evaluated using HWTT as per Illinois modified AASHTO T324. The laboratory and plant mixtures had PG 58-28, which requires a rut depth of no more than 12.5 mm at 5,000 passes. Figure 57 shows that all mixtures passed the HWTT test. In laboratory mixtures, the S5 mix performed the worst, while the modifier G mix performed the best. In the case of plant mixtures, mix PM2 (modified) performed better than PM1 (unmodified), while for plant mixes PM3 and PM4, the latter mix showed better rutting resistance than the former.

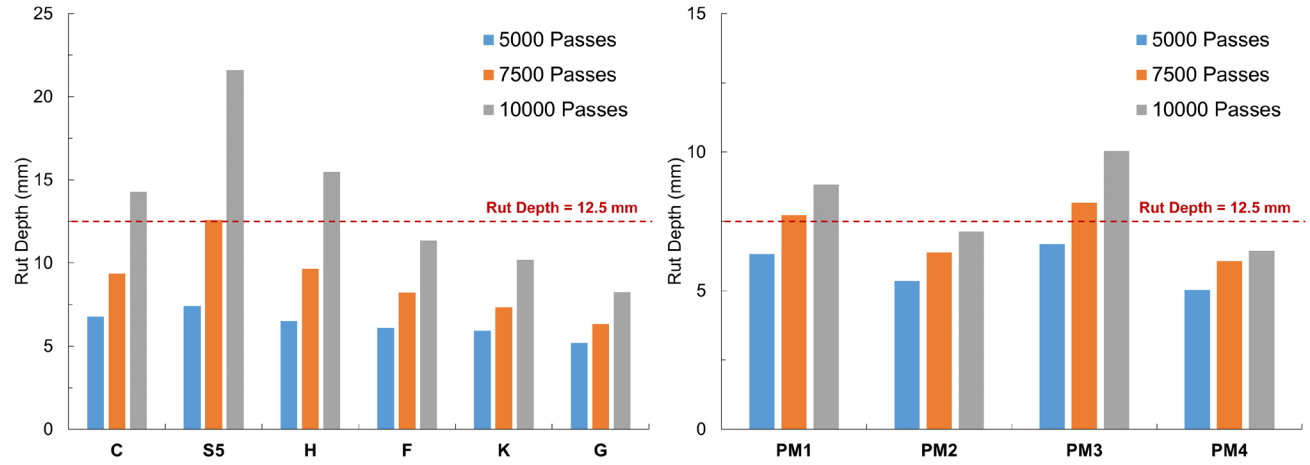

Figure 57. Graphs. Rut depths from HWTT for laboratory and plant asphalt concrete mixtures.

BALANCED MIX PERFORMANCE

Figure 58 presents the balanced mix performance of the lab and plant mixtures evaluated in the study. All laboratory mixtures, except K- and G-modified mixtures, pass the criteria for cracking and rutting at both unaged and LTA conditions for Illinois. K- and G-modified mixtures marginally fail the cracking criterion at LTA condition as per IDOT's current recommendations. PM1 and PM2 also had

acceptable rutting and cracking performance required in Illinois for unaged and LTA conditions. The Minnesota PM3 and PM4 mixtures had acceptable rutting performance but their cracking performance for the unaged condition was less than 8.0 (as required by Illinois). However, for the LTA condition, PM4 showed acceptable performance in both rutting and cracking, while PM3 failed the cracking performance criteria required in Illinois (FI > 4.0 for plant mixtures).

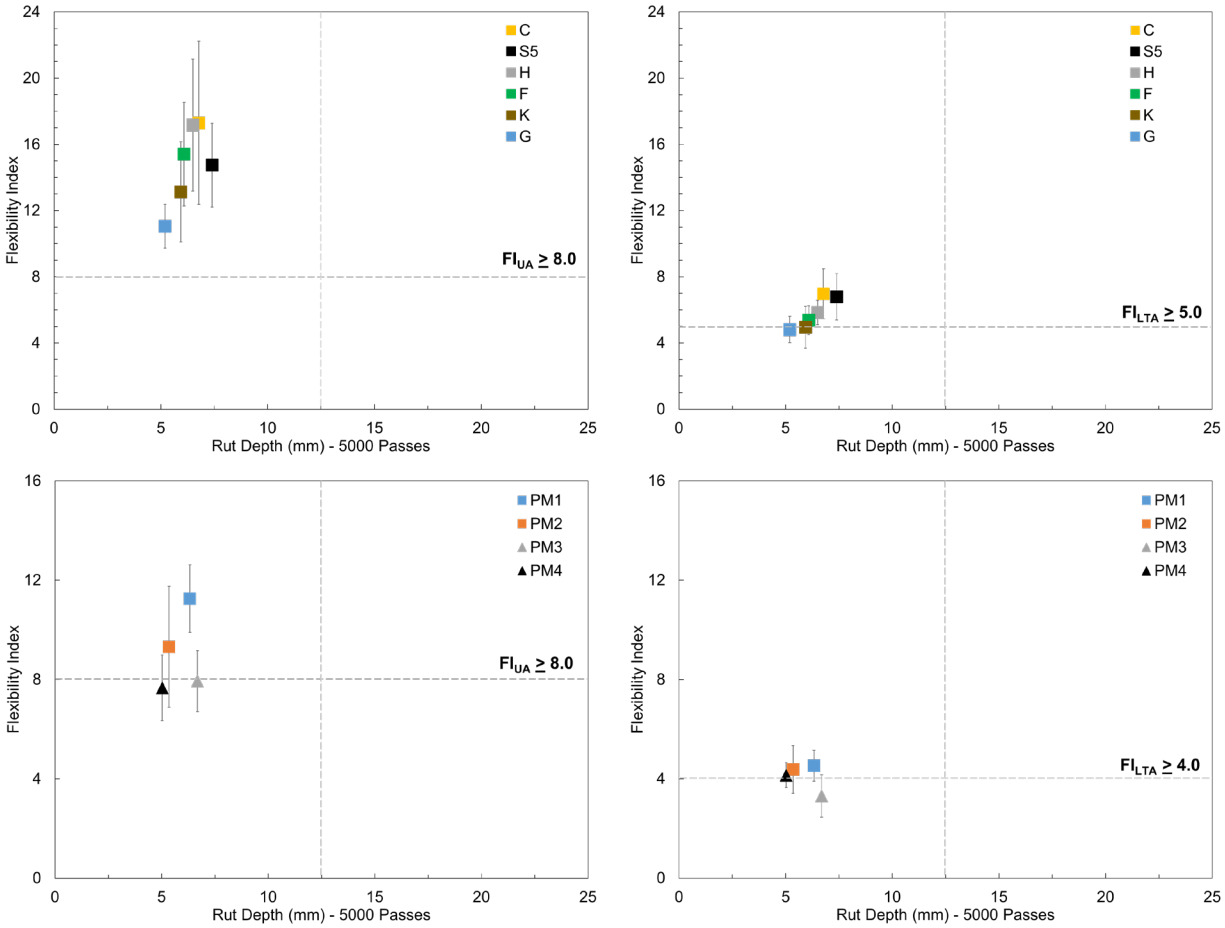

Figure 58. Graphs. Balanced mix design for unaged and long-term aging for laboratory and plant asphalt concrete mixtures.

BINDER-MIX RELATIONSHIP

Relationships between asphalt binders' rheological parameters and their respective mixes' FI and HWTT rutting indices were sought. Table 14 and Table 15 are covariance matrices. Values higher than 0.85 are in bold. Fracture energy during I-FIT appears to be related the binder's rheology. These relationships are illustrated with examples in Figure 59; high correlations are an artifact of the similarity between binder' parameters. It appears there is no significant correlation between asphalt binders' rheological parameters and their respective mixes' I-FIT and HWTT results. The solicitations asphalt binders are subjected to during binder testing are not present or similar to those occurring in mixture tests. Therefore, a correlation is not expected.

A better correlation was observed between FE and rheological binder parameters. This may be because fracture energy (FE) in the I-FIT experiment is significantly affected by initial mixture stiffness before crack propagation starts. Initial mixture stiffness can be better correlated with the changes in the binder stiffness represented by a list of rheological parameters studied, as also shown in Table 14. Therefore, the modulus type of experiments can be used in the future to verify the correlation between binder and mixture properties. Still, a moderate correlation of FI with VETT and $\Delta G^*_{Peak\ \tau}$ was observed when the mix modified with binder G was excluded (Figure 60 and Figure 61). The unaged FI showed better correlation than LTA aged FI. However, the data set is limited; hence, further evaluation is required to establish any relationship between these parameters.

Table 14. Covariance Matrix for I-FIT Parameters and Binder Parameters

		PAV							
		GRP	VETT	R-value	Black Angle	$GRP_{f,\ adjusted}$	$\Delta G^*_{Peak\ \tau}$	ΔT_c	GRP_f
STA	FE.UA	**−0.95**	**−0.92**	**−0.91**	**0.96**	**−0.9**	0.85	**0.89**	**−0.94**
	FI.UA	−0.28	−0.47	−0.46	0.29	−0.32	0.58	0.11	−0.41
	Slope.UA	0.19	−0.01	−0.01	−0.18	0.14	0.15	−0.31	0.07
	S.UA	−0.46	-0.3	−0.31	0.46	−0.36	0.17	0.56	−0.34
LTA	FE	−0.61	−0.64	−0.58	0.58	−0.77	0.6	0.45	−0.73
	FI	−0.61	−0.57	−0.53	0.59	−0.69	0.51	0.5	−0.66
	Slope	−0.38	−0.35	−0.33	0.38	−0.39	0.32	0.31	−0.39
	Strength	−0.53	−0.56	−0.56	0.53	−0.48	0.55	0.51	−0.53
		2PAV							
		GRP	VETT	R-value	Black Angle	$GRP_{f,\ adjusted}$	$\Delta G^*_{Peak\ \tau}$	ΔT_c	GRP_f
STA	FE.UA	**−0.92**	**−0.97**	**−0.95**	**0.93**	**−0.9**	**0.91**	**0.98**	**−0.9**
	FI.UA	−0.26	−0.41	−0.43	0.59	−0.37	0.17	0.36	−0.17
	Slope.UA	0.19	0.07	0.04	0.11	0.08	−0.26	−0.13	0.29
	S.UA	−0.45	−0.38	−0.36	0.21	−0.34	0.56	0.42	−0.5
LTA	FE	−0.65	−0.62	-0.5	0.69	−0.73	0.29	0.6	−0.63
	FI	−0.62	−0.6	−0.52	0.61	−0.64	0.41	0.62	−0.64
	Slope	−0.36	−0.4	−0.38	0.4	−0.35	0.32	0.44	−0.41
	Strength	−0.52	−0.54	−0.53	0.52	−0.54	0.51	0.49	−0.43

Table 15. Covariance Matrix for HWTT Rut Depth and Binder Parameters

		PAV							
		GRP	VETT	R-value	Black Angle	$GRP_{f,\ adjusted}$	$\Delta G^*_{Peak\ \tau}$	ΔT_c	GRP_f
Rut depth at	X5000.Passes	−0.31	−0.33	−0.32	0.3	−0.34	0.33	0.27	−0.34
	X7500.Passes	−0.37	−0.36	−0.37	0.38	−0.35	0.36	0.38	−0.36
	X10000.Passes	−0.37	−0.36	−0.36	0.37	−0.33	0.35	0.38	−0.34
		RTFO							
		GRP	VETT	R-value	Black Angle	$GRP_{f,\ adjusted}$	GRP_f		
Rut depth at	X5000.Passes	−0.78	−0.71	−0.37	0.29	−0.7	−0.37		
	X7500.Passes	−0.59	−0.58	−0.42	0.35	−0.48	−0.11		
	X10000.Passes	−0.56	−0.55	−0.42	0.34	−0.45	−0.08		

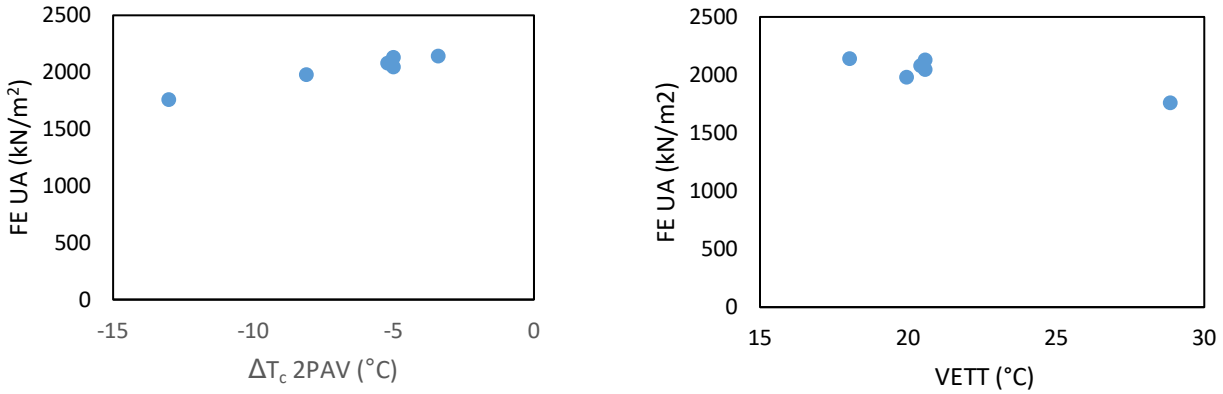

(a) (b)

Figure 59. Graphs. (a) FEUA vs DTC 2PAV and (b) FEUA vs VETT

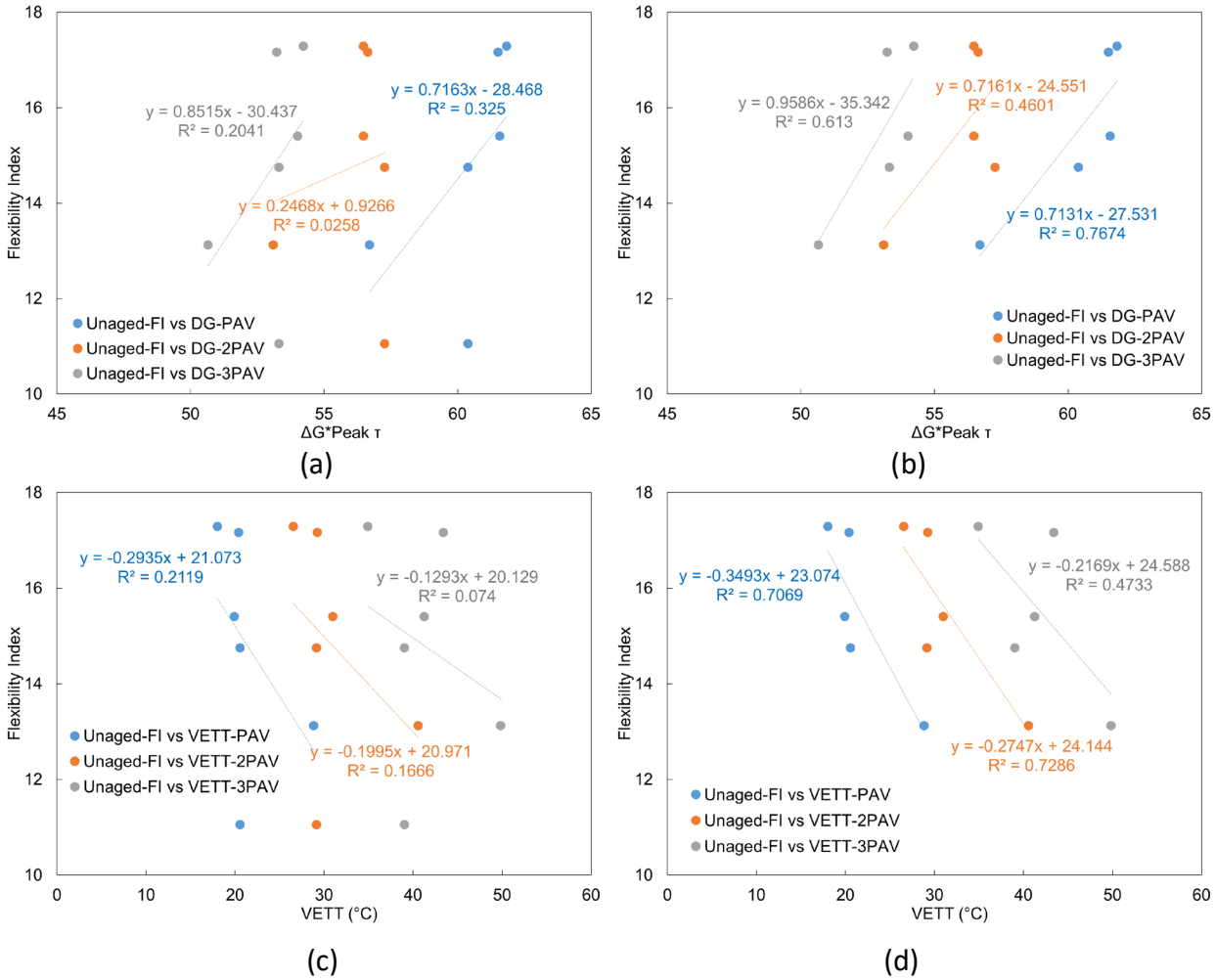

(a) (b)

(c) (d)

Figure 60. Graphs. (a) Unaged-FI vs ΔG*Peak τ, (b) Unaged-FI vs ΔG*Peak τ (without G), (c) Unaged-FI vs VETT, (d) Unaged-FI vs VETT (without G).

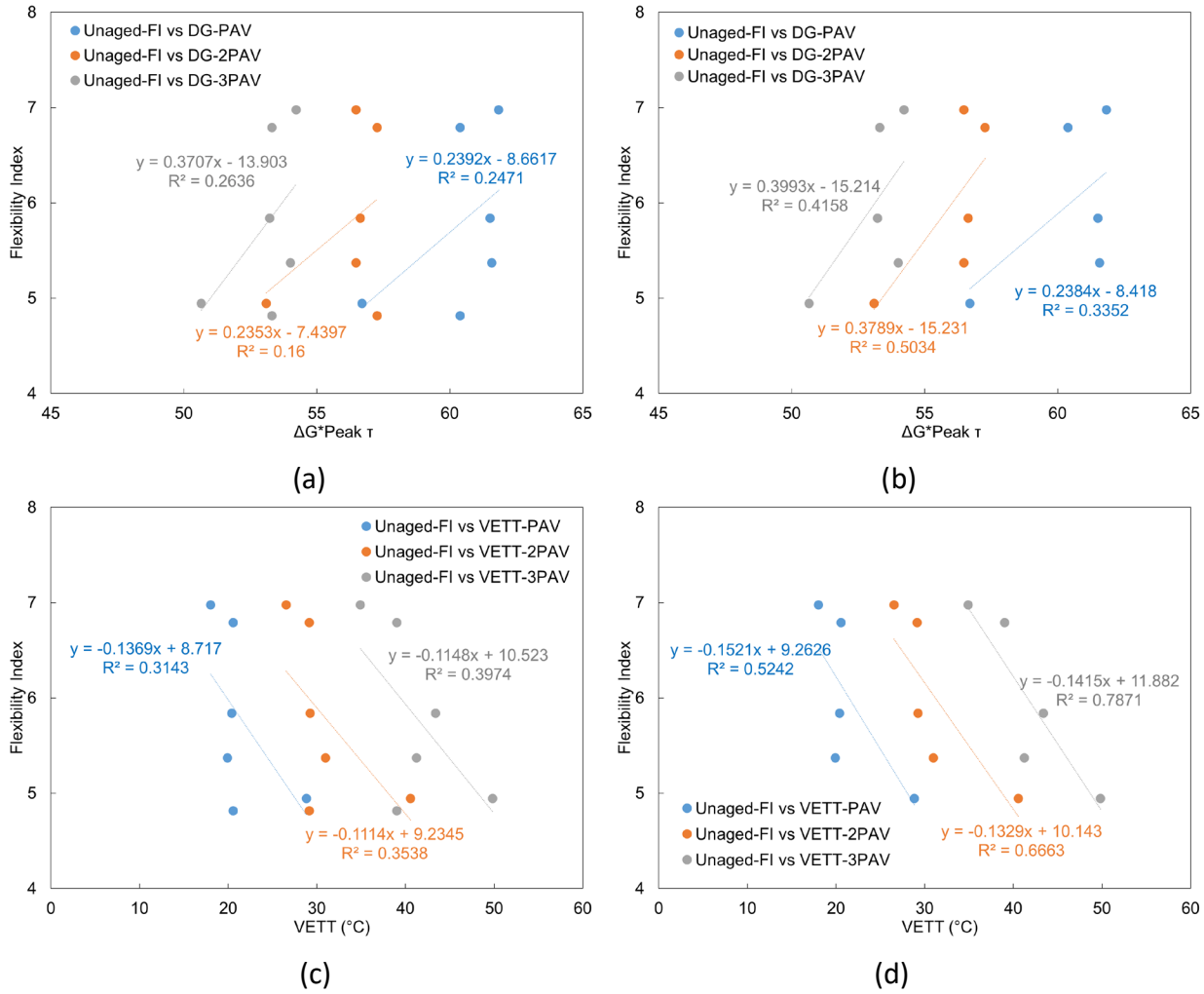

Figure 61. Graphs. (a) LTA-FI vs ΔG*Peak τ, (b) LTA-FI vs ΔG*Peak τ (without G), (c) LTA-FI vs VETT, (d) LTA-FI vs VETT (without G).

SUMMARY

Cracking and rutting tests were conducted on mix designs prepared and compacted in the laboratory as well as the loose mixture samples collected from various sites. Findings from the laboratory tests on mixes containing various modifiers are as follows:

- There are some significant differences between mixes' cracking performance when they are prepared with different types of modifiers. The trends in the mix results are generally consistent with rheological and chemical characteristics. The worst-performing modifier (K) and one of the best-performing modifiers (C) ranked similarly according to FI.

- Modifier G was among the best performing according to rheological and chemical properties. However, it ranked right above modifier K according to FI. Thermal stability and moisture susceptibility characteristics reported in Chapters 4 and 5 for modifier G may have played a role in this result.

- In PM3 and PM4, the outcome of modification seemed successful. The modified mix achieved similar cracking performance compared to the control mix. In the case of PM1 and PM2, the effect of modification was evident when comparing unaged FI. However, the aged FIs were in a similar range.

- Rutting performance of the mixes with different modifiers showed some sensitivity to modifiers. Note that all modified mixes performed better than the unmodified PG 58-28 binder.

- The correlation of the cracking parameter from mixtures to binders does not correlate well and needs further investigation.

CHAPTER 7: SOURCE VARIABILITY

This chapter presents an effort to quantify the importance of base binder properties. The base asphalt binder is the primary component in a modified asphalt binder. The behavior of modified asphalt binders could be defined by their base binder. The base-modifier compound effect might be different if the base is changed.

Modifiers were selected based on the differences in chemical composition and rheological performance. Modifiers were used to modify a different base binder (S2) of the same grade: PG 64-22. One modifier from each of the groups that emerged when analyzing testing data from Chapter 3 was selected: B (fatty acid derivative), G (glycol amine), F (vegetable oil), H (petroleum based), and K (ReOB). The base binder obtained was from a different terminal and make than S1. The same doses of modifiers were used as described in Chapter 3. The same experiments that were ran for modified S1 binders were performed on unaged and 2PAV, modified (S2-B-5.0, S2-G-6.5, S2-F-3.1, S2-H-10, and S2-K-10), and unmodified (S2) binder samples. ΔT_c was obtained at the PAV aging condition because the data was readily available from PG testing.

Rheology testing results of the base binders are presented and discussed. Results of the modified binders are presented and discussed relative to their modified S1 counterparts. Then, chemistry testing results are presented and discussed to explain how modifiers acted in comparison to how they acted with S1. Finally, a discussion is provided about the importance of base binder in dose and modifier selection.

Rheology

Base Comparison: S1 vs S2

Before comparing the modified products, base binders are compared. Table 16 summarizes the rheological testing results. The main differences between the base binders are that binder S2 has a higher modulus at DSR testing frequencies and a lower modulus at BBR testing frequencies as well as a higher phase angle across the whole frequency spectrum, at any aging condition. Figure 62 illustrates this for the 2PAV aging condition. As a result, for S2, the low-temperature PG and ΔT_c are S-controlled, i.e., high stiffness is critical and not relaxation properties (m-value). The crossover modulus and frequency ($|G^*_c|$ and w_c) as well as black angle are higher than those of S1. VETT of S2 is lower than that of S1. GRP_f is similar because it was measured at a frequency in which the behavior of both binders is different. Based on these parameters and master curves compared in Figure 62, these two binders have some distinctive rheological characteristics over a spectrum of temperatures and frequencies despite their same PG. From the low- and intermediate-temperature cracking perspectives, S2 has properties that would be expected to yield better performance.

Table 16. Rheological Comparison between S1 and S2

Binder ID	S1	S2
Performance Grading		
High PG	66.4	65.9
Intermediate PG	22.9	23.9
Low PG (m-value)	−23.7	−24.6
Low PG (Stiffness)	−27.5	−23.4
RTFO Mass Loss (%)	0.28	0.42
Low-temperature non-load-related parameters		
ΔT_c PAV	−3.8	1.3
ΔT_c 2PAV	−7.8 (m-value controlled)	−1.7 (S-controlled)
GRP (kPa, at 15°C and 0.005rad/s) at 2PAV aging condition	875	272
Crossover parameters at 2PAV aging condition		
w_c (Hz, at 15°C)	0.0023	0.070
$\lvert G^*_c \rvert$ (MPa, at w_c)	2.3	8.4
VETT (°C)	37.9	25.9
R-value	2.64	2.08
Fatigue-related parameters at 2PAV aging condition		
Black angle (°)	37.4	44.8
NCHRP 9-59's GRP_f (kPa)	11,503	6971
LAS' $\Delta\lvert G^* \rvert_{peak\ T}$ (%)	55.6	57.0

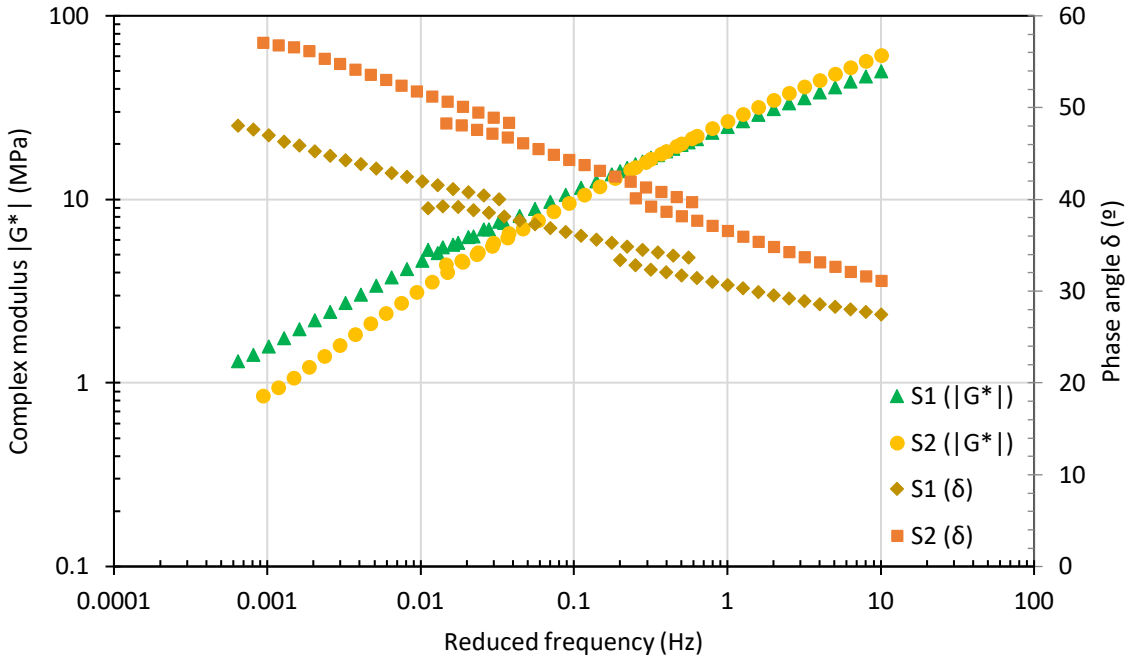

Figure 62. Graph. Master curve and phase angle plot for base binders at 2PAV aging condition.

Modified Binder Comparison

Table 17 provides a rheological result comparison of modified S2 binders and the control PG 58-28 unmodified binder, S5. All modified S2 binders inherited their main properties from the parent S2 binder, such as higher phase angles, higher moduli, and being stiffness controlled at low temperatures (except S2-K-10). S2-B-5.0, S2-F-3.1, S2-G-6.5, and S2-H-10 did not reach PG 58-28 grade. If S2 had been modified with higher dosages, the PG would have been reached. The same dosage may not work for all PG 64-22 base binders.

Table 17. Rheological Comparison between S5 and Modified S2 Binders

Binder ID	S5	S2-B-5.0	S2-F-3.1	S2-G-6.5	S2-H-10	S2-K-10
Performance grading						
High PG	61.1	60.4	59.5	61.7	61.0	59.2
Intermediate PG	17.9	21.2	19.3	19.5	19.2	19.3
Low PG (m-value)	−29.5	−28.0	−29.4	−27.5	−30.2	−32.2
Low PG (Stiffness)	−30.0	−26.1	−28.3	−25.4	−28.8	−30.8
PG	58-28	58-22	58-28*	58-22	58-28*	58-28
RTFO Mass Loss (%)	0.63	0.63	0.36	2.98	0.52	0.38
Low-temperature non-load-related parameters						
ΔT_c PAV	−5.0	1.9	1.2	2.2	1.4	−1.3
ΔT_c 2PAV	−9.0	0.5	0.3	1.1	0.7	−4.4
GRP (kPa, at 15°C and 0.005rad/s) at 2PAV aging condition	248	55	85	49	85	119
Crossover parameters at 2PAV aging condition						
w_c (Hz, at 15°C)	0.0377	0.5194	0.4053	0.6126	0.3267	0.0589
$\lvert G^*_c \rvert$ (MPa, at w_c)	3.6	11.93	10.13	12.53	8.7	3.4
VETT (°C)	29.2	18.9	20.0	18.4	20.9	27.2
R-value	2.44	1.92	1.99	1.90	2.06	2.47
Fatigue-related parameters at 2PAV aging condition						
Black angle (°)	38.1	47.6	45.0	48.0	44.1	39.1
NCHRP 9-59's GRP_f (kPa)	7075	7780	8365	7072	8362	7988
LAS' $\Delta\lvert G^* \rvert_{peak\ \tau}$ (%)	57.3	57.3	59.1	53.6	55.6	54.5

*S2-F-3.1 and S2-H-10 did not pass the intermediate temperature verification for PG 58-28 binders (at 19°C).

S2-F-3.1, S2-H-3.1, and S2-K-10 can still be compared from an iso-stiffness perspective with the control S5, especially because of the mentioned limitations and challenges a priory of using G*sin(δ) to discriminate binders. S2-F-3.1 and S2-H-10 performed similarly to S5 in the small-strain tests but seemed to have a small advantage in large-strain damage tolerance ($\Delta|G^*|_{peak\ \tau}$) because of their phase angle, which also reduced material ejection during the LAS test for S2 and modified S2 binders.

S2-K-10 was the worst performer in both large- and small-strain tests when compared to other modified binders with an S2 base, except GRP_f. Modifier K changed the S2 base to be a PG 58-28 binder but was the worst performer compared to the rest of the S2-modified binders based on black angle, VETT, R-value, GRP, and ΔT_c. S2-K-10 seemed to perform better than the unmodified S5 except for the GRP_f and the large-strain parameter $\Delta|G^*|_{peak\,\tau}$. This is an important observation that highlights the extent of the base binder's impact overshadowing that of the modifiers. Figure 64 shows the importance of the modified binder's base: the relationship between VETT and black angle appears to be defined by the base binder. The relationship on the equation in Figure 22 is only valid for S1 and its modified versions. Note that S2 binders (high m-value) are not commonly found in Illinois. However, we recommend developing a protocol using multiple base binders that are representative of binders commonly used in Illinois.

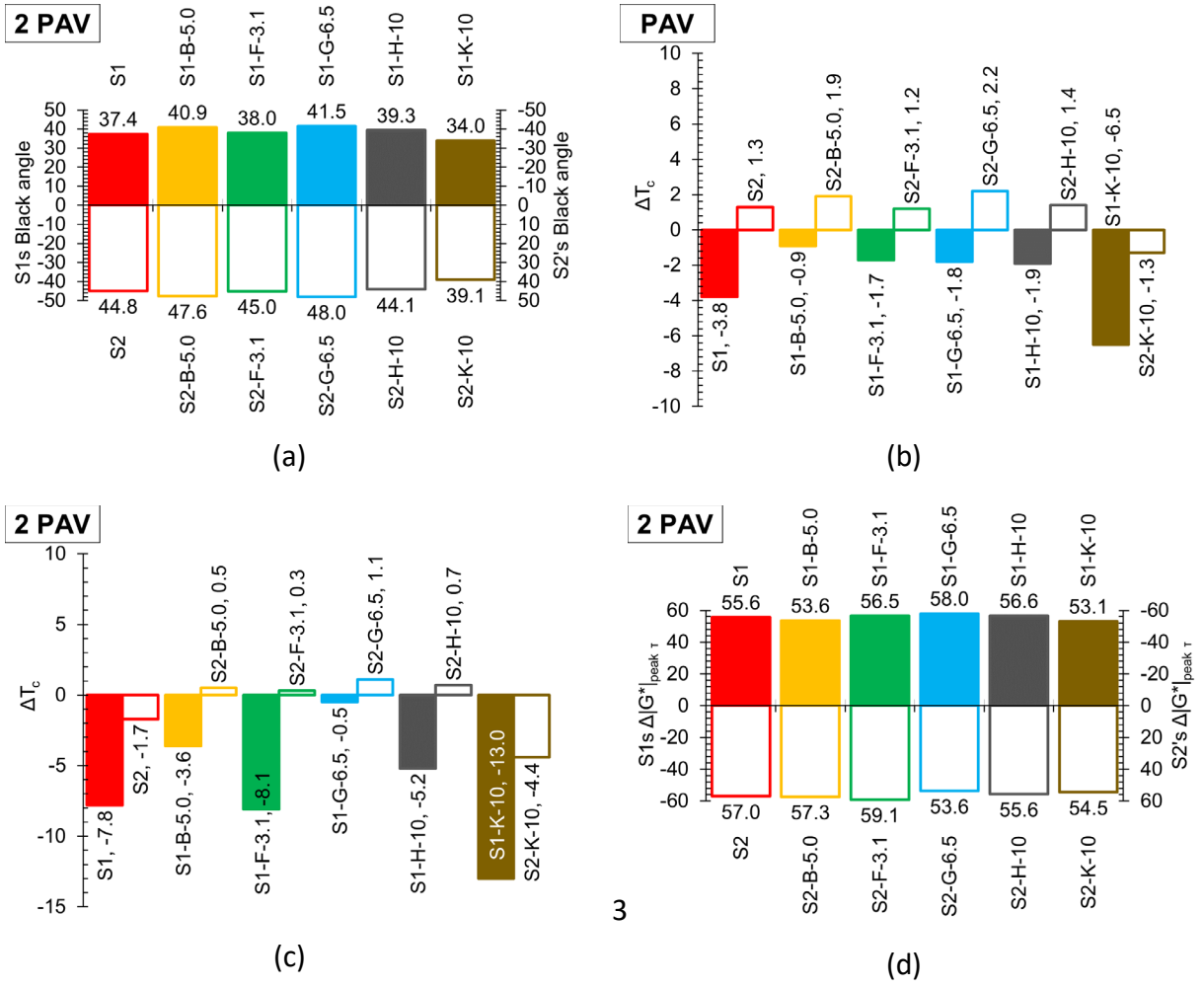

Figure 63. Graphs. Rheological parameter comparison of modified S1 and modified S2 binders at 2PAV aging condition: (a) black angle, (b) ΔT_c, (c) $\Delta|G^*|_{peak\,\tau}$, and (d) ΔT_c.

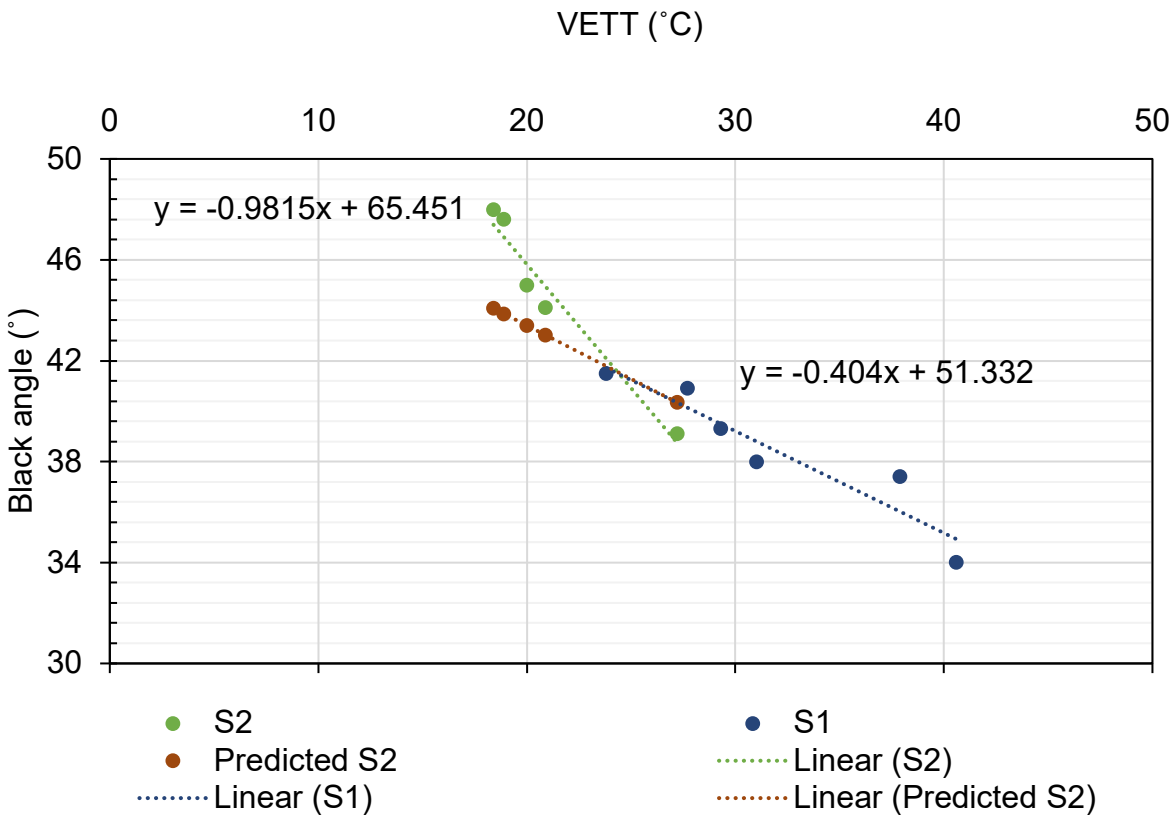

Figure 64. Plot. Relationship between VETT and black angle for modified binders with different base binders.

The required dose to meet PG seems to be dependent on the modulus change needed and not as dependent on the phase angles. In general, modifiers affected S1 and S2 in the same way: all reduced the moduli of their base binder but affected phase angles differently. In particular:

- Modifier K made the binder more brittle by reducing the phase angle. In general, this can be seen by the black angle parameter. Stiffness was critical for S2 at low temperatures. The K-modified binder (S2-K-10) became a relaxation governed binder at low temperatures (m-value controlled) rather than a stiffness-controlled binder.

- Modifiers B and G, having fatty acid derivative and glycol amine, respectively, increased the phase angle in general. This is consistent with the effects observed with the S1 base binder.

- Modifiers H and F, which include vegetable oils, did not affect phase angle significantly. This is consistent with the effects observed with the S1 base binder.

    - There is a difference in how H and F modified S1's moduli and how they modified S2's moduli. Modifier F was better at reducing the modulus for S1 than S2; modifier H was better at reducing the modulus for S2 than S1. $|G^*_c|$ is a good indicator of this. This may be attributed to the chemistry of binder S1, which showed the presence of an ester-based

functional group. This suggests more vegetable oil–based chemistry, which made modifier F (vegetable oil) more compatible to S1, while modifier H had a combination of both asphalt-like and oil-like properties, making it more compatible to S2 (no presence of ester-based functional group). However, this observation requires further investigation to be proven.

Based on the change of ΔT_c from the PAV to 2PAV aging condition, S1 (−4.0) was more susceptible to aging than S2 (−3.0). The same occurred if any S1-modified and S2-modified binders with the same modifier were compared: modified S1 binders were more susceptible to aging. Aging susceptibility also appears to have been inherited by the base binders. Modifiers F and K produced binders that were more susceptible to aging than their base when blended with S1 but not with S2. This occurred because S2 was a stiffness-controlled binder at low temperatures: the effects on m-value would not be critical at low temperatures and may not be seen with ΔT_c.

Chemistry

Base Binder Comparison: S1 vs S2

The chemical fingerprints for binders S1 and S2 were also different from each other. The FTIR spectra for S1 had a characteristic alkoxy peak at 1,261 cm^{-1} and an ester peak at 1,099 cm^{-1} after RTFO aging (Figure 65). These peaks were absent in S2 binders, indicating differences in their binder chemistries especially post-RTFO aging. Furthermore, the molecular weight distribution suggests S1 had a larger proportion of large to small molecular weight than S2.

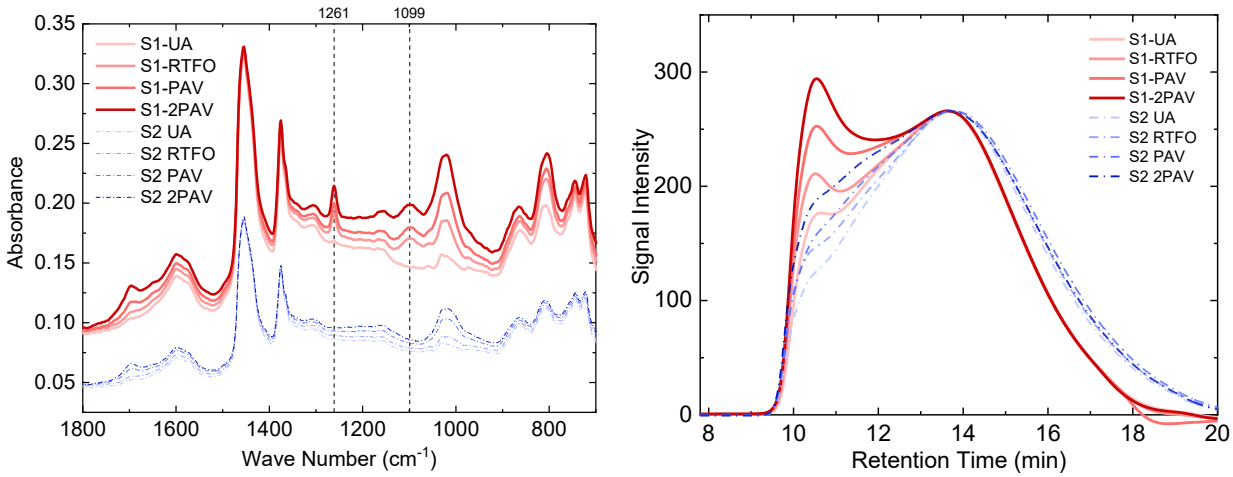

Figure 65. Graphs. (a) Typical molecular weight distribution for S1 and S2 with aging; (b) normalized molecular weight distribution at retention time 13.7 min.

Table 18 summarizes the FTIR- and GPC-based indices for S1 and S2. All evaluated indices had higher values for binder S1 than S2 irrespective of their aging condition. Higher values for the indices suggest increased oxidation, implying more potential for cracking. The molecular weights (M_n and M_w) and polydispersity index are included in Appendix D.

Table 18. FTIR and GPC Parameters for S1 and S2

Binder ID	$FTIR_{C=O}$	$FTIR_{C=O+S=O}$	MWD_{Area}
S1-UA	0.00309	0.042302	0.557793
S1-RTFO	0.005662	0.099653	0.619059
S1-PAV	0.013992	0.168551	0.699809
S1-2PAV	0.027125	0.24838	0.764188
S2-UA	0.006155	0.043614	0.391233
S2-RTFO	0.007604	0.06244	0.42021
S2-PAV	0.018853	0.141081	0.466889
S2-2PAV	0.028033	0.187975	0.542287

Modified Binder Comparison: Chemistry

The oxidation and molecular weight indices for S1 and S2 binders were plotted on the X- and Y-axes, respectively (Figure 66). The line of proportionality is the linear correlation of base binders S1 and S2 and is presented along with the line of equality. The line of quality signifies that the modified binders with S1 and S2 will have similar chemical susceptibility with aging. All S1-modified binders were plotted on the X-axis, and all S2 modified binders were plotted against the Y-axis. For example, in Figure 66, the line of proportionality for $MWD_{N,Area}$ is inclined towards S1, suggesting its higher oxidation potential over binder S2. The effect of modification of S1 with modifiers F, H, and B tends to deviate towards the line of equality, which suggests an improvement in binder aging susceptibility. This suggests these modifiers improve the properties of S1 and makes them more resistant to aging like S2. Similarly, the $FTIR_{C=O+S=O}$ for all the modifiers is shown to deviate towards the line of equality (closer to S2), suggesting that the modification improved the aging susceptibility for S1 modified binders. This suggests modification with base binder S1 is more effective than S2, as S2 is chemically more stable, which is also reflected in its rheological findings.

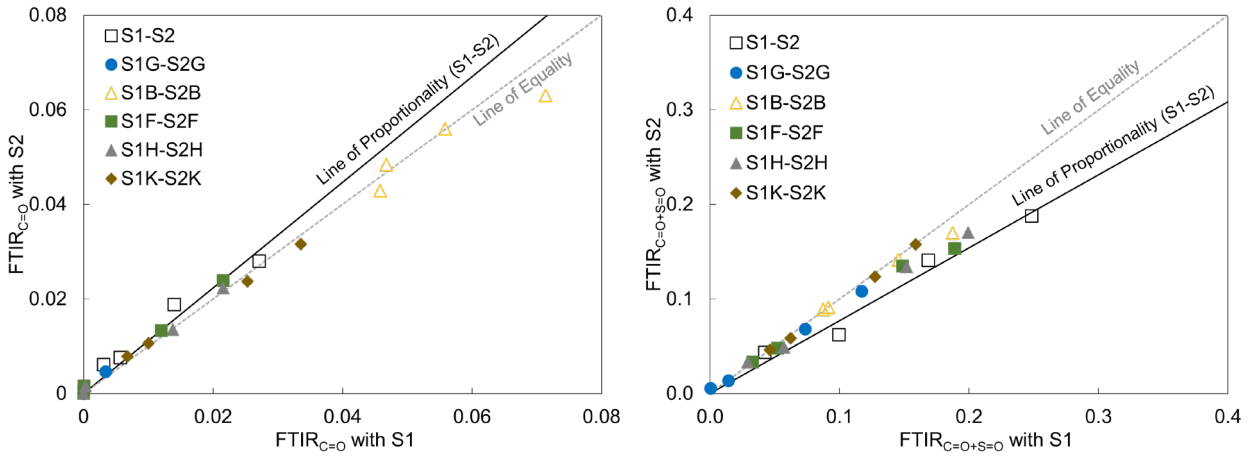

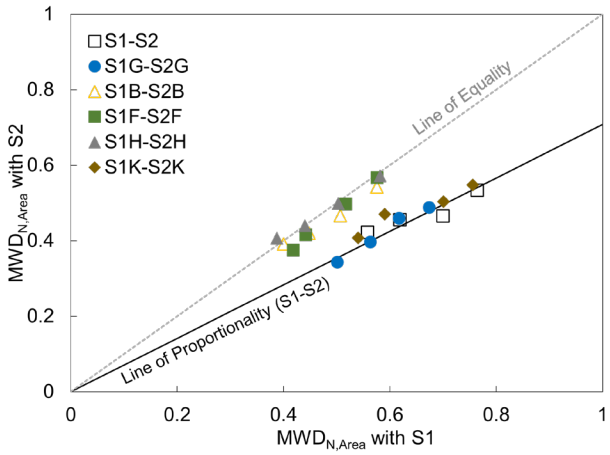

Figure 66. Graphs. Aging kinetics for S1 and S2 binders based on FTIR and GPC indices.

SUMMARY

The chemistry of a base binder impacts the modified binder chemistry and binder rheology, as presented in the findings above. However, note that the dosage required for different base binders may need to be changed to get a similar rheological response. The dosage was kept the same to make a direct comparison between the two base binders. To better evaluate the performance based on source variability, the modifier dosage for S2-modified binders needs to be adjusted to similar stiffness levels for an individual source.

Based on the rheological and chemistry parameters, in general, the ranking of the modified binder was preserved despite a significant shift in rheological and chemical characteristics. Performance based on all small-strain parameters improved after modification for all modified binders but the K-modified binder (ReOB based), even though, based on small-strain parameters, all modified S2 binders (including S2-K-10) appear better than the unmodified benchmark S5. Based on $\Delta|G^*|_{peak\ \tau}$, S2-K-10, S2-H-10, and S2-G-6.5 appear to have had worse fatigue performance than S5. S2-K-10 and S2-G-6.5 were also worse than their base binder (S2).

Modifiers affected S1 and S2 in the same way: all reduced moduli. Modifiers H and F did not affect phase angles, B and G increased them, and K decreased them. Second-order compound effects differentiating the effects of modifiers H and F on the base binder could have taken place.

The performance of these modified binders appears to be dominated by their base binders. The importance of using a wide range of binder performance characteristics that include small- and large-strain rheological and chemistry parameters are highlighted with the source variability data. An acceptable protocol must include all or some of those tests repeated periodically (as characteristics of base binder or modifiers may change) to ensure well-performing binders when they are modified with a range of modifiers. The base binder selection becomes a key parameter and may result in masking worse-performing modifiers like ReOB.

CHAPTER 8: SUMMARY, CONCLUSIONS, AND RECOMMENDATIONS

SUMMARY AND FINDINGS

The impact of a range of asphalt binder modifiers on the rheological and chemical characteristics of two commonly used unmodified binders in Illinois was evaluated. Modified asphalt binders were produced from two sources of PG 64-22 to target a PG 58-28 grade, which is one of the most used binder grades in Illinois with the increasing use of RAP and reclaimed asphalt shingles (RAS) (Trepanier, 2019). The modifiers were proprietary products derived from vegetable oil, bio-oil, fatty acid, amines, and petroleum products. The primary focus of this study was to distinguish modified binders based on their low- and intermediate-temperature cracking performance. These distresses are predominant in flexible pavements in Illinois and could be aggravated with the addition of recycled materials like RAP/RAS.

The experimental program included tests on the modifiers and modified binders at the binder and mixture levels. Fingerprinting of the modifiers was studied using chemical composition and characterization tests. The modified binders were studied at the binder level using state-of-the-practice and state-of-the-art tests at aging conditions from unaged to 3PAV-aged conditions. At the mixture level, I-FIT and HWTT were performed to evaluate the impact on cracking and rutting resistance, respectively.

To realistically evaluate the long-term performance of modified binders, binders were extracted from field-aged cores collected across Illinois. The effectiveness of laboratory long-term aging protocols was evaluated by an analysis of binders recovered from cores.

Major findings and conclusions are discussed as follows:

- There are some differences in binder performance that were not captured by PG testing alone. Even though all modified binders reached the target PG 58-28, a suite of small- and large-strain tests consistently showed that the modified binders show distinctive characteristics beyond their SuperPave grade.

- The rheological tests and the small-strain parameters (GRP, ΔT_c, GRP_f, VETT, and black angle) allowed for consistent grouping of modified binders based on the source of modifiers (vegetable oil, bio-based, fatty acid derivatives, glycol amines, and petroleum based).

- The modified binders showed a more consistent ranking after 2PAV and 3PAV between the small-strain parameters. There is a good correlation between low-and intermediate-temperature small-strain testing parameters. Therefore, there is an opportunity to potentially use some of them as surrogates and reduce the number of tests at the implementation stage.

- The large-strain rheological parameter, $\Delta|G^*|_{peak\,\tau}$, was developed from the LAS tests, allowing a more practical interpretation of extendedly aged and very brittle binders. The $\Delta|G^*|_{peak\,\tau}$ parameter and small-strain parameters were not correlated and described different characteristics of the binders. Rankings of modified binder based on the $\Delta|G^*|_{peak\,\tau}$

parameter and small-strain parameters were different except for the ReOB-based modifier K. Large-strain testing is important to ensure performance because strains in the field are expected to be larger than the linear viscoelastic limits of asphalt binders.

- Extended aging of 2PAV and 3PAV better separates the modified binders' rheological testing parameters than the PAV-aged condition. The PAV aging condition may not simulate field aging properly.

- Both large-strain testing and aging more severe than 2PAV should be considered for inclusion in a softener-modified asphalt binder discrimination protocol. Furthermore, evaluation of field-aged binders showed that binders aged 10–15 years typically correspond to 2PAV to 3PAV laboratory-aged binders.

- Chemistry-based parameters were effective in distinguishing characteristic properties of modified binders in terms of functional groups or molecular weight. However, the rate of aging appeared to be reasonably close to each according to the $FTIR_{C=O}$, $FTIR_{CO+S=O}$, and $MWD_{N,Area}$ indices. Based on the results, it can be concluded that base binder was the main driving factor affecting aging trends.

- Even though it may not be possible to develop performance-related threshold-based chemistry parameters, they were proven to be important in identifying binders with extreme performance (like G, lower rate of aging indices)

- Chemical characterization of modified binders complements the rheological findings, but at this point, chemical testing alone is not sufficient to discriminate modified binders. However, most of the modified binders behaved reasonably close to each other even with distinct modifier types based on their origin (vegetable oil, fatty-acid derivatives, glycol amines, or petroleum based).

- Modifier chemistry tests provided a good description or "fingerprint" characteristics. They can be used as a quick assessment for verifying the production quality of modifiers. Chemical functionalities of modifiers like vegetable oils or amines were demonstrated by the FTIR fingerprint and their molecular weight distribution using GPC tests. The vegetable oil–based modifier shows a presence of distinct fingerprint region with carbonyl and ester functional groups, and the glycol amine–based modifier shows characteristic amide peaks and amine peaks.

- As per SARA analysis, modifier K was high in saturates and insoluble residue, which may result in the formation of a gel-type asphalt structure. This is one of the reasons for poor cracking performance and cannot be identified from tests like FTIR and GPC.

- According to the fingerprint tests, the modifier H, which was initially assumed to be an asphalt-based modifier, showed that it could be a combination of vegetable oil and asphalt-based modifier. Chemical tests have the potential to be used for fast-tracking quality

assessment of the modifiers and modified binders as the formulations may be altered by the manufacturer.

- Based on the binder chemistry and rheology, modifier K (ReOB) was flagged by several tests and has been shown to have detrimental effects on performance. It was the only modifier to reduce the black angle and ΔT_c, as well as increase the VEET, after modifying each of the base binders. While G was one of the modifiers that consistently showed adequate properties when added to the main base binder (S1), it showed the worst relative performance when tested for mixture performance in I-FIT. This may be explained by the high mass loss and lower thermal stability of the G-modified binder. The effect of high mass loss was not clear at binder-level testing but may have a significant impact on mixture volumetrics affecting mixture performance. Another possible reason for its poor performance may be because of moisture damage as modifier G was soluble in water. Additional testing is required to further evaluate the possible reasons for its poor performance.

- Modifier C, in contrast, showed acceptable performance at the binder level and was best performing at mixture-level testing. Even though modified binders can be grouped differently based on rheological and chemical properties, they all showed acceptable mixture performance. There was not enough evidence and data from the mixture performance tests to set an arbitrary threshold to accept or reject the modifiers, except K and G.

- There was a significant change in the modified binders' rheological characteristics when the source of the base binder changed to S2. The same dosage applied to binder S1 did not apply to binder S2 for some of the modifiers. There was a significant shift in the ranking of binders with the S2 base binder. Modifier F performed better than modifier H in S1 while the opposite was observed for S2. Even though modifier K was still the worst performer with S2, the performance of modifier K was comparable to or better than the original unmodified PG 58-28 (S5).

- Based on source variability analysis, the importance of implementing a routine testing protocol was highlighted. It can be expected that base binders and modifiers are subjected to change with different suppliers. It is important to have a testing protocol in place to ensure the quality of modified binders.

- Mixture performance testing proved to be an important indicator to categorize the modifier effect. Based on the results from the cracking and rutting tests, the performance of modifier G was clearly distinguished from the other modifiers. The trend in the mixture tests was opposite of that in the binder-level tests. Thermal stability and high mass loss characteristics resulted in more brittle cracking and lower rutting performance. Furthermore, the effect of ReOB was also captured in the mixture performance tests. However, all modified binders showed acceptable performance in the mixture level as per Illinois requirements, except G and K, which marginally failed the LTA requirements for I-FIT.

- Rheological and chemical characterization of field cores showed a clear differential in aging through the pavement depth. According to the rheological parameters, aging severity can be

as high as 3PAV at the surface and as low as unaged or RTFO aging at 12 in. below the surface. The existing long-term aging protocol (PAV) for binders may not truly represent the field conditions at the pavement surface in Illinois. The laboratory-aged characteristics may fall somewhere between PAV to 2PAV or 2PAV to 3PAV based on the parameter of interest centered on a reference asphalt binder (S1). Therefore, laboratory aging of 2PAV or higher is recommended to distinguish modified binder performance. Because the rankings of binders and performance trends were consistent between 2PAV and 3PAV based on the rheological parameters, 2PAV appears as the recommended aging protocol from a practical standpoint.

- Based on the study findings, Table 19 proposes preliminary thresholds subject to validation upon further testing.

Table 19. Proposed Preliminary Threshold Summary for Rheological Parameters

Corresponding Distress/Behavior described	Aging Condition	Parameter	Suggested Threshold
Low-temperature non-load-related cracking	PAV	ΔT_c	$\geq -5°C$
Intermediate temperature response to solicitation	2PAV	VETT	$\geq 39°C$
Intermediate temperature response to solicitation	2PAV	Black Angle	$\geq 35°$
Intermediate temperature fatigue load associated cracking	2PAV	$GRP_{f,\ adjusted}$	$\leq$ 14,000 kPa
Intermediate temperature damage tolerance, large strain	2PAV	$\Delta G^*_{peak\ \tau}$	$\geq$ 53.5%

Based on a testing program examining the modifiers and modified binders, it can be concluded the modifiers can cause significant changes in the binders' long-term performance characteristics. Furthermore, the changes can be affected by the base binder. There were clear and distinctive groupings of modified binders based on their respective modifiers' origins. Even though there are some differences and clear groupings in the binder- and mixture-level performance of the rest of the modifiers, mixture-level tests resulted in comparable performance with the original unmodified binder.

The differences in the rheological and mixture performance are not significant enough among most of the modified binders to set arbitrary thresholds without any further evidence. However, marginal products can be clearly flagged using the proposed screening protocol. According to the data produced in this study, such a screening protocol should be able to flag modifiers like K and G.

RECOMMENDATIONS

Figure 67 suggests a possible implementation protocol to evaluate the performance of modified binders in Illinois. This protocol was developed considering that binder quality should be adequate and that implementation for IDOT and contractors should be easily attainable. The protocol and all thresholds are based on the limited data set tested in this project and require further validation.

To complement the schematic, note the following for protocol application:

- Two different testing suites are proposed. The first is to support IDOT's existing routine quality assurance protocols. The second is a new protocol that can be implemented at the product approval stage and repeated yearly or when product formulation changes.

For yearly approval:

- Modified binders modified with at least two distinct base binders (e.g., with different m-values) should be provided by the manufacturer because the contribution of base binder is significant on modified binder properties.

- Manufacturers should provide a complete PG in addition to the ΔT_c calculated at the PAV aging condition.

- Additionally, modified binders should be tested at the 2PAV condition for providing intermediate- and low-temperature rheological parameters, as described in Figure 67. The results should comply to the suggested preliminary thresholds as per Table 19

- FTIR spectra and SARA composition for the modifiers and unaged modified binders should be provided by the manufacturers.

For routine testing:

- Once the binder is approved, routine testing should include determination of PG and ΔT_c calculated at the 2PAV aging condition.

- Additional testing for 2PAV-aged binders should be limited to one of the intermediate tests and a low-temperature test complying to suggested thresholds. Details of the implementation recommendation for the selected parameter from each test are highlighted in Figure 67 under the "routine" section.

Furthermore, information about the modifier (FTIR spectra and SARA composition) should be provided to IDOT for approval by manufacturers every time a modifier formulation is changed. This information is primarily to monitor the quality and composition of the modifier. FTIR spectra for unaged modified binder should also be provided to validate the formulation change (Figure 67).

A pilot study based on the implementation strategy should be proposed to fine-tune the proposed thresholds and incorporate changes caused by the inclusion of new softener-based modifier types. It is recommended that, initially, data should be collected based on the proposed "yearly approval" testing and then later transition to "routine" testing as per the procedure proposed.

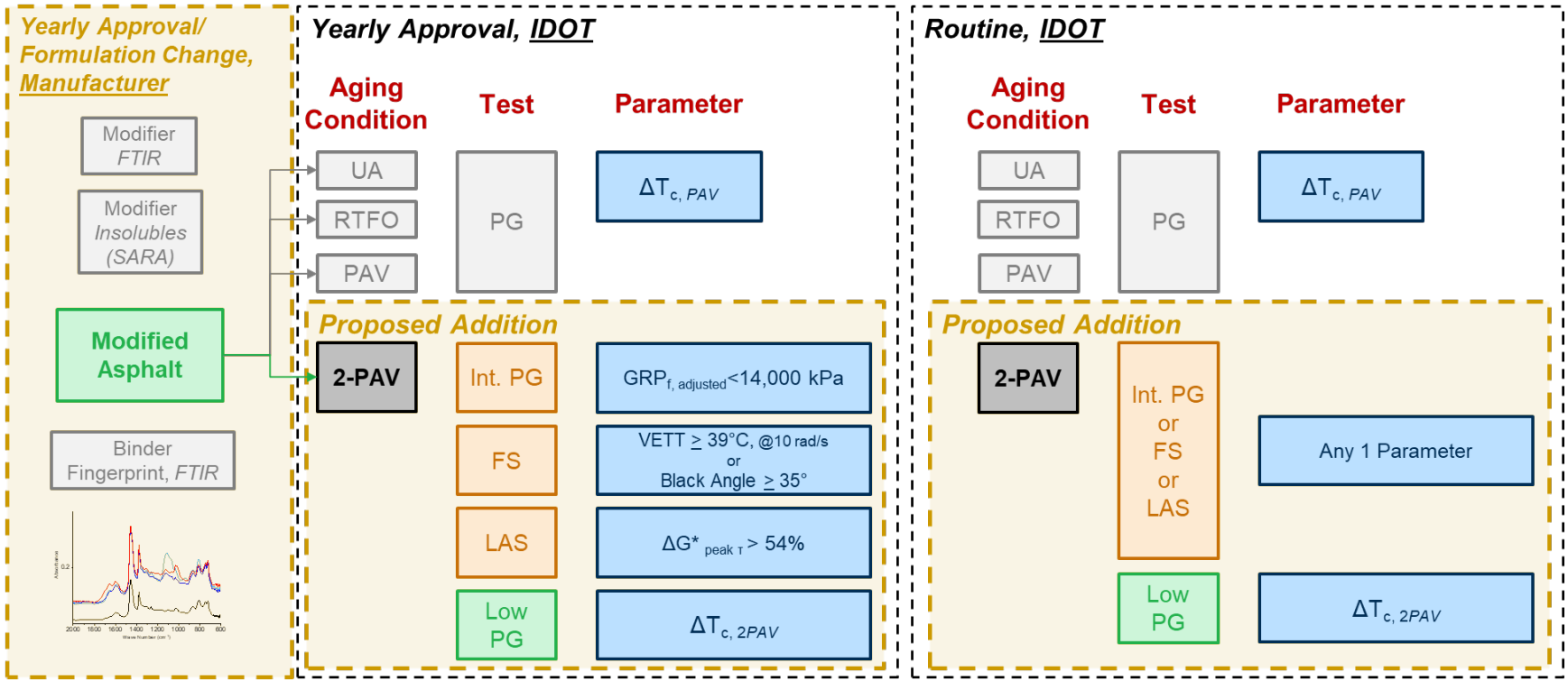

Figure 67. Graph. Protocol implementation strategy.

REFERENCES

Al-Qadi, I. L., Ozer, H., Zhu, Z., Singhvi, P., Ali, M.U., Sawalha, M., Luque, A.E.F., Mainieri, J. J. G., & Zehr, T.G. (2019). *Development of long-term aging protocol for implementation of the Illinois flexibility index test (I-FIT)* (Report No. FHWA-ICT-19-009). Illinois Center for Transportation. https://doi.org/10.36501/0197-9191/19-012

American Association of State Highway Transportation Officials (AASHTO). (2018). *AASHTO Standard TP 101-12: Standard Method of Test for Estimating Fatigue Resistance of Asphalt Binders Using the Linear Amplitude Sweep*. AASHTO.

American Association of State Highway Transportation Officials (AASHTO). (2020). *AASHTO Standard T391-20: Standard Method of Test for Estimating Fatigue Resistance of Asphalt Binders Using the Linear Amplitude Sweep*. AASHTO.

Anderson, D. A., & Kennedy, T. W. (1993). Development of SHRP binder specification. *Journal of the Association of Asphalt Paving Technologists, 62,* 481–507.

Anderson, D. A., Christensen, D. W., Bahia, H. U., Dongre, R., Sharma, M. G., Antle, C. E., & Button, J. (1994). *Binder characterization and evaluation, vol. 3: Physical characterization* (Report No. SHRP-A-369). National Research Council.

Anderson, M. R., King, G. N., Hanson, D.I., & Blankenship, P. B. (2011). Evaluation of the relationship between asphalt binder properties and non-load related cracking. *J. Assoc. Asphalt Paving Technology*, *80*, 615–662. https://trid.trb.org/view/1135500

Asphalt Institute (AI). (2015). *The bitumen industry—A global perspective: Production, chemistry, use, specification and occupational exposure*. Asphalt Institute and Eurobitume.

Asphalt Institute (AI). (2016). *State-of-the-Knowledge the Use of REOB/VTAE in Asphalt IS-235*. Asphalt Institute.

Asphalt Institute (AI). (2019). *Use of the Delta Tc Parameter to Characterize Asphalt Binder Behavior IS-240*. Asphalt Institute. Retrieved July 11, 2020, http://www.asphaltinstitute.org/engineering /delta-tc-technical-document/

Bahia, H. U., Zhai, H., Bonetti, K., & Kose, S. (1999). Non-linear viscoelastic and fatigue properties of asphalt binders. *Asphalt Paving Technology*, *68*, 1–25.

Branthaver, J. F., Petersen, J. C., Robertson, R. E., Duvall, J. J., Kim, S. S., Harnsberger, P. M., … Schabron, J. F. (1993). Binder Characterization and Evaluation, Volume2: Chemistry. In *Strategic Highway Research Program (Vol. 2)*. Retrieved from http://trid.trb.org/view.aspx?id=386723

Cao, W., & Wang, C. (2019). Fatigue performance characterization and prediction of asphalt binders using the linear amplitude sweep based viscoelastic continuum damage approach. *International Journal of Fatigue*, *119*, 112–125. https://doi.org/10.1016/j.ijfatigue.2018.09.028

Christensen, D. W., & Soliman, A. A. (2020). Relationship between asphalt concrete flexibility index and binder rheological properties. Preprints of the 95th Association of Asphalt Paving Technologists Annual Meeting 2020. Retrieved on November 11, 2020, from, https://asphalttechnology.org/wp-content/uploads/sites/6/2020/09/AAPT-2020-Preprints-082620.pdf

Christensen, D. W., & Tran, N. (2019). *NCHRP 9-59: Relating asphalt binder fatigue properties to asphalt mixture fatigue performance* [Draft Final Report]. Submitted to the National Cooperative Highway Research Program, Transportation Research Board.

Christensen, D. W., & Tran, N. (2019). Update on *NCHRP 9-59: Relating asphalt binder fatigue properties to asphalt mixture fatigue performance*. Illinois Bituminous Paving Conference, December 2019. Retrieved on May 5, 2021, https://ict.illinois.edu/outreach/bituminous /conference-history/2019

Crucho, J., Picado-Santos, L., Neves, J., Capitão, S., & Al-Qadi, I. L. (2018). Tecnico accelerated ageing (TEAGE)—a new laboratory approach for bituminous mixture ageing simulation. *International Journal of Pavement Engineering*, 1–13.

D'Angelo, J. A. (2018). *Asphalt binders and aging 20hr or 40hr PAV*. Binder Expert Task Group Meeting, Fall River, Massachusetts. Retrieved on July 12, 2020, http://www.asphaltpavement .org/PDFs/Engineering_ETGs/Binder_201805/16_D'Angelo_Binder_AgingTaskForce_update.pdf

Fini, E. H., Oldham, D., Buabeng, F. S., & Nezhad, S. H. (2015). Investigating the aging susceptibility of bio-modified asphalts. *Airfield and Highway Pavements 2015*, 62–73. https://doi.org/10.1061/9780784479216.007

García Cucalón, L., Kaseer, F., Arámbula-Mercado, E., Epps Martin, A., Morian, N., Pournoman, S., & Hajj, E. (2018). The crossover temperature: Significance and application towards engineering balanced recycled binder blends. *Road Materials and Pavement Design*, *20*(6), 1391–1412. https://doi.org/10.1080/14680629.2018.1447504

García Mainieri, J. J., Singhvi, P., Ozer, H., Sharma, B. K., & Al-Qadi, I. L. (2021). An alternative perspective to fatigue tolerance evaluation using the linear amplitude sweep (LAS) focusing on modified and extendedly aged asphalt binders. *Transportation Research Record*.

Gökalp, I., & Uz, V. E. (2019). Utilizing of waste vegetable cooking oil in bitumen: Zero tolerance aging approach. *Construction and Building Materials*, *227*, 116695. https://doi.org/10.1016/j.conbuildmat.2019.116695

Golalipour, A., & Bahia, H. (2016). Investigation of effect of bio-based and re-refined used oil modifiers on asphalt binder's performance and properties. *Transp. Res. Board* 2016, 1–14.

Haddock, J. E., Tao, B., & Seidel, J. (2009). Examining the feasibility and properties of bio-based pavement binders—Soybean soapstock as a case study of low-value lipids. *36th Rocky Mountain Asphalt Conference and Equipment Show*, (February), 1–8.

Hintz, C., Velasquez, R. A., Johnson, C. M., & Bahia, H. U. (2011a). Modification and validation of the linear amplitude sweep test for binder fatigue specification. *Transportation Research Record*, *2207*(1), 99–106. https://doi.org/10.3141/2207-13

Hintz, C., Velasquez, R., Li, Z., & Bahia, H. U. (2011b). Effect of oxidative aging on binder fatigue performance. *Asphalt Paving Technology*, *80*, 527–548.

Hintz, C., & Bahia, H. (2013a). Simplification of linear amplitude sweep test and specification parameter. *Transportation Research Record*, *2370*(1), 10–16. https://doi.org/10.3141/2370-02

Hintz, C., & Bahia, H. (2013b). Understanding mechanisms leading to asphalt binder fatigue in the dynamic shear rheometer. *Road Materials and Pavement Design*, *14*(sup2) 231–251. https://doi.org/10.1080/14680629.2013.818818

Jacques, C., Daniel, J. S., Bennert, T., Reinke, G., Norouzi, A., Ericson, C., … Kim, Y. R. (2016). Effect of silo storage time on the characteristics of virgin and reclaimed asphalt pavement mixtures. *Transportation Research Record*, *2573*(1), 76–85. https://doi.org/10.3141/2573-10

Jia, X., Huang, B., Moore, J. A., & Zhao, S. (2015). Influence of waste engine oil on asphalt mixtures containing reclaimed asphalt pavement. *Journal of Materials in Civil Engineering*, *27*(12). https://doi.org/10.1061/(ASCE)MT.1943-5533.0001292

Kandhal, P. (1977). Low-*temperature ductility in relation to pavement performance*. American Society for Testing and Materials International. https://doi.org/10.1520/STP27096S

Khojinian, A., Ojum, C., Widyatmoko, D., & D'Angelo, G. (2020). Identifying surface course deterioration using viscous to elastic transition (VET) temperatures. 7th Eurasphalt & Eurobitume Congress. Madrid, Spain. Retrieved on July 15, 2020, from, https://www.researchgate.net /publication/342832922_Identifying_Surface_Course_Deterioration_Using_Viscous_to_Elastic_Transition_VET_Temperatures

Kriz, P., Noel, J., Quddus, M., & Maria, S. (2019). Rheological properties of phase-incompatible bituminous binders. *Proceedings of the 56th Peterson Asphalt Research Conference*, Laramie, Wyoming, United States.

Lei, Z., Bahia, H., & Yi-Qiu, T. (2015). Effect of bio-based and refined waste oil modifiers on low temperature performance of asphalt binders. *Construction and Building Materials*, *86*, 95–100. https://doi.org/10.1016/j.conbuildmat.2015.03.106

National Cooperative Highway Research Program (NCHRP) (2001). *Characterization of modified asphalt binders in superpave mix design* (Research Report 459). Transportation Research Board.

National Cooperative Highway Research Program (NCHRP) (2018). *Long-term aging of asphalt mixtures for performance testing and prediction* (Research Report 871). https://doi.org/10.17226/24959

Ozer, H., Al-Qadi, I. L., Singhvi, P., Khan, T., Rivera-Perez, J., & El-Khatib, A. (2016). Fracture characterization of asphalt mixtures with high recycled content using Illinois semicircular bending test method and flexibility index. *Transportation Research Record*, *2575*(1), 130–137. https://doi.org/10.3141/2575-14

Ozer, H., Renshaw, G., Hasiba, K., & Al-Qadi, I.L. (2016). *Evaluation of the impacts of re-refined engine oil bottoms (ReOB) on performance graded asphalt binders and asphalt mixtures* (Report No. FHWA-ICT-16-006). Illinois Center for Transportation. https://apps.ict.illinois.edu/projects /getfile.asp?id=4772

Paliukaite, M., Assuras, M., & Hesp, S. A. M. (2016). Effect of recycled engine oil bottoms on the ductile failure properties of straight and polymer-modified asphalt cements. *Construction and Building Materials*, *126*, 190–196.

Pauli, A., Farrar, M., & Huang, S.-C. (2018). Characterization of pavement performance based on field

validation test site data interpreted by an asphalt composition model of binder oxidation. *Transportation Research Circular E-C234*, 34–62. http://onlinepubs.trb.org/onlinepubs/circulars/ec234.pdf

Prapaitrakul, N. (2009). Towards an improved model of asphalt binder oxidation in pavements. Thesis, Texas A & M University.

Rohman, A., & Che Man, Y. B. (2013). Application of FTIR spectroscopy for monitoring the stabilities of selected vegetable oils during thermal oxidation. *International Journal of Food Properties*, *16*(7), 1594–1603. https://doi.org/10.1080/10942912.2011.603874

Reinke, G. (2017). *The relationship of binder delta Tc (ΔTc) to mixture fatigue*. Southeastern Asphalt User/Producer Group Meeting. Jacksonville, Florida. Retrieved July 12, 2020, from, http://www.seaupg.org/PDF/2017/Wednesday/11-Reinke-Relationship-Binder-Delta-Tc_1ppg.pdf

Reinke, G., Baumgardner, G., Hanz, A., & King, S. (2017). Investigation of sterol chemistry to retard the aging of asphalt binders. *Transportation Research Record*, *2633*(1), 127–135. https://doi.org/10.3141/2633-15

Reinke, G., Hanz, A., Anderson, R. M., Ryan, M., Engber, S., & Herlitzka, D. (2016). Impact of Re-refined engine oil bottoms on binder properties and mix performance on two pavements in Minnesota. *Proceedings of the 6th Eurasphalt & Eurobitume Congress*, Prague, Czech Republic.

Rose, A. A., Lenz I. R., Than, C. T., & Glover, C. J. (2016). Investigation of the effects of recycled engine oil bottoms on asphalt field performance following an oxidation modeling approach. *Petroleum Science and Technology*, 34(21), 1768–1776. https://doi.org/10.1080/10916466.2016.1230753

Rowe, G. M. (2014). *Analysis of SHRP core asphalts—New 2013/14 test results*. Binder Expert Task Group Meeting. San Antonio, Texas.

Rowe, G. M. (2016). *ΔTc – Some thoughts on the historical development*. Binder Expert Task Group Meeting. Fall River, Massachusetts. Retrieved July 13, 2020, from, https://www.asphaltpavement.org/PDFs/Engineering_ETGs/Binder_201604/13%20Rowe%20-%20DTc%20-%20Historical%20development.pdf

Rowe, G. M. (2019). Critical properties of asphalt binders in the high stiffness region. International Airfield and Highway Pavements Conference Poster. American Society of Civil Engineers (ASCE). Chicago, Illinois.

Rowe, G. M., King, G., & Anderson, M. (2014). The influence of binder rheology in the cracking of asphalt mixes in airport and highway projects. *Journal of Testing and Evaluation*, *42*(5), 1063–1072. https://doi.org./10.1520/JTE20130245

Rowe, G. M., & Sharrock. M. J. (2016). Cracking of asphalt pavements and the development of specifications with rheological measurements. 6th Eurasphalt and Eurobitume Congress. Prague, Czech Republic. Retrieved July 12, 2020, from, https://www.h-a-d.hr/pubfile.php?id=1027

Sabouri, M., Mirzaiyan, D., & Moniri, A. (2018). Effectiveness of linear amplitude sweep (LAS) asphalt binder test in predicting asphalt mixtures fatigue performance. *Construction and Building Materials*, *171*, 281–290. https://doi.org/10.1016/j.conbuildmat.2018.03.146

Sabrina N. Rabelo, Vany P. Ferraz, Leandro S. Oliveira, and Adriana S. Franca. (2015). FTIR analysis for quantification of fatty acid methyl esters in biodiesel produced by microwave-assisted transesterification. *International Journal of Environmental Science and Development*, *6*(12)

Sadek, H., Rahaman, M. Z., Lemke, Z., Bahia, H. U., & Swiertz, D. (2020). Effect of low-temperature modifiers on HMA mixture aging and cracking resistance. *Construction and Building Materials*, *237*, 117456. https://doi.org/10.1016/j.conbuildmat.2019.117456

Safaei, F., Castorena, C., & Kim, Y. R. (2016). Linking asphalt binder fatigue to asphalt mixture fatigue performance using viscoelastic continuum damage modeling. *Mechanics of Time-Depend Materials*, *20*, 299–323. https://doi.org/10.1007/s11043-016-9304-1

Safaei, F., Lee, J., Hermann do Nascimento, L. A., Hintz, C., & Kim, Y. R. (2014). Implications of warm-mix asphalt on long-term oxidative ageing and fatigue performance of asphalt binders and mixtures. *Road Materials and Pavement Design*, *15*(sup1), 45–61. https://doi.org/10.1080/14680629.2014.927050

Shell International Petroleum Company. (1978). *Pavement design manual—Asphalt pavements and overlays for road traffic*. Shell International Petroleum Company Ltd. https://trid.trb.org/view/149309

Shi, L., Liu, Z., Li, J., & Qin, Z. (2017). Analysis of edible vegetable oils by infrared absorption spectrometry. In *Proceedings of the 2nd International Conference on Electrical, Automation and Mechanical Engineering (EAME 2017)* (pp. 286–289). Atlantis Press.

Sigmaaldrich. (n.d.) *IR spectrum table & chart*. https://www.sigmaaldrich.com/technical-documents/articles/biology/ir-spectrum-table.html#ir-spectrum-table-by-range

Sinclair, R. G., McKay, A. F., & Jones, R. N. (1952). The infrared absorption spectra of saturated fatty acids and esters. *Journal of the American Chemical Society 74*(10), 2570–2575, https://doi.org/10.1021/ja01130a033

Singhvi, P., García Mainieri, J. J., Ozer, H., Sharma, B. K., & Al-Qadi, I. L. (2020). Effect of chemical composition of bio- and petroleum-based modifiers on asphalt binder rheology. *Applied Sciences*, *10*(9), 3249. https://doi.org/10.3390/app10093249

Tarhan, İ., Ismail, A. A., & Kara, H. (2017). Quantitative determination of free fatty acids in extra virgin olive oils by multivariate methods and Fourier transform infrared spectroscopy considering different absorption modes. *International Journal of Food Properties*, 20(sup1), S790–S797, https://doi.org/10.1080/10942912.2017.1312437

Trepanier, J. (2019). IDOT HMA Update. *60th Annual Bituminous Conference*. Champaign, IL.

Wang, C., Castorena, C., Zhang, J., & Kim, Y. R. (2015). Unified failure criterion for asphalt binder under cyclic fatigue loading. *Road Materials and Pavement Design*, *16*(sup2), 125–148. https://doi.org/10.1080/14680629.2015.1077010

Widyatmoko, D., Elliott, R. C., & Heslop, M. W. (2004). Mapping crack susceptibility of bituminous materials with binder durability. Fifth RILEM International Conference on Cracking in Pavements—Mitigation, Risk Assessment and Prevention, University of Limoges, ENSIL, France.

Williams, M. L., Landel, R. F., & Ferry, J. D. (1955). The temperature dependence of relaxation

mechanisms in amorphous polymers and other glass-forming liquids. *J. Am. Chem. Soc*., *77*, 3701−3707.

Williams, B. A., Willis, R. J., & Ross, C. T. (2018). *Annual Asphalt Pavement Industry Survey on Recycled Materials and Warm-Mix Asphalt Usage 2018*. National Asphalt Pavement Association.

Wu, S., Pang, L., Liu, G., & Zhu, J. (2010). Laboratory study on ultraviolet radiation aging of bitumen. *Journal of Materials in Civil Engineering*, *22*(8), 767–772.

Yut, I., & Zofka, A. (2011). Attenuated total reflection (ATR) fourier transform infrared (FT-IR) spectroscopy of oxidized polymer-modified bitumens. *Appl. Spectrosc., 65,* 765–770.

Zeng, W., Wu, S., Wen, J., & Chen, Z. (2015). The temperature effects in aging index of asphalt during UV aging process. *Construction and Building Materials*, 93, 1125–1131.

Zhang, L., Bahia, H., Tan, Y., & Cheng L. (2017). Effect of refined waste and bio-based oil modifiers on rheological properties of asphalt binders. *Construction and Building Materials*, *148*, 504–511. https://doi.org/10.1016/j.conbuildmat.2017.05.101

Zhu, C. (2015). Evaluation of Thermal Oxidative Aging Effect on the Rheological Performance of Modified Asphalt Binders. Thesis. University of Nevada, Reno

APPENDIX A: ASPHALT BINDER CHARACTERIZATION LITERATURE REVIEW

STATE-OF-THE-PRACTICE BINDER GRADING

SuperPave performance grading (PG) is a rheology-based system, currently used to grade and specify AB in the United States. The PG system has limited ability to identify the long-term performance of modified asphalt binder (MAB). Various softening type modifiers with a range of chemical compositions and origins are used in modifying AB to achieve a target PG. The use of proprietary modifiers can significantly impact AB chemistry, hence its performance. The modifier effects on the AB chemistry may not be captured by the testing protocols of the current SuperPave grading system. SuperPave grading tests only apply small strains and are performed at limited temperatures, one frequency, and limited aging conditions. The current challenges for characterization of MAB and developing AB specifications using MAB are (i) their complex chemistry, (ii) their uncertain long-term rheological performance, and (iii) lack of a robust grading system that can discriminate them to ensure long-term performance.

STATE-OF-THE-ART RHEOLOGICAL TESTING AND PARAMETERS

Strain amplitude, used in asphalt binder testing, affects the binders' rheological behavior (Anderson et al., 1994). Different binder rheological behaviors would be expected when testing at strains within and beyond the LVER. Strains within the LVER are commonly referred to as "small," while "non-linear" strains are commonly referred to as "large." Bahia et al. (1999) proposed that the role of the asphalt binder could be better defined using a more realistic large-strain amplitude because strains experienced by flexible pavements are often larger than what is considered in small-strain asphalt binder tests.

Small-strain Rheological Testing Parameters

There are numerous rheological index parameters derived from small strain tests conducted using SuperPave equipment such as the DSR and BBR. Pavement cracking intensity has been associated with lower ductility at low temperatures (39.2 and 60˚F / 4 and 15˚C) (Kandhal, 1977). Glover et al. (2005) linked a rheological parameter obtained using a dynamic shear rheometer (DSR) (at 15˚C and 0.005rad/s) and ductility (at 15˚C and 1cm/min elongation rate). The Glover-Rowe parameter (GRP) is a simplification of this otherwise complex problem (Rowe, 2014). The ΔT_c parameter is obtained from the BBR test conducted at low temperatures. Both ΔT_c and GRP were widely accepted as a quality indicator related to non-load-associated low-temperature cracking parameters due to age-hardening (Anderson et al., 2011).

The GRP was observed to effectively capture various damage levels in AC mixtures (Rowe et al., 2014). This parameter captures the effects of complex shear modulus and stress relaxation through viscous dissipation via the phase angle (Rowe & Sharrock, 2016). On the other hand, Reinke (2017) proposed that ΔT_c is the most straightforward approach to quantifying the binder relaxation properties needed to avoid cracking (based on Kandhal, 1977). Reinke (2017) indicated that there was

a relationship between ΔT_c and fatigue cracking and disagreed that such a relationship existed for the GRP and fatigue cracking. On the other hand, Jacques et al. (2016) suggested that the GRP, ΔT_c, crossover frequency (w_c), and R-value are all related to predicting the long-term fatigue behavior of pavements under traffic loading.

The draft report from Project 9-59 of the National Cooperative Highway Research Program (NCHRP 9-59) identified asphalt binder properties related to AC mixture fatigue behavior. A new version of the GRP was proposed to measure GRP at 10rad/s and at a temperature that depends on low-temperature performance grade—herein referred to as GRP_f. The new parameter was closely correlated to the fatigue strain capacity of the binders (Christensen & Soliman, 2020).

The penetration index (PI) has been used in the Shell fatigue equations (Shell, 1978). The Rheological Index (R-value) is a parameter derived from the viscoelastic master curve of asphalt and related to the PI (Anderson et al., 1994). The R-value is the logarithmic difference between the complex modulus |G*| when the phase angle is 45 degrees, and the glassy modulus is often assumed to be 1 GPa. Figure 68-A shows the point where phase angle equates to 45 degrees is commonly referred to as the "crossover" point at which the elastic and viscous components of G* are equal. Therefore, R-value can also be considered as a crossover parameter. Other crossover parameters include the crossover complex shear modulus ($|G^*|_c$), the crossover reduced frequency (w_c), and the crossover temperature or visco elastic transition temperature (VETT) in Figure 68-B. These parameters can describe the shape of the binder's shear modulus master curve.

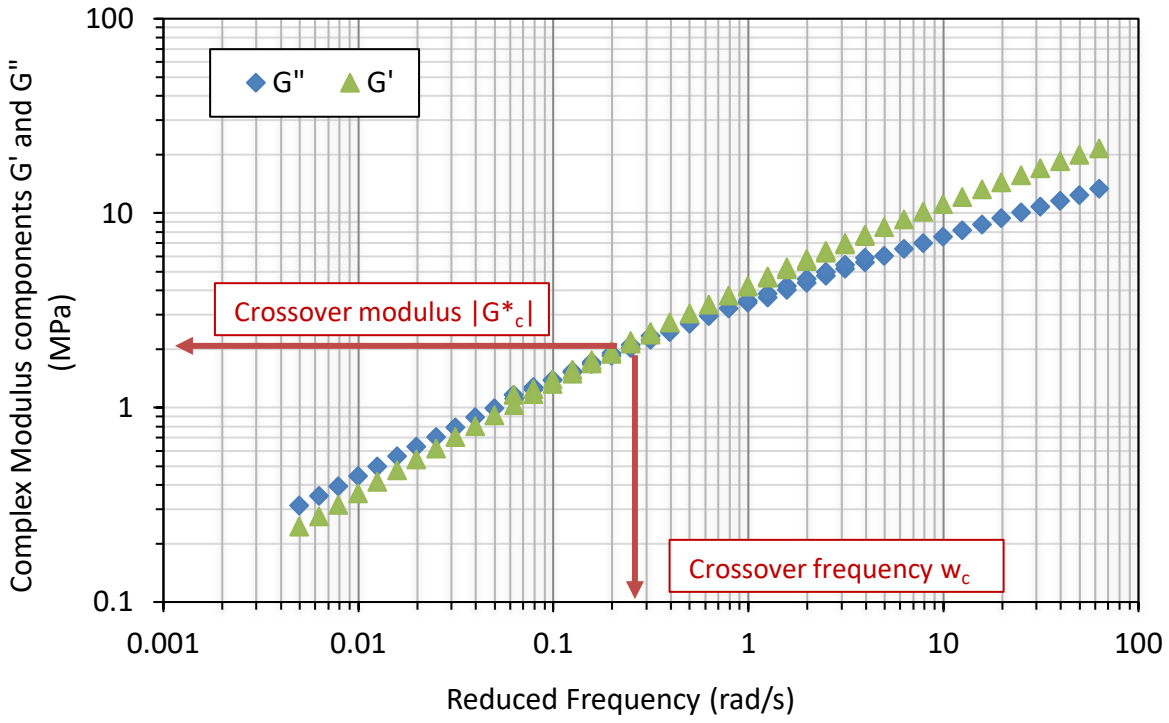

(a)

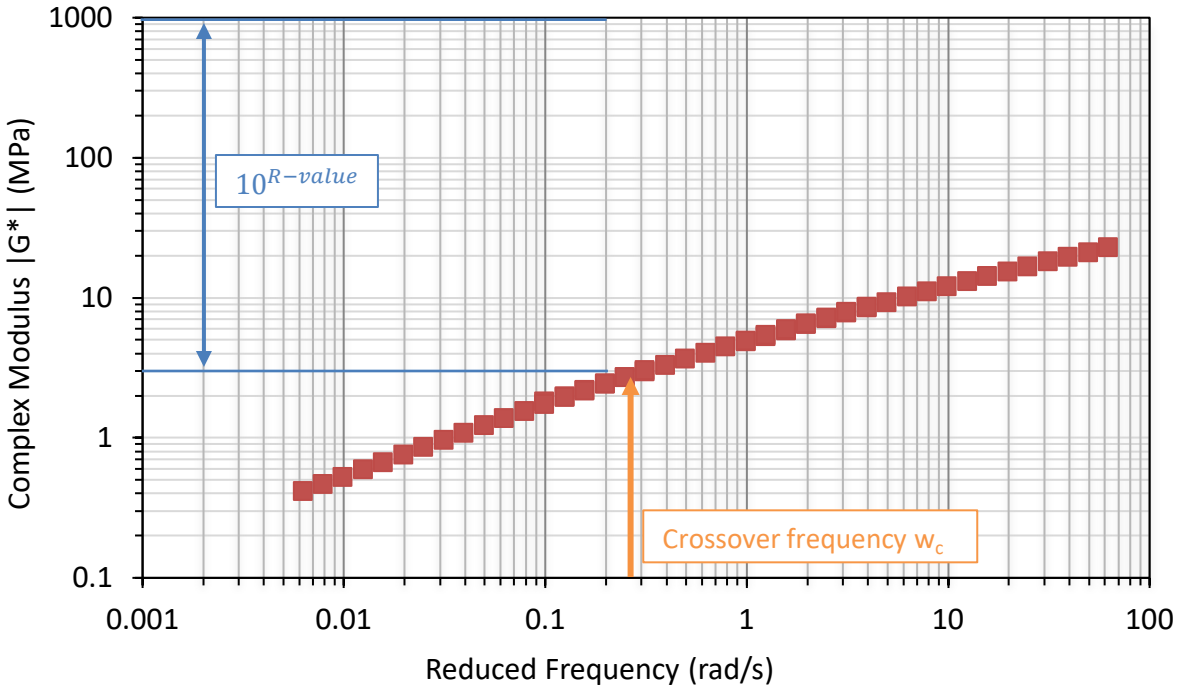

(b)

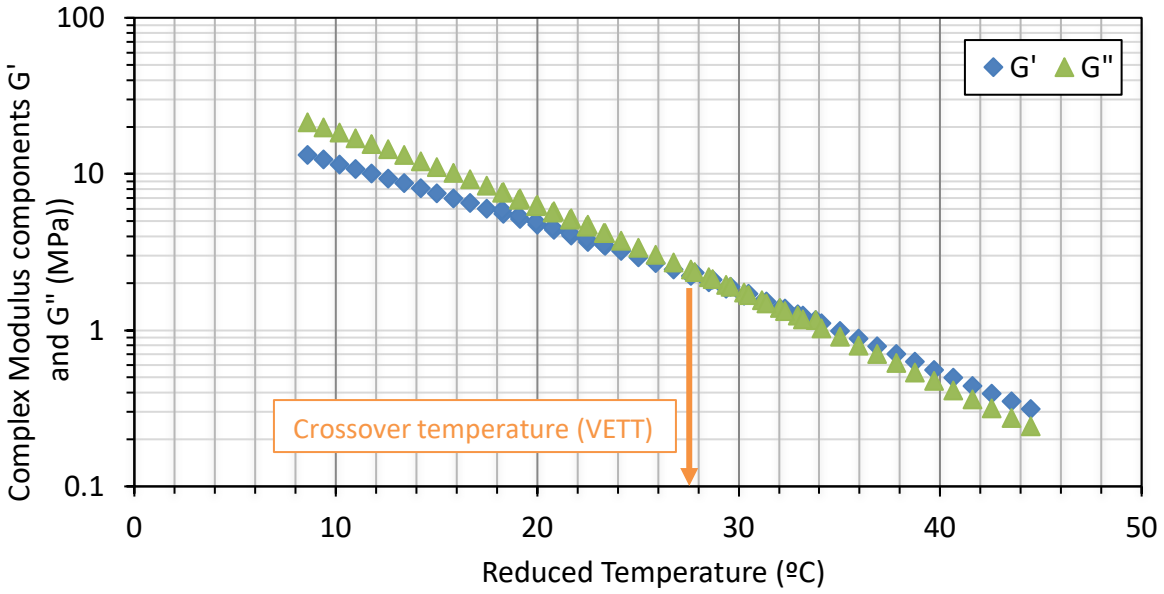

(c)

Figure 68. Graphs. (a) Crossover point illustration, (b) R-value illustration, and (c) crossover point illustration in the reduced temperature domain.

García Cucalón et al. (2018) used the crossover temperature, also known as the VETT, to assess compatibility between base binders, recycled binders, and recycling additives. The crossover temperature was also observed to correlate to ΔT_c (D'Angelo, 2018). Additionally, ΔT_c was related to

several in-service distresses such as raveling and cracking (Khojinian et al., 2020; Widyatmoko et al., 2004).

A good correlation was demonstrated between phase angle (10 rad/s frequency, especially at 50 °C) and test-pavement cracking severity (Pauli et al., 2018). More recently, in the NCHRP 9-59 study, the fatigue exponent was found to be inversely proportional to phase angle at 10 rad/s (Christensen & Soliman, 2020). The phase angle at |G*| = 8967 kPa is herein referred to as the "black angle," as it is easily read from a black space diagram as shown in Figure 69.

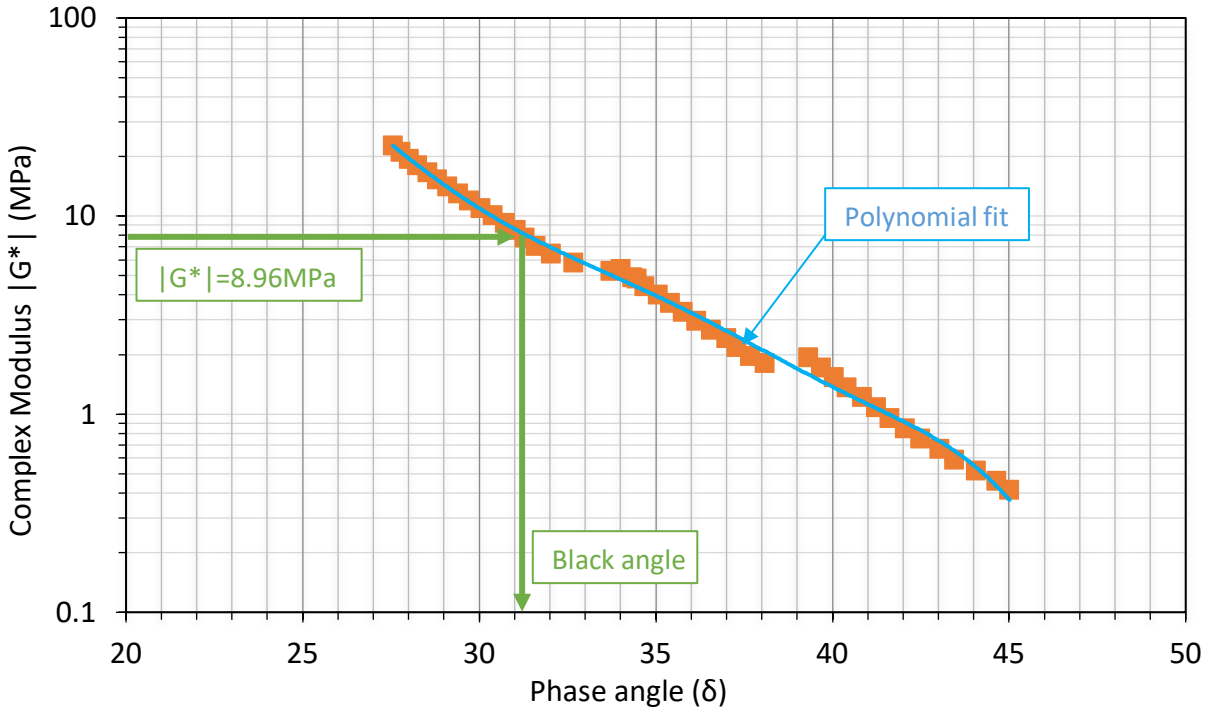

Figure 69. Graph. Black space diagram and black angle.

The black angle describes the mechanical behavior (viscous/elastic) for a range of loading frequencies and temperatures that represent typical field conditions for binders. This is because the black angle is measured at equal stiffness conditions; the corresponding |G*| at which the black angle is measured is equivalent to a typical binder passing SuperPave intermediate temperature criteria (Kriz et al., 2019). The phase angle was found to be related to chemical composition and capable of identifying phase-incompatible asphalt binders (Kriz et al., 2019).

Large-strain Rheological Testing Parameter

To improve the current PG specification, the time sweep (TS) test was developed during the National Cooperative Highway Research Program (NCHRP) Project 9-10 (NCHRP, 2001). However, the TS test is not practical for specifying asphalt binder fatigue behavior because of the uncertainty in testing time (Hintz & Bahia, 2013a). The LAS, a large-strain test, has been proposed as an efficient method to rank asphalt binders (including modified asphalt binders and extendedly aged binders) by measuring their

tolerance to fatigue loading (Hintz et al., 2011a, 2011b; Wang et al., 2015; Safaei et al., 2016; Cao & Wang, 2019). Studies have shown that LAS, coupled with simplified-viscoelastic continuum damage (S-VECD) analysis, captures the binders' contributions to AC mixture fatigue (Safaei et al., 2014; Safaei et al., 2016; Sabouri et al., 2018).

The Multiple-Stress Creep Recovery (MSCR) is another large strain test that was introduced to predict permanent deformation resistance and correctly capture polymer-modified asphalt binder's elastic recovery (AASHTO T350). Since the MSCR parameters are associated with pavement rutting, it is not commonly used in studies evaluating the effects of stiff and aged binders.

The LAS test procedure and its viscoelastic continuum damage (VECD) interpretation was standardized in 2012 in AASHTO TP101-12 (now AASHTO T391-20). It comprises two steps. First, a frequency sweep is conducted as a fingerprint test to determine the undamaged material response of the sample. A load is applied to develop a 0.1% strain over a frequency range from 0.2 to 30Hz. The frequency sweep should not cause damage. Second, a linear oscillatory strain sweep with strain amplitudes ranging from 0.1% to 30%, at 10Hz frequency, is conducted to measure the asphalt binder's damage tolerance (Hintz et al., 2011). The constant-strain rate (CSR) that results from running the standard LAS test is 0.001s-1 or 0.01%/cycle. Both steps use standard 8-mm parallel-plate geometry and a 2-mm gap and are performed at the SuperPave-intermediate temperature.

After the test, a damage accumulation function is calibrated using the undamaged moduli data, and a damage characteristic curve: integrity ($|G^*|\sin(\delta)$) vs damage is fit to obtain three parameters: C_0, C_1, and C_2.

$$|G^*|\sin(\delta) = C_0 - C_1(D)^{C_2}$$

Figure 70. Equation. Damage characteristic curve.

The fit is completed by inputting the data from the linear amplitude sweep in the damage accumulation function. Then, an arbitrary integrity limit of 35% reduction in $G^*\sin(\delta)$ is selected and damage at failure is obtained from the damage characteristic curve (D_f). The D_f value is used to obtain A_{35} and B for the following fatigue performance model:

$$N_f = A_{35}(\gamma_{max})^{-B}$$

Figure 71. Equation. Fatigue performance model.

where Υ_{max}, is the maximum expected binder strain for a given pavement structure, B depends on the undamaged data and A_{35} depends on D_f.

However, there are some challenges with the implementation and interpretation of the LAS test results. García Mainieri et al. (2021) proposed the percent reduction in $|G^*|$ from the start of the LAS test until the peak shear stress (τ_{pp} or peak τ), expressed as $\Delta|G^*|_{peak\,\tau}$, as a parameter that measures the capacity of an asphalt binder to lose integrity before failure. A higher $\Delta|G^*|_{peak\,\tau}$ denotes a higher fatigue tolerance. The alternative parameter addresses the limitations mentioned previously.

STATE-OF-THE-ART CHEMICAL TESTING AND PARAMETERS

Asphalt binders possess unique chemical characteristics and have the potential to characterize binders. These characteristics vary with origin source, exposure to climate, moisture, loading, and intensity of ultraviolet (UV)-rays from sunlight (Crucho et al., 2018; Wu et al., 2010; Zeng et al., 2015). In the 1990s, the SHRP study for the development of Superpave specification, attempted to relate the chemical nature of asphalt to rheological properties but was not successful due to complexities of chemical composition that may not be uniquely translated to rheology (Branthaver et al., 1993).

However, the SHRP study showed that chemical properties do have an impact on the binder's rheological behavior (Branthaver et al., 1993). Since then, significant work has been carried out to investigate asphalt binder chemical properties some of which include molecular size, chemical functional groups, elemental composition, and classification based on polarizability in terms of saturates, aromatics, resins, and asphaltenes. Furthermore, several microscopic techniques have been developed to understand asphalt binder morphology which includes atomic force microscopy, fluorescence microscopy, and darkfield microscopy (Loeber et al., 1996, D'Angelo & Dongre, 2009, Allen et al., 2012, and Ramm et al., 2015).

Oxidation in asphalt binders is one of the major reasons for cracking in binders (Branthaver et al., 1993). The qualitative evaluation of asphalt binder oxidation using FTIR spectroscopy has been significantly studied by researchers (Peterson, 1998, Hofko et al., 2017, Sharma et al., 2017, Singhvi et al., 2019, Mirwald et al., 2020). These studies have shown that the chemical functional groups like carbonyls and sulfoxides strongly correlates with binder oxidation. Typical spectral distribution for asphalt binder is presented in Figure 72. Carbonyl peaks typically appear in the wavenumber range 1600-1800 cm^{-1} which represents functional groups like esters, aldehydes, ketones, and carboxylic acids. Sulfoxide peaks typically appear in the range 980 – 1030 cm^{-1} (Liu & Glover, 2015, Hofko et al., 2017). Laboratory aging tests have shown that the intensity of peaks due to these functional groups increase with aging. Indices based on area under the peak of FTIR spectra corresponding to carbonyl and sulfoxide functional groups have been developed and used as indicators for predicting binder cracking (Sharma et al., 2017, Poulikakos et al., 2019).

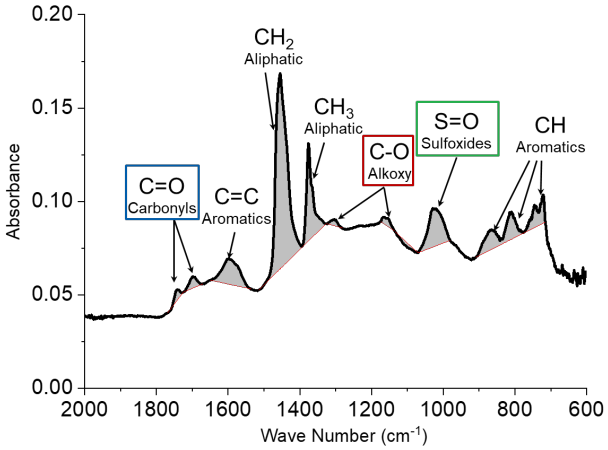

Figure 72. Illustration. Typical FTIR illustrating range of wavenumbers corresponding to functional groups existing in typical asphalt binders.

However, the range of wavenumbers corresponding to these functional groups used in the determination of oxidation parameters varies from one study (Liu & Glover, 2015) to the other (Hofko et al., 2017). For example, Lau et al. (1992) and Liu et al. (1998) studied binder aging using carbonyl area which ranged from wavenumber 1650-1820 cm^{-1} as an indicator for binder oxidation while some used sulfoxides (Petersen and Harnsberger, 1998, Petersen and Glaser, 2011). Some used a combination of sulfoxide and carbonyl to characterize overall oxidation (Zofka et al., 2013, Yut and Zofka, 2014). However, there are limited studies that show which of the specific carbonyl and sulfoxide functionalities truly represent realistic field aging (Hofko et al., 2017).

The composition of asphalt is characterized based on polarity and is classified as saturates, aromatics, resins, and asphaltenes in the order of increasing polarity, respectively (Corbett, 1969). Saturates, aromatics, resins, and asphaltenes are often referred to as SARA composition. In general, it has been shown in the literature that the ratio of polar compounds increases with aging (Sharma et al. 2017). Higher content of asphaltenes has been correlated to poor cracking resistance due to increase in viscosity (Branthaver et al., 1993).). However, there is no direct relation of asphaltene content to cracking performance when comparing different binders. The specific proportions of SARA are responsible for achieving the colloidal structure of asphalt (Eilers, 1948). The SARA composition is responsible for the phase compatibility in asphalt binders and resulting rheological response. However, a direct correlation of rheological behavior to SARA components is still not established. Several techniques have been developed over time to determine the SARA composition some of which include TLC-FID and SARAD. (Karlsen & Larter, 1991, Boysen & Schabron, 2013). However, there are limited studies that compare these different techniques from one another which makes it challenging to compare the results obtained from different methods.

Size exclusion chromatography (SEC) or gel permeation chromatography (GPC) is a method to determine the molecular weight distribution of organic compounds. Molecular weights were thoroughly investigated during the SuperPave development in the SHRP study using SEC (Branthaver et al., 1993). Typical molecular weight distribution for asphalt binders shows bimodal distribution. An increase in molecular weights is observed with an increase in aging (Lee et al., 2009, Sharma et al., 2017). Several molecular weight parameters have been used in the literature which include number-average molecular weight, weight-average molecular weight, and z- average molecular weight. Polydispersity index is another parameter to represent the molecular weight distribution (Branthaver et al., 1993). Molecular weight distribution is further divided into large (LMS), medium (MMS), and small (SMS) molecular size and have been used in the literature to evaluate the effect of aging in asphalt binders (Doh et al., 2007).

Among other techniques, thermal characterization using TGA and differential scanning calorimetry (DSC) provides insights on asphalt binder thermal properties. Parameters like activation energy and rate of mass loss obtained from these techniques have the potential to differentiate binders with potential for oxidation and degradation (Lucena et al., 2004).

APPENDIX B: BBR MEASUREMENTS, AVERAGES, STANDARD DEVIATIONS, AND COEFFICIENTS OF VARIATION

Table 20. Summary of BBR results

Binder ID	Aging Condition	Test Temperature °C	Parameter	R1	R2	Average	St Dev	CoV
S1	PAV	−12	BBR (m-value)	*		0.313	0.002	0.7%
		−18	BBR (m-value)			0.268	0.002	0.9%
		−12	BBR (Stiffness)			166.1	8.8	5.3%
		−18	BBR (Stiffness)			317.7	7.0	2.2%
	2PAV	−6	BBR (m-value)	0.308	0.309	0.309	0.001	0.2%
		−12	BBR (m-value)	0.280	0.281	0.281	0.001	0.3%
		−6	BBR (Stiffness)	97.7	87.6	92.7	7.1	7.7%
		−12	BBR (Stiffness)	182	205	193.5	16.3	8.4%
	3PAV	0	BBR (m-value)	0.314	0.316	0.315	0.001	0.4%
		−6	BBR (m-value)	0.281	0.283	0.282	0.001	0.5%
		0	BBR (Stiffness)	65.1	65.2	65.2	0.1	0.1%
		−6	BBR (Stiffness)	125	117	121.0	5.7	4.7%
S5	PAV	−18	BBR (m-value)	0.319	0.322	0.321	0.002	0.7%
		−24	BBR (m-value)	0.244	0.238	0.241	0.004	1.8%
		−18	BBR (Stiffness)	257	226	241.5	21.9	9.1%
		−24	BBR (Stiffness)	461	455	458.0	4.2	0.9%
	2PAV	−12	BBR (m-value)	0.314	0.317	0.316	0.002	0.7%
		−18	BBR (m-value)	0.279	0.277	0.278	0.001	0.5%
		−12	BBR (Stiffness)	141	144	142.5	2.1	1.5%
		−18	BBR (Stiffness)	261	256	258.5	3.5	1.4%
	3PAV	−6	BBR (m-value)	0.32	0.323	0.322	0.002	0.7%
		−12	BBR (m-value)	0.291	0.299	0.295	0.006	1.9%
		−6	BBR (Stiffness)	78.7	80.1	79.4	1.0	1.2%
		−12	BBR (Stiffness)	143	139	141.0	2.8	2.0%
S1-A-3.5	PAV	−18	BBR (m-value)	0.318	0.315	0.317	0.002	0.7%
		−24	BBR (m-value)	0.267	0.267	0.267	0.000	0.0%
		−18	BBR (Stiffness)	180	181	180.5	0.7	0.4%
		−24	BBR (Stiffness)	362	393	377.5	21.9	5.8%
	2PAV	−12	BBR (m-value)	0.318	0.321	0.320	0.002	0.7%
		−18	BBR (m-value)	0.276	0.28	0.278	0.003	1.0%
		−12	BBR (Stiffness)	98.5	105	101.8	4.6	4.5%
		−18	BBR (Stiffness)	201	198	199.5	2.1	1.1%
	3PAV	−6	BBR (m-value)	0.316	0.317	0.317	0.003	0.9%
		−12	BBR (m-value)	0.282	0.284	0.283	0.004	1.5%
		−6	BBR (Stiffness)	75.7	73.3	74.5	1.7	2.3%

Binder ID	Aging Condition	Test Temperature °C	Parameter	R1	R2	Average	St Dev	CoV
		−12	BBR (Stiffness)	145	148	146.5	2.1	1.4%
S1-C-3.1	PAV	−18	BBR (m-value)	0.324	0.321	0.323	0.002	0.7%
		−24	BBR (m-value)	0.258	0.26	0.259	0.001	0.5%
		−18	BBR (Stiffness)	213	214	213.5	0.7	0.3%
		−24	BBR (Stiffness)	442	442	442.0	0.0	0.0%
	2PAV	−12	BBR (m-value)	0.324	0.325	0.325	0.001	0.2%
		−18	BBR (m-value)	0.28	0.28	0.280	0.000	0.0%
		−12	BBR (Stiffness)	118	124	121.0	4.2	3.5%
		−18	BBR (Stiffness)	284	260	272.0	17.0	6.2%
	3PAV	−6	BBR (m-value)	0.324	0.32	0.322	0.003	0.9%
		−12	BBR (m-value)	0.284	0.288	0.286	0.003	1.0%
		−6	BBR (Stiffness)	84.2	91.5	87.9	5.2	5.9%
		−12	BBR (Stiffness)	173	171	172.0	1.4	0.8%
S1-D-3.1	PAV	−18	BBR (m-value)	0.304	0.301	0.303	0.002	0.7%
		−24	BBR (m-value)	0.254	0.259	0.257	0.004	1.4%
		−18	BBR (Stiffness)	214	205	209.5	6.4	3.0%
		−24	BBR (Stiffness)	403	417	410.0	9.9	2.4%
	2PAV	−12	BBR (m-value)	0.312	0.311	0.312	0.001	0.2%
		−18	BBR (m-value)	0.275	0.281	0.278	0.004	1.5%
		−12	BBR (Stiffness)	134	118	126.0	11.3	9.0%
		−18	BBR (Stiffness)	250	278	264.0	19.8	7.5%
	3PAV	−6	BBR (m-value)	0.313	0.31	0.312	0.002	0.7%
		−12	BBR (m-value)	0.281	0.283	0.282	0.001	0.5%
		−6	BBR (Stiffness)	78	77.6	77.8	0.3	0.4%
		−12	BBR (Stiffness)	140	140	140.0	0.0	0.0%
S1-E-3.1	PAV	−18	BBR (m-value)	0.323	0.324	0.324	0.001	0.2%
		−24	BBR (m-value)	0.273	0.268	0.271	0.004	1.3%
		−18	BBR (Stiffness)	170	180	175.0	7.1	4.0%
		−24	BBR (Stiffness)	338	358	348.0	14.1	4.1%
	2PAV	−12	BBR (m-value)	0.307	0.312	0.310	0.004	1.1%
		−18	BBR (m-value)	0.274	0.28	0.277	0.004	1.5%
		−12	BBR (Stiffness)	131	110	120.5	14.8	12.3%
		−18	BBR (Stiffness)	220	223	221.5	2.1	1.0%
	3PAV	−6	BBR (m-value)	0.311	0.308	0.310	0.002	0.7%
		−12	BBR (m-value)	0.273	0.274	0.274	0.001	0.3%
		−6	BBR (Stiffness)	81.7	80.9	81.3	0.6	0.7%
		−12	BBR (Stiffness)	145	149	147.0	2.8	1.9%
S1-G-6.5	PAV	−18	BBR (m-value)	0.308	0.304	0.306	0.003	0.9%
		−24	BBR (m-value)	0.245	0.236	0.241	0.006	2.6%
		−18	BBR (Stiffness)	264	267	265.5	2.1	0.8%

Binder ID	Aging Condition	Test Temperature °C	Parameter	R1	R2	Average	St Dev	CoV
		−24	BBR (Stiffness)	518	523	520.5	3.5	0.7%
	2PAV	−12	BBR (m-value)	0.326	0.331	0.329	0.004	1.1%
		−18	BBR (m-value)	0.288	0.286	0.287	0.001	0.5%
		−12	BBR (Stiffness)	150	158	154.0	5.7	3.7%
		−18	BBR (Stiffness)	306	298	302.0	5.7	1.9%
	3PAV	−12	BBR (m-value)	0.303	0.302	0.303	0.001	0.2%
		−18	BBR (m-value)	0.261	0.261	0.261	0.000	0.0%
		−12	BBR (Stiffness)	170	169	169.5	0.7	0.4%
		−18	BBR (Stiffness)	301	287	294.0	9.9	3.4%
S1-K-10	PAV	−12	BBR (m-value)	0.333	0.331	0.332	0.001	0.4%
		−18	BBR (m-value)	0.298	0.293	0.296	0.004	1.2%
		−12	BBR (Stiffness)	63.7	64.6	64.2	0.6	1.0%
		−18	BBR (Stiffness)	148	133	140.5	10.6	7.5%
	2PAV	−6	BBR (m-value)	0.306	0.312	0.309	0.004	1.4%
		−12	BBR (m-value)	0.274	0.278	0.276	0.003	1.0%
		−6	BBR (Stiffness)	56.7	56.12	56.4	0.4	0.7%
		−12	BBR (Stiffness)	111	113	112.0	1.4	1.3%
	3PAV	0	BBR (m-value)	0.301	0.301	0.301	0.000	0.0%
		−6	BBR (m-value)	0.275	0.274	0.275	0.001	0.3%
		0	BBR (Stiffness)	40.9	44.7	42.8	2.7	6.3%
		−6	BBR (Stiffness)	74.2	72	73.1	1.6	2.1%
S1-B-5.0	PAV	−18	BBR (m-value)	0.303	0.3	0.302	0.002	0.7%
		−24	BBR (m-value)	0.254	0.253	0.254	0.001	0.3%
		−18	BBR (Stiffness)	279	255	267.0	17.0	6.4%
		−24	BBR (Stiffness)	500	496	498.0	2.8	0.6%
	2PAV	−12	BBR (m-value)	0.32	0.319	0.320	#REF!	#REF!
		−18	BBR (m-value)	0.272	0.271	0.272	0.001	0.3%
		−12	BBR (Stiffness)	157	149	153.0	5.7	3.7%
		−18	BBR (Stiffness)	294	302	298.0	5.7	1.9%
	3PAV	−6	BBR (m-value)	0.333	0.33	0.332	0.002	0.6%
		−12	BBR (m-value)	0.291	0.293	0.292	0.001	0.5%
		−6	BBR (Stiffness)	85.6	90	87.8	3.1	3.5%
		−12	BBR (Stiffness)	164	169	166.5	3.5	2.1%
S1-F-3.1	PAV	−18	BBR (m-value)	0.318	0.319	0.319	0.001	0.2%
		−24	BBR (m-value)	0.262	0.269	0.266	0.005	1.9%
		−18	BBR (Stiffness)	194	187	190.5	4.9	2.6%
		−24	BBR (Stiffness)	365	417	391.0	36.8	9.4%
	2PAV	−12	BBR (m-value)	0.309	0.306	0.308	0.002	0.7%
		−18	BBR (m-value)	0.27	0.273	0.272	0.002	0.8%
		−12	BBR (Stiffness)	116	121	118.5	3.5	3.0%

Binder ID	Aging Condition	Test Temperature °C	Parameter	R1	R2	Average	St Dev	CoV
		−18	BBR (Stiffness)	214	217	215.5	2.1	1.0%
	3PAV	−6	BBR (m-value)	0.315	0.316	0.316	0.001	0.2%
		−12	BBR (m-value)	0.285	0.287	0.286	0.001	0.5%
		−6	BBR (Stiffness)	71	69.1	70.1	1.3	1.9%
		−12	BBR (Stiffness)	133	139	136.0	4.2	3.1%
S1-I-3.5	PAV	−18	BBR (m-value)	0.319	0.315	0.317	0.003	0.9%
		−24	BBR (m-value)	0.273	0.263	0.268	0.007	2.6%
		−18	BBR (Stiffness)	190	197	193.5	4.9	2.6%
		−24	BBR (Stiffness)	372	374	373.0	1.4	0.4%
	2PAV	−12	BBR (m-value)	0.311	0.315	0.315	0.003	0.9%
		−18	BBR (m-value)	0.278	0.28	0.279	0.001	0.5%
		−12	BBR (Stiffness)	115	118	116.5	2.1	1.8%
		−18	BBR (Stiffness)	232	230	231.0	1.4	0.6%
	3PAV	−6	BBR (m-value)	0.312	0.307	0.310	0.004	1.1%
		−12	BBR (m-value)	0.285	0.287	0.286	0.001	0.5%
		−6	BBR (Stiffness)	79	79.3	79.2	0.2	0.3%
		−12	BBR (Stiffness)	133	139	136.0	4.2	3.1%
S1-H-10	PAV	−18	BBR (m-value)	0.314	0.313	0.314	0.001	0.2%
		−24	BBR (m-value)	0.268	0.267	0.268	0.001	0.3%
		−18	BBR (Stiffness)	184	167	175.5	12.0	6.8%
		−24	BBR (Stiffness)	367	336	351.5	21.9	6.2%
	2PAV	−12	BBR (m-value)	0.313	0.316	0.315	0.002	0.7%
		−18	BBR (m-value)	0.282	0.282	0.282	0.000	0.0%
		−12	BBR (Stiffness)	112	115	113.5	2.1	1.9%
		−18	BBR (Stiffness)	231	245	238.0	9.9	4.2%
	3PAV	−6	BBR (m-value)	0.317	0.315	0.316	0.001	0.4%
		−12	BBR (m-value)	0.288	0.281	0.285	0.005	1.7%
		−6	BBR (Stiffness)	76.1	73	74.6	2.2	2.9%
		−12	BBR (Stiffness)	140	148	144.0	5.7	3.9%
S1-J-3.0	PAV	−18	BBR (m-value)	0.314	0.307	0.311	0.005	1.6%
		−24	BBR (m-value)	0.257	0.267	0.262	0.007	2.7%
		−18	BBR (Stiffness)	176	195	185.5	13.4	7.2%
		−24	BBR (Stiffness)	387	396	391.5	6.4	1.6%
	2PAV	−12	BBR (m-value)	0.324	0.327	0.326	0.002	0.7%
		−18	BBR (m-value)	0.286	0.287	0.287	0.001	0.2%
		−12	BBR (Stiffness)	118	111	114.5	4.9	4.3%
		−18	BBR (Stiffness)	225	243	234.0	12.7	5.4%
	3PAV	−6	BBR (m-value)	0.313	0.313	0.313	0.000	0.0%
		−12	BBR (m-value)	0.281	0.281	0.281	0.000	0.0%
		−6	BBR (Stiffness)	79.6	77.1	78.4	1.8	2.3%

Binder ID	Aging Condition	Test Temperature °C	Parameter	R1	R2	Average	St Dev	CoV
		−12	BBR (Stiffness)	134	133	133.5	0.7	0.5%
S8	PAV	−18	BBR (m-value)	0.302	0.307	0.305	0.004	1.2%
		−24	BBR (m-value)	0.258	0.256	0.257	0.001	0.6%
		−18	BBR (Stiffness)	247	227	237.0	14.1	6.0%
		−24	BBR (Stiffness)	548	536	542.0	8.5	1.6%
	2PAV	−12	BBR (m-value)	0.332	0.334	0.333	0.001	0.4%
		−18	BBR (m-value)	0.294	0.292	0.293	0.001	0.5%
		−12	BBR (Stiffness)	126	133	129.5	4.9	3.8%
		−18	BBR (Stiffness)	293	270	281.5	16.3	5.8%
	3PAV	−6	BBR (m-value)	0.324	0.319	0.322	0.004	1.1%
		−12	BBR (m-value)	0.293	0.29	0.292	0.002	0.7%
		−6	BBR (Stiffness)	83.3	78.5	80.9	3.4	4.2%
		−12	BBR (Stiffness)	180	165	172.5	10.6	6.1%
S9-L-NA	PAV	−18	BBR (m-value)	0.305	0.311	0.308	0.004	1.4%
		−24	BBR (m-value)	0.253	0.252	0.253	0.001	0.3%
		−18	BBR (Stiffness)	226	231	228.5	3.5	1.5%
		−24	BBR (Stiffness)	485	508	496.5	16.3	3.3%
	2PAV	−12	BBR (m-value)	0.331	0.327	0.329	0.003	0.9%
		−18	BBR (m-value)	0.284	0.279	0.282	0.004	1.3%
		−12	BBR (Stiffness)	135	129	132.0	4.2	3.2%
		−18	BBR (Stiffness)	276	267	271.5	6.4	2.3%
	3PAV	−6	BBR (m-value)	0.318	0.324	0.321	0.004	1.3%
		−12	BBR (m-value)	0.28	0.283	0.282	0.002	0.8%
		−6	BBR (Stiffness)	81	81	81.0	0.0	0.0%
		−12	BBR (Stiffness)	163	159	161.0	2.8	1.8%

APPENDIX C: INTERPRETING LINEAR AMPLITUDE SWEEP TEST RESULTS OF AGED SOFTENER-MODIFIED BINDERS

WHAT IS THE LAS TEST?

The Linear amplitude sweep (LAS) test was introduced as a method to determine the cyclic fatigue life of binders (AASHTO TP101-12, now T391-20). The test is conducted using a Dynamic Shear Rheometer (DSR) and the following loading scheme:

Table 21. LAS Procedure Steps

Step	Frequency	Amplitude	Temperature
1. Frequency Sweep	0.2 to 30Hz	0.1%	User selected
2. Linear Amplitude Sweep	10Hz	0.1 to 30%	User selected

WHY A NEW PARAMETER?

A comprehensive analysis of the test results using the approach in the specifications and others found in the literature were performed. Inconsistencies were observed in explaining the outcome and interpreting the result for modified binders. From small distortions to large strain deformations and cracking, the theories and equations used to explain the stress-strain relationship become incompatible. The theoretical framework for DSR is not valid anymore past a point where rotations cause such cracking and distortions as the ones shown in Figure 73 and Figure 24-B. Stiffness of the specimen (changing with aging and modifiers) affects the result to a great extent and in an unpredictable manner.

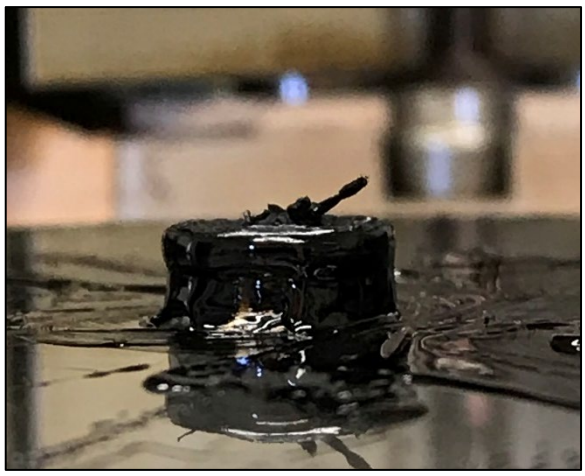

Figure 73. Photo. The bottom plate of the DSR at the end of the LAS test.

Therefore, a new and more practical approach is proposed. The method describes the calculation of the reduction in stiffness ($\Delta|G^*|_{peak\ \tau}$ or delta G) as a parameter to distinguish the cyclic fatigue response of modified binders. The parameter was sought to reduce the inconsistencies.

$\Delta|G^*|_{peak\,\tau}$ is a measurement of the reduction of complex shear modulus ($|G^*|$) from the start of a LAS until the peak shear stress is reached during the test.

OBTAINING DELTA G

The procedure is explained as follows:

1. Find the initial complex shear modulus ($|G^*|_{start}$) recorded as the first $|G^*|$ reading at the start of the test (Figure 74).

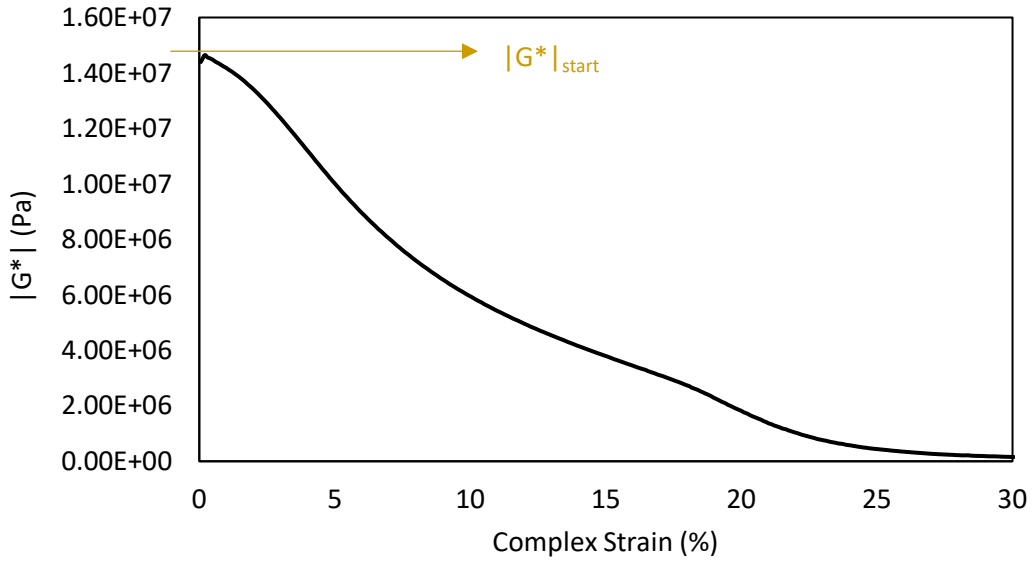

Figure 74. Illustration. Illustration of $|G^*|_{start}$.

2. Find the highest shear stress (τ_{pp}) measured. This should be determined by searching for the maximum $|G^*|$ measured (Figure 76-A).

3. Determine the $|G^*|$ corresponding to τ_{pp} as the complex shear modulus at the peak shear stress condition ($|G^*|_{peak\,\tau}$).

4. Calculate $\Delta|G^*|_{peak\,\tau}$ as the percentage difference between $|G^*|_{start}$ and $|G^*|_{peak\,\tau}$ (Figure 76-B):

$$\Delta|G^*|_{peak\,\tau} = \frac{|G^*|_{start} - |G^*|_{peak\,\tau}}{|G^*|_{start}} \times 100$$

Figure 75. Equation. Calculation for Delta G.

The figure below depicts how Delta G is obtained from two-line graphs: complex shear stress (τ) vs. number of cycles (N) graph and a complex shear modulus normalized by the complex shear modulus at the beginning of the test ($|G^*|$ /$|G^*|_{start}$) vs number of cycles (N) graph.

An example calculation is provided in Section 7.

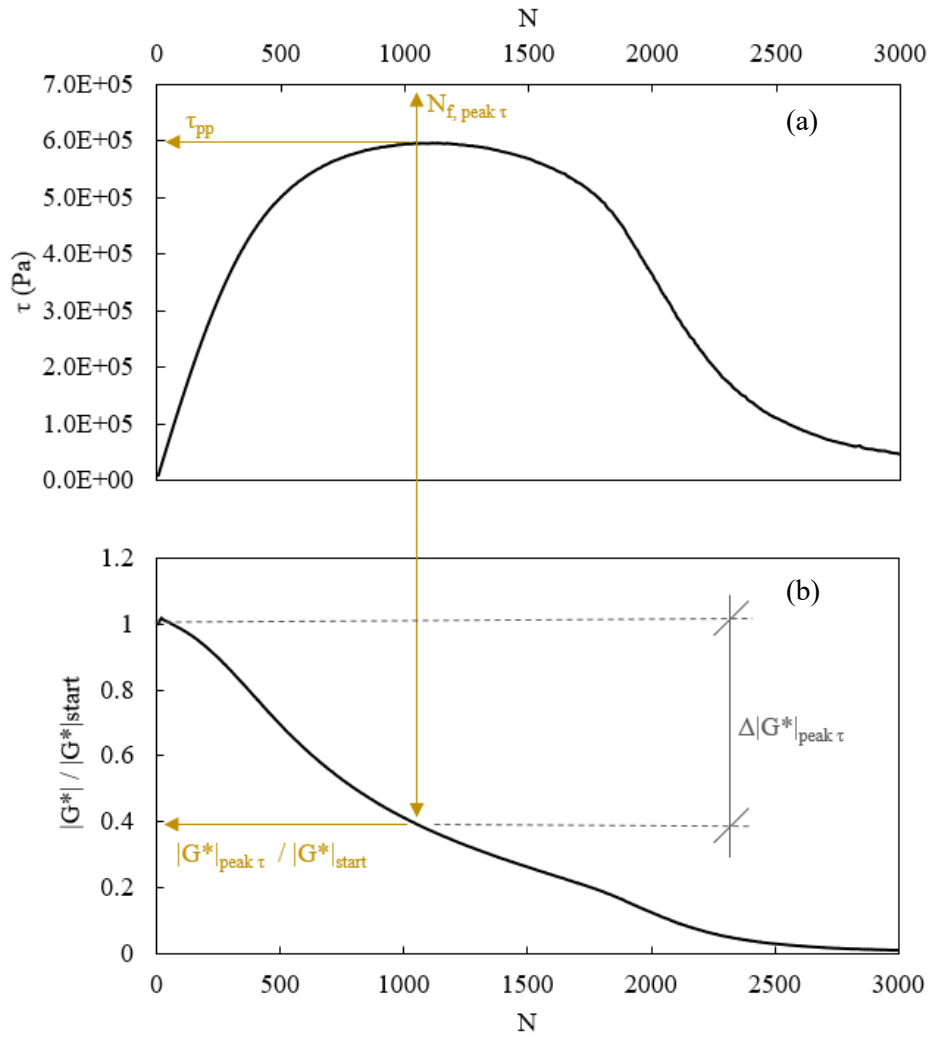

Figure 76. Illustration. Illustration of $\Delta|G^*|_{peak\ \tau}$ for a vegetable-oil-modified binder at PAV-aged condition. (N is the cycle number.)

DELTA G AT DIFFERENT AGING CONDITIONS

When developing this interpretation of the LAS results, binders in several aging conditions were tested: unaged, RTFO-, PAV-, 2PAV- and 3PAV-aged. Degassing was performed after single or multiple PAV aging. Multiple PAV aging cycles were applied continuously with no additional depressurization cycles. This interpretation has been found to correlate well with other tests performed for all aging conditions. The results from different modified binders were distinguished more clearly and reliably at the 2PAV-aged condition.

INTERPRETING DELTA G

The key to understanding delta G is the fact that every sample no matter what aging condition and modification is subjected to the same magnitude of strains. On the other hand, stress and applied

energy depend on the initial complex modulus and phase angle of each sample. An asphalt binder that tolerates greater $\Delta|G^*|_{peak\,\tau}$ before reaching τ_{pp} is a better performer. After peak shear stress is measured, the capacity of the binder to resist deformation decreases. In contrast, a material that withstands a lower $\Delta|G^*|_{peak\,\tau}$ before its shear stress response decreases is considered to perform worse.

Example for Interpreting Delta G Results

The next figure represents the $\Delta|G^*|_{peak\,\tau}$ values (averaged from two replicates) obtained for two non-modified binders (B1 and B2), 11 modified binders with the same base binder (A-K), and one additional modified binder with a different base binder (Z). They are ordered from best (left) to worst (right) performance in the standard LAS loading conditions.

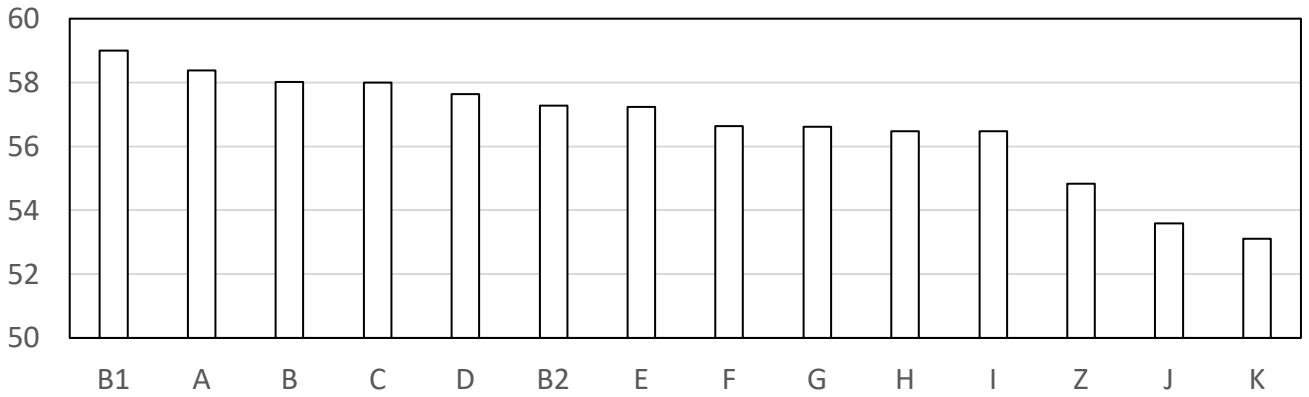

Figure 77. Bar chart. Example $\Delta|G^*|_{peak\,\tau}$ values for binders at the 2PAV-aged condition.

REPEATABILITY FOR DELTA G

The following are best practices to achieve better repeatability within $\Delta|G^*|_{peak\,\tau}$ values of the same asphalt binder:

- The frequency sweep can be omitted to obtain $\Delta|G^*|_{peak\,b}$ecause the values from the frequency sweep detailed in AASHTO TP101-12 are not used herein. However, it is recommended that $|G^*|_{LVER}$ be obtained at the same temperature of the LAS, using strains within the linear viscoelastic range (LVER), and at a 10Hz frequency (same as in LAS), to verify that the $|G^*|_{start}$ is equal or approximately similar. The LAS should be re-run if the results differ considerably (CoV>15%).

- It is recommended to use at least two replicates for each asphalt binder. If stress measurements vary by more than 10% (of the average) in any of the selected readings (from the 5th to the 150th), an additional replicate should be tested to replace the outlier.

EXAMPLE FOR OBTAINING DELTA G FROM TESTING RAW DATA

Table 22is a portion of the data obtained from a standard LAS test on a sample binder.

1. The initial complex shear modulus ($|G^*|_{start}$) recorded as the first $|G^*|$ reading at the start of the test is 1.41E+07Pa.

2. The highest shear stress (τ_{pp}) measured is 5.90E+05Pa (marked with a gray background).

3. The $|G^*|$ corresponding to τ_{pp} ($|G^*|_{peak\,\tau}$) is 5.56E+06Pa.

4. $\Delta|G^*|_{peak\,\tau}$ is the percentage difference between $|G^*|_{start}$ and $|G^*|_{peak\,\tau}$:

$$\Delta|G^*|_{peak\,\tau} = \frac{|G^*|_{start} - |G^*|_{peak\,\tau}}{|G^*|_{start}} \times 100 = \frac{1.41E+07 - 5.56E+06}{1.41E+07} \times 100 = 60.57\%$$

Figure 78. Equation. Example calculation of Delta G.

Table 22. Example Extract Data from Standard LAS

Complex shear strain (%)	Complex shear stress (Pa)	Shear modulus (complex component) (Pa)
0.0613781	8.68E+03	1.41E+07
0.598527	8.55E+04	1.43E+07
1.09758	1.54E+05	1.40E+07
1.59649	2.18E+05	1.37E+07
2.09538	2.77E+05	1.32E+07
2.59741	3.30E+05	1.27E+07
3.0946	3.75E+05	1.21E+07
3.60082	4.15E+05	1.15E+07
4.09988	4.49E+05	1.09E+07
4.60062	4.77E+05	1.04E+07
5.10524	5.01E+05	9.81E+06
5.59852	5.19E+05	9.27E+06
6.10143	5.35E+05	8.77E+06
6.61099	5.49E+05	8.30E+06
7.10566	5.59E+05	7.86E+06
7.60784	5.68E+05	7.46E+06
8.10884	5.74E+05	7.08E+06
8.61029	5.80E+05	6.73E+06
9.09977	5.83E+05	6.41E+06
9.60336	5.86E+05	6.11E+06
10.112	5.88E+05	5.82E+06
10.6179	5.90E+05	5.56E+06
11.1038	5.89E+05	5.31E+06
11.6046	5.89E+05	5.07E+06
12.124	5.88E+05	4.85E+06
12.6169	5.85E+05	4.64E+06

Complex shear strain (%)	Complex shear stress (Pa)	Shear modulus (complex component) (Pa)
13.1094	5.81E+05	4.44E+06
13.6126	5.77E+05	4.24E+06
14.1213	5.72E+05	4.05E+06
14.6203	5.66E+05	3.87E+06
15.1244	5.59E+05	3.69E+06
15.6235	5.50E+05	3.52E+06
16.128	5.42E+05	3.36E+06
16.6247	5.33E+05	3.21E+06
17.1375	5.23E+05	3.05E+06
17.6139	5.12E+05	2.91E+06
18.1521	5.00E+05	2.75E+06
18.6443	4.84E+05	2.60E+06
19.1792	4.63E+05	2.42E+06
19.6594	4.38E+05	2.23E+06
20.1596	4.12E+05	2.04E+06
20.685	3.86E+05	1.87E+06
21.2856	3.58E+05	1.68E+06
21.7198	3.26E+05	1.50E+06
22.1993	2.96E+05	1.33E+06
22.717	2.67E+05	1.18E+06
23.2124	2.40E+05	1.03E+06
23.69	2.17E+05	9.17E+05
24.2248	1.98E+05	8.15E+05
24.7266	1.78E+05	7.19E+05
25.2354	1.58E+05	6.28E+05
25.6903	1.38E+05	5.36E+05
26.2156	1.21E+05	4.60E+05
26.6949	1.08E+05	4.03E+05
27.1858	9.58E+04	3.52E+05
27.676	8.67E+04	3.13E+05
28.2084	7.82E+04	2.77E+05
28.6704	7.04E+04	2.46E+05
29.1616	6.47E+04	2.22E+05
29.6823	5.87E+04	1.98E+05
30.0649	5.45E+04	1.81E+05

DATA INTERPRETATION FOR THE DEVELOPMENT OF DELTA G

The development of delta G is based on the following plots. Figure 79 show adhesion problems during the test, which can be overcome by increasing the loading temperature and testing binders within a 12-60MPa G* range. Figure 80 show normal stresses developed during the LAS test that

corresponds to roll and ridge formation in the samples. Figure 81 to Figure 99 show that data is inadequate after peak stress and that pseudo strain energy variables (proportional to τ x N) are affected by normal stresses after this point making them not repeatable. Figure 100 to Figure 114 present how C-N curves change with aging which demonstrates that stiffness induces quicker integrity loss (G* or C) and that failure is not occurring at the same level of C (which is implied by AASHTO T391-20). Figure 115 to Figure 129 also presents that the phase angle did not have defined peaks and therefore was not used for failure definitions.

Adhesion Loss Manifestations Evident in Linear Amplitude Sweep Measurements

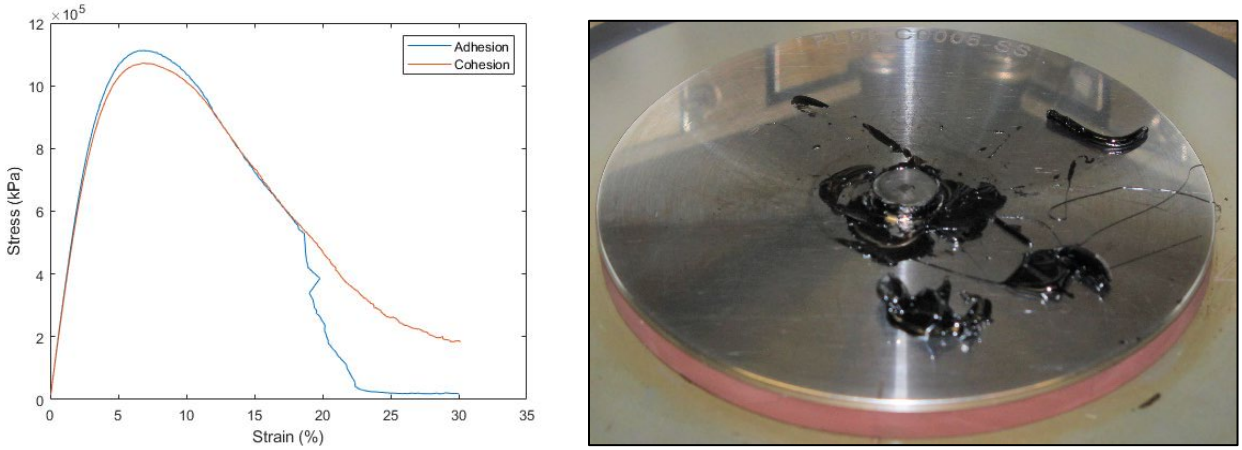

Figure 79. Graph and Photo. Total adhesion loss.

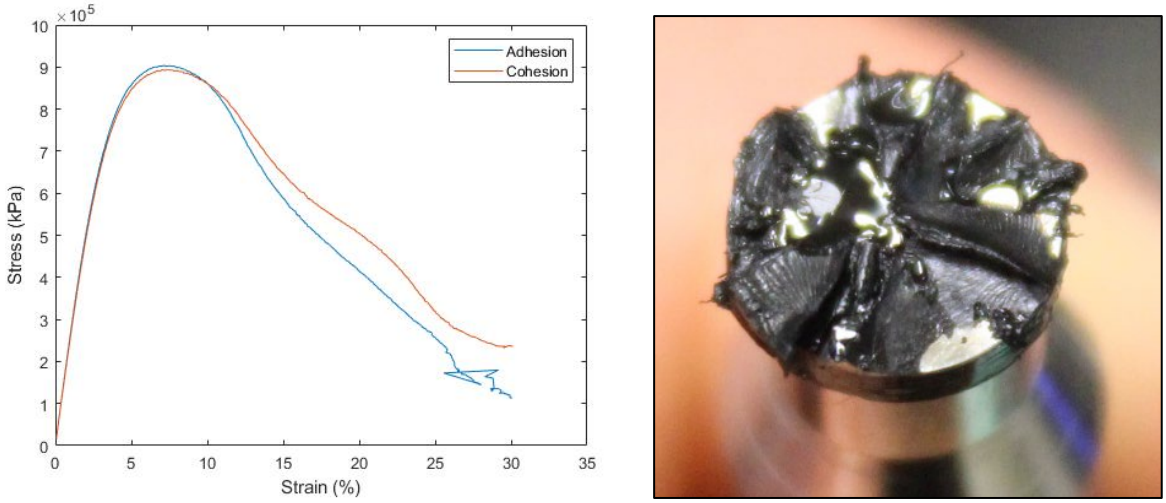

Figure 80. Graph and Photo. Partial (localized) adhesion loss.

Normal Forces and Torques Measured during Several Linear Amplitude Sweeps on Different Binders and Aging Conditions

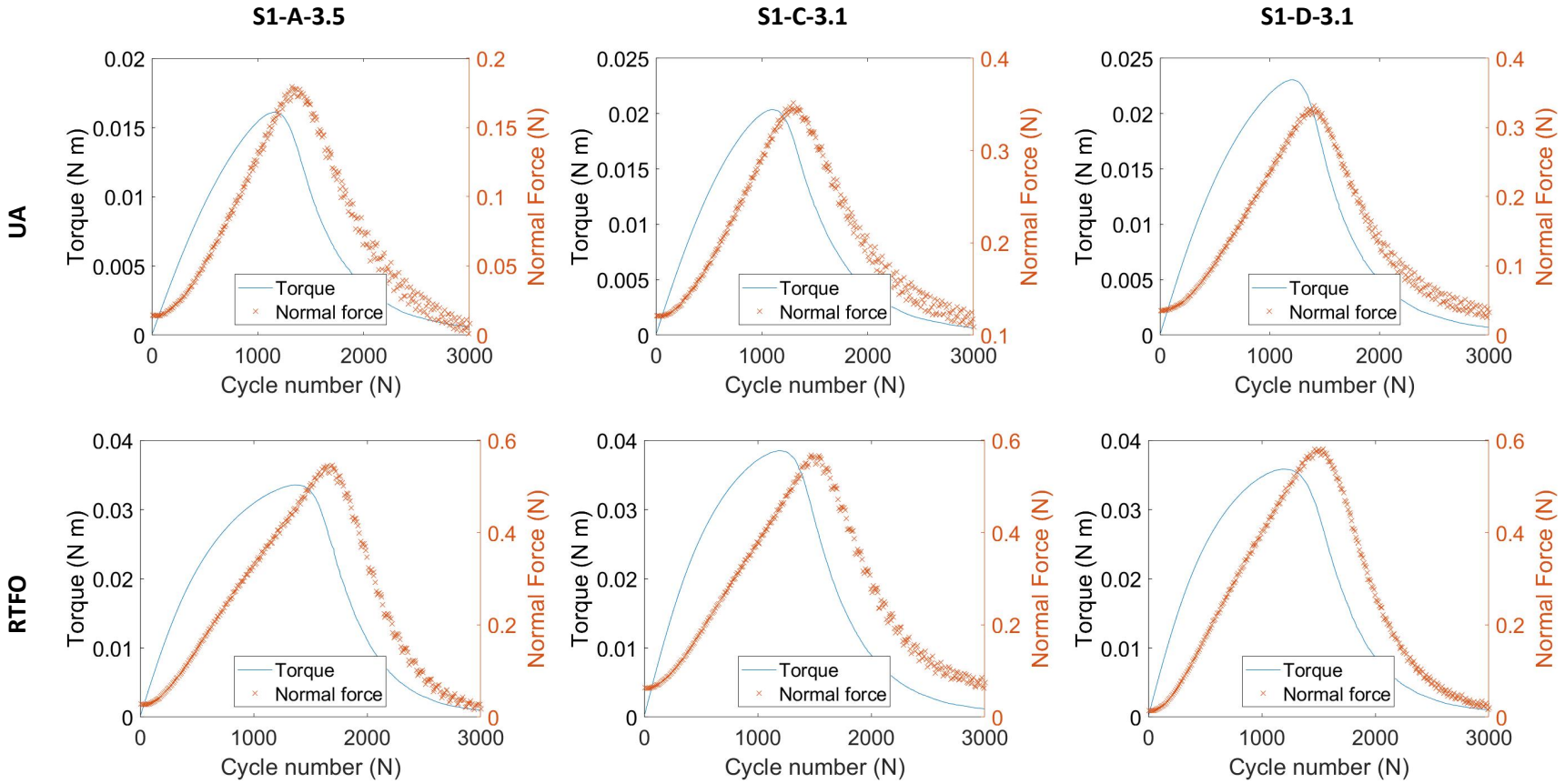

Figure 81. Graphs. Torque vs cycle number for UA and RTFO aging for binders S1-A-3.5, S1-C-3.1 and S1-D-3.1.

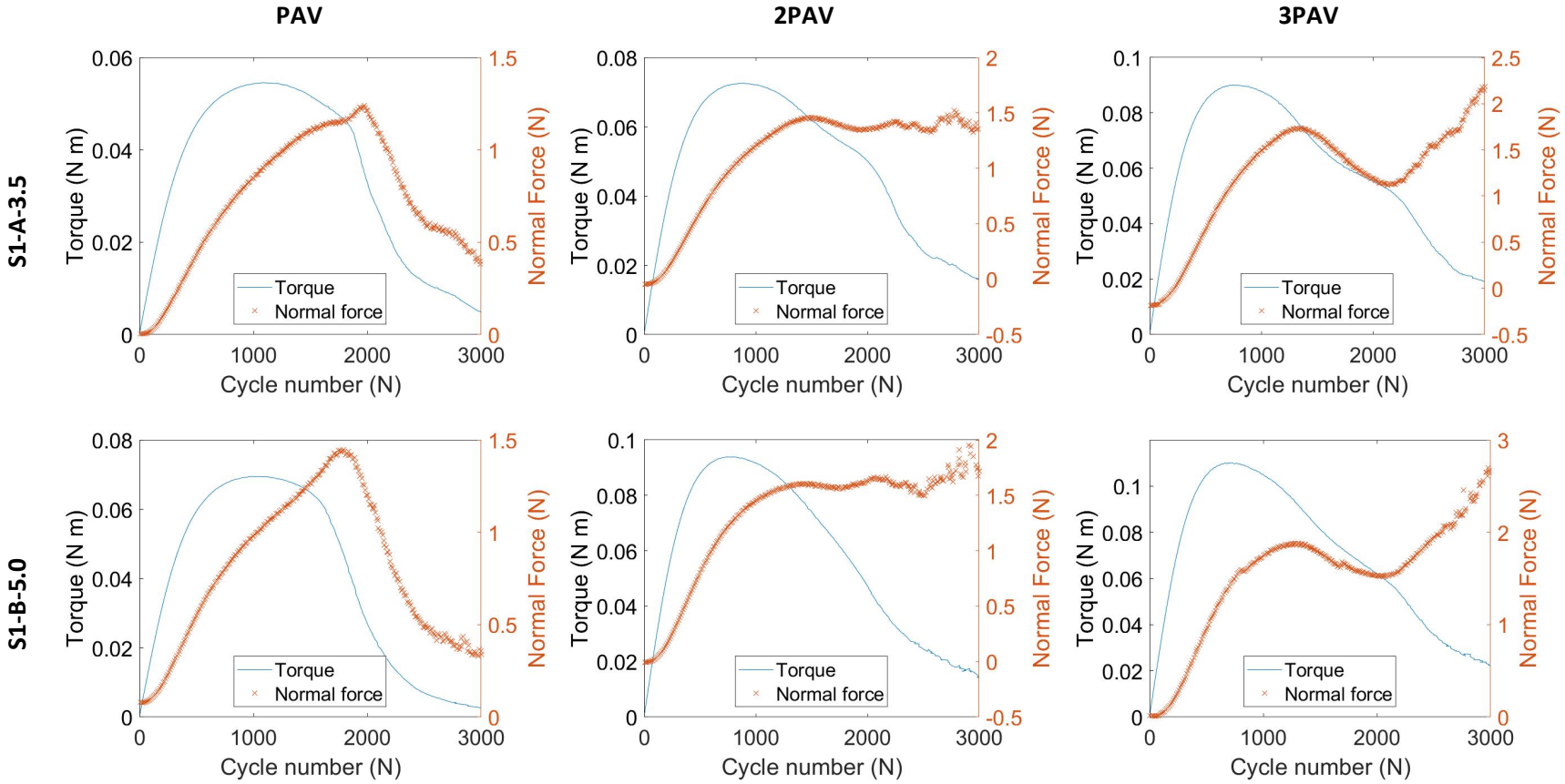

Figure 82. Graphs. Torque vs cycle number for PAV, 2PAV and 3PAV aging for binders S1-A-3.5 and S1-B-5.0.

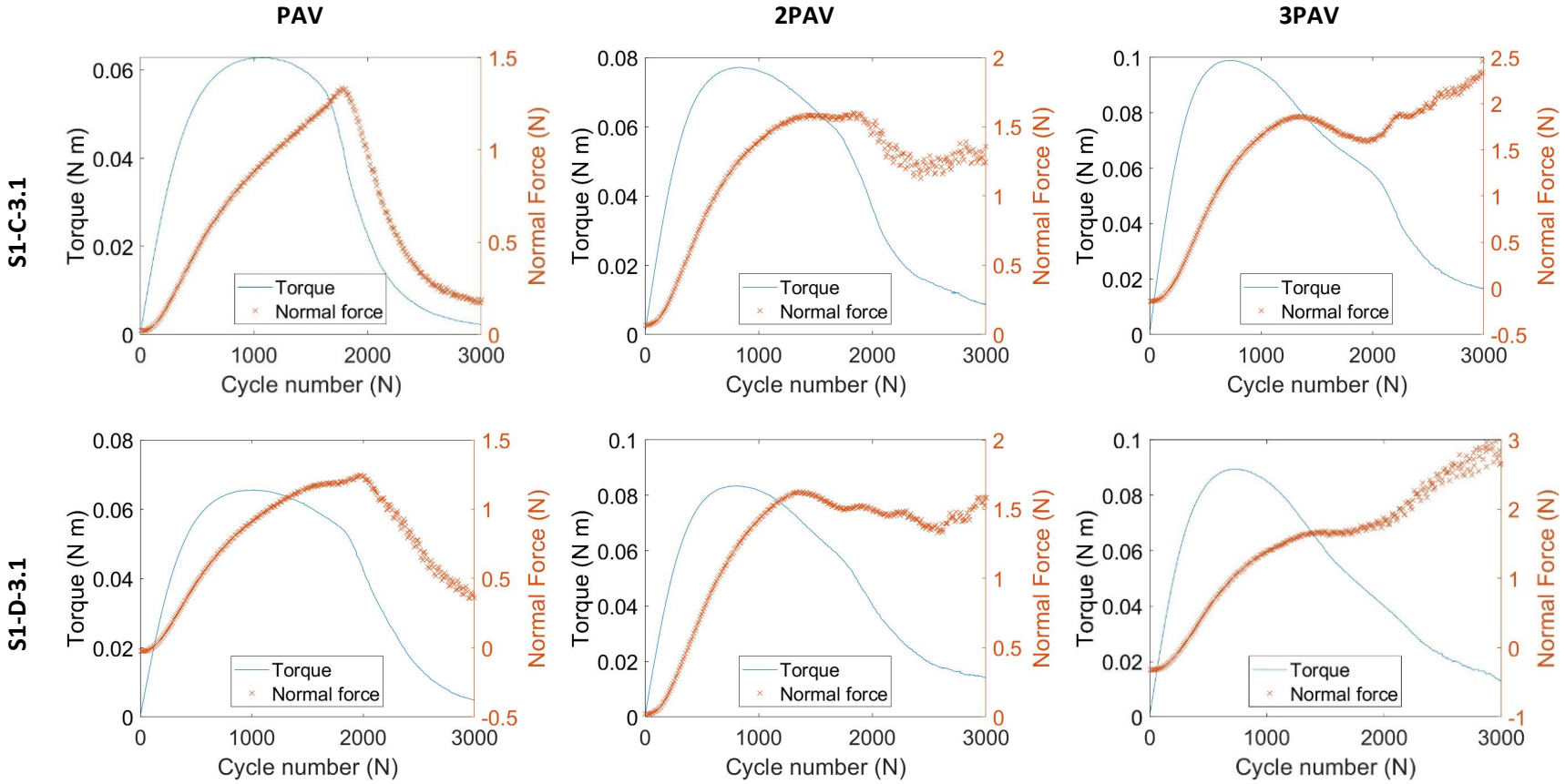

Figure 83. Graphs. Torque vs cycle number for PAV, 2PAV and 3PAV aging for binders S1-C-3.1 and S1-D-3.1.

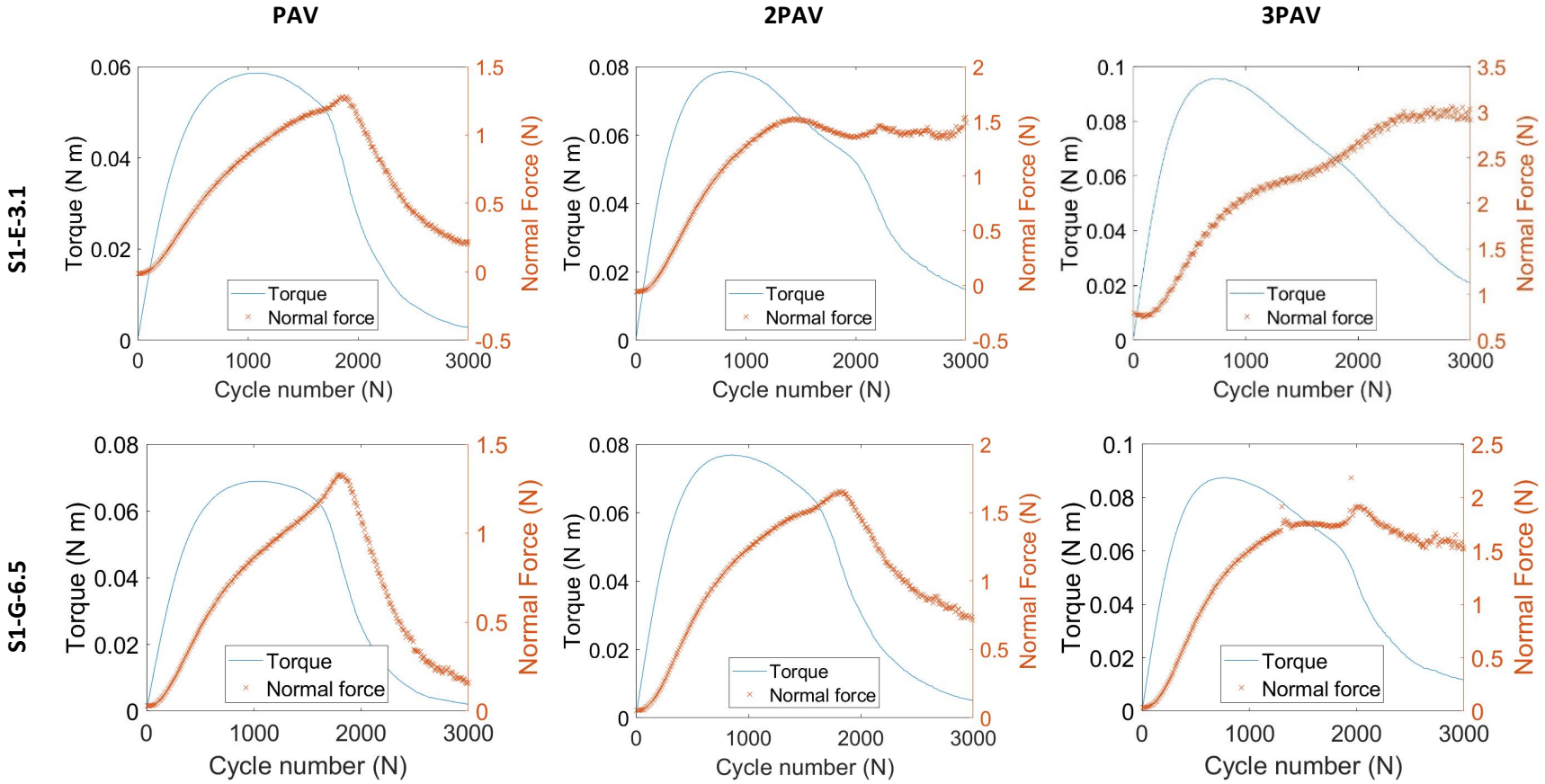

Figure 84. Graphs. Torque vs cycle number for PAV, 2PAV and 3PAV aging for binders S1-E-3.1 and S1-G-6.5.

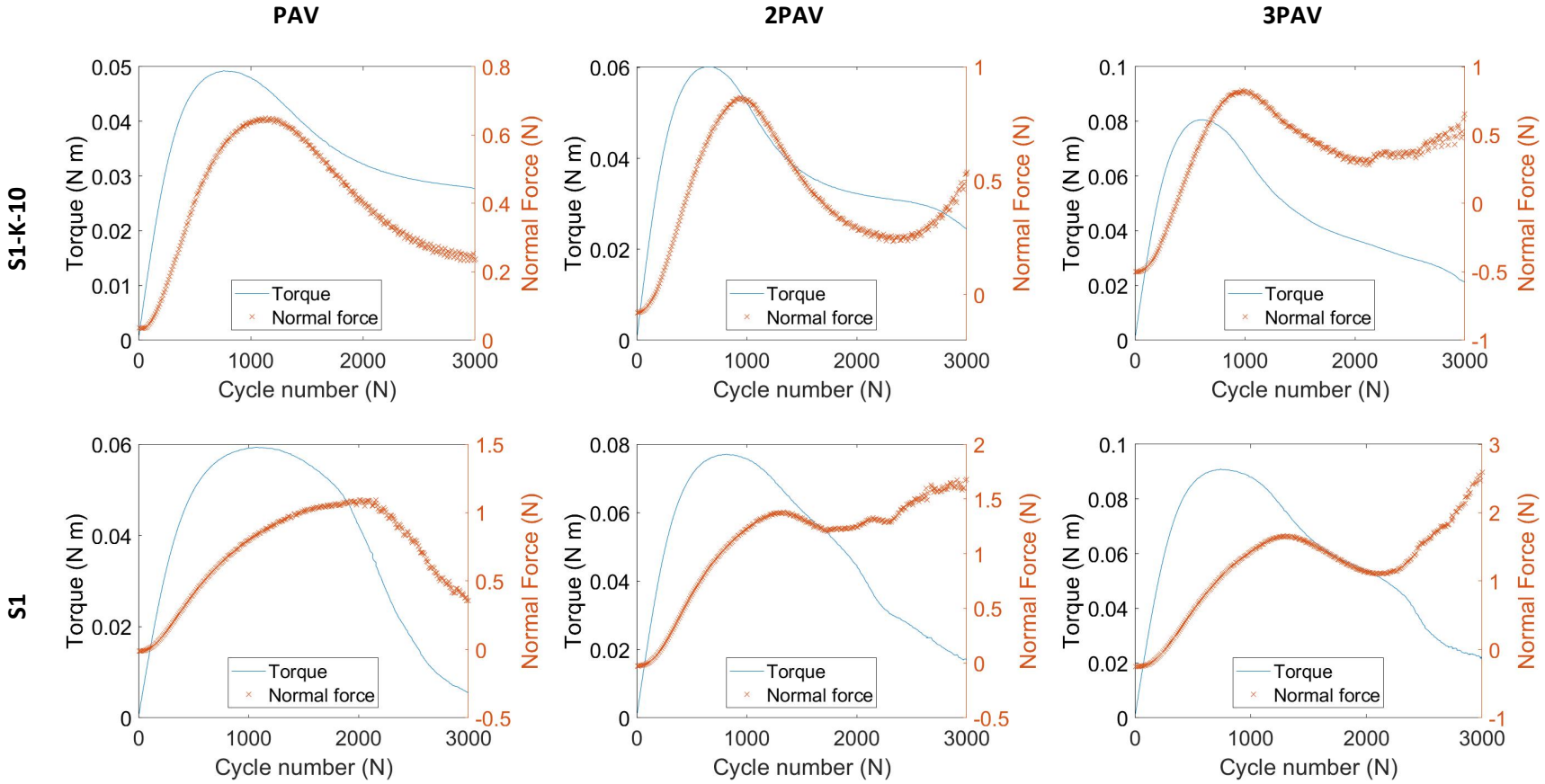

Figure 85. Graphs. Torque vs cycle number for PAV, 2PAV and 3PAV aging for binders S1-K-10 and S1.

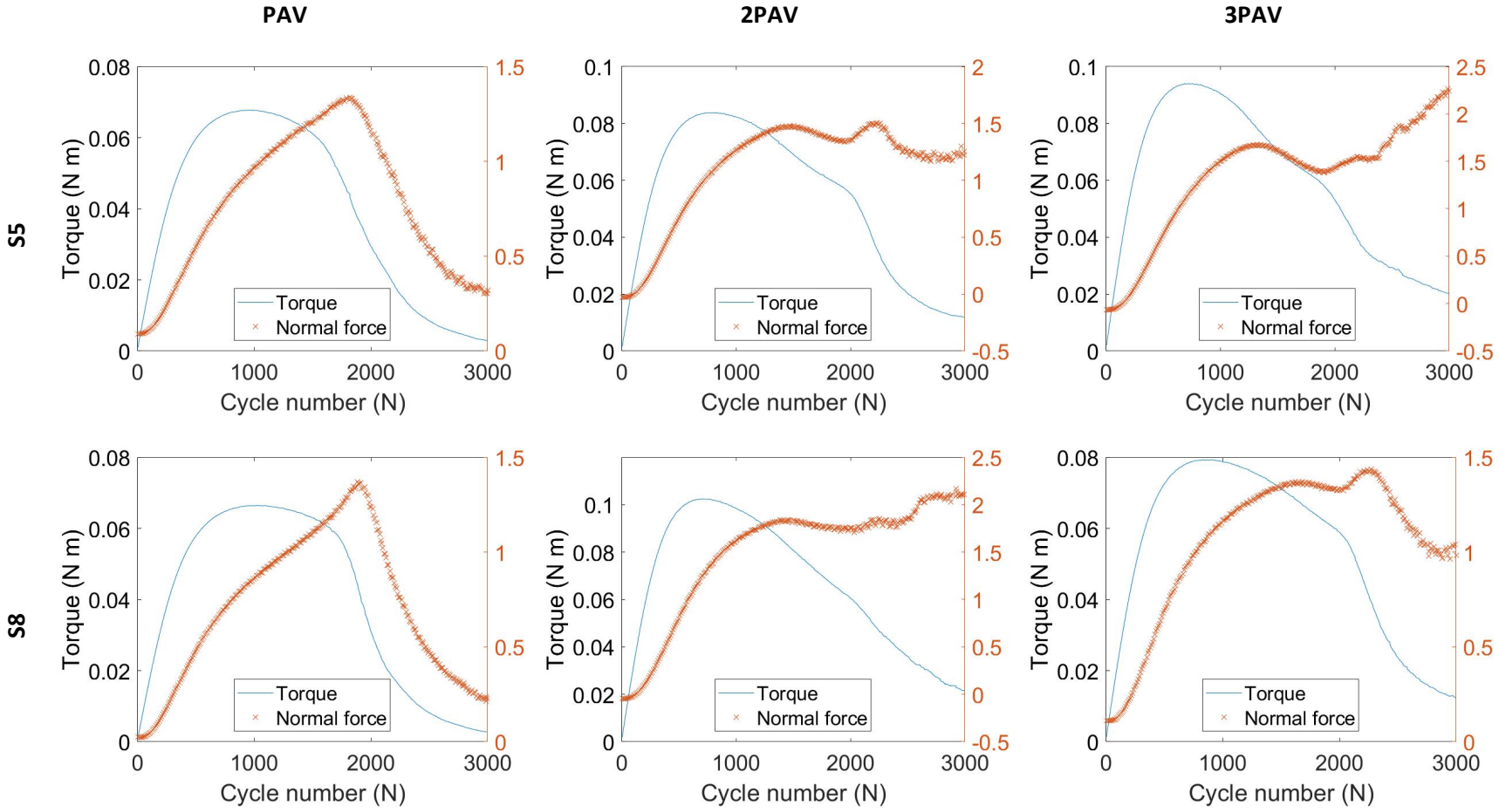

Figure 86. Graphs. Torque vs cycle number for PAV, 2PAV and 3PAV aging for binders S5 and S8.

τ, τ x N and C x τ x (1-C) for Every Cycle for Two Replicates of All Tested Binders at All Tested Aging Conditions

S5

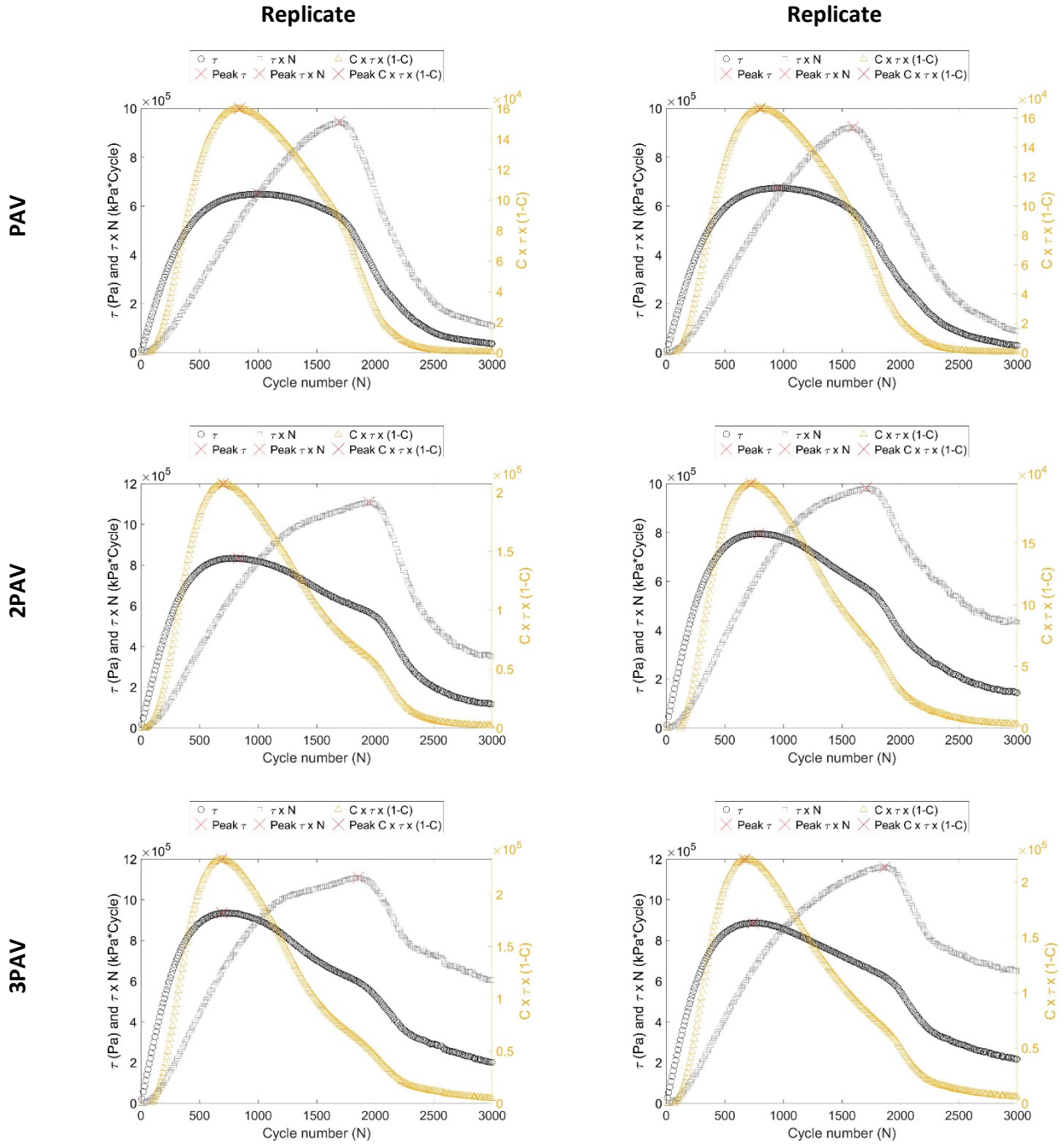

Figure 87. Graphs. Replicates of Torque (τ), τ x N, and C x τ x (1-C) vs cycle number for PAV, 2PAV and 3PAV aging for binder S5.

S8

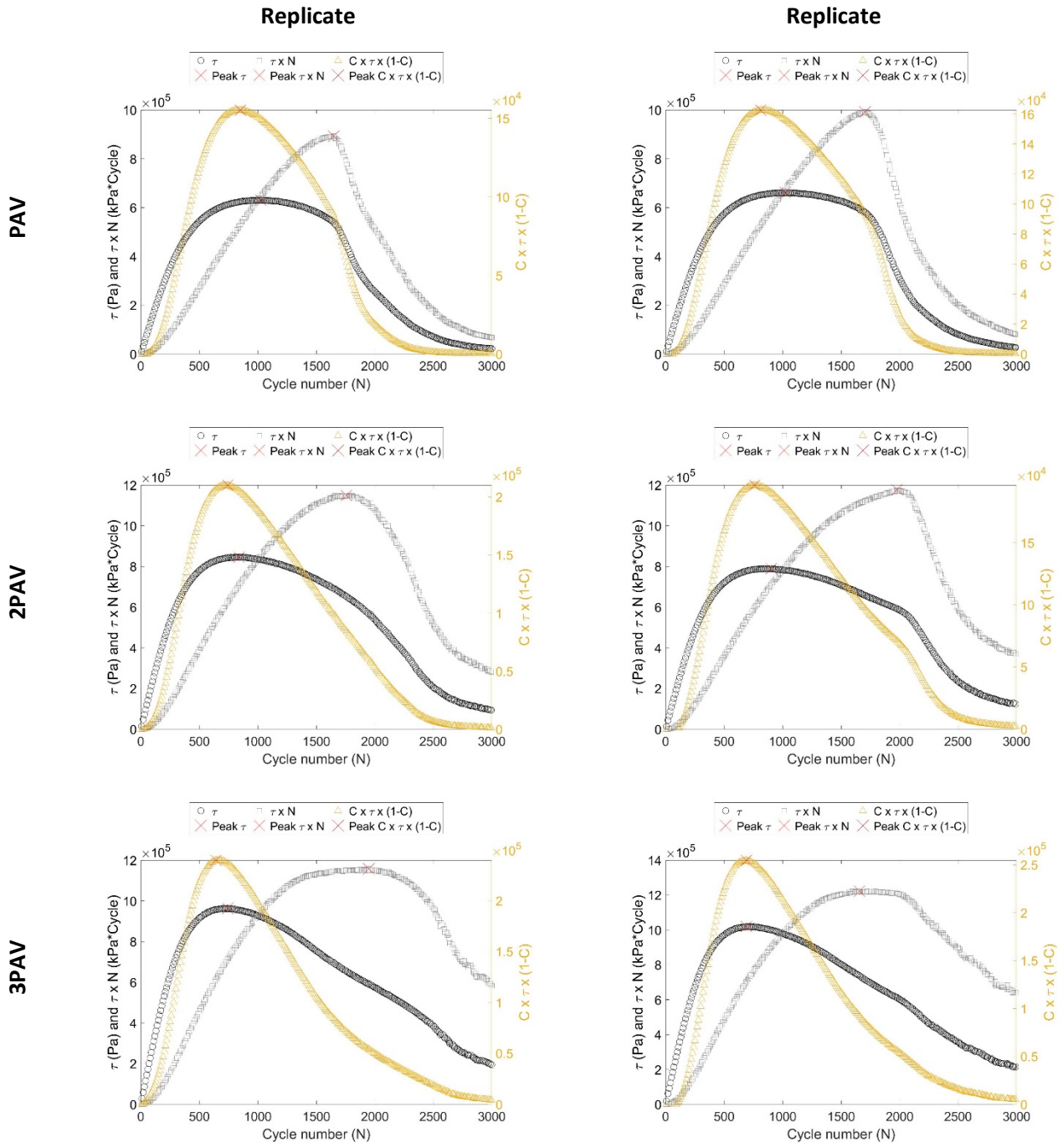

Figure 88. Graphs. Replicates of Torque (τ), τ x N, and C x τ x (1-C) vs cycle number for PAV, 2PAV and 3PAV aging for binder S8.

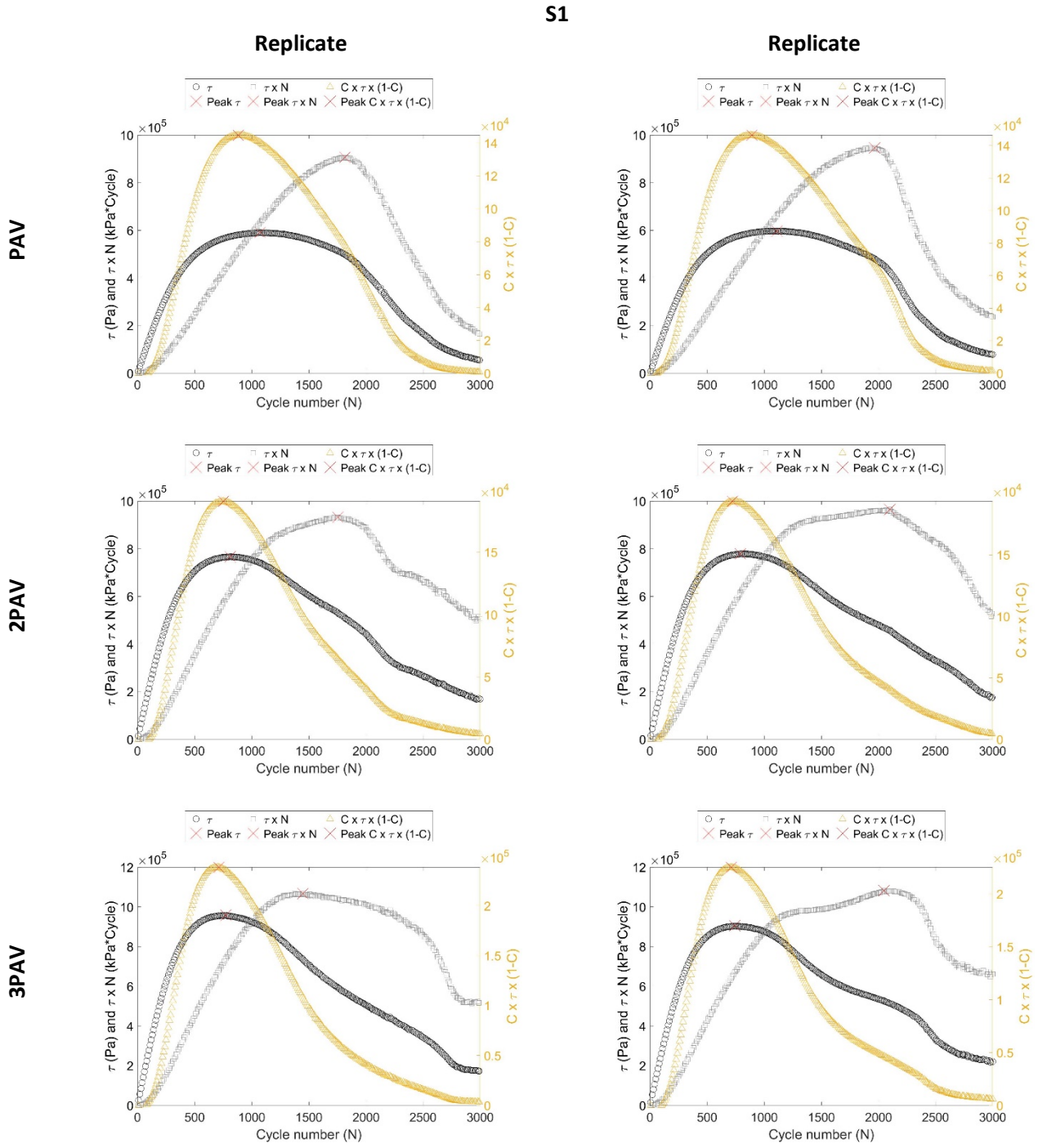

Figure 89. Graphs. Replicates of Torque (τ), τ x N, and C x τ x (1-C) vs cycle number for PAV, 2PAV and 3PAV aging for binder S1.

S1-A-3.5

	Replicate	Replicate
UA	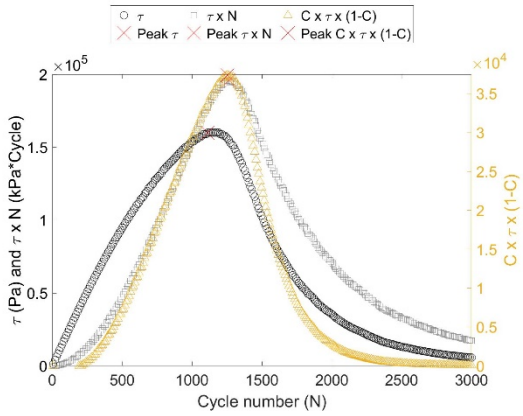	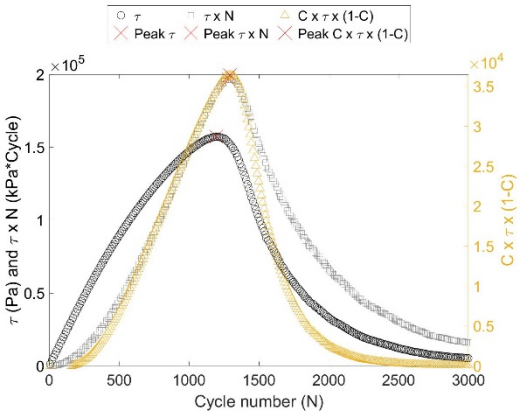
RTFO	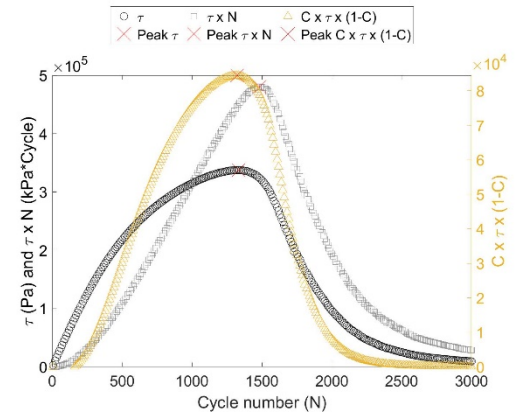	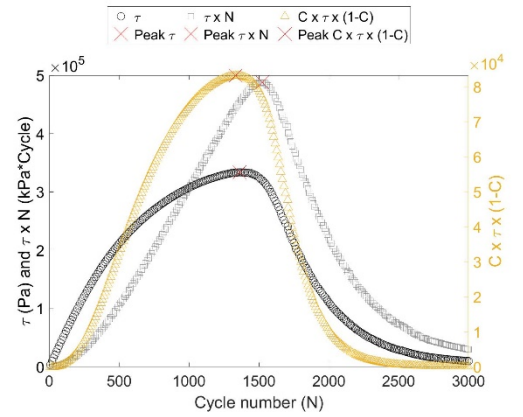
PAV	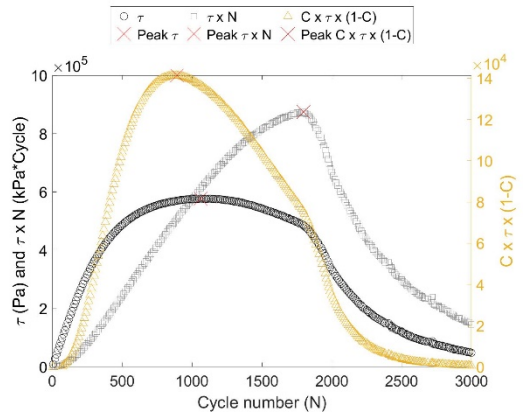	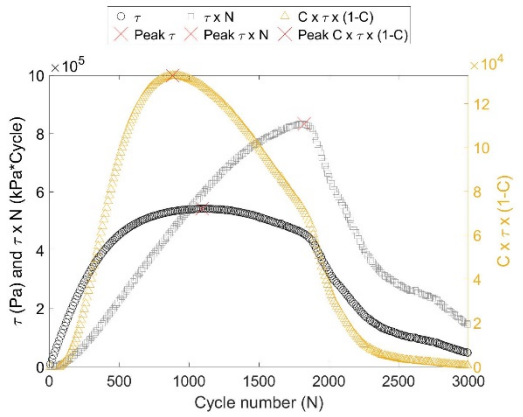

S1-A-3.5

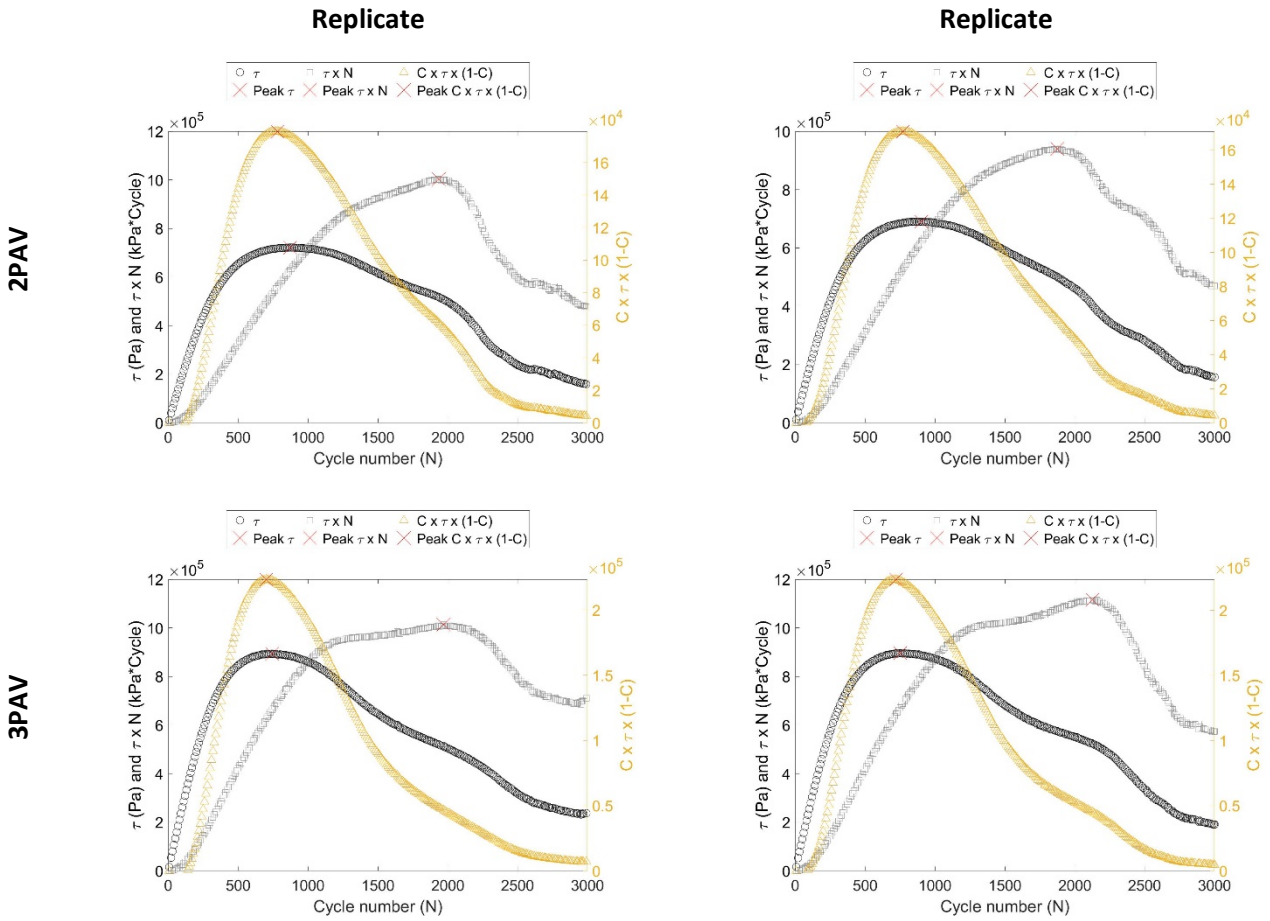

Figure 90. Graphs. Replicates of Torque (τ), τ x N, and C x τ x (1-C) vs cycle number for UA, RTFO, PAV, 2PAV and 3PAV aging for binder S1-A-3.5.

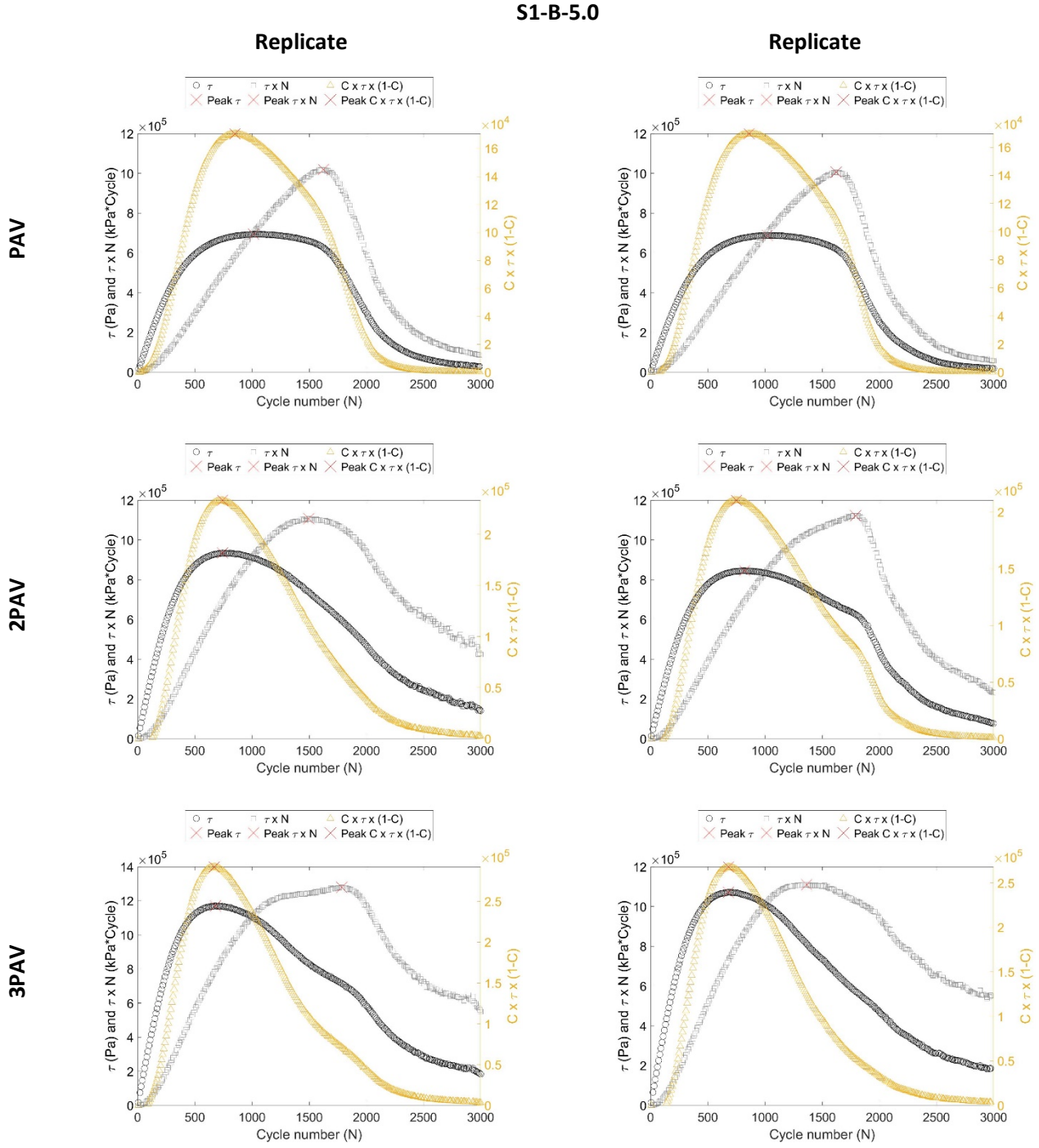

Figure 91. Graphs. Replicates of Torque (τ), τ x N, and C x τ x (1-C) vs cycle number for PAV, 2PAV and 3PAV aging for binder S1-B-5.0.

S1-C-3.1

	Replicate	Replicate
UA	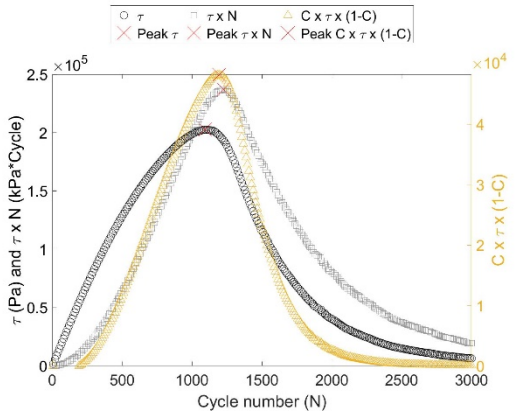	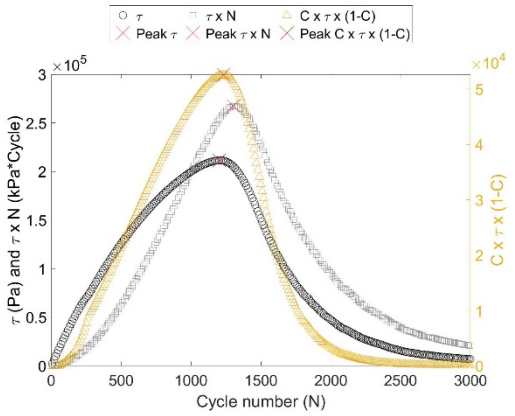
RTFO	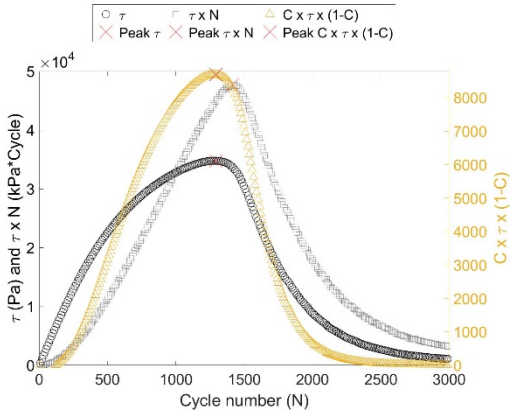	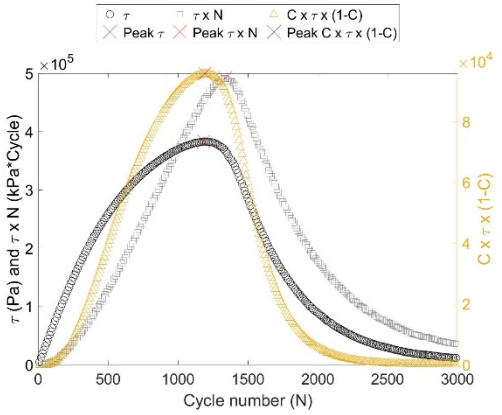
PAV	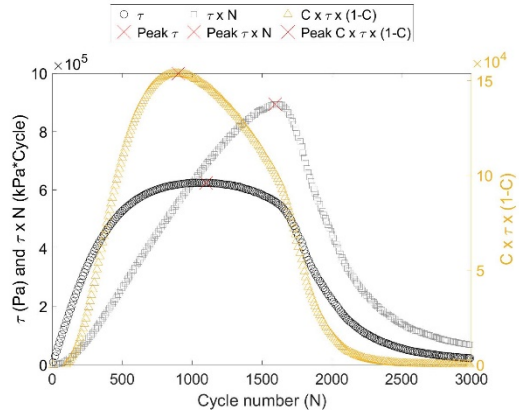	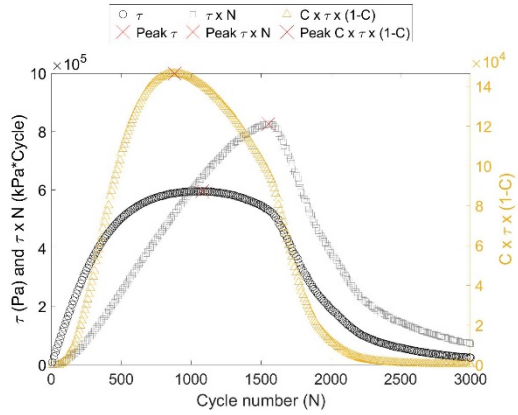

S1-C-3.1

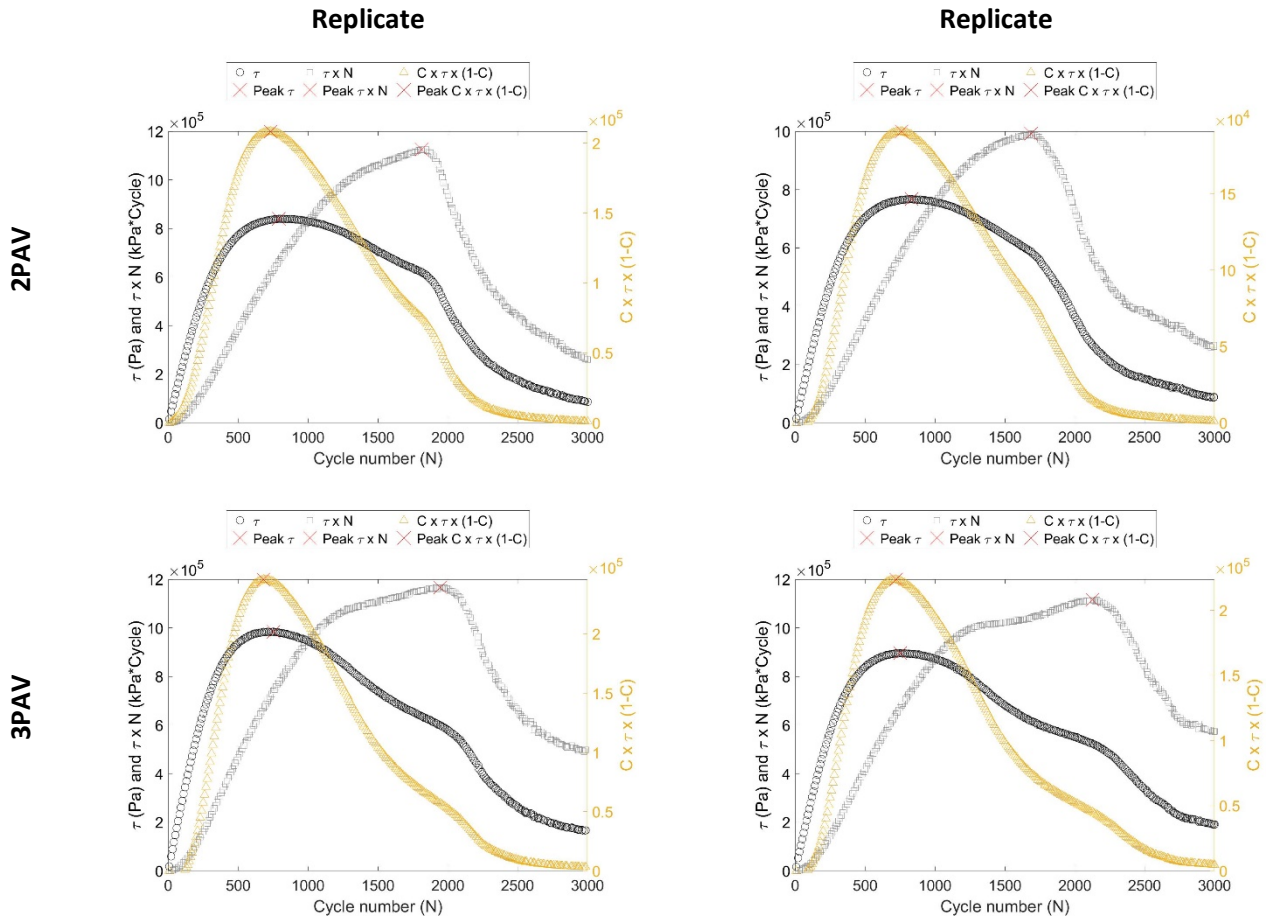

Figure 92. Graphs. Replicates of Torque (τ), τ x N, and C x τ x (1-C) vs cycle number for UA, RTFO, PAV, 2PAV and 3PAV aging for binder S1-C-3.1.

S1-D-3.1

	Replicate	Replicate
UA	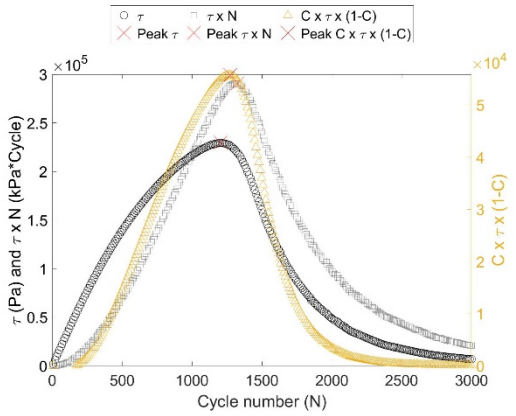	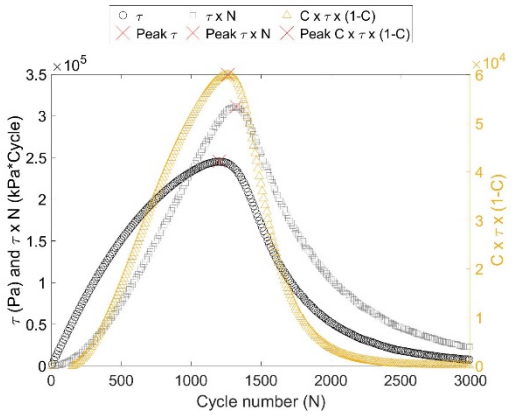
RTFO	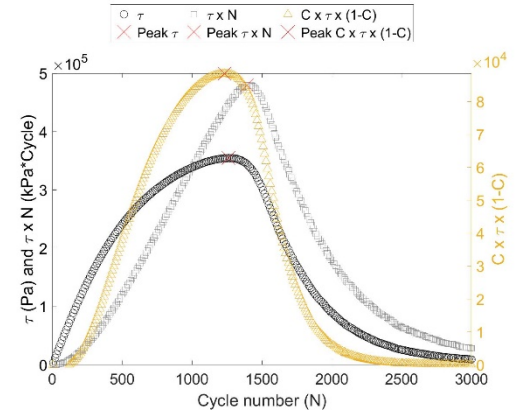	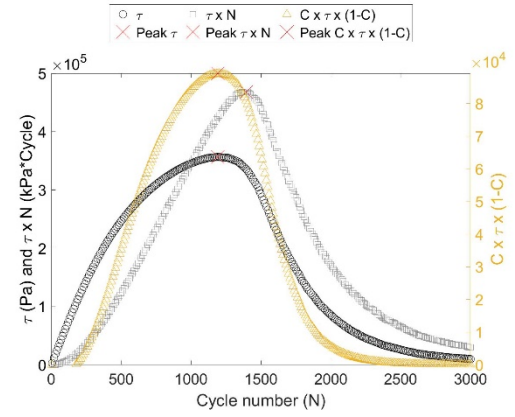
PAV	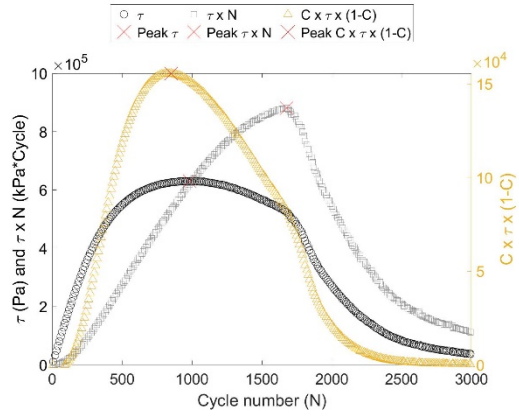	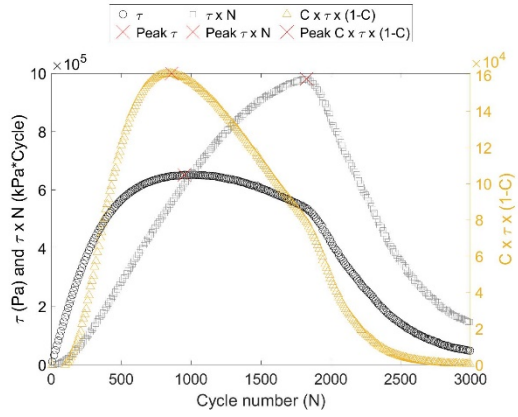

S1-D-3.1

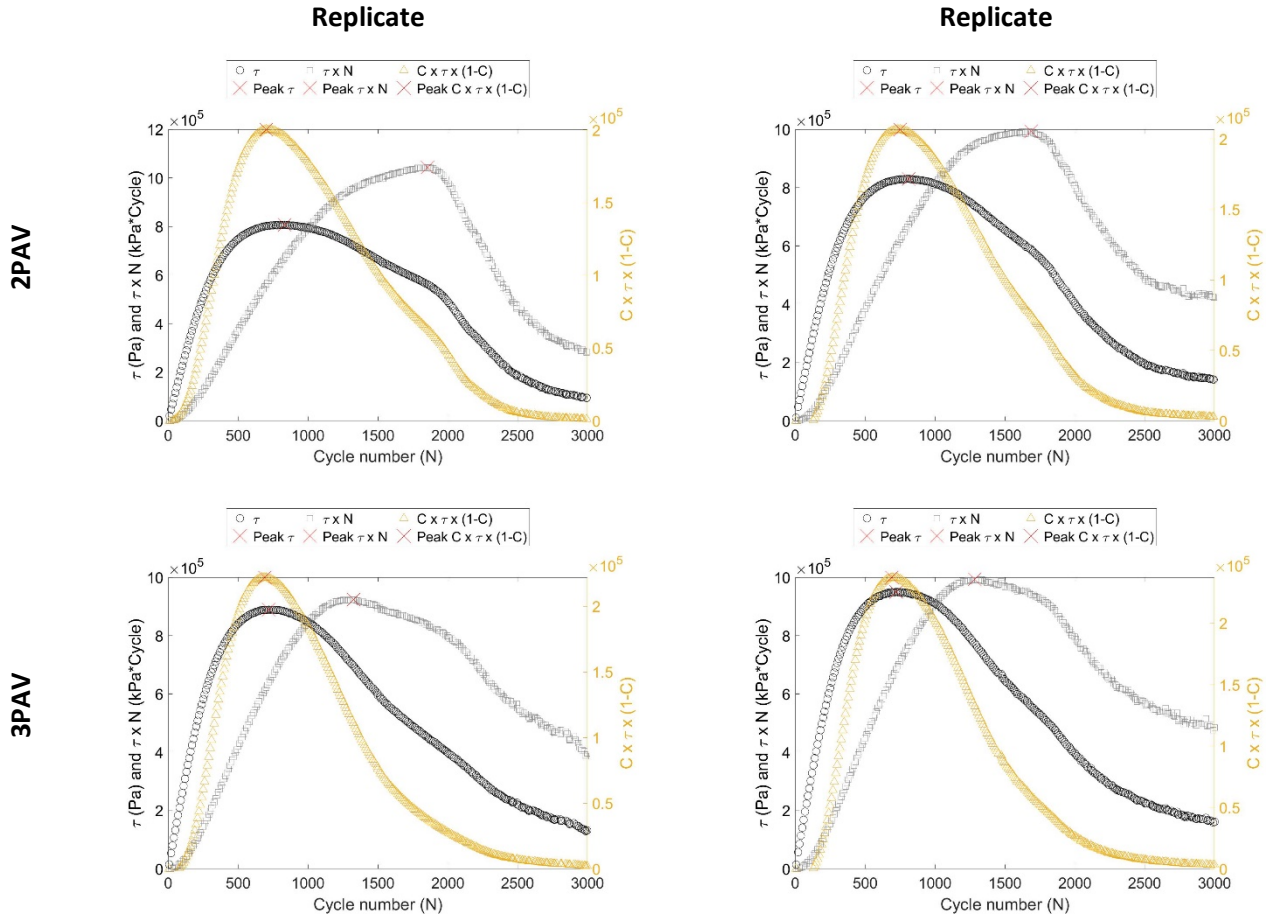

Figure 93. Graphs. Replicates of Torque (τ), τ x N, and C x τ x (1-C) vs cycle number for UA, RTFO, PAV, 2PAV and 3PAV aging for binder S1-D-3.1.

S1-E-3.1

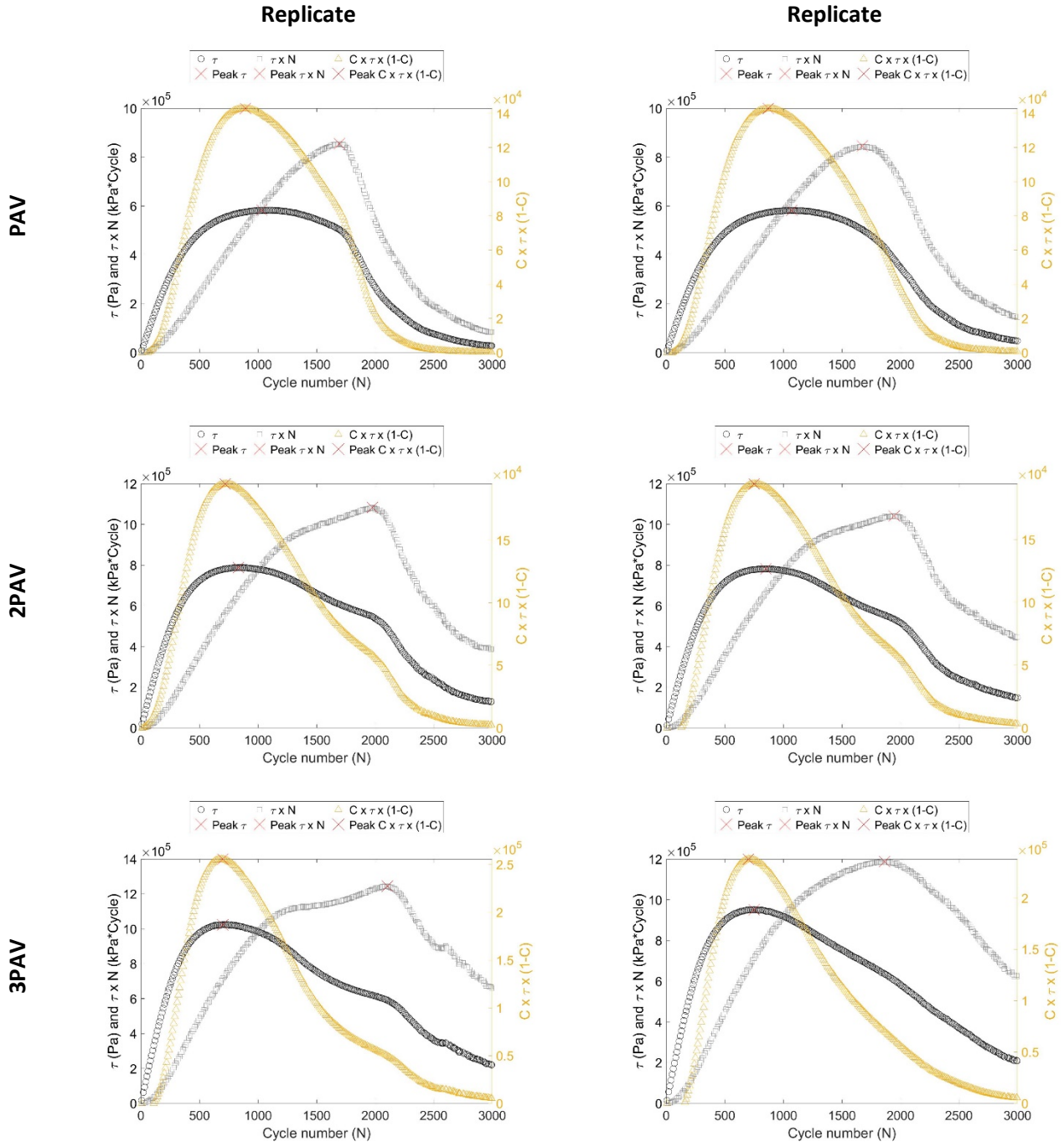

Figure 94. Graphs. Replicates of Torque (τ), τ x N, and C x τ x (1-C) vs cycle number for PAV, 2PAV and 3PAV aging for binder S1-E-3.1.

S1-F-3.1

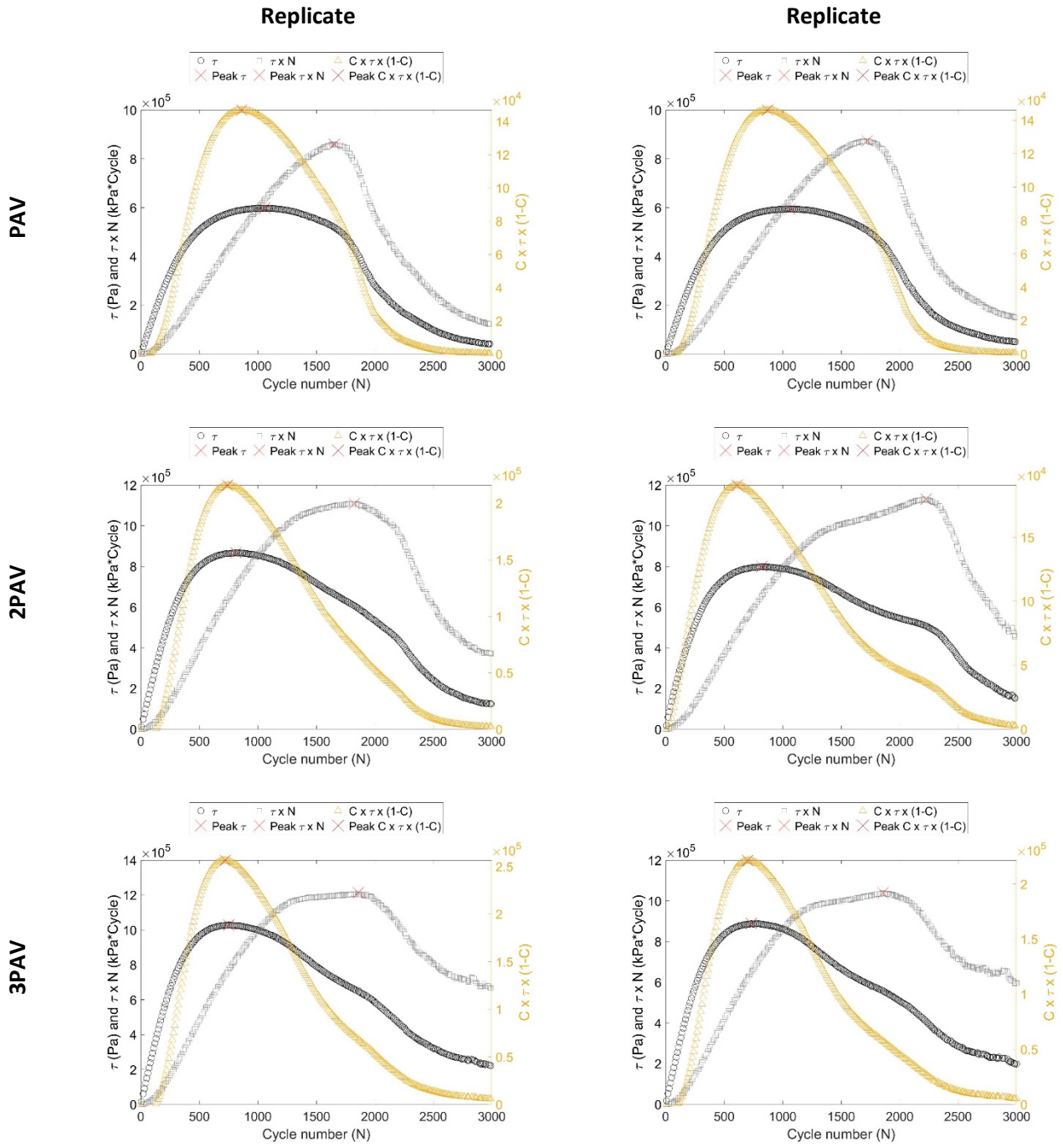

Figure 95. Graphs. Replicates of Torque (τ), τ x N, and C x τ x (1-C) vs cycle number for PAV, 2PAV and 3PAV aging for binder S1-F-3.1.

S1-G-6.5

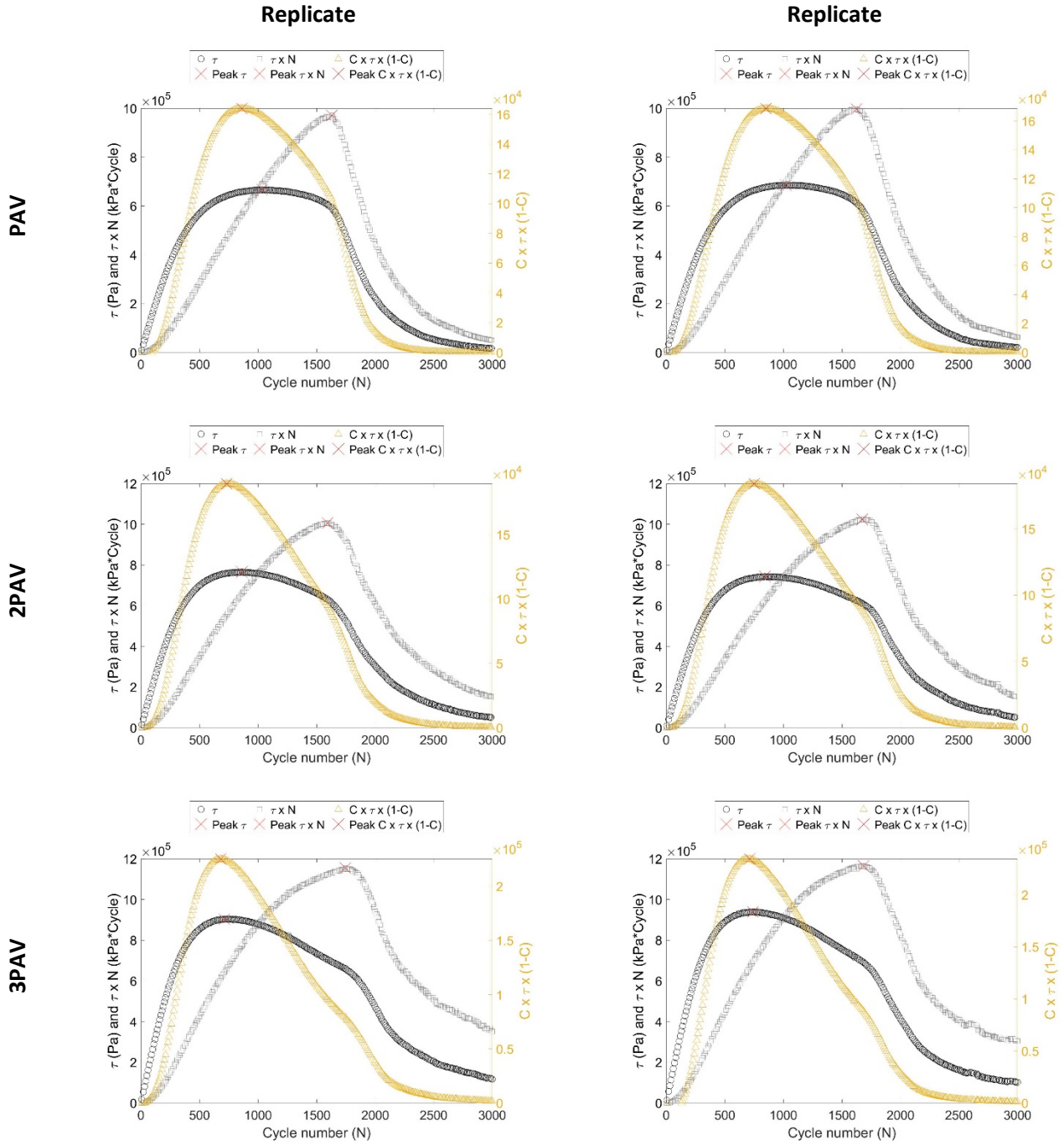

Figure 96. Graphs. Replicates of Torque (τ), τ x N, and C x τ x (1-C) vs cycle number for PAV, 2PAV and 3PAV aging for binder S1-G-6.5.

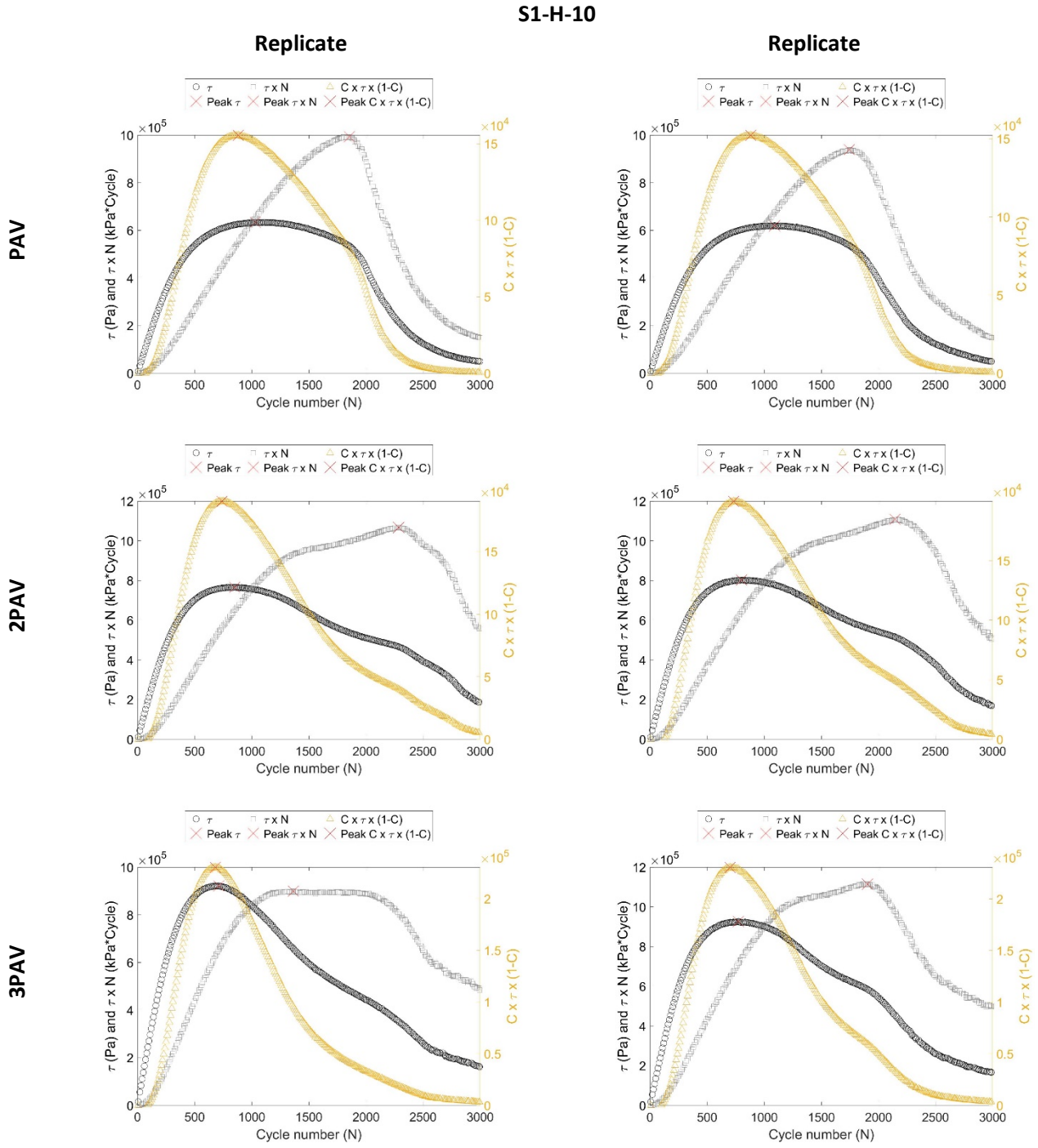

Figure 97. Graphs. Replicates of Torque (τ), τ x N, and C x τ x (1-C) vs cycle number for PAV, 2PAV and 3PAV aging for binder S1-H-10.

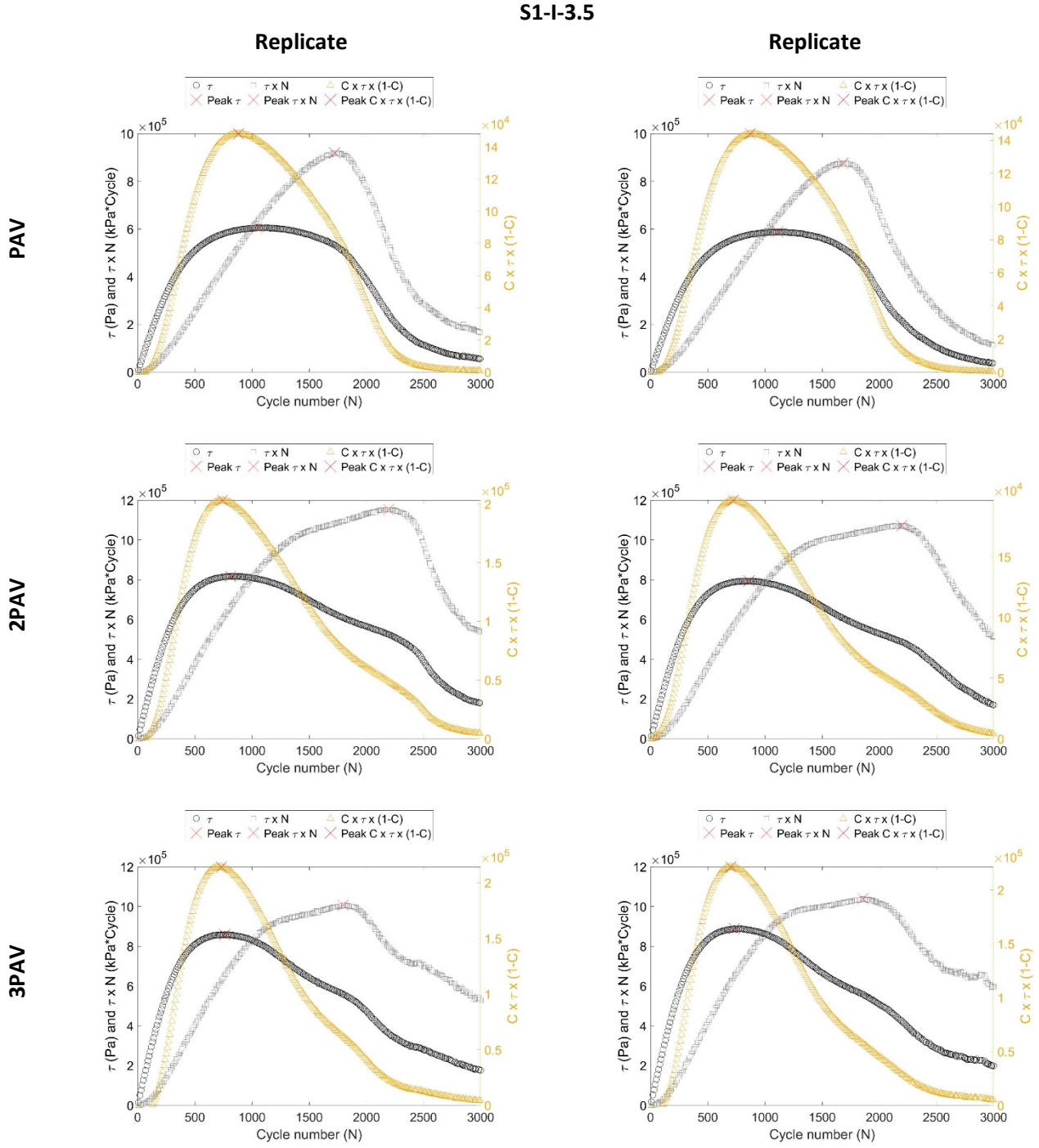

Figure 98. Graphs. Replicates of Torque (τ), τ x N, and C x τ x (1-C) vs cycle number for PAV, 2PAV and 3PAV aging for binder S1-I-3.5.

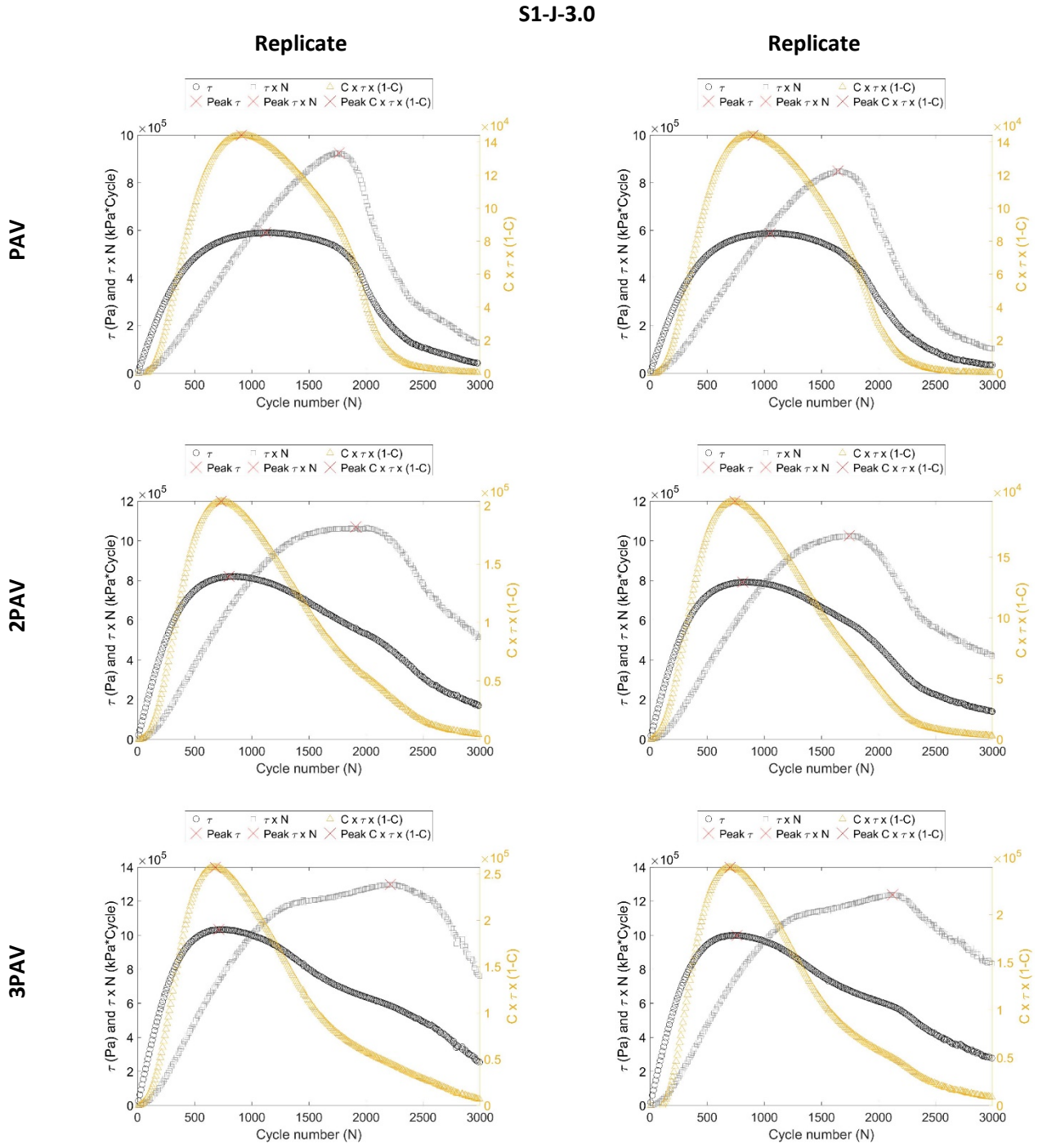

Figure 99. Graphs. Replicates of Torque (τ), τ x N, and C x τ x (1-C) vs cycle number for PAV, 2PAV and 3PAV aging for binder S1-J-3.0.

S1-K-10

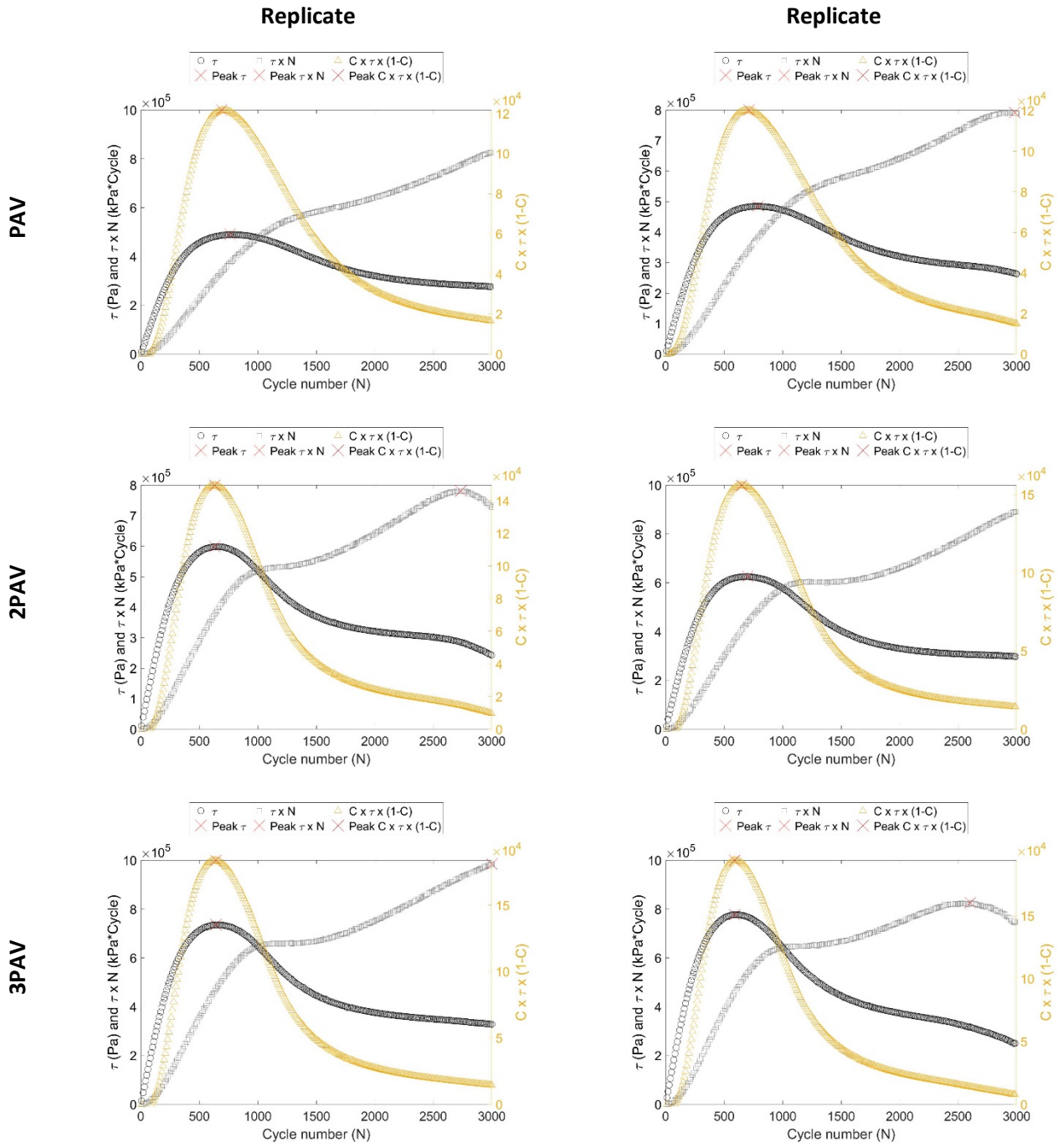

Figure 100. Graphs. Replicates of Torque (τ), τ x N, and C x τ x (1-C) vs cycle number for PAV, 2PAV and 3PAV aging for binder S1-K-10.

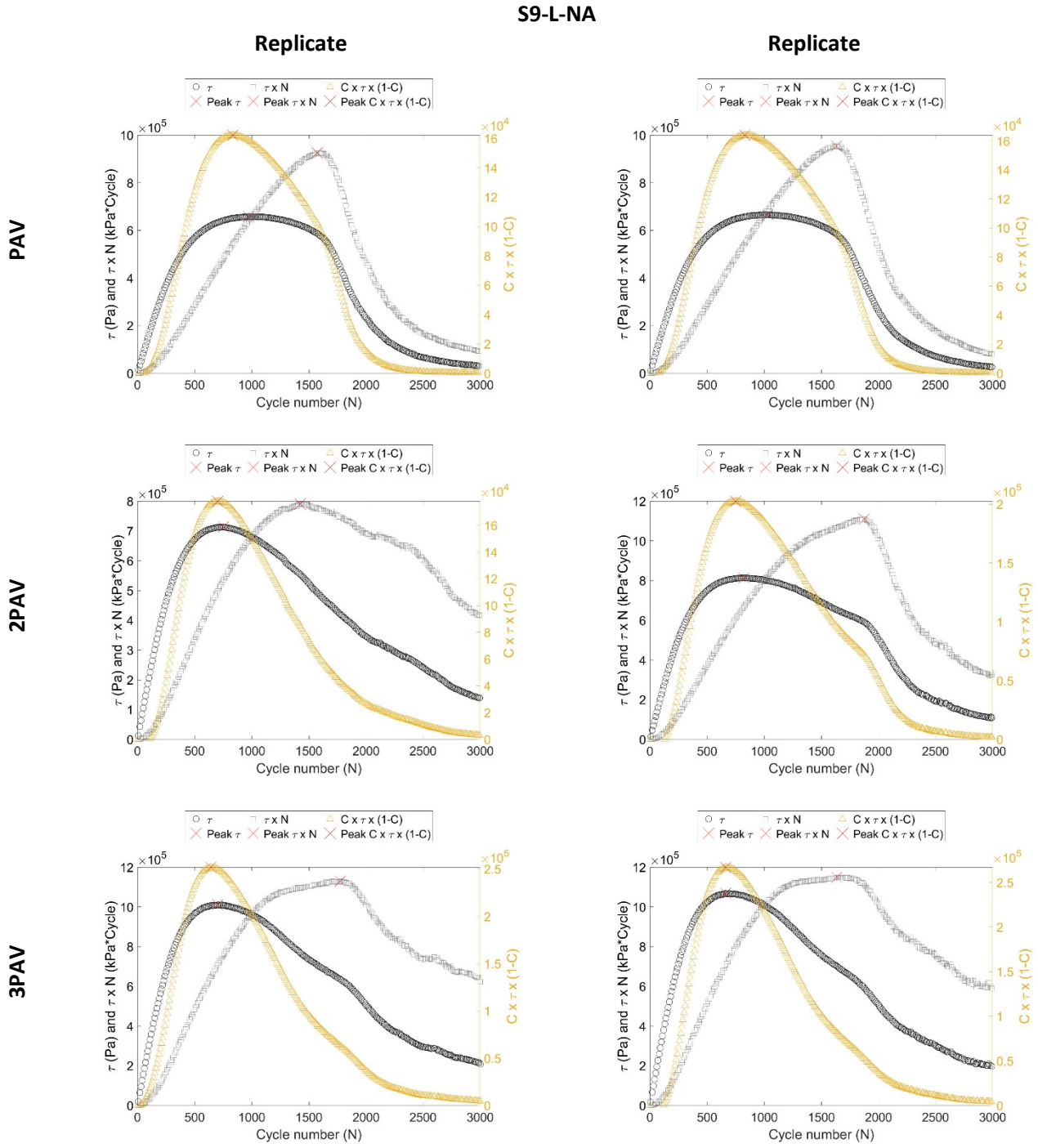

Figure 101. Graphs. Replicates of Torque (τ), τ x N, and C x τ x (1-C) vs cycle number for PAV, 2PAV and 3PAV aging for binder S9-L-NA.

C-N Curves for All Binders at All Aging Conditions Marked at Peak Shear Stress Cycle

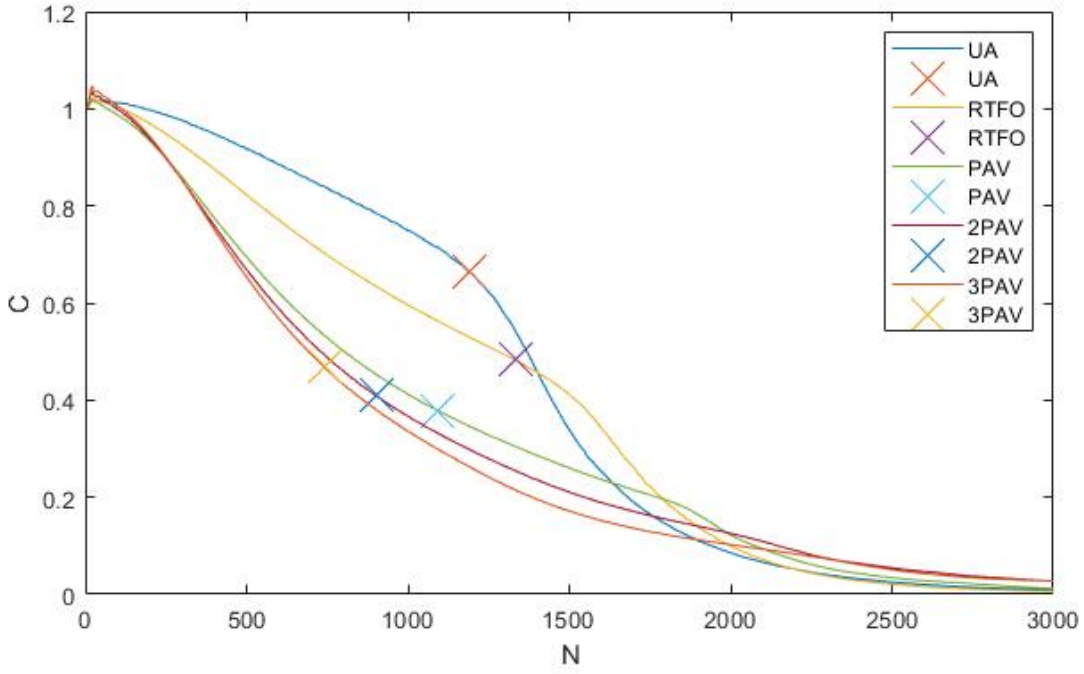

Figure 102. Graph. C-N curves for S1-A-3.5 at UA, RTFO, PAV, 2PAV, and 3PAV aging conditions.

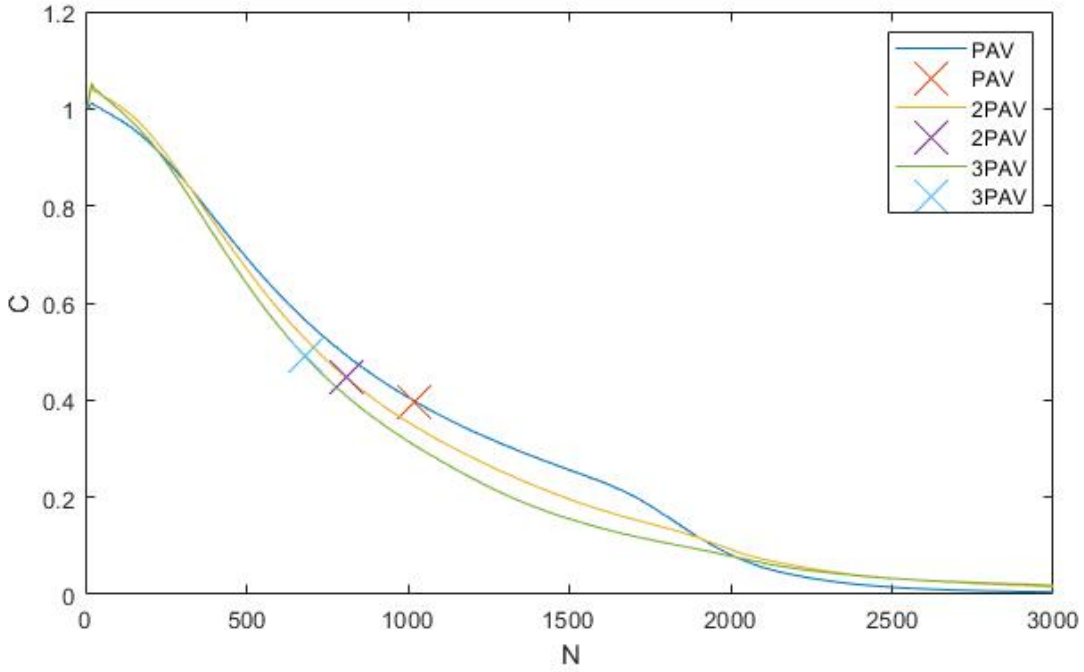

Figure 103. Graph. C-N curves for S1-B-5.0 at PAV, 2PAV, and 3PAV aging conditions.

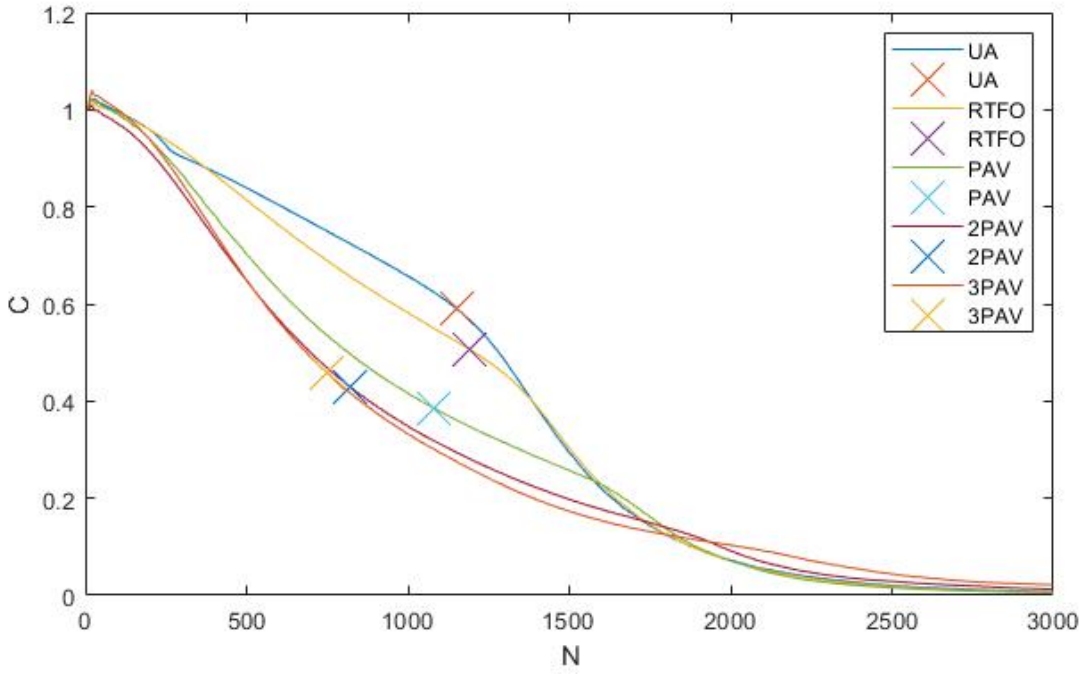

Figure 104. Graph. C-N curves for S1-C-3.1 at UA, RTFO, PAV, 2PAV, and 3PAV aging conditions.

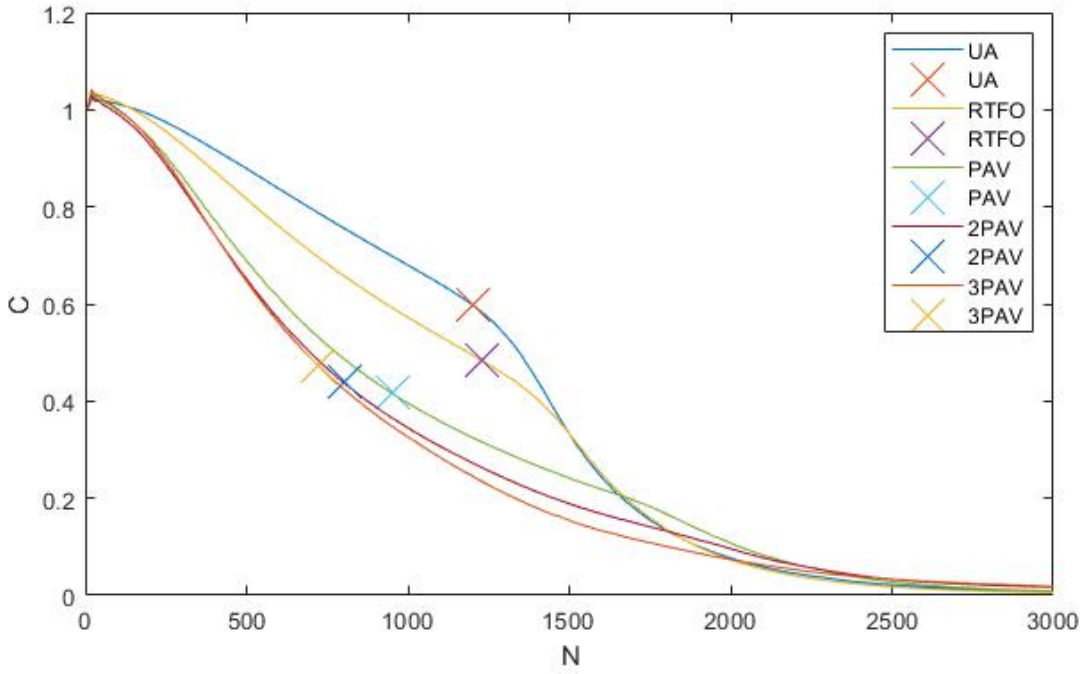

Figure 105. Graph. C-N curves for S1-D-3.1 at UA, RTFO, PAV, 2PAV, and 3PAV aging conditions.

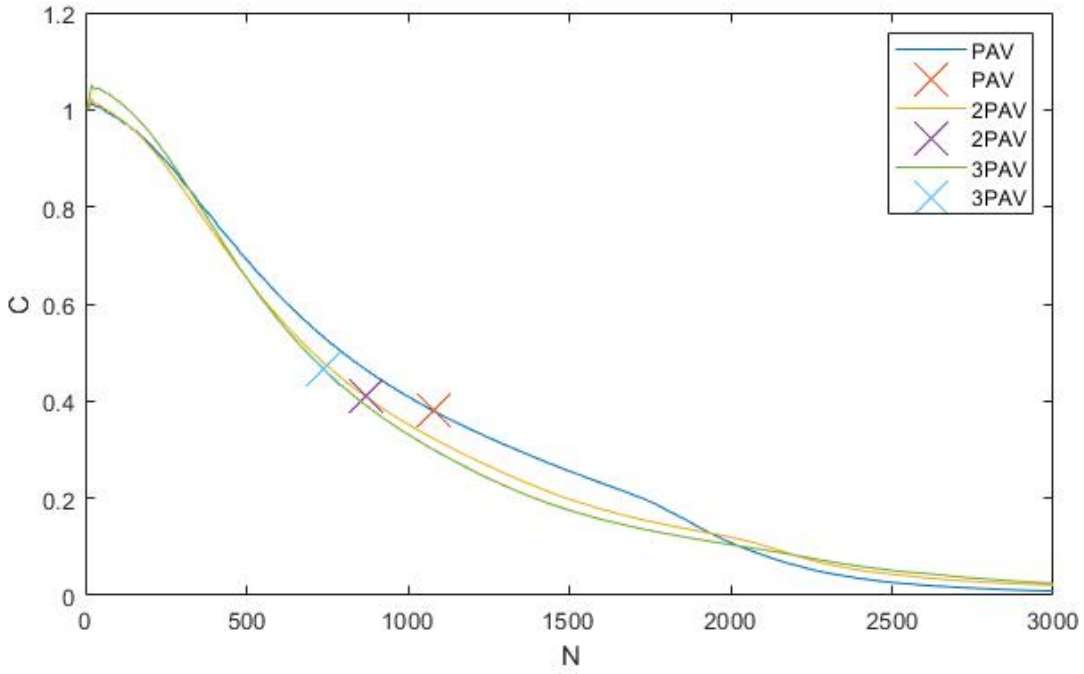

Figure 106. Graph. C-N curves for S1-E-3.1 at PAV, 2PAV, and 3PAV aging conditions.

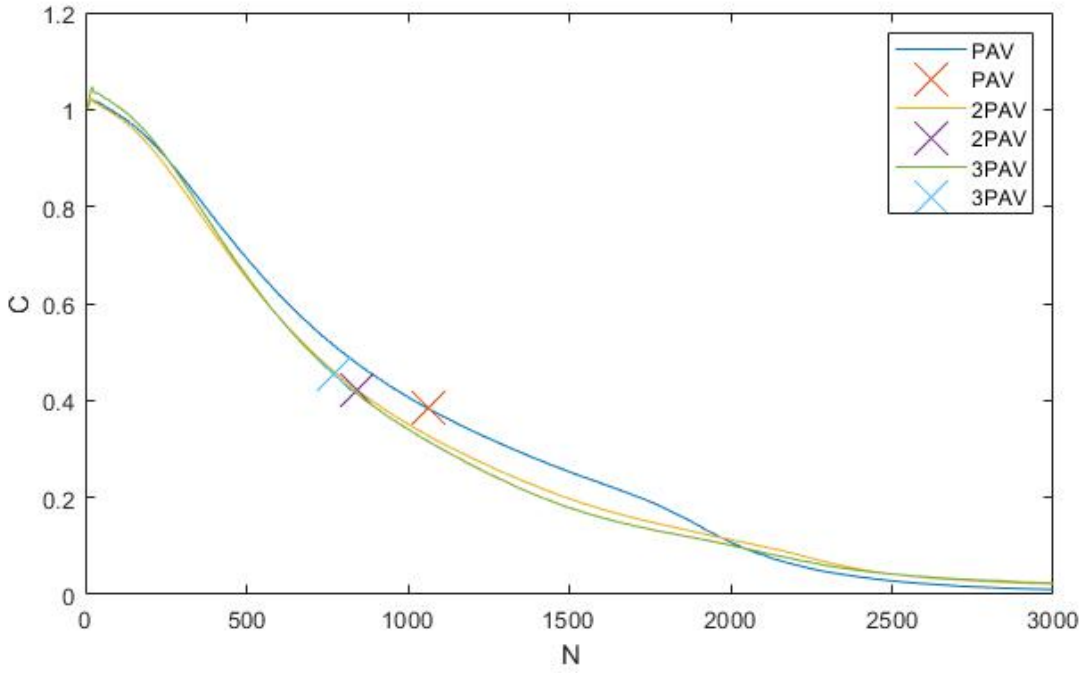

Figure 107. Graph. C-N curves for S1-F-3.1 at PAV, 2PAV, and 3PAV aging conditions.

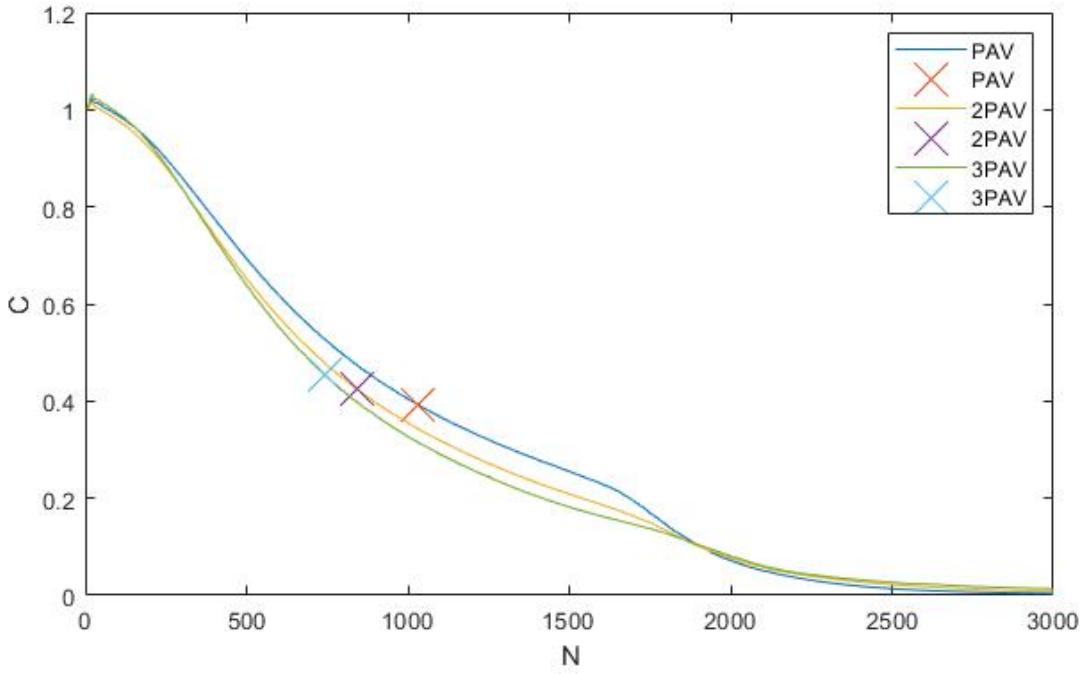

Figure 108. Graph. C-N curves for S1-G-6.5 at PAV, 2PAV, and 3PAV aging conditions.

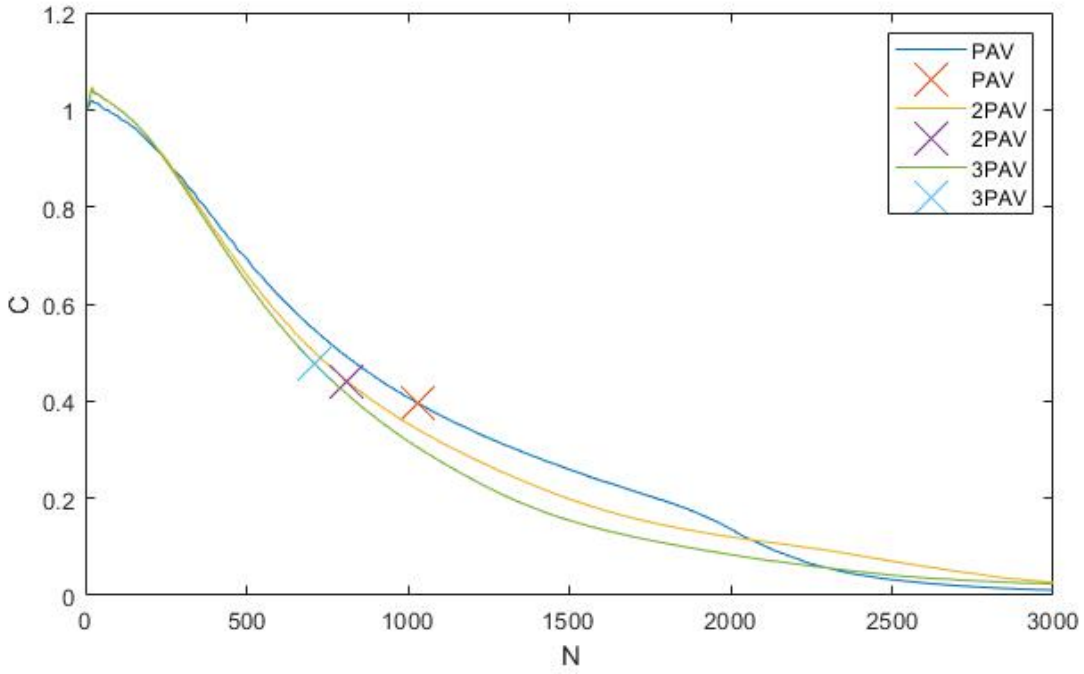

Figure 109. Graph. C-N curves for S1-H-10 at PAV, 2PAV, and 3PAV aging conditions.

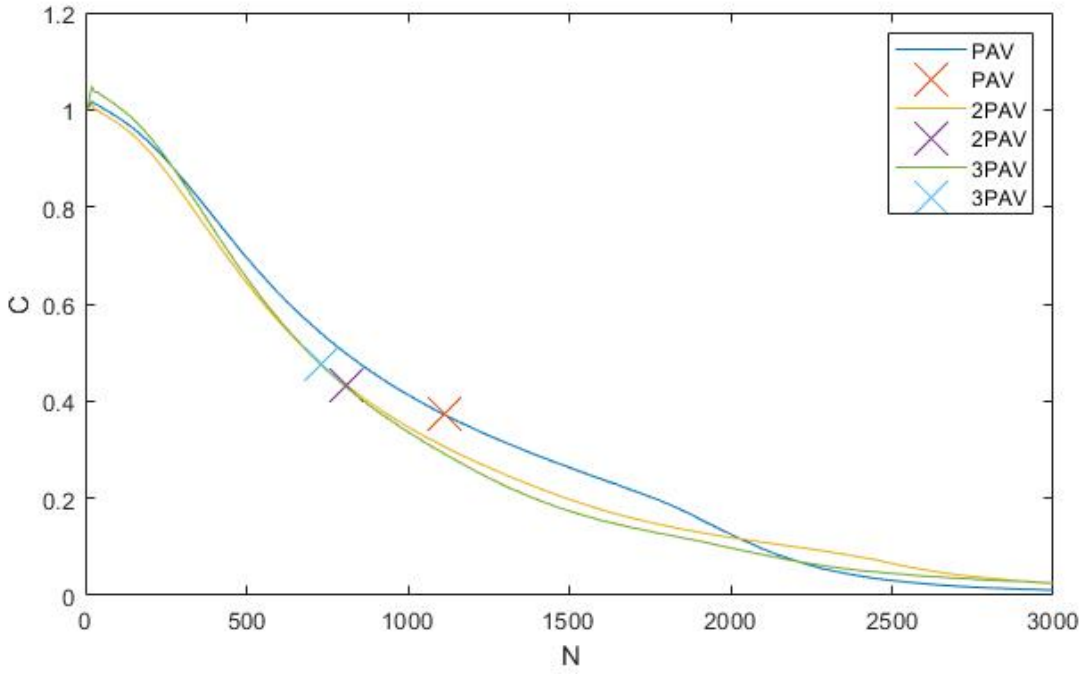

Figure 110. Graph. C-N curves for S1-I-3.5 at PAV, 2PAV, and 3PAV aging conditions.

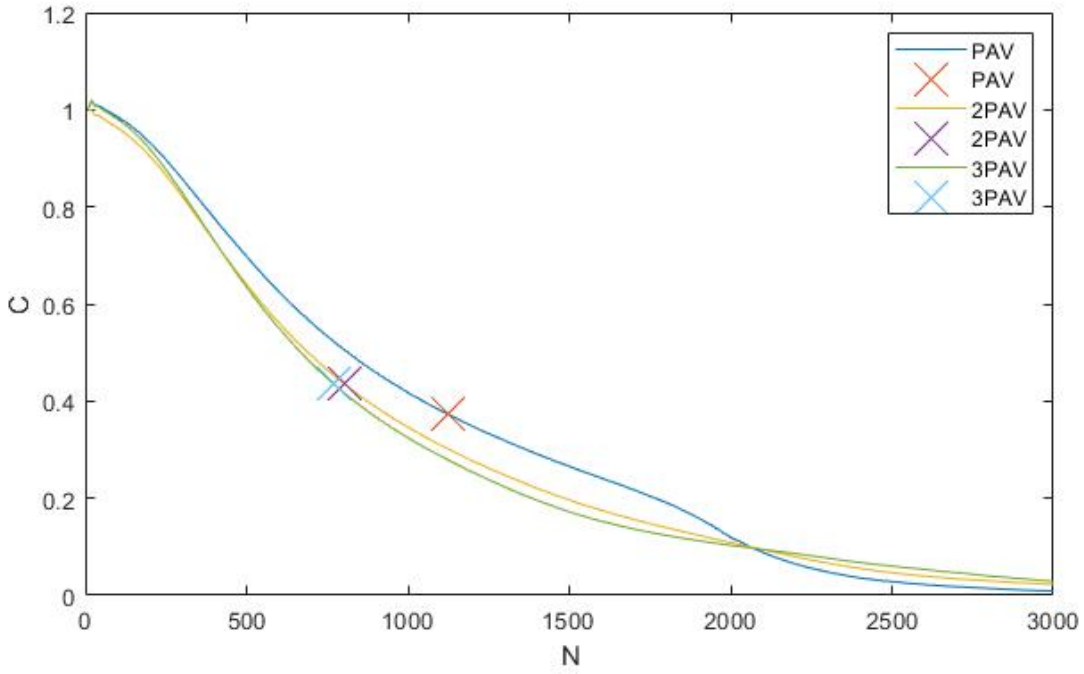

Figure 111. Graph. C-N curves for S1-J-3.0 at PAV, 2PAV, and 3PAV aging conditions.

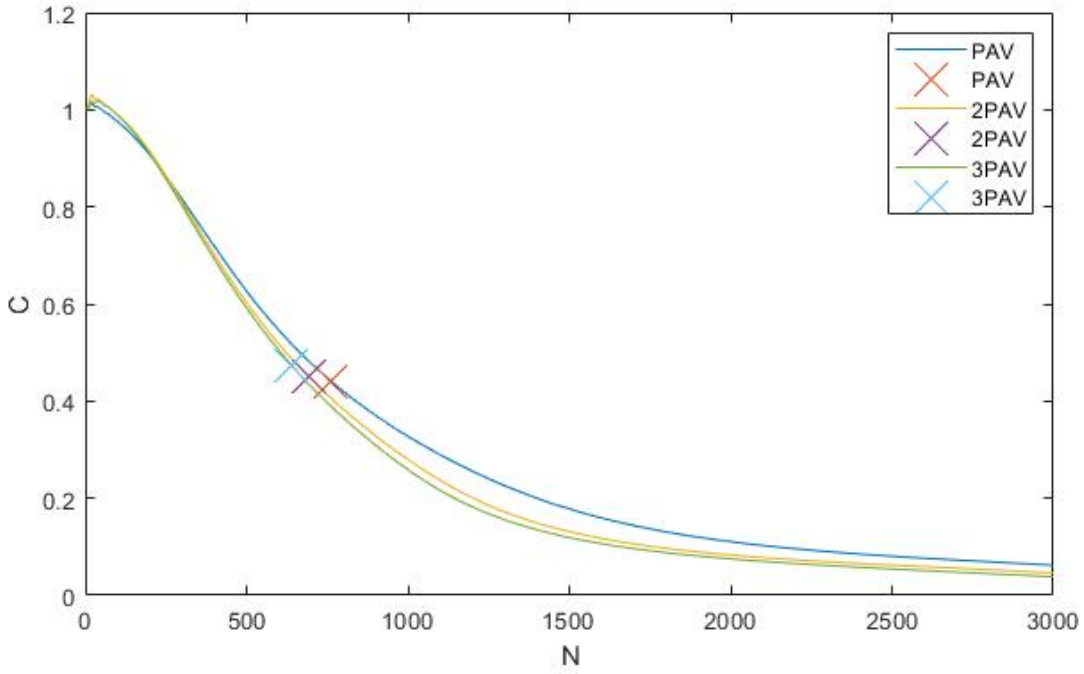

Figure 112. Graph. C-N curves for S1-K-10 at PAV, 2PAV, and 3PAV aging conditions.

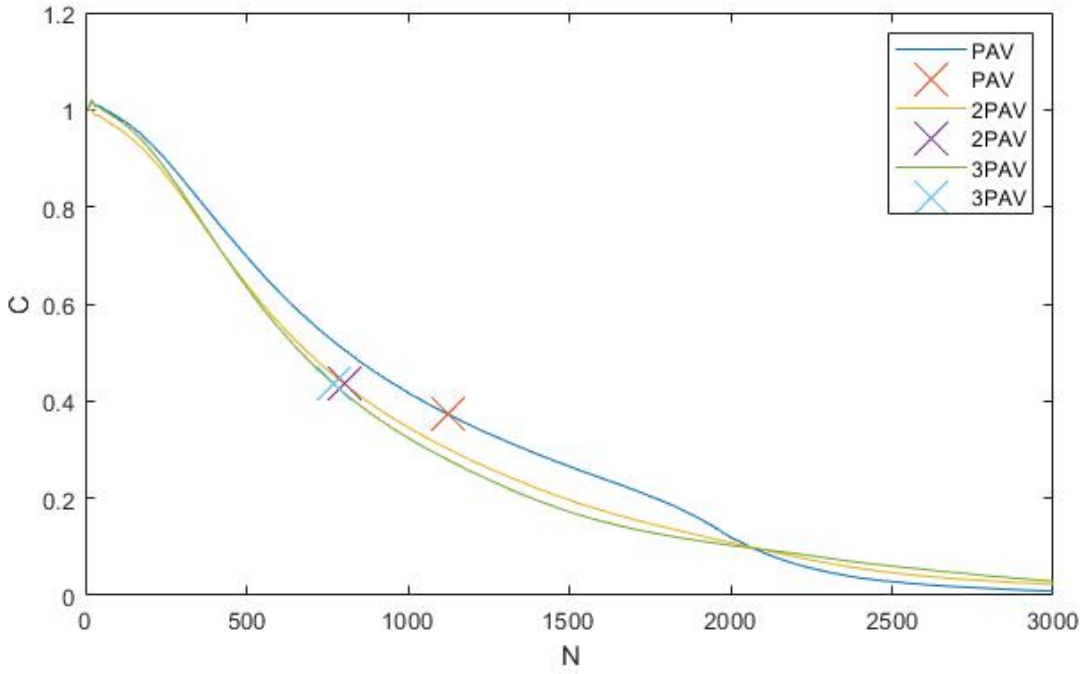

Figure 113. Graph. C-N curves for S9-L-NA at PAV, 2PAV, and 3PAV aging conditions.

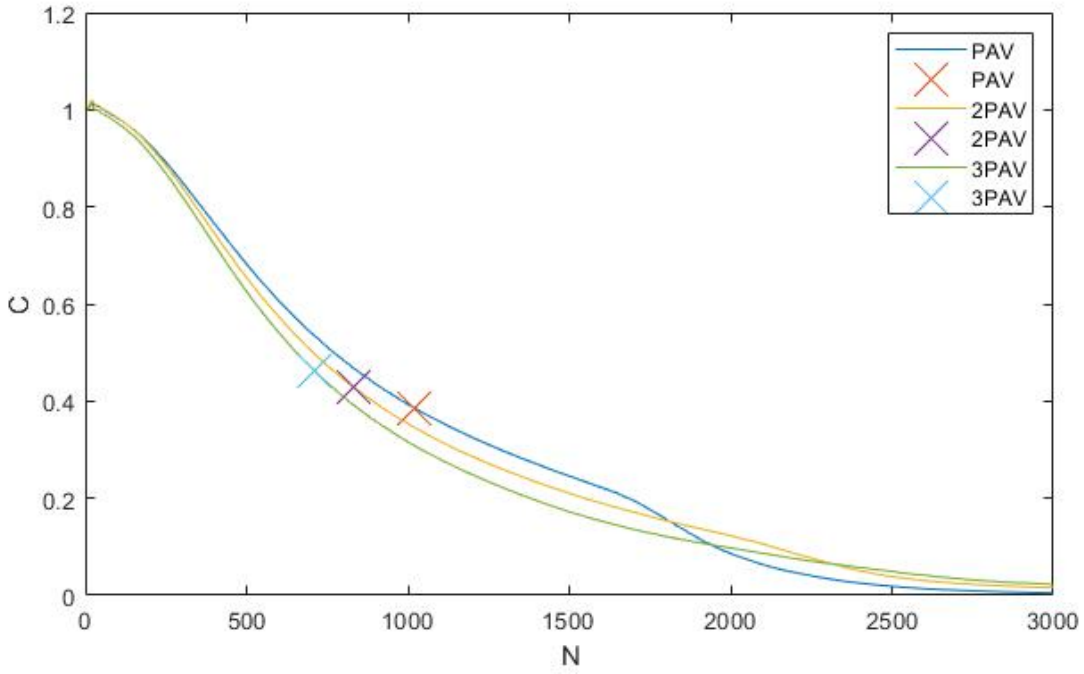

Figure 114. Graph. C-N curves for S8 at PAV, 2PAV, and 3PAV aging conditions.

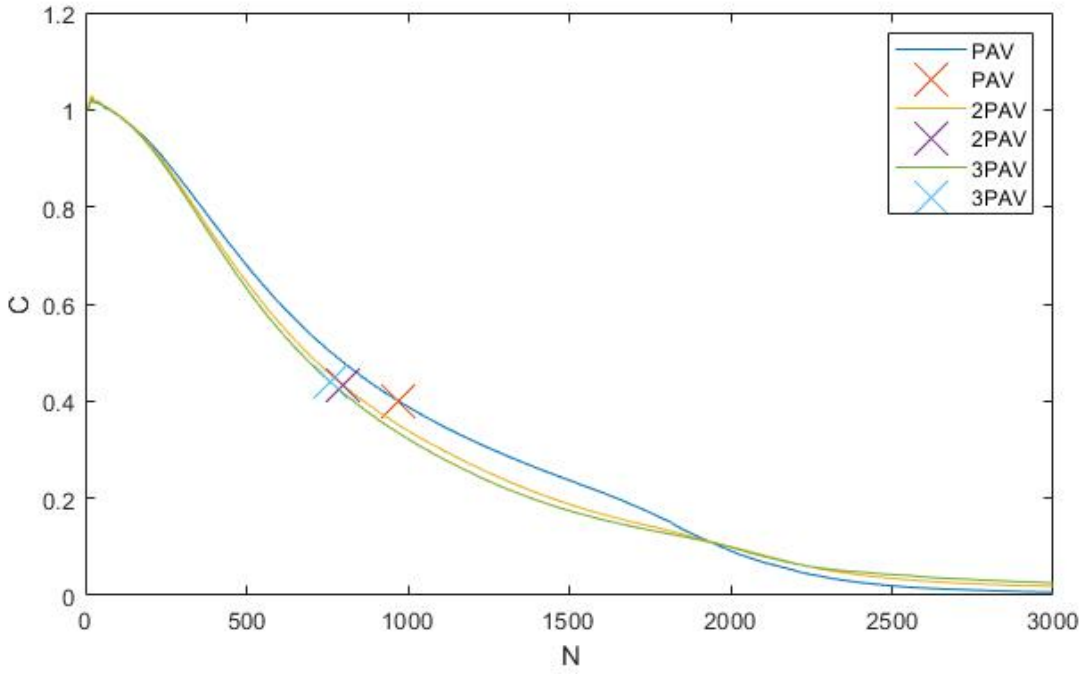

Figure 115. Graph. C-N curves for S5 at PAV, 2PAV, and 3PAV aging conditions.

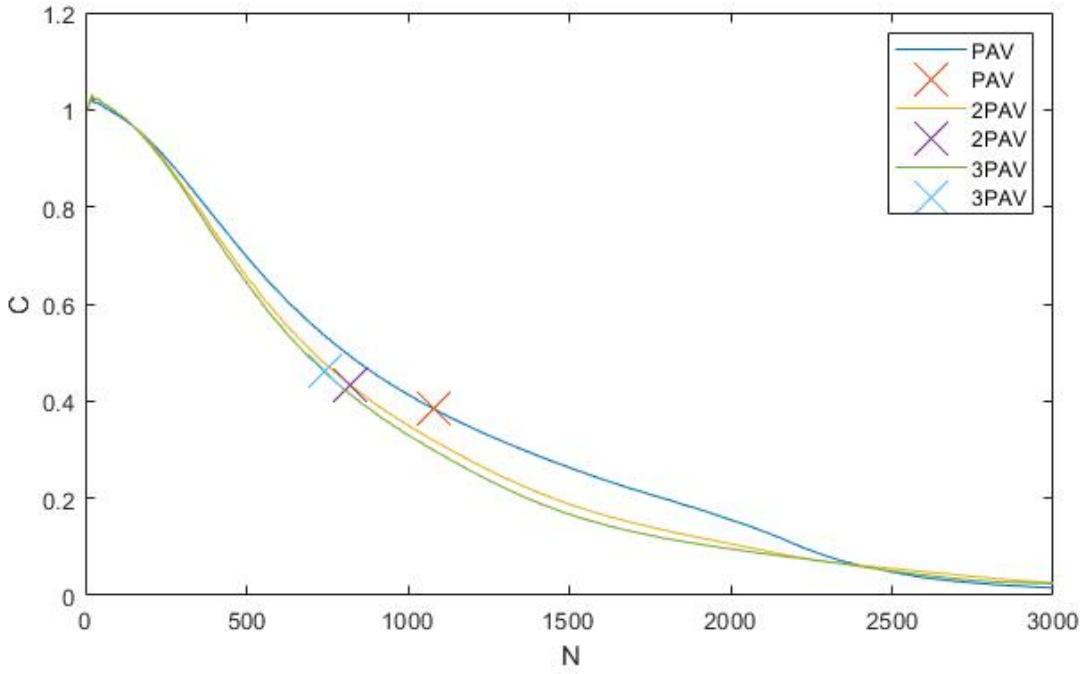

Figure 116. Graph. C-N curves for S1 at PAV, 2PAV, and 3PAV aging conditions.

δ during LAS for All Binders at All Aging Conditions

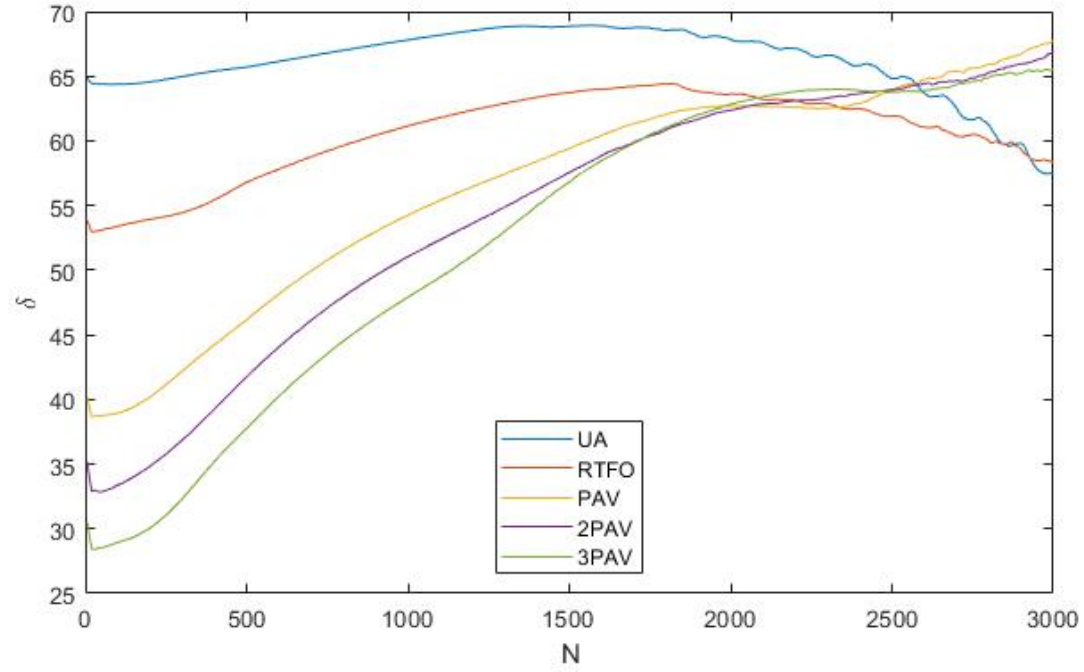

Figure 117. Graph. Phase angle vs cycle number for S1-A-3.5 at UA, RTFO, PAV, 2PAV, and 3PAV aging conditions.

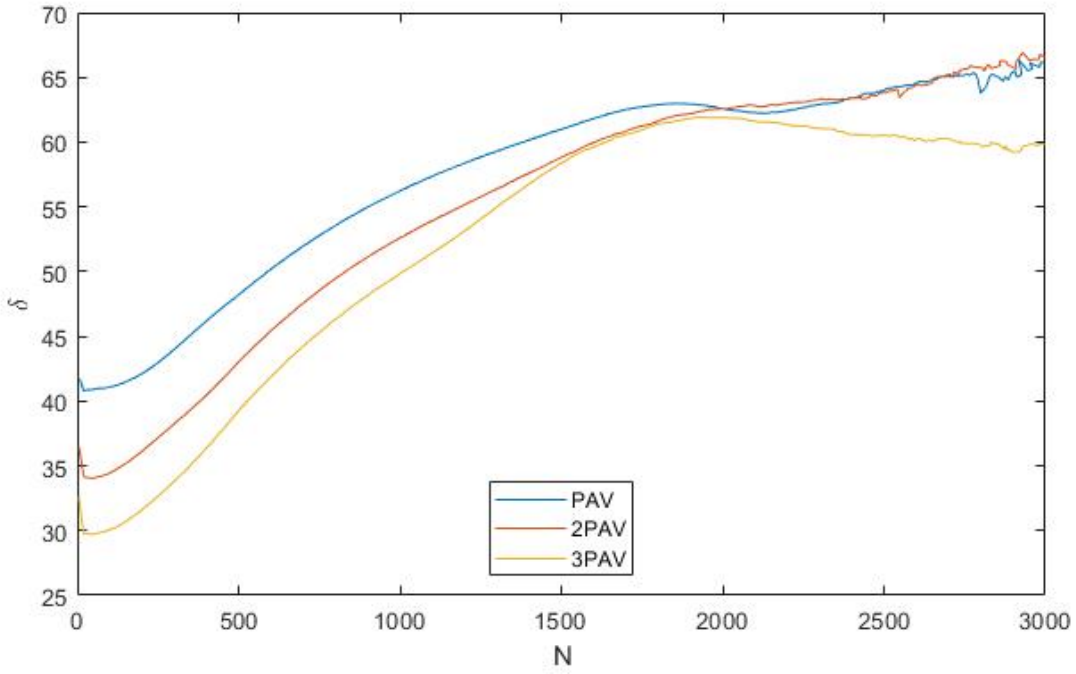

Figure 118. Graph. Phase angle vs cycle number for S1-B-5.0 at PAV, 2PAV, and 3PAV aging conditions.

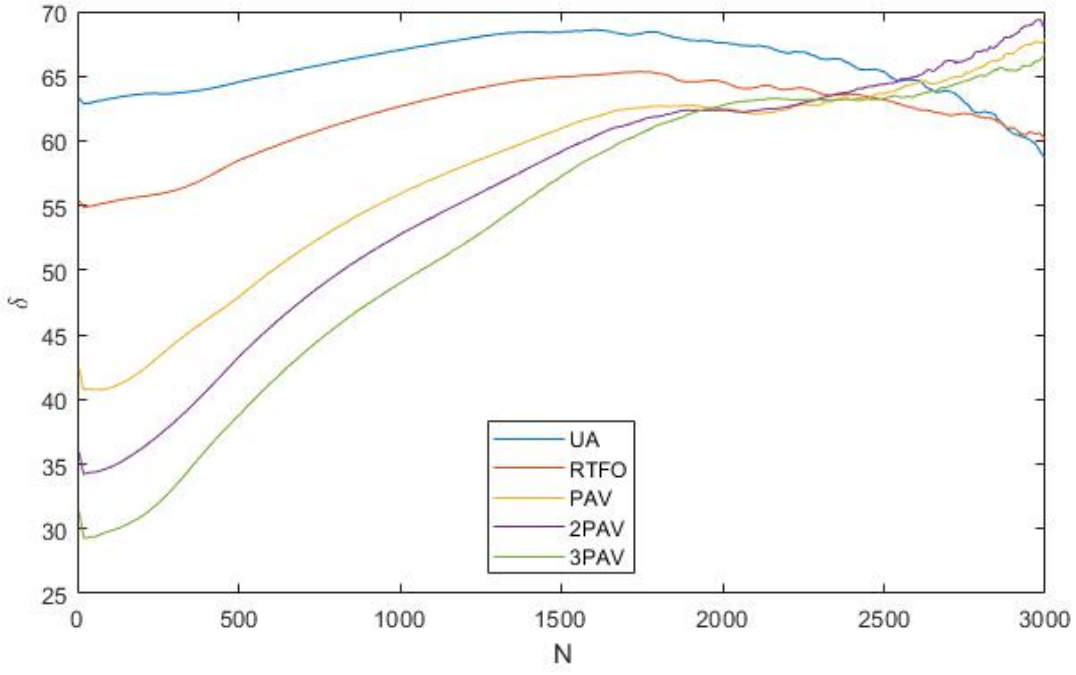

Figure 119. Graph. Phase angle vs cycle number for S1-C-3.1 at UA, RTFO, PAV, 2PAV, and 3PAV aging conditions.

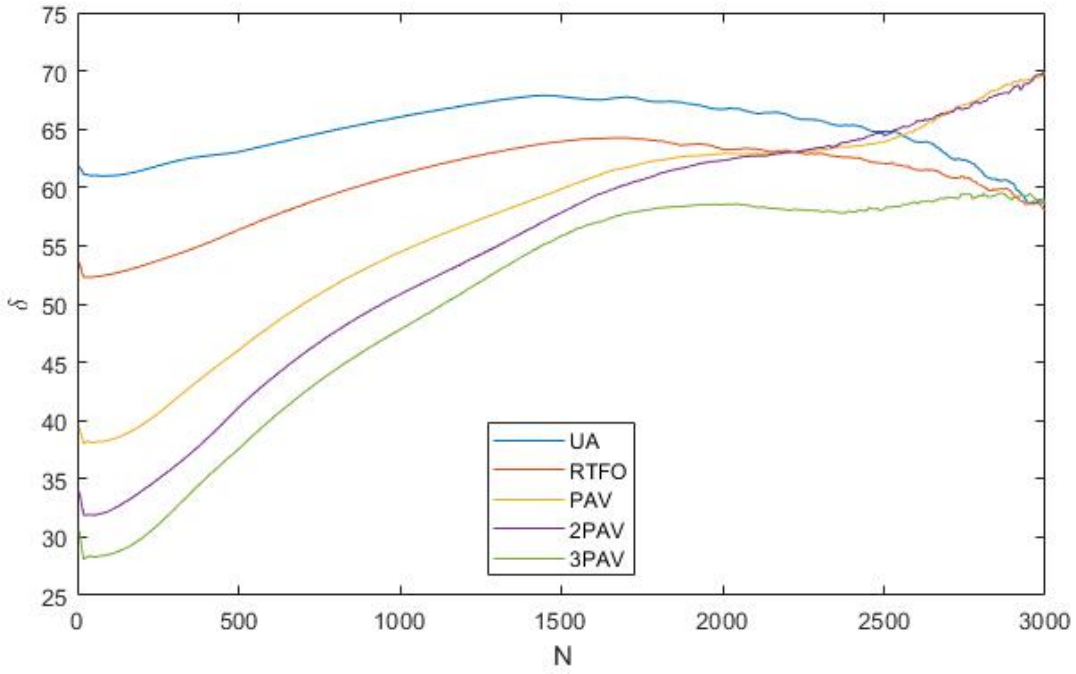

Figure 120. Graph. Phase angle vs cycle number for S1-D-3.1 at UA, RTFO, PAV, 2PAV, and 3PAV aging conditions.

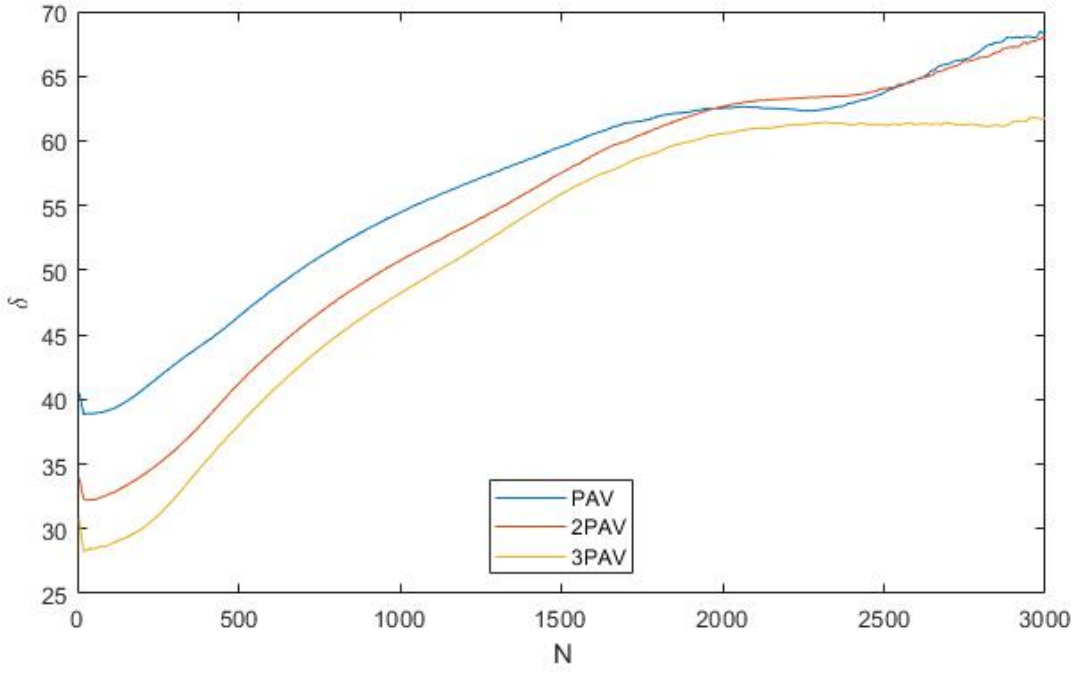

Figure 121. Graph. Phase angle vs cycle number for S1-E-3.1 at PAV, 2PAV, and 3PAV aging conditions.

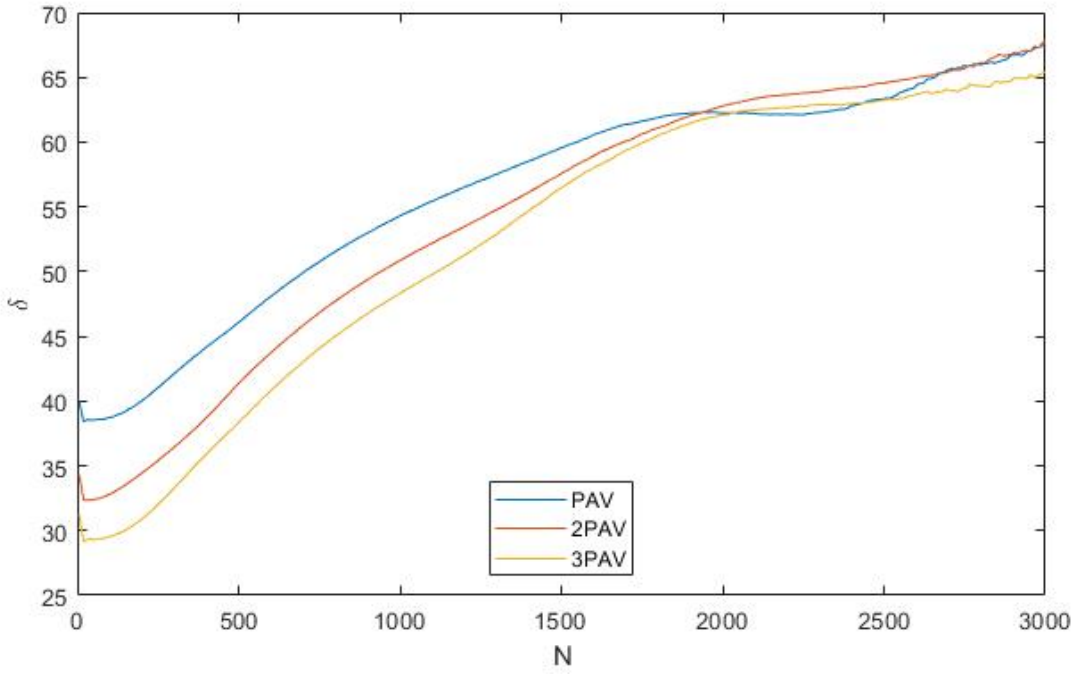

Figure 122. Graph. Phase angle vs cycle number for S1-F-3.1 at PAV, 2PAV, and 3PAV aging conditions.

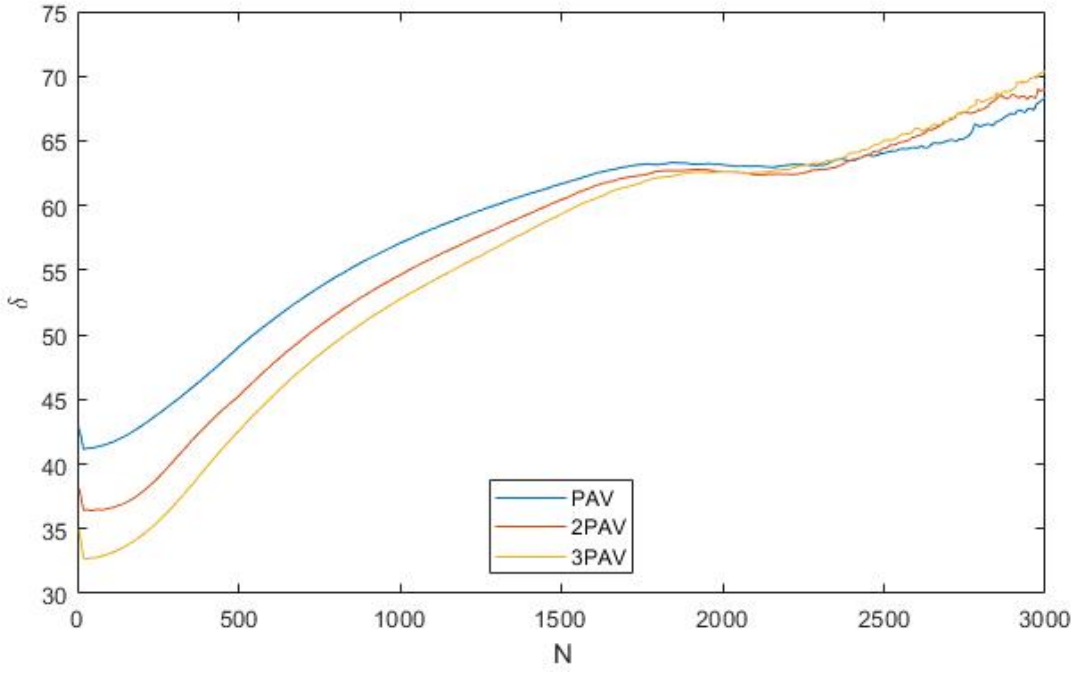

Figure 123. Graph. Phase angle vs cycle number for S1-G-6.5 at PAV, 2PAV, and 3PAV aging conditions.

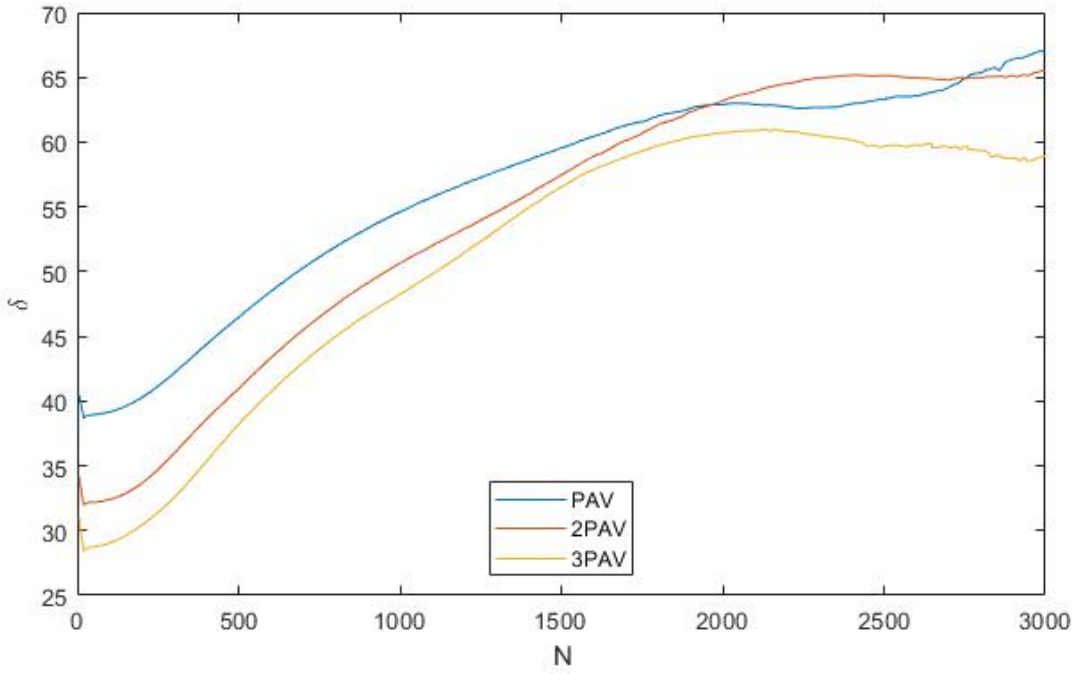

Figure 124. Graph. Phase angle vs cycle number for S1-H-10 at PAV, 2PAV, and 3PAV aging conditions.

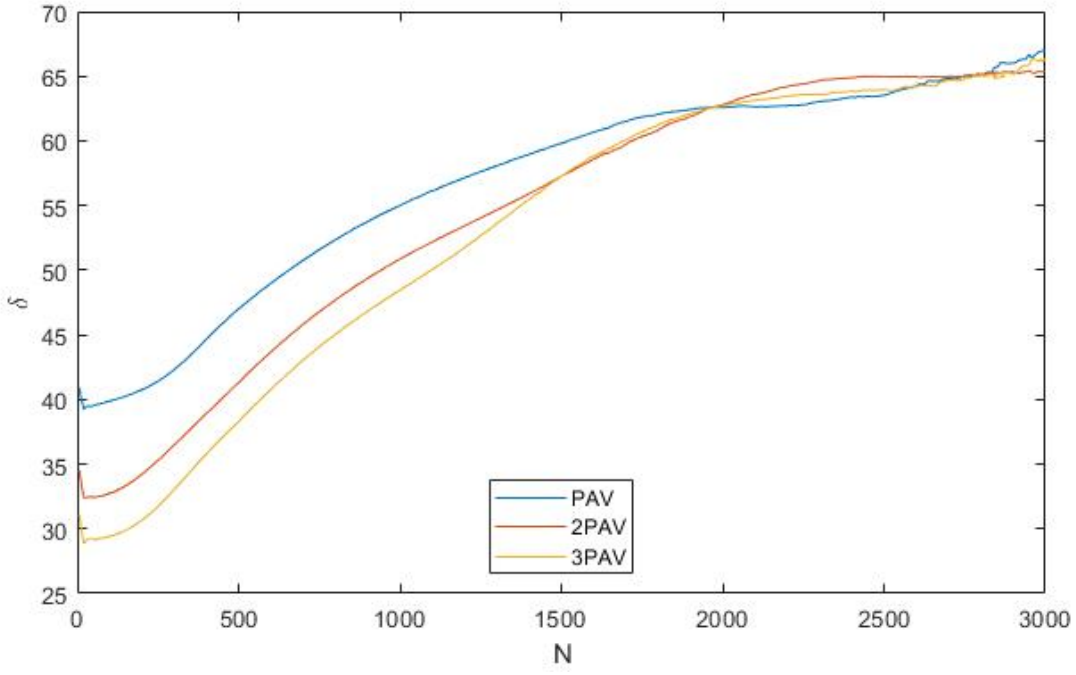

Figure 125. Graph. Phase angle vs cycle number for S1-I-3.5 at PAV, 2PAV, and 3PAV aging conditions.

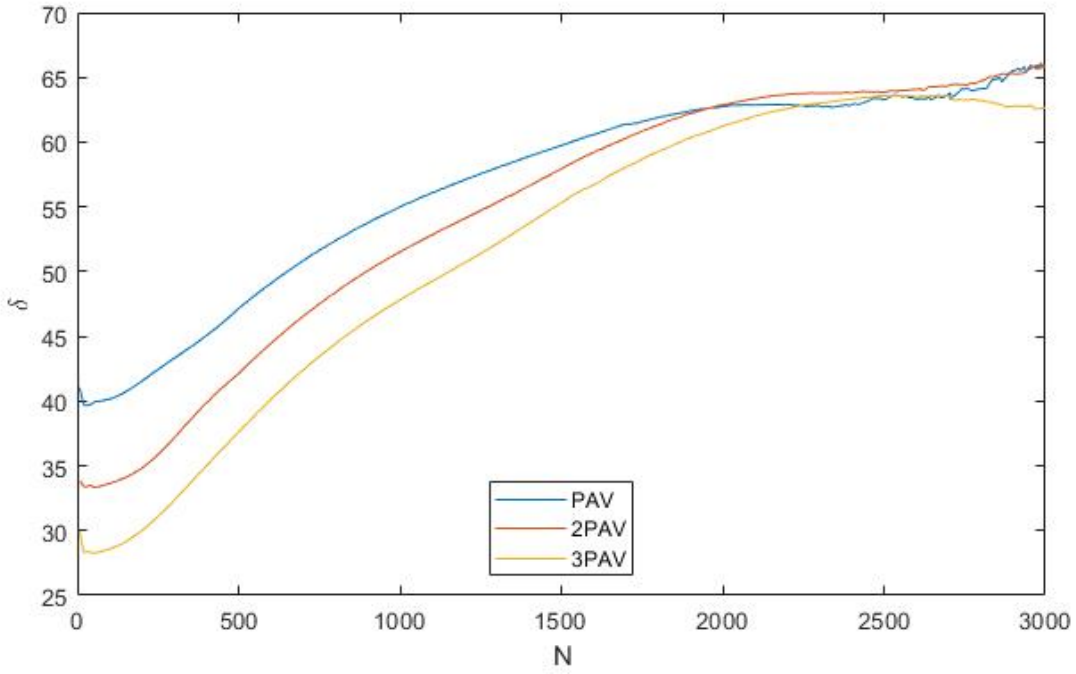

Figure 126. Graph. Phase angle vs cycle number for S1-J-3.0 at PAV, 2PAV, and 3PAV aging conditions.

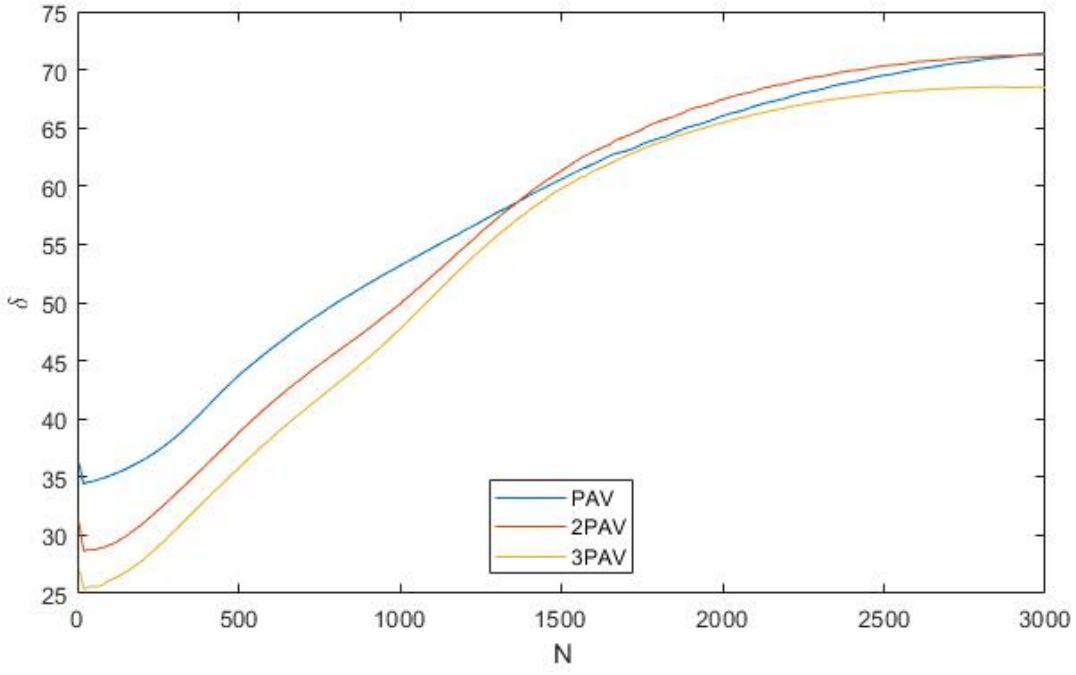

Figure 127. Graph. Phase angle vs cycle number for S1-K-10 at PAV, 2PAV, and 3PAV aging conditions.

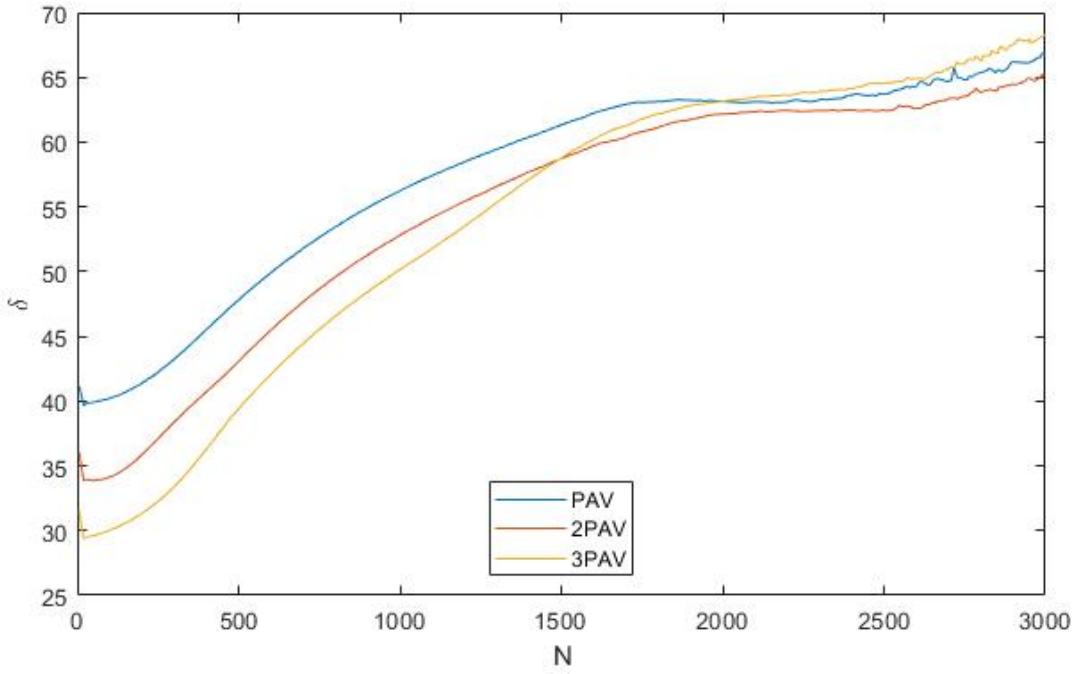

Figure 128. Graph. Phase angle vs cycle number for S9-L-NA at PAV, 2PAV, and 3PAV aging conditions.

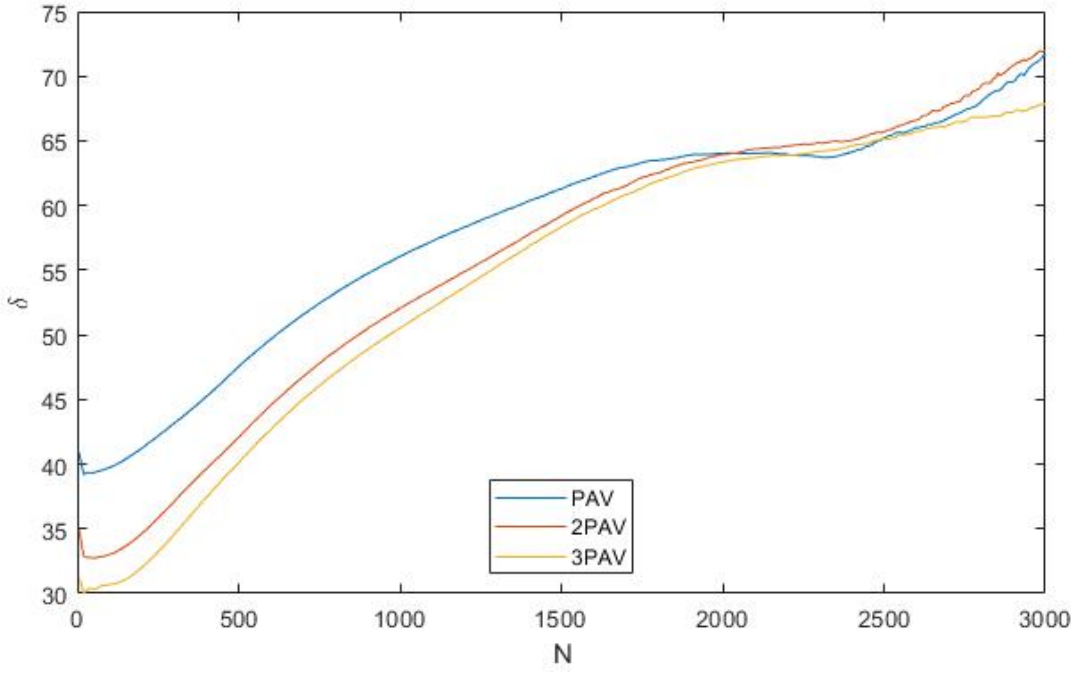

Figure 129. Graph. Phase angle vs cycle number for S5 at PAV, 2PAV, and 3PAV aging conditions.

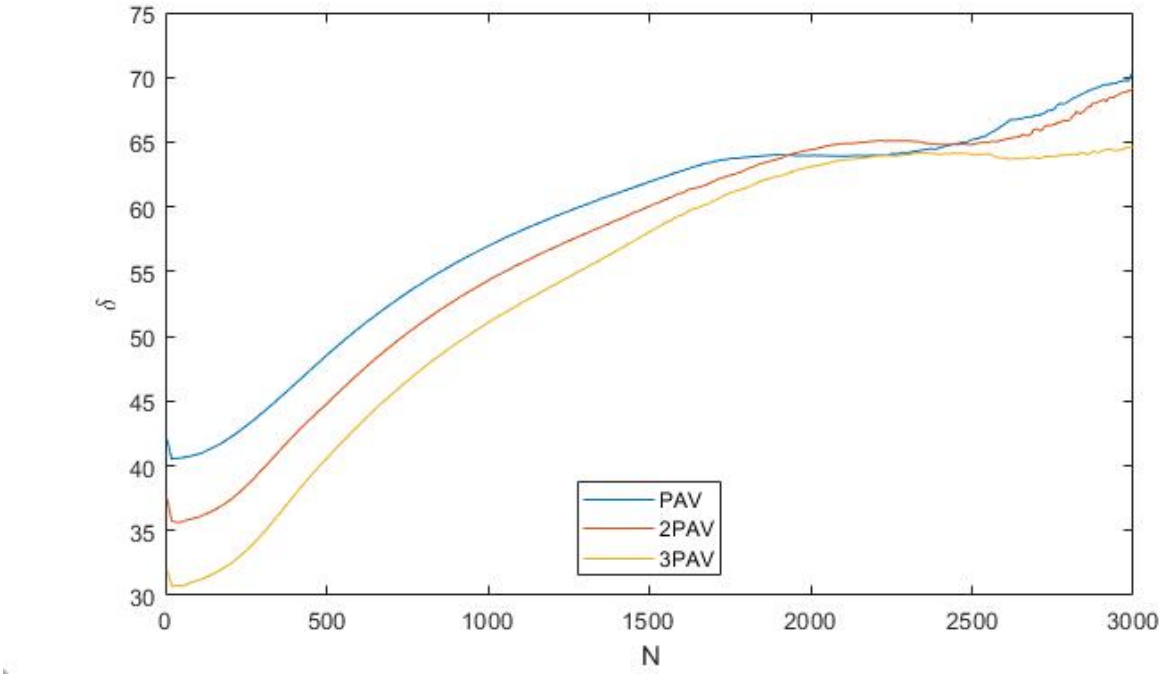

Figure 130. Graph. Phase angle vs cycle number for S8 at PAV, 2PAV, and 3PAV aging conditions.

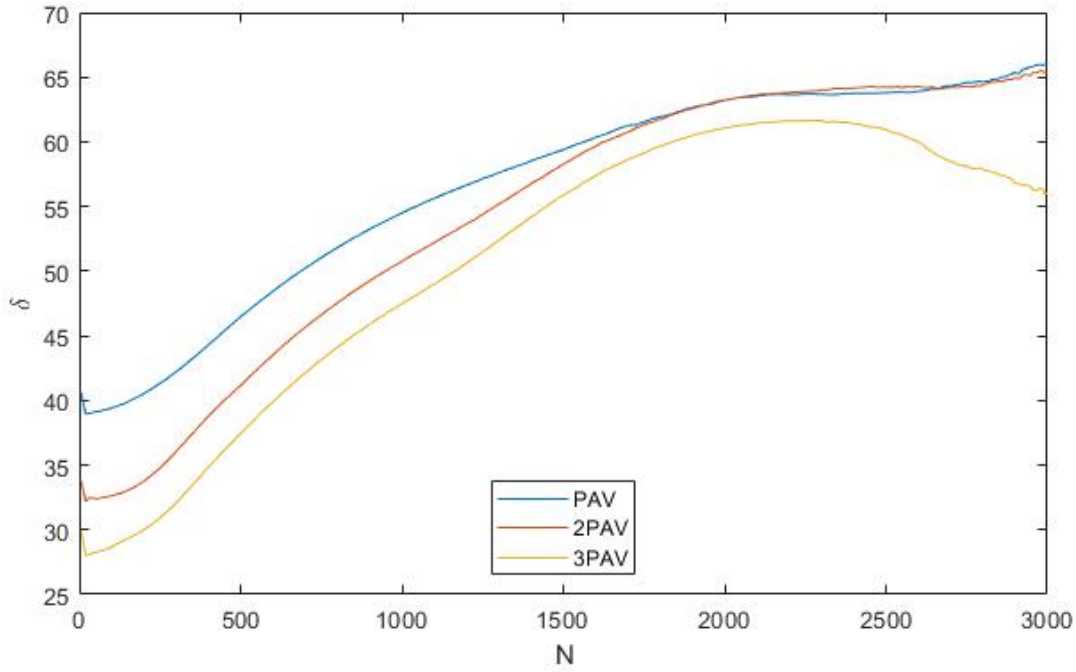

Figure 131. Graph. Phase angle vs cycle number for S1 at PAV, 2PAV, and 3PAV aging conditions.

APPENDIX D: CHEMICAL TESTING SUMMARY

FTIR SUMMARY

Table 23. Area under FTIR Spectra for Different Functional Groups

Area	A1	A2	A3	A4	A5	A6	A7	A8	A9	A10
Functional group	C=O	C=O	Aromaticity	Aliphacity	C-N/C-O	C-O	C-O	C-O	S=O	C-H
Wavenumbers (cm^{-1})	1725-1770	1670-1725	1535-1650	1325-1515	1280-1325	1245-1275	1135-1175	1070-1135	980-1070	715-910
Sample ID										
S1-OB	0.000	0.035	1.498	9.679	0.158	0.020	0.103	0.000	0.438	0.000
S1-RTFO	0.000	0.063	1.549	9.561	0.140	0.211	0.087	0.242	1.044	0.000
S1-PAV	0.000	0.153	1.519	9.388	0.129	0.246	0.088	0.266	1.686	0.000
S1-2PAV	0.000	0.295	1.519	9.354	0.131	0.311	0.100	0.316	2.406	0.000
S1-3PAV	0.000	0.389	1.549	8.874	0.141	0.242	0.112	0.202	2.234	0.000
S1-A-3.5 OB	0.204	0.000	0.669	5.188	0.060	0.045	0.106	0.056	0.285	0.204
S1-A-3.5 RTFO	0.213	0.005	0.686	4.996	0.062	0.000	0.101	0.000	0.383	0.213
S1-A-3.5 PAV	0.206	0.066	0.713	4.959	0.068	0.000	0.111	0.000	0.772	0.206
S1-A-3.5 2PAV	0.197	0.108	0.727	4.915	0.070	0.001	0.120	0.000	0.946	0.197
S1-A-3.5 3PAV	0.141	0.160	0.773	4.880	0.072	0.000	0.115	0.000	0.943	0.141
S1-B-5.0 OB	0.006	0.812	1.556	9.827	0.106	0.005	0.097	0.000	0.182	0.006
S1-B-5.0 RTFO	0.006	0.632	1.606	9.710	0.105	0.001	0.102	0.001	0.403	0.006
S1-B-5.0 PAV	0.003	0.514	1.648	9.562	0.113	0.000	0.110	0.000	1.118	0.003
S1-B-5.0 2PAV	0.000	0.508	1.579	9.298	0.116	0.000	0.125	0.000	1.530	0.000
S1-B-5.0 3PAV	0.000	0.592	1.623	9.206	0.121	0.000	0.138	0.000	1.441	0.000
S1-C-3.1 OB	0.067	0.000	0.696	5.152	0.063	0.000	0.089	0.001	0.139	0.067
S1-C-3.1 RTFO	0.076	0.000	0.691	5.088	0.068	0.000	0.086	0.000	0.341	0.076
S1-C-3.1 PAV	0.070	0.039	0.707	5.060	0.065	0.000	0.086	0.000	0.759	0.070
S1-C-3.1 2PAV	0.043	0.097	0.721	5.030	0.065	0.000	0.081	0.000	0.871	0.043
S1-C-3.1 3PAV	0.017	0.152	0.749	4.997	0.069	0.000	0.086	0.000	0.900	0.017
S1-D-3.1 OB	0.135	0.000	0.685	5.097	0.066	0.016	0.075	0.013	0.264	0.135
S1-D-3.1 RTFO	0.136	0.004	0.702	5.092	0.066	0.019	0.081	0.003	0.395	0.136
S1-D-3.1 PAV	0.140	0.068	0.703	4.989	0.061	0.000	0.095	0.000	0.803	0.140
S1-D-3.1 2PAV	0.085	0.128	0.760	4.799	0.068	0.075	0.088	0.045	1.131	0.085
S1-D-3.1 3PAV	0.176	0.161	0.784	4.895	0.075	0.001	0.126	0.000	0.912	0.176
S1-E-3.1 UA	0.226	0.000	0.694	5.063	0.067	0.003	0.107	0.004	0.216	0.226
S1-E-3.1 RTFO	0.242	0.002	0.692	5.035	0.065	0.002	0.117	0.002	0.408	0.242
S1-E-3.1 PAV	0.232	0.066	0.723	4.982	0.065	0.001	0.110	0.001	0.742	0.232
S1-E-3.1 2PAV	0.182	0.120	0.744	4.879	0.068	0.000	0.116	0.000	0.925	0.182
S1-E-3.1 3PAV	0.096	0.153	0.764	4.910	0.074	0.001	0.102	0.000	0.963	0.096
S1-F-3.1 O	0.492	0.000	1.480	9.646	0.131	0.000	0.214	0.002	0.365	0.492
S1-F-3.1 R	0.476	0.001	1.503	9.537	0.122	0.000	0.210	0.000	0.575	0.476
S1-F-3.1 P	0.473	0.130	1.511	9.350	0.121	0.000	0.226	0.000	1.483	0.473
S1-F-3.1 2P	0.440	0.233	1.526	9.277	0.122	0.000	0.225	0.000	1.808	0.440
S1-F-3.1 3P	0.381	0.316	1.600	9.137	0.135	0.000	0.234	0.000	1.597	0.381
S1-G-6.5 UA	0.005	0.000	1.066	9.433	0.197	0.114	0.000	0.685	0.006	0.005
S1-G-6.5 RTFO	0.002	0.000	1.162	9.405	0.149	0.000	0.000	0.160	0.152	0.002
S1-G-6.5 PAV	0.000	0.000	0.980	9.379	0.142	0.000	0.000	0.095	0.761	0.000
S1-G-6.5 2PAV	0.000	0.035	0.885	9.344	0.134	0.004	0.000	0.084	1.163	0.000
S1-G-6.5 3PAV	0.000	0.108	0.973	9.339	0.138	0.001	0.000	0.068	1.435	0.000
S1-H-10 O	0.452	0.000	1.493	9.794	0.136	0.006	0.206	0.003	0.326	0.452
S1-H-10 R	0.446	0.003	1.479	9.657	0.125	0.011	0.205	0.005	0.631	0.446

Area	A1	A2	A3	A4	A5	A6	A7	A8	A9	A10
Functional group	C=O	C=O	Aromaticity	Aliphacity	C-N/C-O	C-O	C-O	C-O	S=O	C-H
Wavenumbers (cm^{-1})	1725-1770	1670-1725	1535-1650	1325-1515	1280-1325	1245-1275	1135-1175	1070-1135	980-1070	715-910
S1-H-10 P	0.448	0.152	1.517	9.551	0.129	0.011	0.227	0.001	1.529	0.448
S1-H-10 2P	0.398	0.237	1.555	9.438	0.138	0.015	0.233	0.000	1.953	0.398
S1-H-10 3P	0.336	0.323	1.601	9.328	0.140	0.031	0.234	0.000	1.912	0.336
S1-I-3.5 O	0.407	0.000	1.468	9.756	0.129	0.008	0.197	0.010	0.436	0.407
S1-I-3.5 R	0.409	0.002	1.483	9.680	0.130	0.013	0.197	0.007	0.627	0.409
S1-I-3.5 P	0.393	0.136	1.522	9.501	0.125	0.003	0.224	0.002	1.501	0.393
S1-I-3.5 2P	0.363	0.232	1.569	9.397	0.138	0.004	0.230	0.001	1.878	0.363
S1-I-3.5 3P	0.293	0.283	1.570	8.990	0.142	0.001	0.208	0.000	1.733	0.293
S1-J-3 O	0.439	0.000	1.494	9.686	0.131	0.000	0.187	0.000	0.243	0.439
S1-J-3 R	0.448	0.007	1.535	9.559	0.119	0.001	0.190	0.000	0.548	0.448
S1-J-3 P	0.428	0.114	1.516	9.420	0.116	0.000	0.187	0.000	1.409	0.428
S1-J-3 2P	0.389	0.235	1.568	9.261	0.115	0.000	0.205	0.000	1.706	0.389
S1-J-3 3P	0.337	0.345	1.627	9.126	0.137	0.008	0.212	0.000	1.761	0.337
S1-K-10 OB	0.002	0.075	1.417	9.633	0.141	0.000	0.128	0.006	0.435	0.002
S1-K-10 RTFO	0.001	0.110	1.420	9.570	0.132	0.000	0.134	0.003	0.573	0.001
S1-K-10 PAV	0.000	0.277	1.446	9.485	0.131	0.000	0.166	0.002	1.115	0.000
S1-K-10 2PAV	0.000	0.361	1.444	9.337	0.140	0.000	0.189	0.000	1.350	0.000
S1-K-10 3PAV	0.000	0.446	1.480	9.108	0.137	0.051	0.213	0.035	1.396	0.000
S9-L-NA O	0.350	0.012	1.596	9.581	0.130	0.000	0.172	0.000	0.365	0.350
S9-L-NA R	0.354	0.020	1.611	9.482	0.132	0.000	0.168	0.000	0.627	0.354
S9-L-NA P	0.329	0.182	1.657	9.311	0.129	0.000	0.175	0.000	1.393	0.329
S9-L-NA 2P	0.304	0.286	1.701	9.213	0.132	0.000	0.187	0.000	1.655	0.304
S9-L-NA 3P	0.255	0.389	1.758	9.046	0.144	0.000	0.187	0.000	1.696	0.255
S5 OB	0.003	0.003	0.711	5.132	0.081	0.081	0.043	0.066	0.345	0.003
S5 RTFO	0.006	0.026	0.682	4.983	0.091	0.027	0.044	0.006	0.350	0.006
S5 PAV	0.000	0.101	0.730	5.110	0.092	0.000	0.048	0.000	0.756	0.000
S5 2PAV	0.000	0.161	0.751	4.965	0.095	0.000	0.059	0.000	0.916	0.000
S5 3PAV	0.000	0.222	0.754	4.872	0.092	0.082	0.053	0.038	1.051	0.000
S8 O	0.001	0.025	1.623	9.720	0.145	0.010	0.104	0.000	0.766	0.001
S8 R	0.001	0.054	1.611	9.626	0.145	0.001	0.095	0.000	0.738	0.001
S8 P	0.000	0.234	1.678	9.465	0.141	0.003	0.109	0.000	1.468	0.000
S8 2P	0.000	0.351	1.733	9.295	0.148	0.003	0.119	0.000	1.566	0.000
S8 3P	0.000	0.460	1.769	9.206	0.156	0.002	0.124	0.000	1.682	0.000
S2 UA	0.003	0.040	0.843	5.640	0.086	0.002	0.054	0.000	0.243	0.003
S2 RTFO	0.001	0.049	0.856	5.603	0.086	0.002	0.057	0.000	0.354	0.001
S2 PAV	0.000	0.121	0.870	5.534	0.083	0.002	0.063	0.000	0.783	0.000
S2 2PAV	0.000	0.179	0.887	5.514	0.083	0.002	0.065	0.000	1.024	0.000
S2-B-5.0 UA	0.001	0.401	0.806	5.562	0.062	0.004	0.053	0.000	0.166	0.001
S2-B-5.0 RTFO	0.002	0.357	0.839	5.545	0.064	0.001	0.053	0.000	0.225	0.002
S2-B-5.0 PAV	0.000	0.273	0.872	5.489	0.066	0.000	0.060	0.000	0.626	0.000
S2-B-5.0 2PAV	0.000	0.300	0.862	5.326	0.071	0.000	0.070	0.001	0.751	0.000
S2-F-3.1 UA	0.238	0.001	0.797	5.575	0.078	0.001	0.116	0.001	0.213	0.238
S2-F-3.1 RTFO	0.246	0.010	0.804	5.541	0.079	0.001	0.115	0.000	0.295	0.246
S2-F-3.1 PAV	0.239	0.084	0.820	5.491	0.077	0.002	0.122	0.000	0.767	0.239
S2-F-3.1 2PAV	0.223	0.151	0.872	5.439	0.079	0.000	0.126	0.000	0.816	0.223
S2-G-6.5 UA	0.005	0.000	0.734	5.636	0.098	0.001	0.000	0.217	0.036	0.005
S2-G-6.5 RTFO	0.002	0.000	0.650	5.577	0.083	0.002	0.000	0.120	0.085	0.002
S2-G-6.5 PAV	0.000	0.010	0.604	5.546	0.080	0.002	0.000	0.057	0.409	0.000
S2-G-6.5 2PAV	0.000	0.028	0.549	5.522	0.082	0.006	0.000	0.058	0.629	0.000
S2-H-10 UA	0.219	0.001	0.800	5.621	0.079	0.002	0.109	0.000	0.213	0.219
S2-H-10 RTFO	0.219	0.010	0.810	5.561	0.079	0.000	0.111	0.000	0.303	0.219

Area	A1	A2	A3	A4	A5	A6	A7	A8	A9	A10
Functional group	C=O	C=O	Aromaticity	Aliphacity	C-N/C-O	C-O	C-O	C-O	S=O	C-H
Wavenumbers (cm^{-1})	1725-1770	1670-1725	1535-1650	1325-1515	1280-1325	1245-1275	1135-1175	1070-1135	980-1070	715-910
S2-H-10 PAV	0.216	0.086	0.840	5.498	0.074	0.000	0.114	0.000	0.765	0.216
S2-H-10 2PAV	0.198	0.142	0.868	5.475	0.079	0.000	0.116	0.000	0.940	0.198
S2-K-10 UA	0.000	0.051	0.790	5.641	0.082	0.000	0.073	0.003	0.246	0.000
S2-K-10 RTFO	0.000	0.068	0.802	5.605	0.078	0.000	0.076	0.004	0.306	0.000
S2-K-10 PAV	0.000	0.151	0.815	5.564	0.079	0.000	0.089	0.000	0.638	0.000
S2-K-10 2PAV	0.000	0.201	0.825	5.520	0.077	0.000	0.105	0.000	0.801	0.000
IL-125#1	0.000	0.350	1.022	5.453	0.099	0.047	0.047	0.035	1.142	0.000
IL-125#8	0.002	0.180	0.952	5.483	0.090	0.064	0.050	0.039	0.910	0.002
IL-125#18	0.002	0.040	0.936	5.567	0.087	0.072	0.045	0.048	0.601	0.002
US-51#1	0.004	0.298	0.981	5.493	0.108	0.103	0.053	0.054	1.445	0.004
US-51#8	0.008	0.069	0.900	5.667	0.100	0.088	0.060	0.086	0.973	0.008
US-51#18	0.001	0.018	0.778	5.716	0.092	0.105	0.054	0.083	0.707	0.001
US-51#25	0.008	0.000	0.833	5.730	0.108	0.066	0.068	0.163	0.521	0.008
US-51#2425-3PAV	0.000	0.217	0.954	5.527	0.101	0.081	0.066	0.093	0.951	0.000
I-90#1	0.000	0.282	0.984	5.518	0.076	0.078	0.059	0.044	1.202	0.000
I-355#1	0.000	0.333	1.132	5.632	0.103	0.111	0.041	0.116	1.356	0.000
I-72 1E#1	0.000	0.296	1.055	5.544	0.102	0.138	0.059	0.122	1.432	0.000
L1-1019#1	0.000	0.250	1.042	5.541	0.091	0.055	0.056	0.005	1.224	0.000
22SRT2#1	0.000	0.279	1.014	5.536	0.090	0.076	0.086	0.030	1.327	0.000
2RT26#1	0.000	0.267	1.029	6.164	0.115	0.067	0.046	0.012	1.237	0.000
L2#1	0.000	0.276	0.947	5.054	0.092	0.041	0.036	0.000	1.240	0.000
L2#2	0.000	0.255	0.946	5.162	0.082	0.030	0.037	0.000	1.170	0.000
L2#3	0.000	0.230	0.901	5.024	0.074	0.062	0.033	0.006	1.226	0.000
L2#8	0.000	0.265	0.948	5.163	0.088	0.030	0.033	0.000	1.260	0.000

Table 24. FTIR Oxidation Indices Calculation

Indices	$A_2/(\sum Ai)$	$(A_2+A_9)/(\sum Ai)$	$(A_2+A_9+A_5+A_6+A_7+A_8)/(\sum Ai)$	$A_2/(A_3+A_4+A_{10})$	$(A_2+A_9)/(A_3+A_4+A_{10})$	$(A_2+A_9+A_5+A_6+A7+A8)/(A3+A4+A10)$	(A2+A9+A5+A6+A7+A8)/(A3+A4)	(A2+A9)/(A3+A4)	A2/(A3+A4)
Sample ID								$FTIR_{C=O}$	$FTIR_{C=O+S=O}$
S1-OB	0.000	0.031	0.049	0.002	0.032	0.051	0.068	0.042	0.003
S1-RTFO	0.000	0.065	0.104	0.004	0.072	0.117	0.161	0.100	0.006
S1-PAV	0.000	0.104	0.145	0.010	0.122	0.170	0.235	0.169	0.014
S1-2PAV	0.000	0.144	0.190	0.019	0.178	0.235	0.327	0.248	0.027
S1-3PAV	0.000	0.148	0.187	0.027	0.182	0.231	0.319	0.252	0.037
S1-A-3.5 OB	0.025	0.035	0.067	0.000	0.038	0.073	0.094	0.049	0.000
S1-A-3.5 RTFO	0.027	0.050	0.071	0.001	0.055	0.079	0.097	0.068	0.001
S1-A-3.5 PAV	0.025	0.103	0.125	0.009	0.121	0.147	0.179	0.148	0.012
S1-A-3.5 2PAV	0.024	0.128	0.151	0.016	0.155	0.183	0.221	0.187	0.019
S1-A-3.5 3PAV	0.017	0.132	0.154	0.023	0.159	0.186	0.228	0.195	0.028
S1-B-5.0 OB	0.000	0.067	0.081	0.060	0.073	0.088	0.106	0.087	0.071
S1-B-5.0 RTFO	0.000	0.070	0.084	0.047	0.076	0.092	0.110	0.091	0.056
S1-B-5.0 PAV	0.000	0.108	0.122	0.039	0.123	0.139	0.165	0.146	0.046
S1-B-5.0 2PAV	0.000	0.134	0.149	0.039	0.157	0.175	0.210	0.187	0.047
S1-B-5.0 3PAV	0.000	0.134	0.151	0.046	0.158	0.178	0.212	0.188	0.055
S1-C-3.1 OB	0.009	0.018	0.038	0.000	0.019	0.040	0.050	0.024	0.000
S1-C-3.1 RTFO	0.010	0.044	0.063	0.000	0.047	0.068	0.086	0.059	0.000
S1-C-3.1 PAV	0.009	0.097	0.116	0.005	0.111	0.132	0.165	0.138	0.007

Indices	$A_2/(\sum Ai)$	$(A_2+A_9)/(\sum Ai)$	$(A_2+A_9+A_5+A_6+A_7+A_8)/(\sum Ai)$	$A_2/(A_3+A_4+A_{10})$	$(A_2+A_9)/(A_3+A_4+A_{10})$	$(A_2+A_9+A_5+A_6+A7+A8)/(A3+A4+A10)$	(A2+A9+A5+A6+A7+A8)/(A3+A4)	(A2+A9)/(A3+A4)	A2/(A3+A4)
Sample ID								$FTIR_{C=O}$	$FTIR_{C=O+S=O}$
S1-C-3.1 2PAV	0.005	0.116	0.133	0.014	0.135	0.155	0.194	0.168	0.017
S1-C-3.1 3PAV	0.002	0.127	0.146	0.022	0.149	0.171	0.210	0.183	0.026
S1-D-3.1 OB	0.017	0.033	0.054	0.000	0.035	0.058	0.075	0.046	0.000
S1-D-3.1 RTFO	0.017	0.049	0.070	0.001	0.054	0.077	0.098	0.069	0.001
S1-D-3.1 PAV	0.017	0.106	0.125	0.010	0.123	0.146	0.181	0.153	0.012
S1-D-3.1 2PAV	0.009	0.140	0.170	0.017	0.170	0.207	0.276	0.227	0.023
S1-D-3.1 3PAV	0.021	0.127	0.151	0.023	0.153	0.182	0.225	0.189	0.028
S1-E-3.1 UA	0.029	0.027	0.050	0.000	0.030	0.055	0.069	0.037	0.000
S1-E-3.1 RTFO	0.030	0.051	0.075	0.000	0.057	0.084	0.104	0.072	0.000
S1-E-3.1 PAV	0.028	0.097	0.118	0.009	0.113	0.138	0.173	0.142	0.012
S1-E-3.1 2PAV	0.022	0.125	0.147	0.017	0.150	0.176	0.219	0.186	0.021
S1-E-3.1 3PAV	0.011	0.133	0.154	0.022	0.159	0.184	0.228	0.197	0.027
S1-F-3.1 O	0.033	0.024	0.047	0.000	0.026	0.051	0.064	0.033	0.000
S1-F-3.1 R	0.032	0.039	0.061	0.000	0.042	0.067	0.082	0.052	0.000
S1-F-3.1 P	0.030	0.103	0.125	0.010	0.122	0.149	0.181	0.149	0.012
S1-F-3.1 2P	0.028	0.128	0.150	0.018	0.156	0.182	0.221	0.189	0.022
S1-F-3.1 3P	0.024	0.121	0.144	0.024	0.146	0.174	0.213	0.178	0.029
S1-G-6.5 UA	0.000	0.000	0.065	0.000	0.000	0.069	0.095	0.001	0.000
S1-G-6.5 RTFO	0.000	0.011	0.032	0.000	0.011	0.034	0.044	0.014	0.000
S1-G-6.5 PAV	0.000	0.053	0.070	0.000	0.057	0.075	0.096	0.074	0.000
S1-G-6.5 2PAV	0.000	0.083	0.099	0.003	0.093	0.110	0.139	0.117	0.003
S1-G-6.5 3PAV	0.000	0.105	0.119	0.008	0.119	0.135	0.170	0.150	0.010
S1-H-10 O	0.029	0.021	0.044	0.000	0.023	0.047	0.060	0.029	0.000
S1-H-10 R	0.029	0.042	0.064	0.000	0.046	0.071	0.088	0.057	0.000
S1-H-10 P	0.028	0.104	0.127	0.011	0.123	0.150	0.185	0.152	0.014
S1-H-10 2P	0.024	0.134	0.157	0.018	0.163	0.192	0.234	0.199	0.022
S1-H-10 3P	0.021	0.137	0.161	0.024	0.167	0.197	0.242	0.205	0.030
S1-I-3.5 O	0.027	0.029	0.051	0.000	0.031	0.055	0.070	0.039	0.000
S1-I-3.5 R	0.027	0.041	0.064	0.000	0.045	0.070	0.087	0.056	0.000
S1-I-3.5 P	0.025	0.103	0.125	0.010	0.121	0.147	0.181	0.148	0.012
S1-I-3.5 2P	0.022	0.130	0.153	0.017	0.158	0.186	0.226	0.192	0.021
S1-I-3.5 3P	0.018	0.127	0.149	0.021	0.153	0.180	0.224	0.191	0.027
S1-J-3 O	0.030	0.016	0.038	0.000	0.018	0.041	0.050	0.022	0.000
S1-J-3 R	0.029	0.036	0.057	0.001	0.040	0.062	0.078	0.050	0.001
S1-J-3 P	0.027	0.097	0.116	0.009	0.113	0.136	0.167	0.139	0.010
S1-J-3 2P	0.024	0.122	0.142	0.018	0.147	0.171	0.209	0.179	0.022
S1-J-3 3P	0.021	0.132	0.154	0.026	0.160	0.187	0.229	0.196	0.032
S1-K-10 OB	0.000	0.035	0.054	0.005	0.037	0.057	0.071	0.046	0.007
S1-K-10 RTFO	0.000	0.047	0.066	0.008	0.051	0.071	0.087	0.062	0.010
S1-K-10 PAV	0.000	0.093	0.113	0.021	0.105	0.128	0.155	0.127	0.025
S1-K-10 2PAV	0.000	0.114	0.136	0.028	0.132	0.158	0.189	0.159	0.034
S1-K-10 3PAV	0.000	0.121	0.150	0.035	0.143	0.176	0.215	0.174	0.042
S9-L-NA O	0.023	0.025	0.045	0.001	0.027	0.048	0.061	0.034	0.001
S9-L-NA R	0.023	0.042	0.061	0.001	0.046	0.067	0.085	0.058	0.002
S9-L-NA P	0.021	0.098	0.117	0.013	0.114	0.136	0.171	0.144	0.017
S9-L-NA 2P	0.019	0.120	0.140	0.021	0.143	0.166	0.207	0.178	0.026
S9-L-NA 3P	0.016	0.130	0.151	0.029	0.156	0.181	0.224	0.193	0.036
S5 OB	0.000	0.040	0.072	0.000	0.044	0.077	0.106	0.060	0.001
S5 RTFO	0.001	0.047	0.067	0.003	0.050	0.072	0.096	0.066	0.005
S5 PAV	0.000	0.101	0.118	0.014	0.115	0.133	0.171	0.147	0.017
S5 2PAV	0.000	0.127	0.146	0.022	0.149	0.170	0.216	0.188	0.028
S5 3PAV	0.000	0.140	0.169	0.029	0.168	0.203	0.273	0.226	0.039

Indices	$A_2/(\sum Ai)$	$(A_2+A_9)/(\sum Ai)$	$(A_2+A_9+A_5+A_6+A_7+A_8)/(\sum Ai)$	$A_2/(A_3+A_4+A_{10})$	$(A_2+A_9)/(A_3+A_4+A_{10})$	$(A_2+A_9+A_5+A_6+A7+A8)/(A3+A4+A10)$	(A2+A9+A5+A6+A7+A8)/(A3+A4)	(A2+A9)/(A3+A4)	A2/(A3+A4)
Sample ID								$FTIR_{C=O}$	$FTIR_{C=O+S=O}$
S8 O	0.000	0.049	0.065	0.002	0.052	0.070	0.093	0.070	0.002
S8 R	0.000	0.051	0.066	0.004	0.055	0.071	0.092	0.071	0.005
S8 P	0.000	0.105	0.121	0.016	0.120	0.137	0.175	0.153	0.021
S8 2P	0.000	0.118	0.135	0.025	0.137	0.156	0.198	0.174	0.032
S8 3P	0.000	0.132	0.149	0.033	0.155	0.175	0.221	0.195	0.042
S2 UA	0.000	0.031	0.046	0.005	0.032	0.049	0.066	0.044	0.006
S2 RTFO	0.000	0.044	0.059	0.006	0.046	0.063	0.085	0.062	0.008
S2 PAV	0.000	0.095	0.111	0.014	0.107	0.124	0.164	0.141	0.019
S2 2PAV	0.000	0.124	0.139	0.021	0.144	0.162	0.211	0.188	0.028
S2-B-5.0 UA	0.000	0.067	0.081	0.052	0.073	0.089	0.108	0.089	0.063
S2-B-5.0 RTFO	0.000	0.068	0.082	0.046	0.075	0.090	0.110	0.091	0.056
S2-B-5.0 PAV	0.000	0.103	0.117	0.035	0.116	0.133	0.161	0.141	0.043
S2-B-5.0 2PAV	0.000	0.122	0.138	0.040	0.141	0.160	0.193	0.170	0.048
S2-F-3.1 UA	0.027	0.024	0.046	0.000	0.026	0.050	0.064	0.034	0.000
S2-F-3.1 RTFO	0.028	0.034	0.056	0.001	0.038	0.062	0.079	0.048	0.002
S2-F-3.1 PAV	0.026	0.092	0.113	0.011	0.107	0.132	0.167	0.135	0.013
S2-F-3.1 2PAV	0.024	0.104	0.126	0.019	0.122	0.148	0.186	0.153	0.024
S2-G-6.5 UA	0.001	0.004	0.039	0.000	0.004	0.041	0.055	0.006	0.000
S2-G-6.5 RTFO	0.000	0.010	0.034	0.000	0.010	0.035	0.047	0.014	0.000
S2-G-6.5 PAV	0.000	0.049	0.065	0.001	0.052	0.069	0.091	0.068	0.002
S2-G-6.5 2PAV	0.000	0.076	0.092	0.004	0.083	0.102	0.132	0.108	0.005
S2-H-10 UA	0.024	0.024	0.045	0.000	0.026	0.048	0.063	0.033	0.000
S2-H-10 RTFO	0.025	0.035	0.057	0.001	0.038	0.062	0.079	0.049	0.002
S2-H-10 PAV	0.023	0.092	0.112	0.011	0.106	0.129	0.164	0.134	0.014
S2-H-10 2PAV	0.021	0.114	0.135	0.018	0.135	0.159	0.201	0.171	0.022
S2-K-10 UA	0.000	0.033	0.051	0.006	0.035	0.054	0.071	0.046	0.008
S2-K-10 RTFO	0.000	0.042	0.060	0.008	0.045	0.064	0.083	0.058	0.011
S2-K-10 PAV	0.000	0.088	0.106	0.019	0.098	0.119	0.150	0.124	0.024
S2-K-10 2PAV	0.000	0.110	0.129	0.025	0.126	0.149	0.187	0.158	0.032
IL-125#1	0.000	0.150	0.173	0.043	0.181	0.209	0.266	0.230	0.054
IL-125#8	0.000	0.114	0.140	0.022	0.133	0.163	0.207	0.169	0.028
IL-125#18	0.000	0.068	0.095	0.005	0.076	0.105	0.137	0.099	0.006
US-51#1	0.000	0.164	0.194	0.035	0.204	0.241	0.318	0.269	0.046
US-51#8	0.001	0.103	0.135	0.008	0.119	0.157	0.209	0.159	0.010
US-51#18	0.000	0.075	0.109	0.002	0.084	0.123	0.163	0.112	0.003
US-51#25	0.001	0.054	0.096	0.000	0.060	0.106	0.141	0.079	0.000
US-51#2425-3PAV	0.000	0.118	0.152	0.026	0.139	0.179	0.233	0.180	0.034
I-90#1	0.000	0.147	0.172	0.034	0.177	0.208	0.268	0.228	0.043
I-355#1	0.000	0.156	0.190	0.038	0.192	0.234	0.304	0.250	0.049
I-72 1E#1	0.000	0.159	0.198	0.034	0.199	0.247	0.326	0.262	0.045
L1-1019#1	0.000	0.143	0.162	0.029	0.170	0.194	0.255	0.224	0.038
22SRT2#1	0.000	0.153	0.180	0.032	0.187	0.220	0.288	0.245	0.043
2RT26#1	0.000	0.142	0.164	0.030	0.170	0.197	0.242	0.209	0.037
L2#1	0.000	0.159	0.177	0.035	0.193	0.215	0.281	0.253	0.046
L2#2	0.000	0.148	0.164	0.032	0.177	0.196	0.258	0.233	0.042
L2#3	0.000	0.153	0.172	0.029	0.185	0.207	0.275	0.246	0.039
L2#8	0.000	0.159	0.174	0.033	0.192	0.211	0.274	0.249	0.043

APPENDIX E: FIELD CORE SUMMARY

Table 25. Field Core Summary

Core ID	Core Label	Description	Detail	Route	County	Date of Paving	Date of Coring	Binder Grade
IL-125	C1	10" HMA Base Course (N50 IL19.0 with 2.25" HMA Shoulder (N70 IL9.5	Over Tributary to Lost Creek West of Virginia Eastbound shoulder (stage II Construction Traffic Lane)	IL-125	Cass	Nov-09	2019	64-22
	C2							
	C3							
	C4							
	C5					Top 2.25":		
	C6					May-10		
US-51	J9	Grade: PG 64-22 All Mixes	At Big Muddy River	US 51	Jackson	Fall of 2001	2019	64-22
	J10							
	J11							
	J12							
	J13							
	J14							
	J15							
	J16							
I-90	B1	N70D-Surface and N70-Binder	At Belvedere Toll Plaza Outside shoulder inside the cash lanes, past the Cash Plaza, before the end of the barrier wall between the cash lanes and Ort Lanes	WB I-90	Boone	2006	2019	64-22
	B2							
	B3							
	B4							
	B5							
	B6							
	B7							
	B8							
I-355	W1	N70D-Surface and N70-Binder	Entrance ramp, Outside shoulder	SB I-355	Will	Oct-07	2019	64-22
	W2							
	W3							
	W4							
	W5							
	W6							
	W7							
	W8							

Core ID	Core Label	Description	Detail	Route	County	Date of Paving	Date of Coring	Binder Grade
L1-1019	10/19 L1-1	ICT Test Track 2” Surface (No RAP)	NA	ATLAS	Champaign	2008	2019	64-22
	10/19 L1-2							
	10/19 L1-3							
	10/19 L1-4							
L2-1019	10/19 L2-1	ICT Test Track 4” Surface (No RAP)	NA	ATLAS	Champaign	2009	2019	64-22
	10/19 L2-2							
	10/19 L2-3							
	10/19 L2-4							
L3-1019	10/19 L3-1	ICT Test Track 2” Surface (No RAP)	NA	ATLAS	Champaign	2011	2019	64-22
	10/19 L3-2							
	10/19 L3-3							
	10/19 L3-4							
SMA20	1	2” Surface	NA	NA	NA	1998	2018	NA
	2							
	3							
	4							
ICTParking	ICTP-1	ICT Parking Lot 4” Surface	NA	NA	NA	1989	2020	NA
	ICTP-2							
	ICTP-3							
	ICTP-4							
	ICTP-5							
	ICTP-6							
	ICTP-7							
	ICTP-8							
2RT26		1.5” Surface PG76-28 SBS	Illinois 26 South of Dixon	Northbound Passing Lane	Dixon	2004	2014	76-28
22SRT2		1.5” Surface PG 58-22	Illinois 3 West of Dixon, River Road to Plock Road	Westbound Shoulder Lane, Approx. Station 396+00	Dixon	2003	2014	58-22

APPENDIX F: MIXTURE DESIGN, VOLUMETRICS, AND MIXTURE TESTING

LAB MIX DESIGN

Table 26. Mix Design Summary for Lab Mix

AGGREGATE DETAILS							
Agg. Blending %	CM16 (MS)	FM20 (V)	FA-1	MF	RAP (-3/8")	RAP (+3/8")	Target
	43.8	25.6	5.0	0.6	1.6	23.4	100.0
% Passing Sieve							
1" (25.0 mm)	100.0	100.0	100.0	100.0	100.0	100.0	*100.0*
3/4" (19.0 mm)	100.0	100.0	100.0	100.0	100.0	100.0	*100.0*
1/2" (12.5 mm)	100.0	100.0	100.0	100.0	87.4	100.0	*99.8*
3/8" (9.5 mm)	98.0	100.0	100.0	100.0	62.5	95.9	*97.6*
No. 4 (4.75 mm)	29.0	99.0	99.8	100.0	31.4	75.3	*61.8*
No. 8 (2.36 mm)	4.9	70.8	91.9	100.0	21.2	45.1	*36.4*
No. 16 (1.18 mm)	3.6	36.7	70.0	100.0	15.4	31.3	*22.6*
No. 30 (600 µm)	3.1	18.6	45.0	100.0	11.9	21.3	*14.1*
No. 50 (300 µm)	2.8	9.2	14.6	100.0	8.6	16.2	*8.8*
No. 100 (150 µm)	2.6	6.1	2.8	95.0	6.5	13.8	*6.7*
No. 200 (75 µm)	2.4	4.8	1.5	85.0	5.4	9.6	*5.2*
Bulk Spec Gravity (Gsb)	2.607	2.602	2.566	2.800	2.630	2.630	*2.610*
Apparent Spec Gravity (Gsa)	2.72	2.806	2.698	2.800	2.730	2.730	*2.743*
Absorption (%)	1.6	2.8	1.9	1.0	1.0	1.0	*1.544*

MIX & BINDER DETAILS	
Mix Type	N70-20
Binder Type	PG 58-28
Specific Gravity, G_b	1.03

MIXING CONDITIONS	
Mixing Temperature	*150C*
Compaction Temperature	*150C*
G_{mm}	2.471

DESIGN VOLUMETRICS								
Binder%	Gmb @ N70	VTM	VMA	DP	VFA	Gse	Absorbed Asphalt	Effective Asphalt
6.30%	2.358	4.6%	15.4%	0.83	70.3%	2.727	1.69%	4.72%

PLANT MIX DESIGN (PM1 AND PM2)

Table 27. Mix Design Summary for Plant Mix PM1 and PM2

Mix Design Summary	
Aggregate Type	**% Blend**
032CM16	52.0
028FM20	9.0
038FM20	14.7
004FM02 (Dust)	1.3
017FM3800 (RAP -3/8")	23.0

Target Gradation	
Sieve Size	**% Passing**
1" (25.0 mm)	100.0
3/4" (19.0 mm)	100.0
1/2" (12.5 mm)	100.0
3/8" (9.5 mm)	97.0
No. 4 (4.75 mm)	56.0
No. 8 (2.36 mm)	34.0
No. 16 (1.18 mm)	21.0
No. 30 (600 µm)	16.0
No. 50 (300 µm)	11.0
No. 100 (150 µm)	7.0
No. 200 (75 µm)	6.0

Mixture Volumetrics	
Design gyrations	70
Gmb	2.386
Gmm	2.485
Gsb,Agg	2.653
% Voids	4.0
%VMA	15.5
%VFA	74.2
%AC Total	6.0
%AC RAP	1.2
%ACVirgin	4.8
%ABR	19.7
TSR	0.93

Table 28. Mix Design Summary for Plant Mix PM3

Mix Design Summary	
Aggregate Type	**% Blend**
Washed Sand	28.0
Unwashed 1/2"	13.0
Washed Chips 1/2"	12.0
Washed Chips 3/4"	22.0
SHOP RAP	25.0

Target Gradation	
Sieve Size	**% Passing**
1" (25.0 mm)	100.0
3/4" (19.0 mm)	100.0
1/2" (12.5 mm)	91.1
3/8" (9.5 mm)	81.7
No. 4 (4.75 mm)	60.5
No. 8 (2.36 mm)	48.7
No. 16 (1.18 mm)	35.8
No. 30 (600 µm)	24.1
No. 50 (300 µm)	13.8
No. 100 (150 µm)	7.0
No. 200 (75 µm)	4.1

Mixture Volumetrics	
Design gyrations	100
Gmb	2.387
Gmm	2.481
Gsb,Agg	2.667
% Voids	3.8
%VMA	15.1
%VFA	74.8
%AC Total	5.1
%AC RAP	1.0
%ACVirgin	4.1
%ABR	19.6
TSR	0.83

Table 29. Mix Design Summary for Plant Mix PM4

Mix Design Summary	
Aggregate Type	**% Blend**
Washed Sand	28.0
Unwashed 1/2"	13.0
Washed Chips 1/2"	12.0
Washed Chips 3/4"	22.0
SHOP RAP	25.0

Target Gradation	
Sieve Size	**% Passing**
1" (25.0 mm)	100.0
3/4" (19.0 mm)	100.0
1/2" (12.5 mm)	91.1
3/8" (9.5 mm)	81.7
No. 4 (4.75 mm)	60.5
No. 8 (2.36 mm)	48.7
No. 16 (1.18 mm)	35.8
No. 30 (600 µm)	24.1
No. 50 (300 µm)	13.8
No. 100 (150 µm)	7.0
No. 200 (75 µm)	4.1

Mixture Volumetrics	
Design gyrations	100
Gmb	2.387
Gmm	2.481
Gsb,Agg	2.667
% Voids	3.8
%VMA	15.1
%VFA	74.8
%AC Total	5.1
%AC RAP	1.0
%ACVirgin	4.1
%ABR	20.0
TSR	0.83

Table 30. I-FIT Specimen Volumetrics

MIX	ID	DRY	SUB	SSD	Gmb	AV	CONDITION	THICK 1	THICK 2	NOTCH1	NOTCH2	LIG 1	LIG 2	AVG LIG	AVG THICK	AVG NOTCH
PM1	P1-2	997.8	575.6	999.4	2.354	6.7	3D95C	49.85	50.05	13.85	13.71	59	59.76	59.38	49.95	13.78
PM1	P1-4	1003.4	576.6	1005.4	2.340	7.3	3D95C	49.82	50.09	13.72	13.63	60.29	60.67	60.48	49.955	13.675
PM1	P2-1	994.8	575.9	996.8	2.364	6.4	3D95C	49.66	50.04	13.73	13.22	59.61	59.95	59.78	49.85	13.475
PM1	P2-4	1015.7	585.5	1017.4	2.352	6.8	3D95C	50	50	13.45	13.36	60.81	60.94	60.875	50	13.405
PM1	P3-4	1021.7	589.9	1023.7	2.355	6.7	3D95C	49.76	49.96	13.6	13.6	60.82	61.23	61.025	49.86	13.6
PM1	P4-1	1009.2	584	1011	2.363	6.4	3D95C	50.15	50.46	13.46	13.52	59.94	60.34	60.14	50.305	13.49
PM1	P4-2	1019	588.5	1021	2.356	6.7	3D95C	50.08	50.51	13.6	13.67	60.88	60.44	60.66	50.295	13.635
PM1	P1-1	1008.6	580.6	1010.3	2.347	7.0	UA	50	50.27	14.44	14.01	59.76	60.25	60.005	50.135	14.225
PM1	P1-3	1005.7	578.8	1007.3	2.347	7.0	UA	50.37	49.98	13.87	13.5	59.94	60.19	60.065	50.175	13.685
PM1	P2-2	998.8	574.8	1001.1	2.343	7.2	UA	50.05	49.72	13.52	13.35	59.77	59.83	59.8	49.885	13.435
PM1	P2-3	1013.9	583.9	1015.7	2.348	7.0	UA	49.58	49.71	13.27	13.52	60.9	61.11	61.005	49.645	13.395
PM1	P3-2	1012.1	586	1013.8	2.366	6.3	UA	49.5	49.61	13.46	13.57	59.7	60.64	60.17	49.555	13.515
PM1	P3-3	988.3	568.3	989.7	2.345	7.1	UA	49.66	49.7	13.39	13.58	59.73	59.23	59.48	49.68	13.485
PM1	P4-4	990.5	572.4	992.3	2.359	6.5	UA	49.46	49.55	13.78	13.45	59.92	59.54	59.73	49.505	13.615
PM1	P3-1	1010.8	588	1013	2.378	5.8								#DIV/0!	#DIV/0!	#DIV/0!
PM1	P4-3	1007.6	585.9	1009.2	2.380	5.7								#DIV/0!	#DIV/0!	#DIV/0!
PM2	P1-2	1020.1	586.3	1022.5	2.339	7.1	3D95C	50.78	50.49	13.66	13.2	60.9	61.21	61.055	50.635	13.43
PM2	P1-3	1000.5	578.1	1002.1	2.360	6.3	3D95C	49.79	49.36	13.58	13.49	60.4	60.48	60.44	49.575	13.535
PM2	P2-1	988.3	569.1	990.4	2.346	6.8	3D95C	49.54	50.1	13.43	13.34	59.72	59.55	59.635	49.82	13.385
PM2	P3-1	985.9	567.7	987.7	2.347	6.8	3D95C	49.63	49.68	13.42	13.39	59.91	59.7	59.805	49.655	13.405
PM2	P3-2	1008.6	582.9	1010.8	2.357	6.4	3D95C	50.34	50.3	13.35	13.08	60.95	59.95	60.45	50.32	13.215
PM2	P4-2	1012.1	582.7	1014.6	2.343	6.9	3D95C	50.13	50.02	13.37	13.27	60.59	61.12	60.855	50.075	13.32
PM2	P4-4	992.5	572.6	994.7	2.351	6.6	3D95C	49.26	49.81	13.33	13.53	59.9	59.6	59.75	49.535	13.43
PM2	P1-1	983.1	567.3	984.5	2.356	6.4	UA	49.73	49.35	13.38	13.5	58.81	59.1	58.955	49.54	13.44
PM2	P1-4	975.2	561.1	977.9	2.340	7.1	UA	49.12	48.93	13.7	13.48	59.87	59.93	59.9	49.025	13.59
PM2	P2-2	980.1	563.9	982.2	2.343	6.9	UA	49.04	49.31	13.27	13.38	60.27	59.81	60.04	49.175	13.325
PM2	P2-3	997	575.4	999.2	2.353	6.6	UA	49.17	49.04	13.56	13.44	61	60.02	60.51	49.105	13.5
PM2	P2-4	1014.2	585.9	1016.3	2.356	6.4	UA	49.95	50.26	13.48	13.39	60.65	60.54	60.595	50.105	13.435
PM2	P3-3	989.8	571.2	991.6	2.354	6.5	UA	49.98	49.12	13.22	13.49	59.95	60.36	60.155	49.55	13.355
PM2	P4-3	987.6	568.3	990.3	2.340	7.1	UA	49.69	49.8	13.59	13.43	59.96	59.76	59.86	49.745	13.51
PM2	P3-4	1024.7	594.4	1026.3	2.373	5.8								#DIV/0!	#DIV/0!	#DIV/0!
PM2	P4-1	1010.5	584.4	1012.4	2.361	6.2								#DIV/0!	#DIV/0!	#DIV/0!
PM3	P1-1	985.7	563.1	987.3	2.324	6.6	UA	49.74	50.06	13.66	13.54	59.24	59.68	59.46	49.9	13.6
PM3	P1-4	1008.1	576.6	1009.9	2.327	6.5	UA	49.94	49.68	13.62	13.45	60.81	60.56	60.685	49.81	13.535
PM3	P2-3	1006.6	574.3	1008.1	2.320	6.8	UA	49.9	49.77	13.53	13.48	60.9	60.7	60.8	49.835	13.505
PM3	P3-1	988.4	560.9	989.6	2.306	7.4	UA	49.31	49.19	13.6	13.53	60.3	60.8	60.55	49.25	13.565
PM3	P3-2	1013	580	1014.6	2.331	6.4	UA	50.24	50.33	13.37	13.45	60.3	60.76	60.53	50.285	13.41
PM3	P4-2	1002.9	574.3	1004.5	2.331	6.3	UA	50.35	50.52	13.5	12.9	60.06	60.15	60.105	50.435	13.2

MIX	ID	DRY	SUB	SSD	Gmb	AV	CONDITION	THICK 1	THICK 2	NOTCH1	NOTCH2	LIG 1	LIG 2	AVG LIG	AVG THICK	AVG NOTCH
PM3	P4-3	984.9	559	986.6	2.303	7.5	UA	49.17	49.1	13.66	13.48	60.4	60.66	60.53	49.135	13.57
PM3	P1-2	995.8	566.2	997.2	2.310	7.2	3D95C	49.97	49.98	13.8	13.59	60.13	60.51	60.32	49.975	13.695
PM3	P1-3	992.8	568.4	994	2.333	6.3	3D95C	49.56	49.85	13.65	13.49	59.72	59.82	59.77	49.705	13.57
PM3	P2-2	991.1	566.3	993.1	2.322	6.7	3D95C	50.05	50.35	13.38	13.61	59.8	59.65	59.725	50.2	13.495
PM3	P4-1	973.4	555	974.9	2.318	6.9	3D95C	49.07	49.21	13.5	13.29	59.78	59.68	59.73	49.14	13.395
PM3	P4-4	1008.2	575.4	1010.1	2.319	6.8	3D95C	50.26	50.21	13.45	13.43	60.79	60.43	60.61	50.235	13.44
PM3	P2-4	993.6	563.2	995.5	2.298	7.7	3D95C	49.77	49.54	13.53	13.64	60.64	60.76	60.7	49.655	13.585
PM3	P2-1	973.1	551.2	975.1	2.296	7.8										
PM3	P3-3	1004.2	575.9	1005.8	2.336	6.2										
PM3	P3-4	970.1	548.8	971.8	2.293	7.9										
PM4	P1-1	994.6	566.6	996	2.316	7.1	3D95C	49.44	49.21	13.34	13.69	60.89	60.83	60.86	49.325	13.515
PM4	P1-2	986.8	565.2	988.4	2.332	6.4	3D95C	49.32	50.1	12.89	13.46	60.04	59.84	59.94	49.71	13.175
PM4	P2-2	992	566.5	993.8	2.322	6.8	3D95C	49.33	49.87	13.55	13.17	60.07	60.23	60.15	49.6	13.36
PM4	P2-4	998.9	572.3	1000.9	2.331	6.5	3D95C	49.66	49.59	13.55	13.55	59.96	60.8	60.38	49.625	13.55
PM4	P3-2	985.7	561.5	987.6	2.313	7.2	3D95C	49.37	49.24	13.48	13.4	60.74	60.14	60.44	49.305	13.44
PM4	P4-1	992.4	567.4	994.3	2.325	6.7	3D95C	50.34	49.99	13.61	13.56	59.59	59.66	59.625	50.165	13.585
PM4	P4-4	1001.6	572.4	1002.9	2.327	6.6	3D95C	49.89	49.38	13.42	13.42	60.72	60.86	60.79	49.635	13.42
PM4	P1-3	1005.7	574.7	1007.3	2.325	6.7	UA	50.26	49.98	13.56	13.41	60.54	60.65	60.595	50.12	13.485
PM4	P1-4	968.3	551.7	969	2.320	6.9	UA	49.13	49.37	13.57	13.58	59.5	58.61	59.055	49.25	13.575
PM4	P2-3	1006	575.6	1008	2.327	6.6	UA	50.19	50.82	13.57	13.46	60.16	60.28	60.22	50.505	13.515
PM4	P3-1	979.7	557.8	981.6	2.312	7.2	UA	49.25	49.25	13.54	13.65	60.08	60.55	60.315	49.25	13.595
PM4	P3-3	1017.4	579.5	1019.2	2.314	7.1	UA	50.99	50.17	13.55	13.28	60.59	61.19	60.89	50.58	13.415
PM4	P3-4	980.6	561.8	982	2.334	6.4	UA	48.95	49.85	13.73	12.98	59.76	60.12	59.94	49.4	13.355
PM4	P4-2	986.3	562.3	988.5	2.314	7.1	UA	49.21	49.76	13.5	13.2	60.37	59.95	60.16	49.485	13.35
PM4	P4-3	1002.6	569.1	1005.2	2.299	7.7	UA	50.94	50.03	13.58	13.52	60.91	60.2	60.555	50.485	13.55
PM4	P2-1	994.3	572.4	996	2.347	5.8										
S5	P1-1	1017.7	579.7	1019.2	2.316	6.3	3D95C	50.46	50.27	15.27	15.47	59.25	59.42	59.335	50.365	15.37
S5	P1-4	995.4	561.7	997.2	2.286	7.5	3D95C	50.24	49.87	15.58	15.43	59.08	59.37	59.225	50.055	15.505
S5	P3-1	1008.4	570.3	1010.1	2.293	7.2	3D95C	49.86	50.44	15.52	15.36	59.36	59.05	59.205	50.15	15.44
S5	P3-2	981.5	554.5	983.7	2.287	7.5	3D95C	51.12	50.74	15.32	15.08	57.52	57.62	57.57	50.93	15.2
S5	P4-3	971.8	550.9	973.8	2.298	7.0	3D95C	49.34	50.02	15.33	15.39	57.94	57.78	57.86	49.68	15.36
S5	P4-4	961.4	543.1	963.8	2.285	7.5	3D95C	49.42	49.7	15.18	15.43	57.33	57.78	57.555	49.56	15.305
S5	P1-2	977.2	554.6	979	2.303	6.8	UA	49.9	50.09	15.63	15.28	57.63	57.68	57.655	49.995	15.455
S5	P1-3	985.1	560.1	986.7	2.309	6.5	UA	49.96	49.73	15.31	15.44	58.28	58.08	58.18	49.845	15.375
S5	P3-3	1009.7	575	1011.4	2.314	6.4	UA	50.41	50.37	15.48	15.3	58.88	58.91	58.895	50.39	15.39
S5	P3-4	990.5	560.9	993	2.292	7.2	UA	50.5	50.05	15.36	15.4	58.2	58.7	58.45	50.275	15.38
S5	P4-1	1004.2	569.7	1005.6	2.304	6.8	UA	49.88	50.36	15.44	15.4	59.2	59.2	59.2	50.12	15.42
S5	P4-2	999.4	566.2	1001.1	2.298	7.0	UA	49.21	49.5	15.43	15.54	59.58	59.63	59.605	49.355	15.485
S5	P2-1	983.6	561.3	985.4	2.319	6.1										
S5	P2-2	999.4	569.6	1001	2.317	6.2										

MIX	ID	DRY	SUB	SSD	Gmb	AV	CONDITION	THICK 1	THICK 2	NOTCH1	NOTCH2	LIG 1	LIG 2	AVG LIG	AVG THICK	AVG NOTCH
S5	P2-3	1010.4	578.7	1012.1	2.331	5.7										
S5	P2-4	993	567.3	994.6	2.324	6.0										
C	P1-3	983.1	554.9	985.1	2.285	7.5	3D95C	50.71	51.01	15.4	15.21	57.66	57.77	57.715	50.86	15.305
C	P1-4	1025.6	581.2	1027.5	2.298	7.0	3D95C	51.35	51.19	15.25	15.2	59.61	59.25	59.43	51.27	15.225
C	P2-2	981.4	555	983.3	2.291	7.2	3D95C	50.75	50.63	15.27	15.39	57.66	57.63	57.645	50.69	15.33
C	P2-4	1012.7	575.5	1014.3	2.308	6.6	3D95C	50.23	50.7	15.11	15.34	58.88	59.23	59.055	50.465	15.225
C	P3-3	1020.8	576.3	1022.7	2.287	7.4	3D95C	51.77	51.05	15.32	15.2	59.3	59.19	59.245	51.41	15.26
C	P3-4	1009	573.3	1010.5	2.308	6.6	3D95C	50.27	50.41	15.35	15.28	59.03	58.98	59.005	50.34	15.315
C	P1-1	1004.1	568.4	1006.4	2.292	7.2	UA	49.94	49.96	15.28	15.24	59.54	59.38	59.46	49.95	15.26
C	P1-2	978.4	552.2	980	2.287	7.4	UA	50.6	50.2	15.31	15.42	57.97	57.78	57.875	50.4	15.365
C	P2-1	983.1	556.4	985	2.294	7.1	UA	49.86	50.2	15.5	15.42	58.02	58.06	58.04	50.03	15.46
C	P2-3	993.6	560.7	995.8	2.284	7.5	UA	49.8	49.96	15.31	15.27	59.38	58.9	59.14	49.88	15.29
C	P3-1	983.1	557.1	984.9	2.298	7.0	UA	49.88	50.28	15.41	15.44	57.81	58.4	58.105	50.08	15.425
C	P3-2	986.1	560.2	987.9	2.306	6.7	UA	50.1	50.14	15.28	15.46	58.15	57.88	58.015	50.12	15.37
F	P1-3	980	554	981.8	2.291	7.1	3D95C	50	50.56	15.29	15.08	58.29	58.04	58.165	50.28	15.185
F	P1-4	1021.8	581	1023.1	2.311	6.3	3D95C	50.8	50.72	15.42	15.19	59.57	59	59.285	50.76	15.305
F	P2-2	1006.3	572.3	1007.7	2.311	6.3	3D95C	50.05	50.24	15.32	15.24	58.66	58.93	58.795	50.145	15.28
F	P2-4	993.6	564	995.2	2.304	6.6	3D95C	49.95	50.14	15.51	15.34	58.58	58.57	58.575	50.045	15.425
F	P3-2	1005.7	568.4	1007.6	2.290	7.2	3D95C	50.27	50.44	15.35	15.3	59.15	59.24	59.195	50.355	15.325
F	P3-3	985.2	557.4	986.8	2.294	7.0	3D95C	50.34	50.27	15.28	15.47	57.72	57.75	57.735	50.305	15.375
F	P1-1	968.7	547.4	971	2.287	7.3	UA	49.98	49.36	15.46	15.6	57.72	57.91	57.815	49.67	15.53
F	P1-2	994	564.5	995.3	2.307	6.5	UA	49.1	49.14	15.32	15.42	59.49	59.56	59.525	49.12	15.37
F	P2-1	987.2	560.1	989.1	2.301	6.7	UA	50.77	50.43	15.29	15.38	58.06	57.92	57.99	50.6	15.335
F	P2-3	988.4	563.3	990.3	2.315	6.2	UA	50.12	49.94	15.37	15.38	57.82	58.42	58.12	50.03	15.375
F	P3-1	991.9	563.2	993.7	2.304	6.6	UA	50.57	50.37	15.42	15.48	57.74	57.85	57.795	50.47	15.45
F	P3-4	999.9	563.4	1001.7	2.281	7.5	UA	50.14	49.96	15.44	15.44	59.4	59.24	59.32	50.05	15.44
G	P1-3	971.4	548.6	973.2	2.288	7.5	3D95C	49.71	49.73	15.33	15.3	57.87	58.23	58.05	49.72	15.315
G	P1-4	994.9	564.2	996.4	2.302	7.0	3D95C	50	49.88	15.38	15.34	58.9	58.98	58.94	49.94	15.36
G	P2-3	983.9	559.7	985.5	2.311	6.6	3D95C	50.3	49.88	15.32	15.4	58.12	57.96	58.04	50.09	15.36
G	P2-4	991.3	561.4	993.1	2.296	7.2	3D95C	50.14	49.9	15.2	15.39	58.8	58.86	58.83	50.02	15.295
G	P3-2	992.1	565.1	993.1	2.318	6.3	3D95C	50.28	50.71	15.28	15.42	57.71	58.13	57.92	50.495	15.35
G	P3-3	985.7	558.6	986.9	2.301	7.0	3D95C	49.27	49.56	15.33	15.44	58.58	58.96	58.77	49.415	15.385
G	P1-1	986.2	561.4	988.1	2.311	6.6	UA	50.04	49.98	15.35	15.38	57.88	58.28	58.08	50.01	15.365
G	P1-2	992.1	561.8	994.3	2.294	7.3	UA	49.68	50.16	15.4	15.32	59.1	58.9	59	49.92	15.36
G	P2-1	982	557.1	983.6	2.302	6.9	UA	50.37	50.26	15.53	15.3	58.18	57.61	57.895	50.315	15.415
G	P2-2	1009.1	574.2	1010.6	2.312	6.5	UA	50.1	50.16	15.23	15.31	59.1	59.57	59.335	50.13	15.27
G	P3-1	973.9	551.6	975.4	2.298	7.1	UA	49.75	49.4	15.49	15.39	58.08	58.42	58.25	49.575	15.44
G	P3-4	1008.5	572.7	1010	2.306	6.8	UA	50.49	50.23	15.18	15.41	59.2	58.91	59.055	50.36	15.295
H	P1-3	984	558.8	985.4	2.307	6.4	3D95C	49.77	50.4	15.31	15.46	57.73	57.62	57.675	50.085	15.385
H	P1-4	997.5	564.9	999.2	2.297	6.8	3D95C	49.92	50	15.3	15.5	58.61	59.13	58.87	49.96	15.4

MIX	ID	DRY	SUB	SSD	Gmb	AV	CONDITION	THICK 1	THICK 2	NOTCH1	NOTCH2	LIG 1	LIG 2	AVG LIG	AVG THICK	AVG NOTCH
H	P2-3	980.9	553.5	982.8	2.285	7.3	3D95C	51.1	50.8	15.29	15.32	58	57.6	57.8	50.95	15.305
H	P2-4	1020.2	580.7	1021.5	2.314	6.1	3D95C	50.1	50.5	15.25	15.26	59.53	58.82	59.175	50.3	15.255
H	P3-3	970.7	546.5	972.2	2.280	7.5	3D95C	50.5	50.32	15.39	15.42	57.74	57.31	57.525	50.41	15.405
H	P3-4	1014.5	573.5	1016	2.293	7.0	3D95C	50.45	50.15	15.47	15.31	59.45	59.95	59.7	50.3	15.39
H	P1-1	992.7	564.4	993.9	2.311	6.2	UA	50.02	50.36	15.18	15.48	58.28	58.19	58.235	50.19	15.33
H	P1-2	1009.6	571.5	1011.5	2.295	6.9	UA	50.94	50.43	15.41	15.23	59.14	58.72	58.93	50.685	15.32
H	P2-1	980.7	556.8	982.3	2.305	6.5	UA	49.5	49.8	15.38	15.36	57.85	57.94	57.895	49.65	15.37
H	P2-2	995.8	562.7	997.3	2.291	7.0	UA	49.99	49.64	15.64	15.41	59.02	58.95	58.985	49.815	15.525
H	P3-1	984.1	557.3	985.2	2.300	6.7	UA	49.94	50.15	15.39	15.29	57.95	58.04	57.995	50.045	15.34
H	P3-2	1012.6	570.4	1014.7	2.279	7.5	UA	50.48	50.84	15.31	15.33	59.69	59.74	59.715	50.66	15.32
K	P1-3	985	557.4	986.8	2.294	7.0	3D95C	50	50.11	15.4	15.31	58.18	58.41	58.295	50.055	15.355
K	P1-4	994.3	562.9	996	2.296	6.9	3D95C	49.8	49.94	15.35	15.41	58.57	59.22	58.895	49.87	15.38
K	P2-1	990.1	563	991.6	2.310	6.4	3D95C	50.43	50.39	15.35	15.29	57.59	58.05	57.82	50.41	15.32
K	P2-2	998.9	566	1000.6	2.298	6.8	3D95C	50.05	50.3	15.23	15.3	59	58.96	58.98	50.175	15.265
K	P3-1	977.1	552.1	978.9	2.289	7.2	3D95C	50.22	50.04	15.43	15.21	57.52	57.81	57.665	50.13	15.32
K	P3-2	997.3	564.3	999.4	2.292	7.1	3D95C	49.82	50.11	15.41	15.4	58.71	59.04	58.875	49.965	15.405
K	P1-1	989	562.1	990.6	2.308	6.4	UA	50.34	50.24	15.48	15.48	57.87	57.97	57.92	50.29	15.48
K	P1-2	1004.1	568.9	1006	2.297	6.9	UA	50.07	50.18	15.43	15.36	59.06	59.36	59.21	50.125	15.395
K	P2-3	984.3	556.7	985.8	2.294	7.0	UA	49.93	49.97	15.28	15.32	58.2	58.43	58.315	49.95	15.3
K	P2-4	998.5	564.4	1000.2	2.291	7.1	UA	49.9	49.89	15.42	15.38	58.94	59.27	59.105	49.895	15.4
K	P3-3	979.3	555.3	981	2.300	6.8	UA	50.05	49.76	15.48	15.4	58	58.04	58.02	49.905	15.44
K	P3-4	1001.1	567	1002.7	2.298	6.9	UA	50.18	50.38	15.44	15.32	59.35	59.03	59.19	50.28	15.38


Illinois Department
of Transportation


ILLINOIS